حولية كلية البنات

بجامعة عين شمس

العـــدد الثـــانى عشر

القســـم العلمى

مطبعة كلية البنات
١٩٨٧

UNIVERSITY COLLEGE FOR GIRLS

ANNUAL REVIEW

AIN SHAMS UNIVERSITY

VOLUME : 12

SCIENCE SECTION

COLLEGE FOR GIRLS PRESS

1987

CONTENTS

****

MOTION OF A CONDUCTING FLUID DUE TO AN INFINITE ROTATING DISK

Adel A. Megahed
Department of Engineering Mathematics,
Faculty of Engineering, Cairo University, Giza.

ABSTRACT

In the present paper, the unsteady motion of a weakly conducting, incompressible and viscous fluid due to non-uniform rotation of an infinite flat disk, is considered. The motion is subjected to a uniform external magnetic field normal to the disc and parallel to the axis of rotation. The equations of motion are written assuming low magnetic Reynold's number i.e. The external magnetic field is undisturbed during motion. The general solution is determined by the aid of Green's function, and is obtained in the form of a system of integral equations which can be solved by successive approximation. A special case of the solution, which corresponds to uniform rotation of the disk, is deduced and discussed.

INTRODUCTION

The flow of viscous, electrically conducting fluids in the neighbourhood of a rotating disk is of great practical importance, particularly in connection with rotary magnetohydrodynamic machines. Similar problem in classical hydrodynamics is studied by many authors[1]. The exact solution of the equation of motion of a viscous fluid around a flat infinite disk which rotates about an axis perpendicular to its plane with a uniform angular velocity was studied by Cochran[2], and the steady state solution was obtained by similarity. The motion due to a rotating disk in a fluid at rest, was also examined to study the transition of a three-dimensional boundary layer to turbulence[1], and it was proved that it becomes turbulent at large Reynold's numbers, $Re > 3 \times 10^5$.

In the presence of an external axial magnetic field, the steady flow of an electrically conducting fluid was studied due to the rotation of an infinite cylinder.[3] Other problems of steady motion of conducting fluids due to rotating disks are described in many references[4,5]. Such problems are related to magnetohydrodynamic (MHD) generators and MHD vortex flow, and the solution was obtained mainly by numerical methods.

In the present work, is considered, the non-uniform rotation of an infinite thin disk through the origin, about the z-axis, in an incompressible, viscous and electrically conducting fluid. The fluid is assumed initially at rest, and is subjected to a uniform external magnetic field normal to the disk and parallel to the z-axis. Following the cylindrical-coordinates (r,θ,z), the case considered is a fully three dimensional flow i.e. there exists three components of the velocity of flow v_r, v_θ and v_z. The fluid layer near the disk is carried by it through friction and is thrown outwards owing to the action of centrifugal forces. This is compensated by particles which flow in an axial direction towards the disk to be in turn carried and ejected centrifugally.

FUNDAMENTAL EQUATIONS

Denoting the three components of velocity by $v_r = u(r,z,t)$, $v_\theta = v(r,z,t)$ and $v_z = w(r,z,t)$, and assuming low magnetic Reynold's number $Re_m < 1$, the equations of motion in cylindrical coordinates are written in the form[3,5];

$$\frac{\partial u}{\partial t} + u\frac{\partial u}{\partial r} + w\frac{\partial u}{\partial z} - \frac{v^2}{r} = -\frac{1}{\rho}\frac{\partial P}{\partial r} + \nu\left(\Delta u - \frac{u}{r}\right) - m^2 u$$

$$\frac{\partial v}{\partial t} + u\frac{\partial v}{\partial r} + w\frac{\partial v}{\partial z} + \frac{uv}{r} = \nu\left(\Delta v - \frac{v}{r^2}\right) - m^2 v \quad \ldots (1)$$

$$\frac{\partial w}{\partial t} + u\frac{\partial w}{\partial r} + w\frac{\partial w}{\partial z} = -\frac{1}{\rho}\frac{\partial P}{\partial z} + \nu\Delta w$$

and

$$\frac{\partial u}{\partial r} + \frac{u}{r} + \frac{\partial w}{\partial z} = 0$$

where,

$$\Delta = \frac{\partial^2}{\partial r^2} + \frac{1}{r}\frac{\partial}{\partial r} + \frac{\partial^2}{\partial z^2},$$

$m^2 = \text{const} = \dfrac{\sigma H_o^2}{\rho c^2}$, and H_o = constant external magnetic field.

The angular velocity of the rotation of the disk is a given function of time w(t), so that the inital and boundary conditions can be represented in the form;

$$u = v = w = 0, \quad \text{at} \quad t = 0$$

$$u = 0, \; v = r\,w(t), \; w = 0 \quad \text{at} \quad z = 0, \quad ..(2)$$

and $$u = v = 0. \quad \text{as} \quad z \longrightarrow \infty$$

It is required to obtain the solution of system of equations (1), which satisfies the boundary and initial conditions (2). The solution is assumed in the form;

$$u = rf(z,t), \; v = r\,g(z,t), \; w = 2\psi(z,t),$$

$$P = P(z,t) \qquad \ldots (3)$$

Substituting from (3), the system of equations (1) is reduced to the form;

$$\nu \frac{\partial^2 f}{\partial z^2} - \frac{\partial f}{\partial t} - m^2 f = 2\psi \frac{\partial f}{\partial z} + f^2 - g^2,$$

$$\nu \frac{\partial^2 g}{\partial z^2} - \frac{\partial g}{\partial t} - m^2 g = 2\psi \frac{\partial g}{\partial z} + 2 f g, \qquad \ldots (4)$$

$$\frac{\partial^2 \psi}{\partial z^2} - \frac{\partial \psi}{\partial t} = 2\psi \frac{\partial \psi}{\partial z} + \frac{1}{2\rho}\frac{\partial P}{\partial z},$$

and

$$\frac{\partial \psi}{\partial z} = -f$$

The system of equations (4) is solved with the following boundary and initial conditions;

at $t = 0$, $f = g = \psi = 0$,

at $z = 0$, $f = 0$, $g = w(t)$, $\psi = 0$ ... (5)

and as $z \longrightarrow \infty$, $f = g = 0$.

Introducing the new function $F = f + i\,g$, ... (6)

the two first equations of the system (4) are written in the form;

$$\nu \frac{\partial^2 F}{\partial z^2} - \frac{\partial F}{\partial t} - m^2 F = 2\psi \frac{F}{z} + F^2 \quad \ldots \quad (7)$$

The function ψ will be deduced from the relation;

$$\psi = - \int_0^z \bar{f}\, dz = - \int_0^z \mathrm{Re}\,(F)\, dz, \quad \ldots \quad (8)$$

where,

Re(F) is the real part of the function F.

Boundary and initial conditions of the new function F are;

$F = 0$ at $t = 0$, and $F = i\,w(t)$ at $z = 0$,

while as $z \longrightarrow \infty$, $F \longrightarrow$ zero ... (9)

The method of solution followed here, is described by Sharikadze and Megahed[6]. The unsteady solution is obtained by superposition, as the sum of two parts. The first part is the solution of the homogeneous differential equation which satisfies the given boundary conditions and zero initial conditions, while the second part is the solution of the given differential equation which corresponds to homogeneous boundary conditions.

SOLUTION OF THE PROBLEM

The solution of the left-hand side of equation (7), which satisfie the boundary conditions (9) can be proved to be;

$$F_o(z,t) = \frac{1}{2\sqrt{\pi\nu}} \int_o^t w(\tau) \exp -\left[\frac{z^2}{4\nu(t-\tau)} - m^2(t-\tau)\right] \frac{z\, d\tau}{(t-\tau)^{3/2}} \quad \ldots \quad (10)$$

Introducing Green's function[6,7]

$$G(z,\xi,t) = -\frac{1}{2\sqrt{\pi\nu t}} \exp\left[-\frac{(z-\xi)}{4\nu t} - m^2 t\right] +$$

$$+ \int_o^t \exp\left(-\frac{\xi^2}{4\nu\tau} - m^2\tau\right) \exp\left[-\frac{z^2}{4\nu(t-\tau)}\right] \frac{z\, d\tau}{4\pi\nu\sqrt{\tau(t-\tau)^3}}, \quad \ldots \quad (11)$$

which satisfies at $z \neq \xi$ equation (7) without the right-hand side and tends to zero at $t = 0$, and at $z = 0, \infty$, the final required solution $F(z,t)$ can be represented in the form;

$$F(z,t) = F_o(z,t) + \int_o^t d\tau \int_o^\infty (2\psi\frac{\partial F}{\partial \xi} + F^2) G(z,\xi,t-\tau)\, d\xi \quad \ldots \quad (12)$$

Differentiating equation (12) with respect to z, under the sign of integration, we get;

$$\frac{\partial F}{\partial z} = \frac{\partial F_o}{\partial z} + \int_o^t d\tau \int_o^\infty (2\psi\frac{\partial F}{\partial \xi} + F^2)\frac{\partial G}{\partial z}\, d\xi \quad \ldots \quad (13)$$

The system of equations (12) and (13) and be solved to obtain the unknowns F, $\frac{\partial F}{\partial z}$, hence the two functions f and g can be determined, Equation (8) enables to obtain ψ while the third equation of (4) is applied to determine P. The components of velocity are deduced from f , g and ψ as defined before.

The method of successive approximation is applied to solve the system (12) and (13). Denoting $\frac{\partial F}{\partial z} = W$, the required functions are represented in the form of the following series;

$$F = \sum_{n=o}^{\infty} \lambda^n F_n, \quad W = \sum_{n=o}^{\infty} \lambda^n W_n, \quad \psi = \sum_{n=o}^{\infty} \lambda^n \psi_n \qquad \ldots(14)$$

where,

λ is a parameter. Substitute from (14) into equations (8) , (12) and (13) , starting initially with;

$$F_o , \quad W_o = \frac{\partial F_o}{\partial z} \text{ and } \psi_o = - \int_o^z \text{Re } (F_o) \, dz = 0,$$

we obtain the recurrent formulae;

$$F_{n+1} = \int_o^t d\tau \int_o^{\infty} \sum_{m=o}^{n} (2\psi_{n-m} W_m + F_{n-m} F_m) \, G \, d\xi,$$

$$\psi_{n+1} = - \int_o^z \text{Re } (F_{n+1}) \, dz, \qquad \ldots(15)$$

and $$W_{n+1} = \int_0^t d\tau \int_0^\infty \sum_{m=0}^{\infty} (2\psi_{n-m} W_m + F_{n-m} F_m) \frac{\partial G}{\partial z} d\xi$$

The function F_o could be calculated from (10) as a pure imaginary function with a real part equals zero. The solution deduced in (14) and (15) can be proved to form a system of convergent series within the conditions under consideration.

The first two approximations of such solution are determined. Consider as a first approximation;

$$F_o = 0 \quad , \quad \psi_o = 0 \text{ i.e.} \qquad f_o = \psi_o = 0,$$

Therefore from (4) and (10), we get;

$$u = 0 \quad , \quad w = 0 \quad , \quad P = P_o(t)$$

$$v_\theta = v = \frac{r\ z}{2\sqrt{\pi\nu}} \int_0^t w(\tau) \exp\left[\frac{-z^2}{4\nu(t-\tau)} - m^2(t-\tau)\right] \frac{d\tau}{(t-\tau)^{3/2}}$$

...(16)

The last equations indicates that the first approximation affects only the rotating motion of the fluid, while the radial and axial components of the velocity are zero. If the disc rotates with uniform angular velocity i.e. $w(\tau) = \omega = \text{const.}$, we get after integrating (16);

$$v = \frac{r\omega}{2}\left[\exp\left(-mz/\sqrt{\nu}\right) \operatorname{erfc}\left(\frac{z}{2\sqrt{\nu t}} - m\sqrt{t}\right) + \right.$$

$$\left. + \exp\left(mz/\sqrt{\nu}\right) \operatorname{erfc}\left(\frac{z}{2\sqrt{\nu t}} + m\sqrt{t}\right)\right], \qquad ...(17)$$

where, erfc $x = 1 - \frac{2}{\sqrt{\pi}} \int_0^x e^{-n^2} dn$

Equation (17) represents the distribution of the transverse component of the velocity of flow due to a uniformly rotating infinite disk in the presence of external magnetic field. As m tends to zero the corresponding solution in classical hydrodynamics is obtained.

$$v = r\omega (\text{erfc} \ (z/2\sqrt{\nu t}) \quad \ldots \quad (18)$$

For the second approximation the following results are obtained;

$$F_1 = \int_0^t d\tau \int_0^\infty F_0^2 \, G d\zeta , \quad W_1 = \int_0^t d\tau \int_0^\infty F_0^2 \frac{\partial G}{\partial z} d\zeta ,$$

and the following expressions are deduced;

$$f_1 = \int_0^t d\tau \int_0^\infty F_0^2 \, G \, d\zeta , \quad \psi_1 = - \int_0^t d\tau \int_0^\infty F_0^2 \, d\zeta \int_0^z G \, dz.$$

All the results obtained in this work for the case of infinite disk, can be applied as well to the case of circular rotating disk of finite radius R, provided that the radius is large compared to δ the thickness of the viscous boundary layer i.e. $R \gg \delta$.

Equation (16) which represents the solution for the velocity corresponding to the first approximation, allows to calculate the moment of the force of friction allover a

rotating disc of finite radius R. The moment of the force of friction is defined and calculated as follows;

$$M = -2\pi\rho \int_0^R r^2 \left.\frac{\partial v_\theta}{\partial z}\right|_{z=0} dr =$$

$$= \rho R^4 \sqrt{\pi\nu} \int_0^t \left(\frac{dw}{d\tau} + m^2 w \right) \frac{e^{-m^2(t-\tau)}}{\sqrt{t-\tau}}\, d\tau \quad \ldots (19)$$

It is evident from (16) and (19) that even in the first approximation the magnetic field has an effect on the velocity distribution and the frictional moment.

Substituting m = 0 in the obtained results, the corresponding results of classical hydrodynamics are obtained, without taking into consideration the conductivity of the fluid or the presence of external magnetic field.

REFERENCES

1. H. Schlichting; Boundary Layer Theory, 6th edition, McGraw-Hill (1968).
2. W.G. Cochran; Proc. Cambridge Phil. Soc., 30, 365 (1934).
3. I.J. Novykov, Applied Magnetohydrodynamics, Atomuzdat, Moscow (in russian) (1969).
4. C. Mannal, and N.W. Mather; Engineering Aspects of Magnetohydro-dynamics, New York (1962)

5. A.B. Vatagen, G.A. Lyobemov, and C.A. Regurer;
Magnetohydrodynamic Channel flow, Moscow(1970).

6. A.A. Megahed, Ph.D. Thesis, Tbillisi University, 1973.

7. E. Butkov; Mathematical Physics,
Addison-Wesley Pub. Com., London, 1973.

دراسة حركة مائع موصل ناشئة عن دوران قرص لا نهائي

عادل عبد الرحمن مجاهد

قسم الرياضيات والفيزيقا الهندسية ـ كلية الهندسة ـ جامعة القاهرة

يتناول البحث دراسة حركة مائع لزج وموصل ضعيف للكهربية الناشئة عن دوران قرص رقيق ذي قطر لا نهائي بينما يتعرض المائع لمجال مغناطيسي خارجي عمودي على مستوى القرص . تم الحصول على الحل العام لمركبات سرعة المائع عندما يتحرك القرص بسرعة دورانية تتغير كدالة معطاه للزمن . كما تم استنتاج بعض الحالات الخاصة للحل .

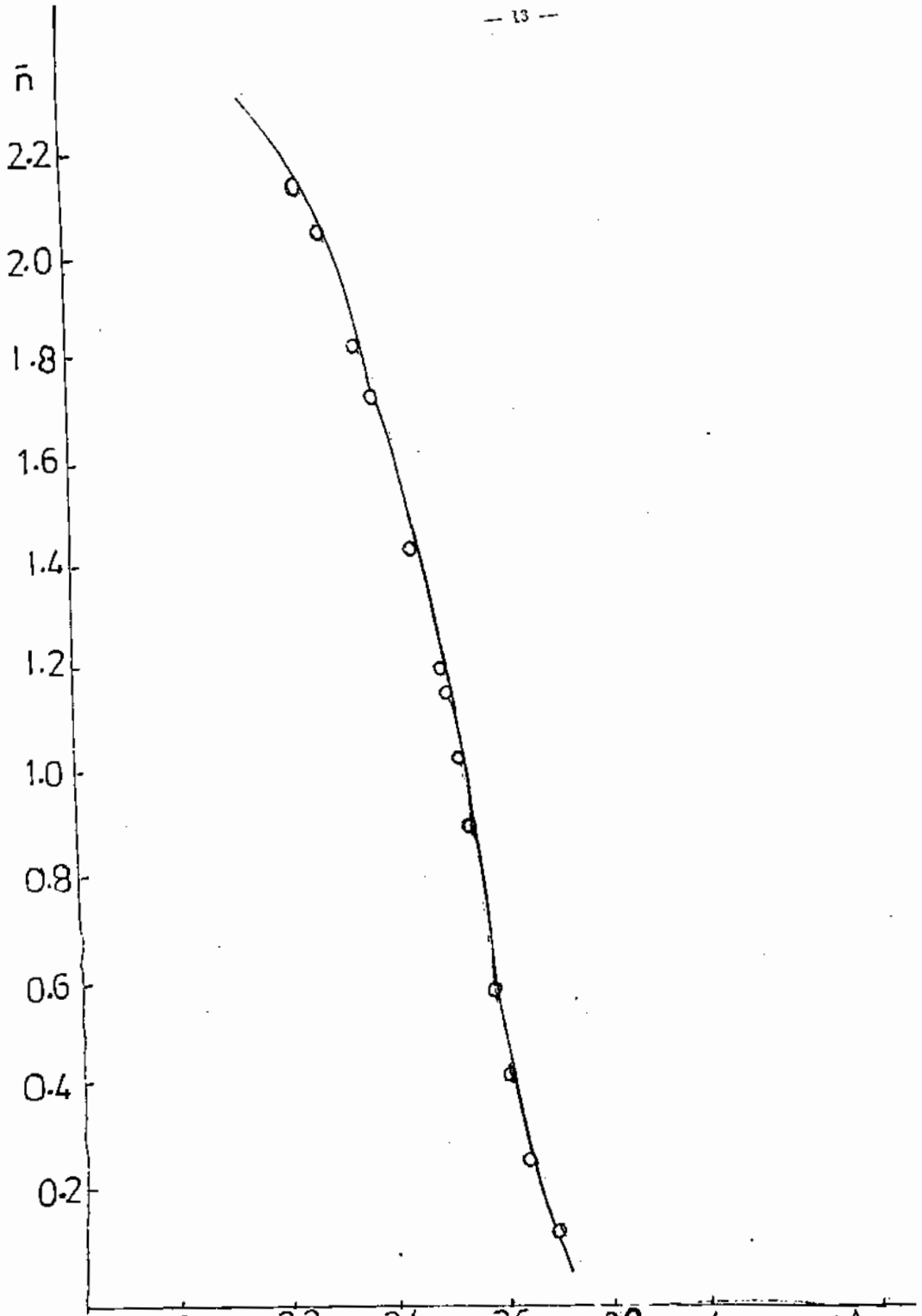

Fig 1

CARTWRIGHT'S THEOREM FOR VECTOR VALUED ENTIRE FUNCTIONS OF n-COMPLEX VARIABLES

M.A. KANDIL

Department of Mathematics, Assiut University, Egypt

Received 30.6.1978

In this paper we deduce an interpolation formula for vector valued entire functions of n-complex variables of exponential types. This formula is used to derive a sufficient condition for these functions to have compact trajectories. The result leads to a generalization of Cartwright's theorem[3] for this class of functions.

§1. Introduction:

The vector valued functions are defined on the field of complex variables $C_z^n - z = (z_1, z_2, \ldots, z_n)$, $z_k = x_k + iy_k$, $k = 1,2,3,\ldots,n$ - to Banach space X. Let $E_{\mu_1,\mu_2,\ldots,\mu_n}^{(X)}$ be the space of such vector valued functions satisfying the following two conditions :

(1) They are entire functions of exponential types $\mu_1, \mu_2, \mu_3, \ldots, \mu_n$ relative to $z_1, z_2, \ldots, z_n$ respectively, where $\mu_k < \pi, k = 1,2, \ldots, n$.

(2) They are bounded functions on the n-dimensional Euclidean Space R^n. So if $F(z_1,z_2,\ldots,z_n) \in E_{\mu_1,\mu_2,\ldots,\mu_n}^{(X)}$

then

(i) $F(z_1,z_2,\ldots,z_n) = \sum_{i_1=0}^{\infty} \sum_{i_1=0}^{\infty} \cdots \sum_{i_n=0}^{\infty} a_{i_1,i_2,\ldots,i_n} z_1^{i_1} z_2^{i_2} \ldots z_n^{i_n}$

(ii) $\| F(z_1,z_2, \ldots ,z_n) \|_X < A \exp \sum_{k=1}^{n} (\mu_k + \varepsilon) |z_k|$

where ε is an arbitrary positive number , A is a constant, $\mu_k < \pi$ for all $k = 1,2,\ldots,n$.

(iii) Sup $||F(x_1,x_2,\ldots,x_n)||_X < \infty$

§2. Generalization of Cartwright's Theorem.

Theorem (1). If $F(z_1,z_2,\ldots,z_n) \; E_{\mu_1,\mu_2,\ldots,\mu_n}(X)$, then

$$F(z_1,z_2,\ldots,z_n) = \sum_{m_1=-\infty}^{+\infty} \sum_{m_2=-\infty}^{+\infty} \cdots \sum_{m_n=-\infty}^{+\infty} L_{m_1,m_2,\ldots,m_n}(z_1,z_2,\ldots,z_n)\, F(m_1,m_2,\ldots,m_n)$$

where

$$L_{m_1,m_2,\ldots,m_n}(z_1,z_2,\ldots,z_n) = (-1)^{m_1+m_2+\ldots+m_n} \prod_{i=1}^{n} \frac{\sin \pi z_i}{\pi} \frac{\sin \omega(m_i-z_i)}{(m_i-z_i)^2}$$

$$\omega < \pi - \max_k \mu_k \;, \quad k = 1,2,\ldots,n$$

Proof. This is just a generalization of the one variable expansion [4] .

Theorem (2) . Let $F(z_1,z_2,\ldots,z_n)$ be a vector valued function defined on the n-dimensional Euclidean space R^n to Banach space X with expansion,

$$F(x_1,x_2,\ldots,x_n) = \sum_{m_1=-\infty}^{+\infty} \sum_{m_2=-\infty}^{+\infty} \cdots \sum_{m_n=-\infty}^{+\infty} L_{m_1,m_2,\ldots,m_n}(x_1,x_2,\ldots,x_n)\, F(\alpha_{m_1},\alpha_{m_2},\ldots,\alpha_{m_n})$$

such that :

(i) The set of the numerical function $L_{m_1,m_2,\ldots,m_n}(x_1,x_2,\ldots,x_n)$ satisfies the condition

$$\sum_{m_1=-\infty}^{+\infty} \sum_{m_2=-\infty}^{+\infty} \cdots \sum_{m_n=-\infty}^{+\infty} \left| L_{m_1,m_2,\ldots,m_n}(x_1,x_2,\ldots,x_n) \right| < M$$

(M is a constant)

and ,

(ii) If the set of points

$$\Lambda = (\alpha_{m_1}, \alpha_{m_2}, \ldots, \alpha_{m_n}) \subset R^n$$

is defined for all conbinations $(m_1, m_2, \ldots, m_n)$ of positive and negative integers, and if the set $F(\alpha_{m_1}, \alpha_{m_2}, \ldots, \alpha_{m_n})$ of values of the function $F(x_1, x_2, \ldots, x_n)$ at the set is compact, then the function $F(x_1, x_2, \ldots, x_n)$ is of compact trajectory.

Proof. For any arbitrary positive number ε, there exists a finite set of points in R^n,

$$\Gamma = \left[(\gamma_1^r, \gamma_2^r, \ldots, \gamma_n^r) \right] \quad r = 1, 2, \ldots, s;$$

The set Γ generates a finite number of divisions of the set of points ξ

$$\xi = \sum_{r=1}^{s} \beta_r$$

such that for any point $(\alpha_1, \alpha_2, \ldots, \alpha_n) \in \beta_r$ we get,

$$\left| F(\alpha_1, \alpha_2, \ldots, \alpha_n) - P(\gamma_1^r, \gamma_2^r, \ldots, \gamma_n^r) \right|_x < \varepsilon.$$

Consider the following equality :

$$F(x_1, x_2, \ldots, x_n) = \sum_{r=1}^{s} \sum_{\beta_r} \sum_{m_1, m_2, \ldots, m_n} L(x_1, x_2, \ldots, x_n) \left\{ P(\alpha_{m_1}, \ldots \alpha_{m_n}) - F(\gamma_1^r, \ldots, \gamma_n^r) \right\} +$$

$$+ \sum_{r=1}^{s} \sum_{\beta_r} \sum_{m_1, m_2, \ldots, m_n} L(x_1, x_2, \ldots, x_n) F(\gamma_1^r, \ldots, \gamma_n^r) \quad \ldots\ldots\ldots\ldots\ldots\ldots\ldots\ldots (1)$$

For the last term in (1) we get

$$\sum_{r=1}^{s} \sum_{\beta_r} \sum_{m_1, m_2, \ldots, m_n} L(x_1, x_2, \ldots, x_n) F(\gamma_1^r, \gamma_2^r, \ldots, \gamma_n^r) =$$

$$= \sum_{r=1}^{s} F(\gamma_1^r, \gamma_2^r, \ldots, \gamma_n^r) \sum_{\beta_r} \sum_{m_1, m_2, \ldots, m_n} L(x_1, x_2, \ldots, x_n)$$

Let

$$\sum_{\beta_r\, m_1,m_2,\ldots,m_n} L(x_1,x_2,\ldots,x_n) = G_r(x_1,x_2,\ldots,x_n)$$

From condition (1) of the theorem we get that the numerical function $G_r(x_1,x_2,\ldots,x_n)$ is bounded, and so it has a compact trajectory.

Let

$$F_s(x_1,x_2,\ldots,x_n) = \sum_{r=1}^{s} G_r(x_1,x_2,\ldots,x_n)\, F(\gamma_1^r,\gamma_2^r,\ldots,\gamma_n^r) \qquad (2)$$

It is clear that $F_s(x_1,x_2,\ldots,x_n)$ is a polynomial in the bounded numerical functions $G_r(x_1,x_2,\ldots,x_n)$, $r = 1,2,\ldots, s$, and so the vector valued function $F_s(x_1,x_2,\ldots,x_n)$ is of compact trajectory .

From (1) and (2) we have

$$F(x_1,x_2,\ldots,x_n) - F_s(x_1,x_2,\ldots,x_n) =$$

$$= \sum_{r=1}^{s} \sum_{\beta_r\, m_1,m_2,\ldots,m_n} L(x_1,x_2,\ldots,x_n)\left\{F(\alpha_{m_1},\ldots,\alpha_{m_n}) - F(\gamma_1^r,\ldots,\gamma_n^r)\right\}$$

$$\therefore \; \|F(x_1,x_2,\ldots,x_n) - F_s(x_1,x_2,\ldots,x_n)\| < \varepsilon M.$$

Thus the trajectory of the vector valued function $F_s(x_1,x_2,\ldots,x_n)$ is εM net for the trajectory of the function $F(x_1,x_2,\ldots,x_n)$, and so the trajectory of the vector valued function $F(x_1,x_2,\ldots,x_n)$ is compact, Q.E.D.

Theorem (3). If $F(z_1,z_2,\ldots,z_n) \in E_{\mu_1,\mu_2,\ldots,\mu_n}(X)$, and if the set $\left[F(m_1,m_2,\ldots,m_n)\right]$ of values of the function $F(x_1,x_2,\ldots,x_n)$ at the lattice point * is compact, then the function $F(x_1,x_2,\ldots,x_n)$ is of a compact trajectory.

Proof. From theorem (1), we have the expansion

---

* All combinations $(m_1,\ldots,m_n)$ of positive and negative integers

$$F(x_1,x_2,\dots,x_n) = \sum_{m_1=-\infty}^{+\infty} \sum_{m_2=-\infty}^{+\infty} \cdots \sum_{m_n=-\infty}^{+\infty} L(x_1,x_2,\dots,x_n)\, F(m_1,m_2,\dots,m_n)$$

where

$$L_{m_1,m_2,\dots,m_n}(x_1,x_2,\dots,x_n) = (-1)^{m_1+m_2+\dots+m_n} \prod_{i=1}^{n} \frac{\sin \pi z_i \, \sin\omega(m_i-z_i)}{\pi^n \omega^n (m_i-z_i)^2}$$

So we have

$$\sum_{m_1=-\infty}^{+\infty} \sum_{m_2=-\infty}^{+\infty} \cdots \sum_{m_n=-\infty}^{+\infty} L_{m_1,m_2,\dots,m_n}(x_1,x_2,\dots,x_n) =$$

$$= \sum_{m_1=-\infty}^{+\infty} \sum_{m_2=-\infty}^{+\infty} \cdots \sum_{m_n=-\infty}^{+\infty} \prod_{i=1}^{n} \left| \frac{\sin z_i \, \sin \omega(m_i-z_i)}{\pi^n \omega^n (m_i-z_i)^2} \right|$$

$$= \sum_{m_1=-\infty}^{+\infty} \left| \frac{\sin \pi z_i \, \sin \omega(m_1-z_1)}{\pi\omega (m_1-z_1)} \right| \dots \sum_{m_n=-\infty}^{+\infty} \left| \frac{\sin z_n \, \sin \omega (m_n-z_n)}{\pi \omega(m_n-z_n)} \right| \leq \left(\frac{\pi}{\omega}\right)^n$$

From theorem (2) we get the required result .

From the above we can generalize the Cartwright's theorem to be :

If $F(z_1,z_2,\dots,z_n)$ is a vector valued entire function of n-variables $z_1,z_2,\dots,z_n$ of exponential types $\mu_1,\mu_2,\dots,\mu_n$ repectively , $\mu_i < k$,$i = 1,2,\dots,n$, and if the set of its values at the lattice points is compact, then the function $F(x_1,x_2,\dots,x_n)$ is of compact trajectory.

References

1- E. Hille and R.S. Phillips, Functional analysis and semigroups, Amer. Math. Soc. Colloq. Publ., vol. 31, rev. ed., Amer. Math. Soc., Providence, R.I., 1974.

2- A. Zygmund , Trigonometric series, Cambridge Univ. Press, New York, 1959.

3- B.Ja. Levin, Distribution of the zeros of entire functions, GITTL, Moscow, 1956; English transl., Transl. Math. Monographs, vol. 5, Amer. Math. Soc., Providence, R.I., 1964.

4- M.A. KANDIL, The Wiener-Paley theorem and other questions in the theory of abstract function Mat. Sbornik Tom 73 (115) (1967). No. 3 p 306-319 ; English transl., Math. USSR Sbornik Vol. 2 (1967). No. 3- p 271-284.

ON THE PLANE TEMPERATURE WAVES METHOD FOR THE DETERMINATION OF THERMAL PROPERTIES OF SOLIDS

BY

M.A. Kenawy*, S.R. Atala** and A.A. El-Sharkawy**

Abstract:

Theory of plane temperature waves was analysed for a flat heater generating periodic heat flux and sandwitched between two identical solid specimens, taking into consideration the role of both heater and radiation.

Theoretical expressions for the determination of different theraml parameters from data of temperature oscillations in different ways are obtained.

The experimental results for olivine confirm the proposed scheme of measuring the thermal diffusivity, conductivity and heat capacity coefficients in one experiment using a multiproperty apparatus.

Introduction:

Measurement of the theraml properties of solids may be done using a great variety of steady and nonsteady state method. The best of these are the so-called periodic temperature methods, since they enable us to measure the heat capacity, thermal diffusivity and conductivity coefficients in one experiment[1,2]. When such an experiment is properly designed, it is possible to have extra information about the distribution of the amplitude and phases of the temperature oscillations in the investigated sample. So an extra control for the results treated in various ways is provided. Moreover, the random errors at suchan experiment are reduced.

* Univ. College for Girls, Ain Shams University, Cairo, Egypt.

** Fac. of Science, Al-Azhar Univ., Cairo, Egypt.

In this work we deduced the essential formulae for the determination of thermal diffusivity, conductivity, capacity coefficients in different ways by processing the experimental diagrams of temperature oscillations corresponding to emf variations of two thermocouples. One of them is sandwitched with the heater generating periodic heat flux between two identical specimens, while the other is fixed on the outer surface of the specimen this set-up is explained elsewhere[3,4].

Theoretical approach:

The plane temperature waves is an infinite slab are described by the following differential equation[5,6].

$$\partial^2\theta/\partial x^2 - (i\omega/a)\,\theta = 0 \qquad (1)$$

where θ represents the temperature oscillations.

ω the angular frequency and

a the thermal diffusivity coefficient

solution of this equation:

$$\theta = A \exp\left(\frac{i\omega}{a}\right)^{1/2} x + B \exp\left(-\frac{i\omega}{a}\right)^{1/2} x \qquad (2)$$

The boundary conditions to find A and B for the case under discussion (Fig. 1), considering radiation from the unheated surface (x = 0), are of the following from:

$$-\lambda\,\partial\theta/\partial x\Big|_{x=-L} = \tilde{q} \quad \text{and} \quad -\lambda\,\partial\theta/\partial x\Big|_{x=0} = \alpha\theta \qquad (3)$$

Where λ is the thermal conductivity coefficient, $\tilde{q}$ - heat flux,

α - heat transfer coefficient.

From the above an expression for the temperature oscillations at both heated (θ_h) and unheated surfaces (θ_{uh}) is obtained:

$$\theta_h = \tilde{q}/\lambda \left(\frac{i\omega}{a}\right)^{1/2} \cdot \left[\exp(-\mathcal{X}\sqrt{i}) + \exp(\mathcal{X}\sqrt{i})\right] + \frac{Bi}{\mathcal{X}\sqrt{i}}\left[\exp(\mathcal{X}\sqrt{i}) - \exp(\mathcal{X}\sqrt{i})\right] \quad (4)$$

$$/\left[\exp(\mathcal{X}\sqrt{i} - \exp(-\mathcal{X}\sqrt{i})\right] - \frac{Bi}{\mathcal{X}\sqrt{i}}\left[\exp(-\mathcal{X}\sqrt{i}) + \exp(\mathcal{X}\sqrt{i})\right]$$

$$\theta_{uh} = 2\,\tilde{q}/\lambda \left(\frac{i\omega}{a}\right)^{1/2} / \left[\exp(\mathcal{X}\sqrt{i}) - \exp(-\mathcal{X}\sqrt{i})\right] - \frac{Bi}{\mathcal{X}\sqrt{i}}\left[\exp(-\mathcal{X}\sqrt{i}) + \exp(\mathcal{X}\sqrt{i})\right] \quad (5)$$

The reduced amplitude and the phase of temperature oscillations at both heated and unheated surfaces could be expressed.

$$F_h = |\theta_h/\theta_o| = \left[\left((S_1 + S_2) + \frac{Bi\sqrt{2}}{\mathcal{X}}\left(S_4^2 + S_6^2 + S_1 S_2\right)\right)^2 + \left((S_2 - S_1) - \frac{Bi\sqrt{2}}{\mathcal{X}}\left(S_5^2 + S_3^2\right)\right)^2\right]^{1/2} /$$

$$S_3^2 + S_2^2 + \frac{Bi\sqrt{2}}{\mathcal{X}}(S_1 - S_2)$$

$$\Phi_h = \arctan\left[(S_2 - S_1) - \frac{Bi\sqrt{2}}{\mathcal{X}}\left(S_5^2 - S_3^2\right)\right] / (S_1 + S_2) + \frac{Bi\sqrt{2}}{\mathcal{X}}\left(S_4^2 + S_6^2 + S_1 S_2\right) \quad (6)$$

$$F_{uh} = |\theta_{uh}/\theta_o| = \mathcal{X} / \left[(S_3^2 + S_5^2) + \frac{Bi}{\mathcal{X}\sqrt{2}}(S_2 - S_1)\right]^{1/2}$$

$$\Phi_{uh} = \arctan\left[(S_3 + S_5) - \frac{Bi\sqrt{2}}{\mathcal{X}} S_4\right] / (S_5 - S_3) + \frac{Bi\sqrt{2}}{\mathcal{X}} S_6 \quad (7)$$

where $\mathcal{X} = \left(\frac{\omega}{a}\right)^{1/2} L$, $Bi = \alpha L/\lambda$ = Biot number (8)

$\theta_o = \tilde{q}/H w c_p$, $\chi = 4\sigma\epsilon T^3$

σ - Stefan - Boltzman constant, ϵ - emissivity (9)

$S_1 = \mathrm{Ch}\,\mathcal{X}/\sqrt{2}\ \mathrm{Sh}\,\mathcal{X}/\sqrt{2}$, $S_2 = \sin \mathcal{X}/\sqrt{2} \cos \mathcal{X}/\sqrt{2}$

$S_3 = \mathrm{Ch}\,\mathcal{X}/\sqrt{2} \sin \mathcal{X}/\sqrt{2}$, $S_4 = \mathrm{Sh}\,\mathcal{X}/\sqrt{2} \sin \mathcal{X}/\sqrt{2}$

$S_5 = \mathrm{Sh}\,\mathcal{X}/\sqrt{2} \cos \mathcal{X}/\sqrt{2}$, $S_6 = \mathrm{Ch}\,\mathcal{X}/\sqrt{2} \cos \mathcal{X}/\sqrt{2}$

The dependence of $\left|\theta_h/\theta_o\right|$, $\left|\frac{\theta_{uh}}{\theta_o}\right|$, Φ_h & Φ_{uh} on $\mathcal{X}$ and $Bi^{(5)}$ is plotted in Figures 2,3,4 and 5.

The ratio of the complex temperature oscillations at both heated and unheated surfaces could be expressed as:

$$\psi_1 = \theta_h / \theta_{uh} = \frac{1}{2}\left[\exp(\varkappa\sqrt{i}) + \exp(-\varkappa\sqrt{i})\right] + \frac{Bi}{\varkappa\sqrt{i}}\left[\exp(\varkappa\sqrt{i}) - \exp(-\varkappa\sqrt{i})\right] \quad (10)$$

Modulus of this expression is:

$$\theta_h/\theta_{uh} = \left[\left(s_6 + Bi/\varkappa\sqrt{2}(s_5 + s_3)\right)^2 + \left(s_4 + Bi/\varkappa\sqrt{2}(s_3 - s_6)\right)^2\right]^{1/2} \quad (11)$$

The difference of phases is:

$$\phi_h - \phi_{uh} = \Delta\phi = \arctan\left[s_4 + Bi/\varkappa\sqrt{2}(s_3 - s_5)\right] / \left[s_6 + \frac{Bi}{\varkappa\sqrt{2}}(s_5 + s_3)\right] \quad (12)$$

The dependence of θ_h/θ_{uh} and $\Delta\phi$ upon factor $\varkappa$ and Bi is shown in Figures 6 and 7.

The difference between θ_h and θ_{uh} will be:

$$(\theta_h - \theta_{uh}) = \tilde{q}/\lambda\left(\frac{\omega}{a}\right)^{1/2}\left[\varkappa\left(\exp(\varkappa\sqrt{i}) + \exp(-\varkappa\sqrt{i})\right) + \frac{Bi}{\varkappa\sqrt{i}}\left(\exp(\varkappa\sqrt{i}) - \exp(-\varkappa\sqrt{i})\right) - 2\right]$$

$$/\ 2\sqrt{i}\left(\exp(\varkappa\sqrt{i}) - \exp(-\varkappa\sqrt{i})\right) - \frac{Bi}{\varkappa\sqrt{i}}\left(\exp(-\varkappa\sqrt{i}) + \exp(\varkappa\sqrt{i})\right) \quad (13)$$

Modulus of this expression is given by

$$|\theta_h - \theta_{uh}| = |\Delta\theta| = \tilde{q}L/\lambda\varkappa\left[(s_1 - s_2 + 2(s_3 - s_5) + Bi\sqrt{2}/\varkappa(2s_6 - s_6^2 - s_4^2)\right] /$$

$$s_5^2 + s_3^2 + Bi\sqrt{2}/\varkappa(s_2 - s_1) \quad (14)$$

In Figure 8, $|\Delta\theta|$ as a functionof $\varkappa$ and Bi is shown.

Using the previous formulae and graphs, it is possible to determine factor $\mathcal{X}$ by processing thhe experimental curves to get ϕ_h, ϕ_{uh} and $\Delta\phi$. It is also easy to determine $\mathcal{X}$ by measuring the ratio θ_h / θ_{uh}.

Factor Bi is found from the measurement of ϕ_h or ϕ_{uh} at two frequencies ω and 2ω (6).

Thermal diffusivity coefficient is then obtained from

$$a = \frac{\omega}{\mathcal{X}^2} L^2 \tag{15}$$

It could be also obtained using the following relation (quasi-steady state method).

$$a = \frac{\pi^2 L^2 \theta_0}{\tau \Delta T} \tag{16}$$

where

τ = period, ΔT = steady-state temperature difference across the specimen, or by measuring time lag between the power and the temperature oscillations at unheated surface

So, $$a = \frac{L^2}{6 \Delta t}$$

where Δt = time lag.

The heat capacity can be determined using either.

$$C_p = \frac{\tilde{q}}{M \omega \theta_h} F_h \tag{17}$$

or

$$C_p = \frac{\tilde{q}}{M \omega \theta_{uh}} F_{uh} \tag{18}$$

M-mass of the specimen.

The thermal conductivity coefficient is determined from the steady-state temperature gradient across the specimen according to

$$\lambda = \frac{\tilde{q} L}{f \Delta T} \tag{19}$$

where f = area of the specimen.

It can also be determined using the relation:

$$\lambda = \frac{\tilde{q} L}{f |\Delta\theta|} F \tag{20}$$

Finally λ can be determined from

$$\lambda = \rho C a \tag{21}$$

Thus using the information about the temperature oscillations obtained from the two thermocopuples, the thermal properties may be determined according to the previous scheme.

It is worthy to mention, that in case of rectangular modulation of the heat flux (switching on and off of the heating current), it is possible to use a much simpler way for processing the experimental curves, to deduce the thermal properties.

This adds extra informations necessary for internal control of the obtained results.

Role of heater:

For the given arrangement in Figure (1) we should take into consideration the distribution of amplitudes and phases of temperature oscillations due to the presence of the heater.

It is worthy to mention that the presence of the heater does not affect the amplitude ratio method.

The influence of the heater upon the amplitude difference is expressed as; $\frac{\delta(\Delta\theta)}{(\Delta\theta)} = \frac{M_1 C_1}{MC} \cdot (S_1^2 + S_2^2)^{1/2} / (S_5^2 + S_3^2)$

When $\frac{M_1 C_1}{MC}$ is small (less than 1%) this correction may be neglected, otherwise it must be taken into consideration.

All the illustrated functions have been computed using computer ICL-600.

Experimental:

This theory was used for processing the experimental curves obtained during the course of calibration of the mentioned apparatus, while varyin widely the experimental condtions.

In Table I the obtained results of measuring the thermal diffusivity for olivine using phase method, time lag method, amplitude ratio method and quasi-steady state method are given.

From the table, one can see that the obtained experimental values differ by about 2% randomly each other.

The experimental error in the phase method and amplitude-ratio method was 4-7%, in time lag method (for rectangular heat flux modulation) the error was 3.5% and in the quasi-steady state it was 6-8%.

Table (I): The thermal diffusivity coefficient of olivine (a x 10^{-3} $\frac{cm^2}{sec}$)

Temp. °K	Biot number	Phase method at heat, surface		Phase method at unheated surface		Phase difference method		Time lag method		Amplitude method		Quasi steady state method	
		2ω	ω	2ω	ω	2ω	ω	2ω	ω	2ω	ω	2ω	ω
		τ=30.5 sec	τ=61.5 sec	τ=30.5 sec	τ=61.5 sec	τ=30.5 sec	τ=61.5 sec	τ=30.5 sec'	τ=61.5 sec	τ=30.5 sec	τ=61.5 sec	τ=30.5 sec	τ=61.5 sec
435	0.10	8.9	8.2	8.2	8.1	8.1	8.1	8.3	8.2	8.2	8.4	8.1	8.1
545	0.15	6.6	6.6	7.1	7.1	7.0	6.6	6.8	7.2	7.4	7.0	6.9	6.7

The heat capacities of olivine calculated by different methods is tabulated in Table II.

Table (II): Heat capacity of olivine

Temp.	Biot number	Heat capacity at heared surface Cal/gm. °K		Heat capacity at unheated surface	
		τ =30.5sec	τ =61.5sec	τ =30.5 sec	τ =61.6 sec
435	0.10	0.176	0.179	0.177	0.178
545	0.15	0.214	0.213	0.213	0.215

The obtained experimental results differe by 2-2.5% for the heat capacity of olivine. This seems to be quite satisfactory agreement with the experimental results.The experimental error of measuring heat capacity was, 5%.

The thermal conductivity of olivine calculated by different methods is tabulated in Table III.

Table (III): The thermal conductivity coefficient of olivine

Temp	Biot number	Using equation (λ= Ca) Cal/cm sec. °K				Difference method
		heat. surface		unheat. surface		
		τ =30.5	τ =61.5	τ =30.5	τ =61.5	
435	0.10	0.0041	0.0040	0.0042	0.0043	0.0039
545	0.15	0.039	0.0039	0.0040	0.0040	0.0034

The agreement among the obtained values from different methods lies within 2-4%, which is less than the general experimental error of 2-5% for the mentioned methods except for formula (21) which gives 3-7%.

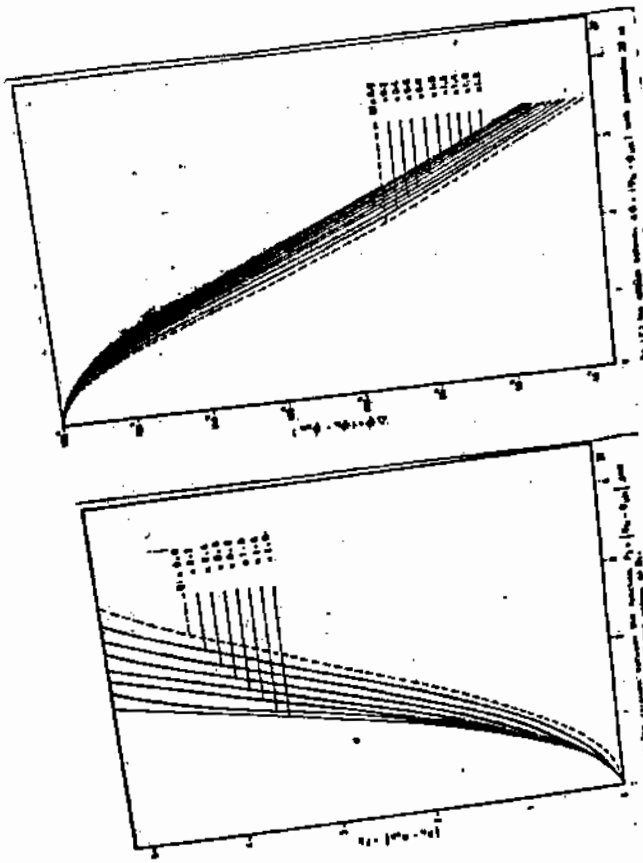

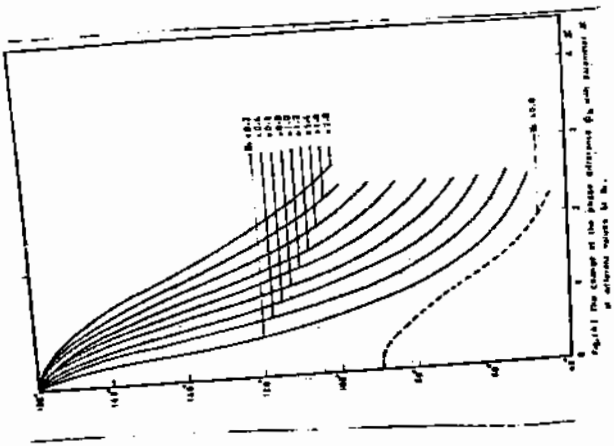

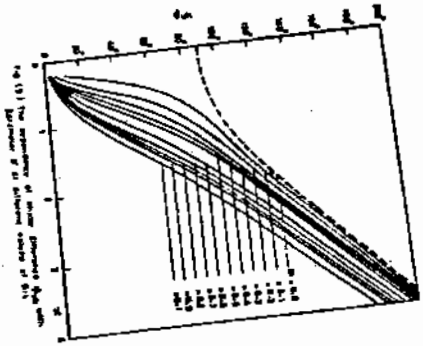

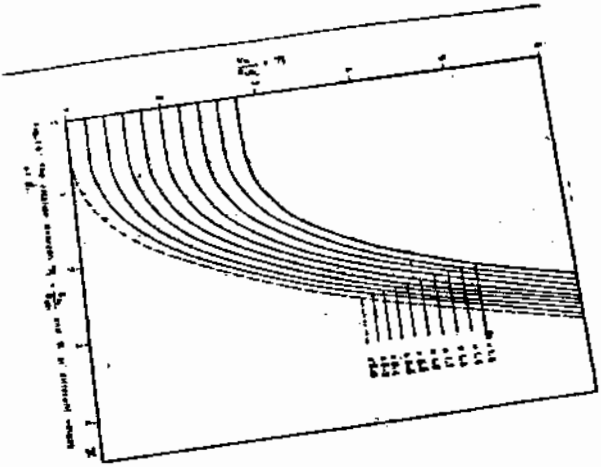

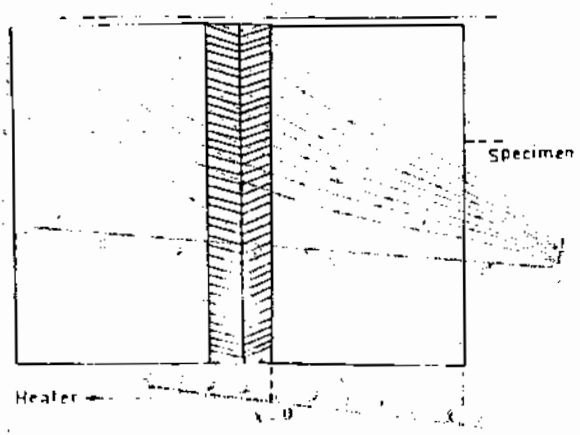

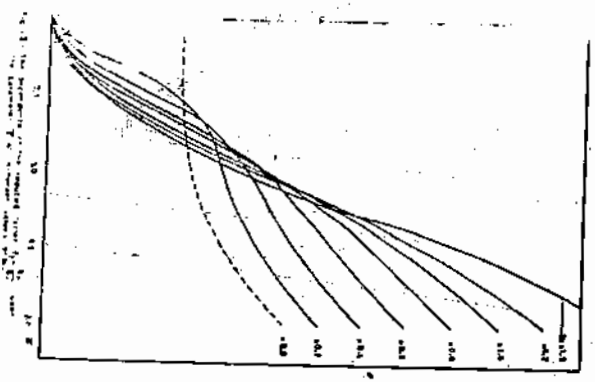

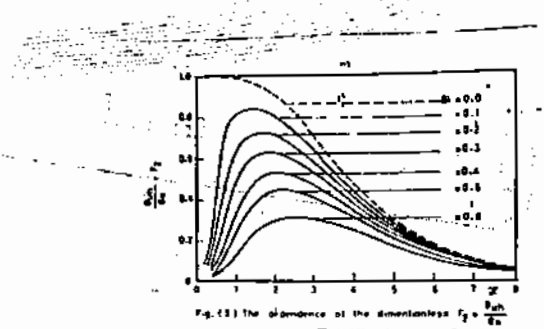

Fig. (3) The dependence of the dimensionless $f_2 = \frac{\partial \theta}{\partial \eta}$ on parameter $\bar{x}$ at different values of B_r.

CHARACTERISTICS OF SINGLE WIRE ANODE STREAMER COUNTER

HOSNIA M. ABU-ZEID and H.M.ABU-DORRA

Faculty of Women, Ain Shams University.

ABSTRACT

Performance of the wire-plane streamer counter in air at normal temperature and pressure have been studied and discussed. Investigations are made on the counting characteristics and corona current in relation to their dependence on various electrode separation and on the anode wire material and diameter.

It is found that the effieiency of detecting the streamer pulses increases with the increase of the anode diameter as well as the decrease of the electrode spacing. The material of the anode has negligible effect on both the counting and corona characteristics.

INTRODUCTION

Tavendale[1] showed that the conventional corona counter in air at atmospheric pressure can be operated in two modes depending on wire diameter and electrode spacing, i.e. a spark or corona-streamer discharge can be

produced. At low gaps spark action occurs while at larger spacing breakdown terminals at the streamer stage of spark development.

Harrison[2] gave the conditions which are suitable for good working plateau in a corona streamer counter.

Recently more work has been done on a new type of corona counter namely"Gridded streamer Corona Counter"[3] as well as on "Wire-plane Streamer Counter"[4] intending to furnish data on the operating characteristic and for better understanding of the related mechanism. Also multi-wire anode streamer counters were constructed and their operating characteristics were studied [3,4].

The present work was undertaken to investigate more critically the operation of the streamer counter with different anode diameter and variable electrode spacing.

EXPERIMENT

The form of the single-wire anode streamer counter and the block diagram of electronic circuit is shown in fig. 1. The pulses from the cathode follower are amplified by an amplifier and fed after a pulse shaper into the input of a fast scaler. High voltage poower supply[3] is used to supply the detector with stabilized high voltage from 0-to-20 KV. Three other stablilized power units are used as power supply to the cathode follower, amplifier and pulse shaper.

A ^{210}PO alpha-source which was fixed at a constand height from the anode was used for producing streamer pulses.

EXPERIMENTAL RESUITS

Figures (2 and 3) show the results of the counting characterlsties for ankon and Molybdenum wires for various values of the distance h between the wire anode and cathode from 5 to 19 mm. corresponding to different values of anode diameter from 0.15 to 0.38 mm.

It is shown from these curves that an increase in the anode-tocathode spacing is accompanied by considerable decrease in the counting rate.

It can also be observed that for small gaps the counting starts at lower voltage, and at all curves, we notice that the plateaues are perfect flat i.e.have a zero slope.

These families of curves indicate that the counting rate N increases with the decrease of electrode spacing and increase of anode diameter $\emptyset$.

Int the absence of any alpha-source hear the counter we investigated the variation of the corona current with applied voltage under various wire-to-plate spacing, as

Well as, different values of anode diameter. The results are shown in fig. (4 and 5) for ankor and Molybdenum respectively.

These families of curves indicate that I increases with the decrease of either the electrode spacing h or the anode diameter Ø.

To identify clearly the effect of the anode wire diameter on the counter characteristics the operating characteristics of the streamer detector with Ankor (Ø =0.25 and 0.35mm) and Molybdenum(Ø = 0.26 and 0.38mm) as anode wire are represented in fig. 6. With the finest wire the counting starts at lower voltage, but with the largest diameter a better effeciency is obtained.

By increasing the anode diameter the corona current decreases and it occurs at higher voltage as the field around the wire becomes smaller. Moreover companion of the results of the two different materials, shows that the material of anode wire has negligible effect on the counter characteristics.

Fig. 7 shows the family of corona curves for two different wire materials, of which the diameter is (0.27 mm for ankor and 0.26 mm for Md.), (0.32 mm for mol. and 0.33 mm for Ankon), i.e. having nearly the same diameter.

It is clearly seen that the material of the wires have nearly no effect on the threshold voltage or the slope of the corona current curves.

ACKNOWLEDGEMENT

The authors would like to express their thanks and gratitude to prof. Dr. M. Mahrous head of the Physics Department, Girls College, Ain Shams University for his interest and supplying the necessary facilities throughout this experimental work.

The authors also express their thanks to prof. Dr. H.M. Abu-Zeid, Atomic Energy Establishment for his interest and useful advices.

REFERENCES

(1) A.J. Tavenhdale, J.Sci. Instr., 39, 517 (1962).

(2) A.J. Harrison, IEEE Transaction on Nucl. Sci., 12, No. 6, 48 (1965).

(3) H.M. Abu-Zeid, Ph.D.Thesis, Ain shams Univ., Girls College (1971).

( ) E.[illegible] Zaid, Ph. D. Thesis, Ain Shams Univ., Girls College (1972).

.....

خواص المداد الفيضي الاحادي المصعد

د • حسنية محمد ابو زيد والسيدة / هدى محمد ابو غزة

ملخـــص

درست طريقة تشغيل المداد الفيضي احادي المصعد عند معدل الضخ ودرجة الحرارة وبحثت خواصه المميزة عند تغير كل من قطر سلك المصعد ومادته وكذا المسافة بين المصعد والمهبط • ووجد ان كفاءة المداد الفيضي تزداد بزيادة قطر المصعد وكذا يصغر المسافة بين القطبين • وقد يكون تأثير مادة المصعد منعدما على كل من التيار الهالي ومعدل العد •

• • • • • • • •

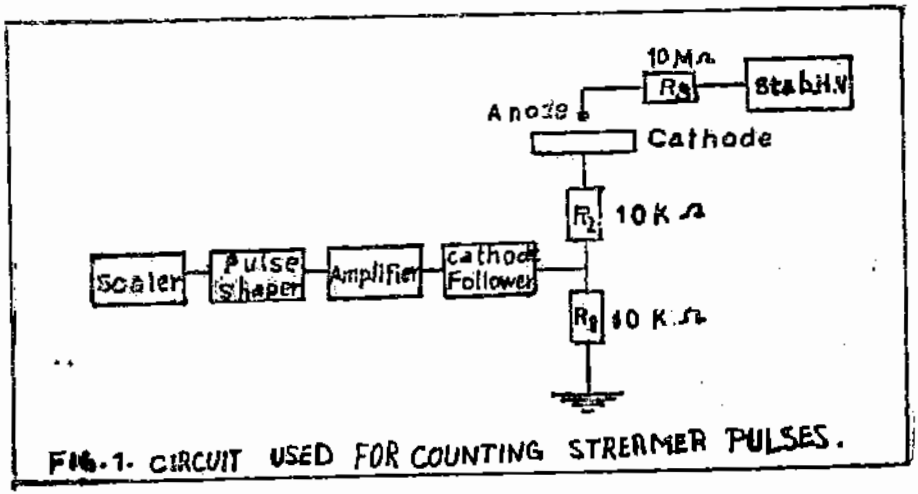

FIG. 1. CIRCUIT USED FOR COUNTING STREAMER PULSES.

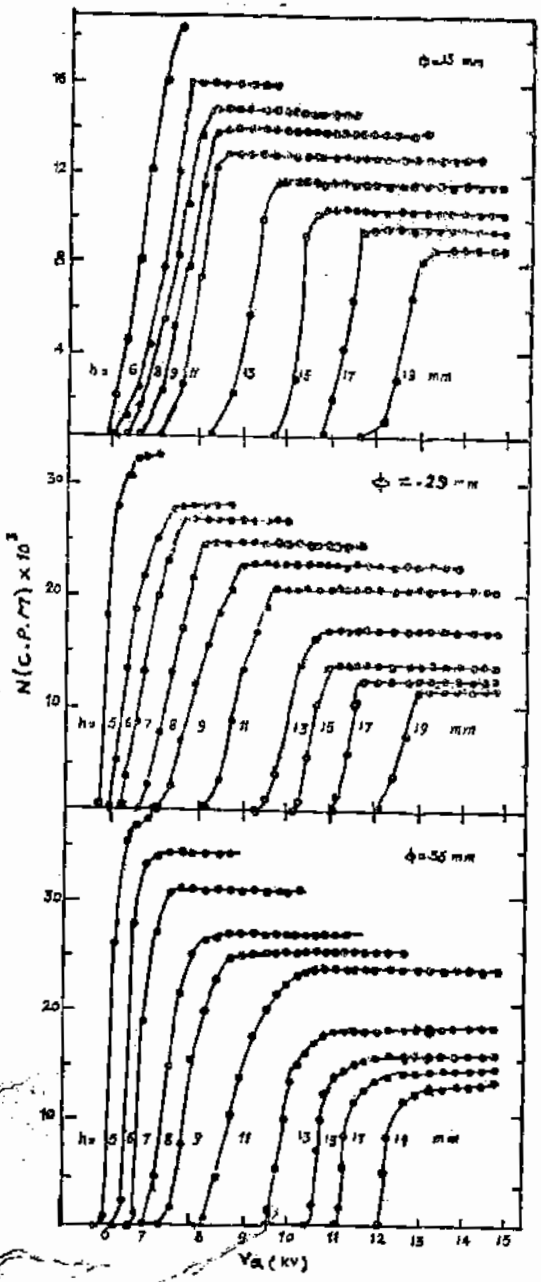

FIG. 2. THE RELATION BETWEEN THE COUNTS PER UNIT TIME AND THE APPLIED VOLTAGE, FOR DIFFERENT ELECTRODE SPACING, (ANKOR).

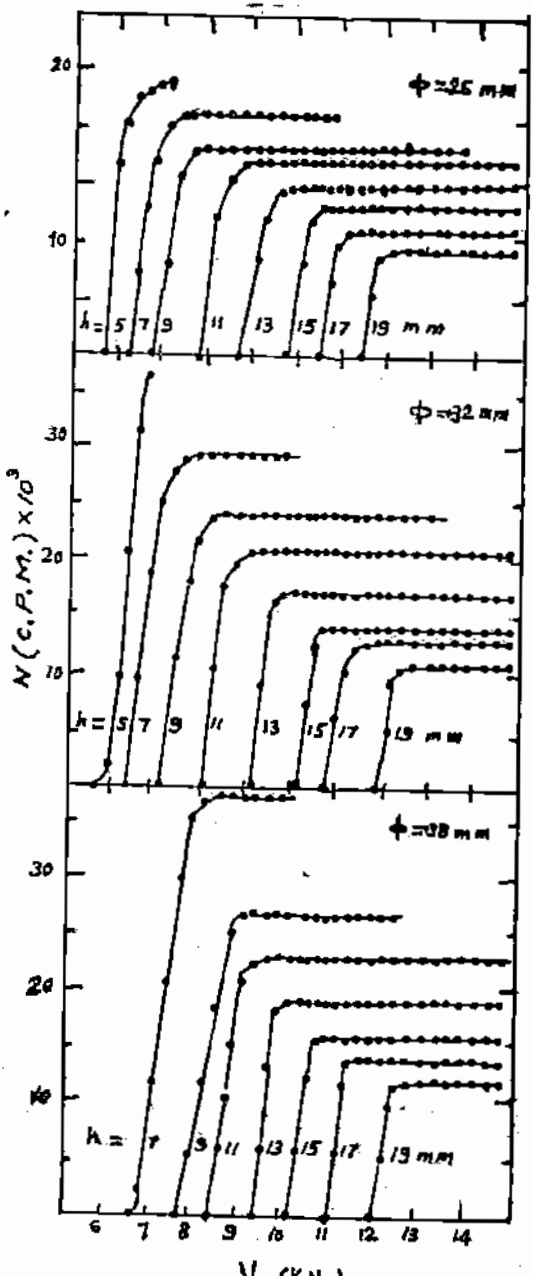

FIG. 3. THE RELATION BETWEEN THE COUNTS PER UNIT TIME AND THE APPLIED VOLTAGE, FOR DIFFERENT ELECTRODE SPACING, (MOLYBDENIUM).

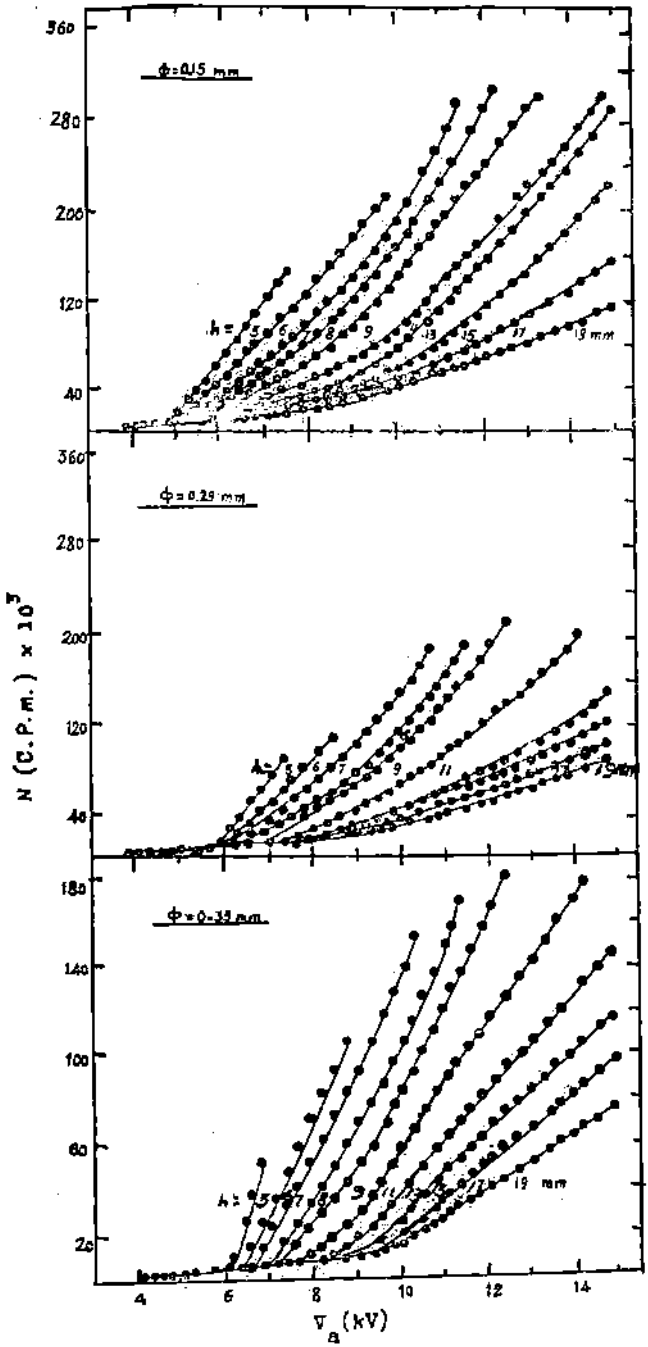

FIG. 4. THE RELATION BETWEEN THE CORONA CURRENT AND THE APPLIED VOLTAGE, FOR DIFFERENT ELECTRODE SPACING (ANKOR).

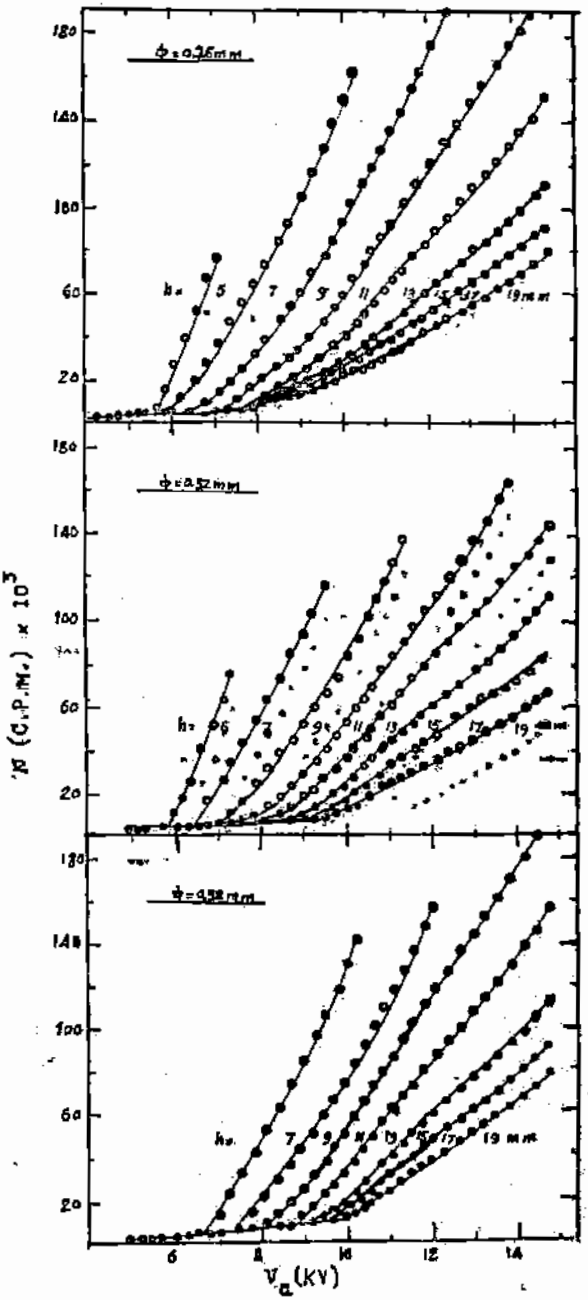

FIG. 5. THE RELATION BETWEEN THE CORONA CURRENT AND THE APPLIED VOLTAGE, FOR DIFFERENT ELECTRODE SPACING (MOLYBDENIUM).

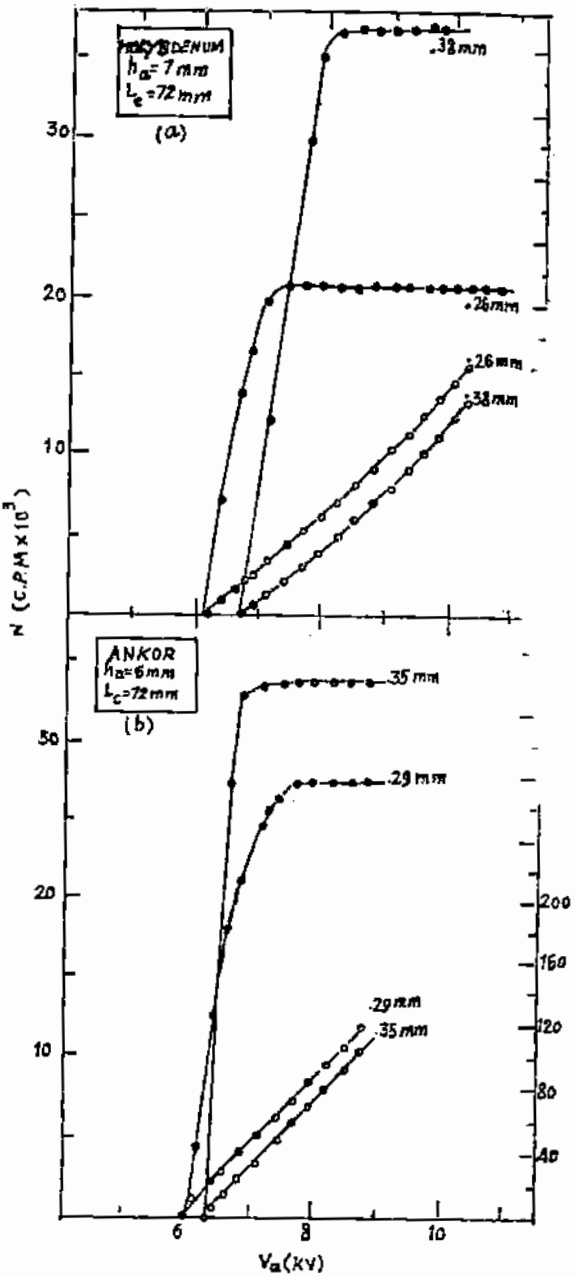

FIG. 6. COUNTING AND CORONA CHARACTERISTICS FOR DIFFERENT DIAMETER ANODE WIRE

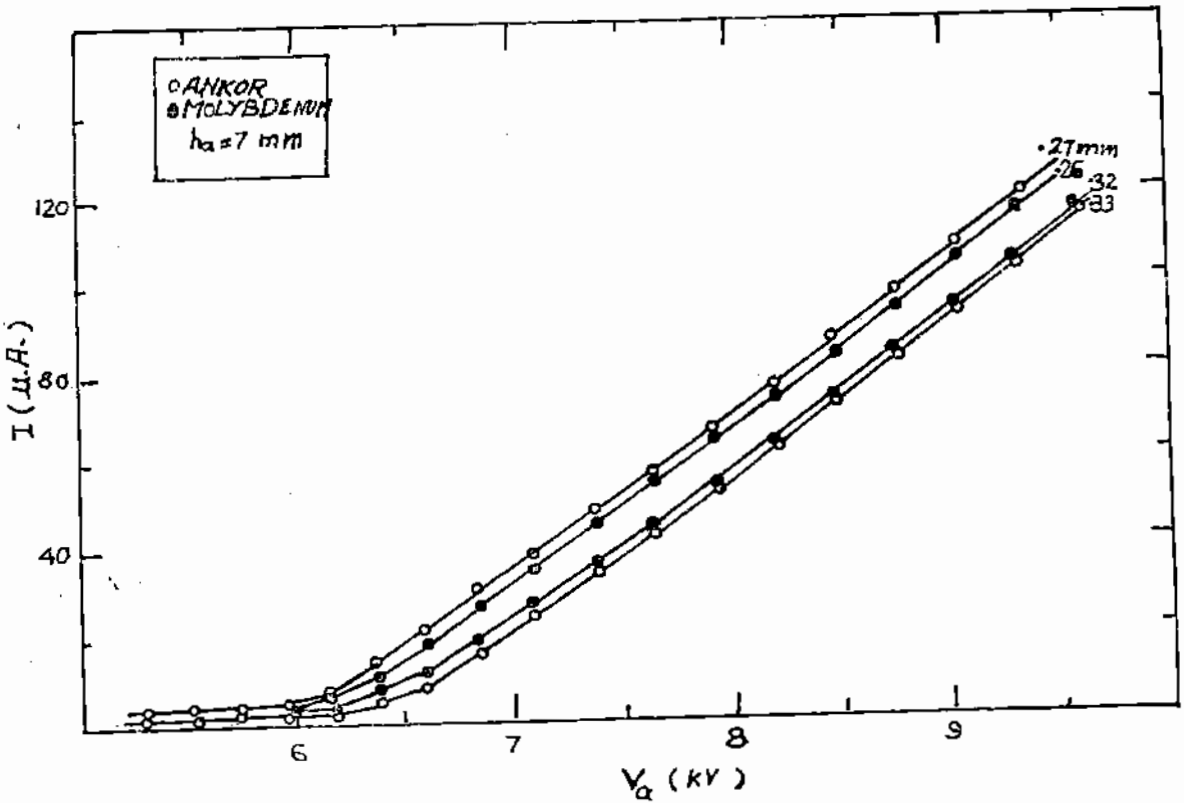

FIG. 7, APPLIED VOLTAGE AND THE CORONA CURRENT FOR TWO MATERIALS OF NEARLY THE SAME DIAMETER.

NUCLEAR LIFETIME MEASUREMENTS USING Pb-LOADED PLASTIC SCINTILLATORS

H. Abou-Leila, S. M. Darwish[1], E. A. Ismail[2], And S. El Menyawi[3]

Nuclear Physics Laboratory, University College For Girls, Ein Shams University, Egypt.

Received 11.2.1975

Abstract

The half-lives of the 81 keV, 160.6 keV , 384 keV and 437 keV levels in ^{133}Cs have been measured using the delayed coincidence techniques and Pb-loaded plastic scintillators. Analysis of the data gave the following half-life values :

$T_{\frac{1}{2}}$ (81 keV level) = 6.15 ± 0.08 ns

$T_{\frac{1}{2}}$ (160.6 keV level) ≤ 0.193 ns

$T_{\frac{1}{2}}$ (384 and/or 437 keV level) $\leq$ 0.36 ns

An explanation for the descripencies between the different results given by different authors is given. From the obtained results the experimental partial transition probabilities are calculated and compared with the single particle Weiskopf estimations.

1. Introduction

Lifetimes in the range 10^{-8} to 10^{-11} sec are usually measured by the time-to-pulse height converter techniques. The scintillation detectors have proved to be the fastest detector for such techniques.

---

1) Physics Department, Faculty of Science, Cairo University, GIZA, EGYPT.

2) Physics Department, Faculty of Education, Ein Shams University, EGYPT.

3) Physics Department, Islamic Faculty of Girls, Al-Azhar University, EGYPT.

The rapidly increasing use of fast scintillation detectors has been greatly facilitated by the development of suitable fast luminescent materials. An important group among them are plastic scintillators (organic scintillators) either pure or in various combinations of solid solutions. These scintillators have the advantage of showing short decay time τ, while have the disadvantages of showing low total detection efficiency, zero photopeak detection efficiency and/or poor energy resolution as compared with the best inorganic scintillators such as NaI(Tl) crystals.

Only few trials[1-3] have been performed by various authors to combine the best properties of both organic (plastic) and inorganic (NaI(Tl) crystal) scintillators. However, these trials did not offer any clear and easy means of measurements and thus no practical applications of such trials have been reported.

Regarding our previous studies[4] on the properties of pure Naton 136 and some Pb-loaded plastic scintillators as well as NaI(Tl) crystal, it has been proved that as far as one is interested in performing a fast timing experimental analysis of low energy gamma-ray transitions with short decay time, high efficiency, high light output as well as relatively good energy resolution, the 2 % Pb-loaded plastic scintillator is better than all other mentioned scintillators.

The decay of ^{133}Ba to ^{133}Cs has recently attracted a certain amount of interest. The decay of ^{133}Ba has been studied by many authors[5-8] and the level scheme may be considered as well established. Although that the decay scheme is relatively simple, some discrepancies remain concerning lifetime measurements of levels and, therefore absolute transition probabilities. This is mainly due to the fact that most of the levels are populated and depopulated by gamma transitions having adjacent energies and thus difficult to be seperated due to the poor energy resolution of fast scintillators. The half-lives of several levels in ^{133}Cs have been measure

by several authors[9-16]. Some of their results agree while the others disagree.

In the present work, the improved properties of the 2 % Pb-loaded plastic scintillators are used to measure the half-lives of the 81 , 160.6 , 384 and/or 437 keV levels in ^{133}Cs. The obtained experimental results are compared with the theoretical single particle estimates.

2. Experimental Arrangements

2.1. SOURCES

The ^{133}Ba sources, used in the present investigation, were obtained from the radiochemical centre in Uppsala. These were made by evaporating commercially available activity onto 800 $\mu g/cm^2$ nickel foils.

2.2. APPARATUS

The experimental set-up used in the half-life measurements consists of an ORTEC model 437A fast time-to-pulse height converter and the energy selection channels. The gamma rays were detected by two scintillation detectors. Each detector consisted of a 2 % Pb-loaded plastic scintillator (25mm dia x 10 mm hight) coupled to an XP 2020 photomultiplier tube. The system is essentially a fast-slow coincidence system based on constant fraction timing spectrometry. The data were recorded on an Intertechnique 400 channel analyser. The system was calibrated with known lengths of well calibrated cables.

The system time resolution at low energy was determined with one of the two 2 % Pb-loaded plastic scintillators selected at 356 keV with a window width of ~ 50 keV on the stop channel and the other 2 % Pb-loaded plastic scintillator selected at 30 keV K X-ray with a window width of ~ 25 keV on the start channel using a ^{22}Na source and was found to have a slope ≃ 0.36 ns and FWHM ≃ 1.10 ns .

3. Measurements and Results

Fig. 1 shows a simplified level scheme[8] of ^{133}Cs . The gamma-ray spectrum of ^{133}Cs nucleus detected by 2 % Pb-loaded plastic scintillator coupled to an XP 2020 photomultiplier tube is shown in fig. 2 .

3. 1. The 81 keV Level

According to the decay scheme of ^{133}Cs nucleus fig. 1 , the gamma-rays populating the 81 keV level are the 356 , the 302 and the 79.6 keV transitions . It can also be seen (fig. 2) that owing to the improved properties of the 2 % Pb loaded plastic scintillators , the gamma line of the 81 keV is seperated in the gamma-ray spectrum of the ^{133}Cs nucleus detected by 2 % Pb-loaded plastic scintillator detector. Thus one has to measure delayed coincidences between the high energy part (above 250 keV) of the gamma-ray spectrum of ^{133}Cs (fig. 2) including the 302 keV and the 356 keV transitions populating this level selected in the start channel and the 81 keV gamma-ray transition depopulating this level selected in the stop channel. A certain admixture of almost prompt coincidences from other levels was registered. The delayed coincidence curve obtained with this adjustment had to be compared with a prompt coincidence curve, as shown in fig. 3 . This curve was measured with the aid of ^{22}Na source with the same channel adjustments. A least squares fit of an exponential function to the experimental data was made by means of a computer programme . Taking into consideration the statistical and systematic errors due to time calibration and electronic instability of the apparatus, the half-life of the 81 keV level was determined to be ,

$$T_{\frac{1}{2}} \text{ (81 keV level)} = 6.75 \pm 0.08 \quad \text{ns}$$

3. 2. The 160.6 keV Level

It is clear from the level scheme of ^{133}Cs (fig. 1) that this level is populated by the 223 keV and the 276 keV transitions and is depopulated by the 79.6 keV and the 160.6 keV transitions. Since both the 223 and 160.6 keV transitions are weak , the most probable coincidence combination is hence between the 276 keV transition populating this level adjusted in the start channel and the 79.6 keV transition depopulating this level adjusted in the stop channel. It seems also natural to measure the lifetime of the 160.6 keV level using the centroi shift method . Therefore, one of the timing single channel analysers was set to accept the 80 keV gamma-ray energy (with window of about 60-100 keV) the other timing single channel analyser was set to accept the 276 keV high gamma-ray energies from 250 keV to 300 keV. The time spectrum obtained with this adjustment , had to be compared with a prompt time coincidence spectrum. This prompt coincidence spectrum was measured with the aid of a ^{60}Co source with the same channel adjustments. The centroi shift between the delayed time coincidence spectrum of ^{133}Cs and the prompt time coincidence spectrum of ^{60}Co should be corrected for the contributions of the other admixed coincidences.

It is clear that the time distribution curve obtained is composed mainly from four contributions :

i) γ ($\geq$ 250 keV) - γ (81 keV) coincidences belonging to a delay time equals to + τ_{81}

ii) γ (276 keV) - γ (79.6 keV) coincidences belonging to a delay time equals to + $\tau_{160.6}$.

iii) γ(276 keV) - γ (K X-ray) coincidences belonging to a delay time equals to - τ_{437} .

iv) γ (302 keV) - γ (53.4 keV)- K X-ray coincidences belonging to a delay time equals to - (τ_{384} + τ_{437}) .

The first contribution was found to be of the order of 5-7 % with a long lived decay time ($T_{\frac{1}{2}}$ of the 81 keV level $\simeq$ 6.15 ns). This was simply substracted from the time distribution curve . Each of the other contributions was calculated from the partial relative intensities of the contributing transitions listed in the nuclear table of isotopes[8].

Having applied these corrections a value for the half-life of the 160.6 keV level in ^{133}Cs was found to be ,

$$\tau_{160.6} = -2.953\ \tau_{total} + 1.238\ \tau_{437} + 0.715\ \tau_{384}$$

where τ_{total} is the observed mean lifetime. The value of τ_{total} was obtained after analyzing about 40000 coincidences in a large number of repeated short measurements and taking into consideration the statistical and instrumental errors due to time calibration and electronic instability of the apparatus, the average value for the centroid shift (mean lifetime) between the 276 keV gamma-rays and the 80 keV gamma-rays in ^{133}Cs and the prompt ^{60}Co curves was found to be ,

$$\tau_{total} = 29 \pm 11.5 \quad ps$$

If we take into consideration the values of the half-lives $T_{\frac{1}{2}}$ (384 keV level) = 40 $\pm$ 20 ps & 50 ps reported by Välivaara et al.[13] & Alkasov et al.[15] , respectively , and $T_{\frac{1}{2}}$ (437 keV level) $\leq$ 150 ps reported by Välivaara et al.[13] & Vartapetian et al.[16], our final result for the half-life time of the 160.6 keV level was found to be ,

$$T_{\frac{1}{2}} \text{ (160.6 keV level)} \leq 193 \quad ps$$

3. 3. The 384 KeV and 437 KeV Levels

As can be seen from the level scheme of ^{133}Cs presented in fig. 1 , the 384 keV level is directly populated by 22 % electron capture and depopulated by the 223 , 303 and 384 keV transitions of relative intensities 1 % , 65 % and 34 % respectively , while the 437 keV level

is directly populated by 78 % electron capture and depopulated by the 53 , 276 and the 356 keV transitions of relative intensities 0.1 % , 9 % , and 91 % , respectively . Since the 53 keV and 223 keV transitions is very weak and either the 356 keV and the 384 keV transitions and/or the 276 keV and the 303 keV transitions depopulating these two levels cannot be resolved in the gamma spectrum, therefore, the most probable way is to measure delayed coincidences between the KX-ray adjusted in one channel and the high energy (above 300 keV) gamma spectrum of ^{133}Cs (fig. 4) including the 356 keV and the 384 keV transitions adjusted in the other channel . The delayed coincidence spectrum obtained with this adjustment, had to be compared with a prompt coincidence spectrum. This spectrum was measured using ^{22}Na source with the same channel adjustments. Since the observed time spectrum for the delayed coincidences has a slope which is equal to the instrumental slope of the prompt time resolution curve, recorded with the same energy settings, an upper limit for the half-life of either the 384 keV or the 437 keV levels was obtained :

$$T_{\frac{1}{2}} \text{ (384 keV or 437 keV level)} \leq 0.36 \text{ ns}$$

4. Results and Discussion

The obtained value for the half-life of the 81 keV level ($T_{\frac{1}{2}} = 6.15 \pm 0.08$ ns) is in good agreement with all previous measurements . Concerning the half-life of the 160.6 keV level, it is clear that the value obtained by ref. 13 is nearly double the values reported by refs. 10, 12 and 14 . This disagreement could be explained by the fact that in the results given by refs. 10 and 11 , the effect of admixed coincidences were not taken into consideration . These admixed coincidences will affect the centroid of the measured time distribution curve and will decrease the value obtained for the half-life of the 160.6 keV level by a factor depending on the selected

windows for each experimental conditions . The effect of these admixed coincidences on the results reported by ref. 13 and 14 is highly attenuated since the desired transitions are selected by a double lens β-spectrometer before measuring their time distribution.

Concerning the results obtained in the present work, unfortunately, the corrected value for the half-life of the 160.6 keV level will depend on the values of the half-lives of the 384 and 437 keV levels . If we take into considerations, the values given by refs. 13 , 15 , and 16 for these two levels, only a limit for the half-life of the 160.6 keV level could be reached ($T_{\frac{1}{2}} \leq$ 0.193 ns) . This limit is in agreement with all previous values[10-14].

An important conclusion could be deduced from this result . This conclusion is that, if the value ($T_{\frac{1}{2}}$ = 0.190 $\pm$ 0.015 ns) given by ref. 13 for the half-life of the 160.6 keV level is confirmed by other measurements , our results will give a value of $T_{\frac{1}{2}}$ = 0.150 ns instead of $T_{\frac{1}{2}} \leq$ 0.150 ns for the half-life of the 437 keV level .

From the experimental point of view, direct measurements of the half-life of the 437 keV level is rather difficult. This is mainly due to the fact that this level is populated and depopulated by gamma transitions whose energies differ slightly from other gamma transitions populating and depopulating the 384 keV level . This small energy difference is much smaller than the possible energy resolution of known fast scintillation detectors. Therefore, the trial done in the present work to measure the half-life of the 437 keV level will lead only to a limit value. This limit value should be only considered as an indication for the capability of Pb-loaded plastic scintillators to measure half-lives of low energy gamma transitions. It is

worthwhile to mention that the present measurement proves the possibility of performing fast time distribution measurements for X- or γ-rays in the energy range of 30 keV using Pb-loaded plastic scintillators. This possibility could not be reached using the common pure plastic scintillators owing to the fact that only Compton interaction is possible in such type of pure plastic scintillators (E_{max} Compton for the 30 keV $\approx$ 3 keV).

The results of our experimental measurements for the half-lives have been collected in table I together with the transition energies, relative gamma-ray intensities, multipole mixing ratios, branching ratios and theoretical internal conversion coefficient[5] collected from other published data[6,19]. These data have been used to calculate the partial gamma-ray half-lives $T_{\frac{1}{2}\gamma}^{exp}$ for all transitions, according to

$$T_{\frac{1}{2}\gamma}^{exp} = \frac{T_{\frac{1}{2}} (1+\alpha)}{X}$$

where α is the total internal conversion coefficient found by interpolation from the tables of Sliv and Band[19], and X is the branching ratio extracted from experimental published data.

From the partial half-lives, the experimental partial transition probabilities were deduced and compared with the theoretical single-particle Weisskopf estimates[20]. To obtain the Weisskopf estimates a nuclear radius constant of 1.2 fm and a statistical factor S = 1 were used[20].

From the theoretical single-particle Weisskopf estimate of the partial transition probabilities $B_{\gamma}^{Weisskopf\,(M1\text{ or }E2)}$ and the experimental partial gamma-ray transition probabilities B_{γ}^{exp}, the retardation and enhancement factors can be evaluated by employing the mixing ratios δ. The retardation and enhancement factors for the M1 and E2 transitions, respectively, are given by :

$$R\,(M1) = \frac{B_{\gamma}^{Weisskopf\,(M1)}}{B_{\gamma}^{Exp}}$$

$$B\,(\,E2\,) \;=\; \frac{B_{\gamma}^{Exp}}{B_{\gamma}^{Weisskopf}(E2)}$$

Table I also shows the calculated retardation and enhancement factors. According to the present values of the above mentioned parameters in this table, the lower limits of the enhancement factors for the 356 keV and 276 keV transitions which are of pure E2 multipolarity and depopulating the 437 keV level support the Weisskopf predictions for the partial transition probabilities of a single proton. The large enhancement factor obtained for the 53 keV transition depopulating the same level gives us an indication of the existence of collective effects.

The lower limits of the enhancement factors for the 384 keV transition of pure E2 multipolarity depopulating the 384 keV level support also the Weisskopf single particle predictions for the partial transition probability of a single proton. The M1 part of the 303 keV transition depopulating the 384 keV level is strongly retarded while the lower limit of the E2 part is enhanced by about the same amount below the single particle estimation, indicating that the E2 part of this transition is somewhat better accounted for in the single particle estimates.

References

1) De Boer, Th. J., S. S. Klein, E. W. Ten Napel, J. Blok, Nucl. Instr. & Meth. 21 (1963) 347 .

2) Vergnes, M., R. David-Boyer : J. de Phys. et Rad. 21 (1960) 65 .

3) Abou-Leila, H. : Doctorat es sciences Thesis, Paris 1967 .

4) Abou-Leila, H., S. M. Darwish, A. A. El Kamhawy, H. A. Ismail and S. M. El Bahi : Atomkernenergie Bd. 28 (1976) Lfg. 2 , 131 .

5) Thun, J. E., S. Törnkvist, K. Bonde Nielsen, H. Snellman, F. Falk and A. Mocorša : Nucl. Phys. 88 (1966) 289 .

6) Notea, A. and Y. Gurfinkel : Nucl. Phys. A 107 (1968) 193 .

7) Bosch, H. E., A. J. Haverfield, E. Szichman and S. M. Abecasis : Nucl. Phys. A 108 (1968) 209 .

8) Lederer, C. M., J. M. Hollander and I. Perlman, Table of Isotopes (J. Wiley & Sons, New York, 1967).

9) Bondenstedt, E., H. J. Körner and E. Matthias, Nucl. Phys. 11 (1959) 584 .

10) Flauger, W., and H. Schneider : Atomkernenergie 8 (1963) 453 .

11) Scharbert, T., Acta Phys. Hung. Tom. 20 (1966) 185 .

12) Imanishi, N., F. Fukuzawa and M. Sakisaka, Nucl. Phys. A 101 (1967) 654 .

13) Välivaara, K. G., A. Marelius and J. Kozyozkowski, Physica Scripta 2 (1970) 19 .

14) Badawy, O. E., Z. Awwad, M. R. El Aassar and A. El-Farrash : Atomkern-energie 19 (1972) 58 .

15) Alkasov, D. G., K. I. Erokina and I. K. Lemberg, Izv. Akad. Nauk. SSSR, ser fiz. 28 (1964) 1667 .

16) Vartapetian, H. A., A. G. Khudaverdia and T. A. Garibian, Compt. Rend. Congres Int. de Phys. Nucl. 2 (1964) 520 .

17) Bond, P. D., J. D. McGervey and S. Jha, Nucl. Phys. A 163 (1971) 571 .

18) Gupta, D. K. and G. N. Rao, Nucl. Phys. A 182 (1972) 669 .

19) Sliv, L. A. and I. M. Band, α-, β - and γ-Spectroscopy ed. by K. Siegbahn (North-Holland Publ. Company, Amesterdam,(1965) App. 5) .

20) Moszkowski, S. A., α -, β - and γ-Spectroscopy, ed. by K. Siegbahn (N.-H. Publ. Co., Amesterdam, 1965, p. 881) .

Table I

The retardation and enhancement factors for M1 and E2 transitions in ^{133}Cs

Level (keV)	Half-life (ns)	E_γ a) (keV)	I_γ a) %	Multi-polarity	Branch ratio b) X	Mixture ratio b) δ^2	I. C. C. α c) M1	I. C. C. α c) E2	R (M1)	E (
81	6.15±0.08	81	100	M1 + E2	1.0	0.0240	1.45	2.30	366± 5	4.6 ±
160.6	≦ 0.193	160.6	12	M1 + E2	0.118	0.3480	0.22	0.28	≦ 501.0	≧ 15
		79.6	88	M1 + E2	0.882	<0.0625	1.53	2.40	≦ 13.5	≧ 333
384	≦ 0.360	384	34	pure E2	0.313	—	—	0.018	—	≧ 1
		303	65	M1 + E2	0.6682	≦0.0144	0.036	0.035	≦703.0	≧ 0
		223	1	M1 + E2	0.0189		0.11	0.10	—	-
437	≦ 0.360	356	91	pure E2	0.741	—	—	0.021	—	≧ 4
		276	9	pure E2	0.0889	—	—	0.047	—	≧ 2
		53	0.1	M1 + E2	0.170	≦0.1160	4.9	6.8	≦ 92.7	≧ 207

a) Ref. 8 b) Ref. 6 c) Ref. 19

Figure Captions

Fig. 1 : A simplified level scheme of ^{133}Cs (Ref. 8) .

Fig. 2 : Direct gamma-ray spectrum of ^{133}Cs nucleus detected by 2 % Pb-loaded plastic scintillator coupled to an XP 2020 photomultiplier tube.

Fig. 3 : (a) Time distribution curve for evaluation of the half-life of the 81 keV level. (b) Prompt

Fig. 4 : (a) Time distribution curve for evaluation of the 384 and / or 437 keV levels . (b) Prompt

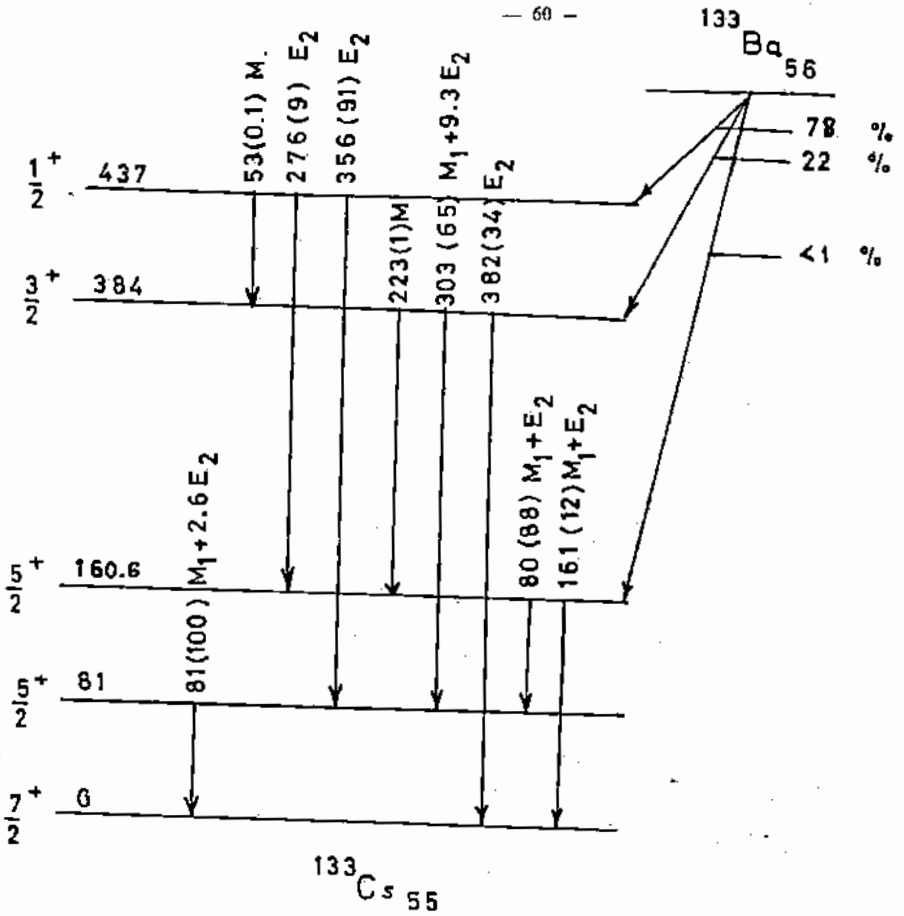
133 Ba 56
78 %
22 %
< 1 %
1/2+ 437
3/2+ 384
5/2+ 160.6
5/2+ 81
7/2+ 0
53(0.1) M1
276(9) E2
356(91) E2
223(1) M1+9.3 E2
303(65) E2
382(34) E2
80(88) M1+E2
161(12) M1+E2
81(100) M1+2.6 E2
133 Cs 55

Fig 1

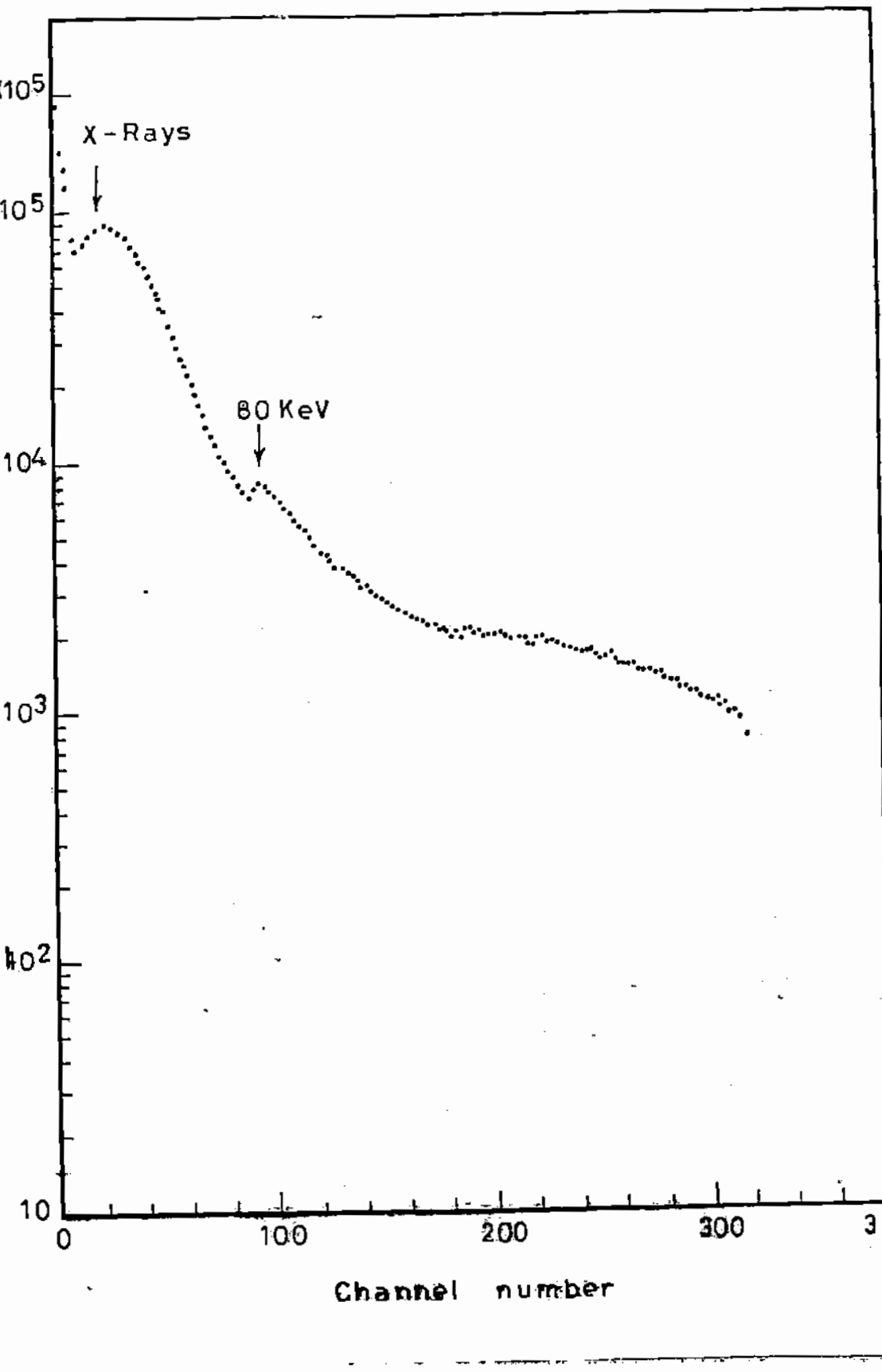
X-Rays
80 KeV
10^5
10^4
10^3
10^2
10
0
100
200
300
Channel number

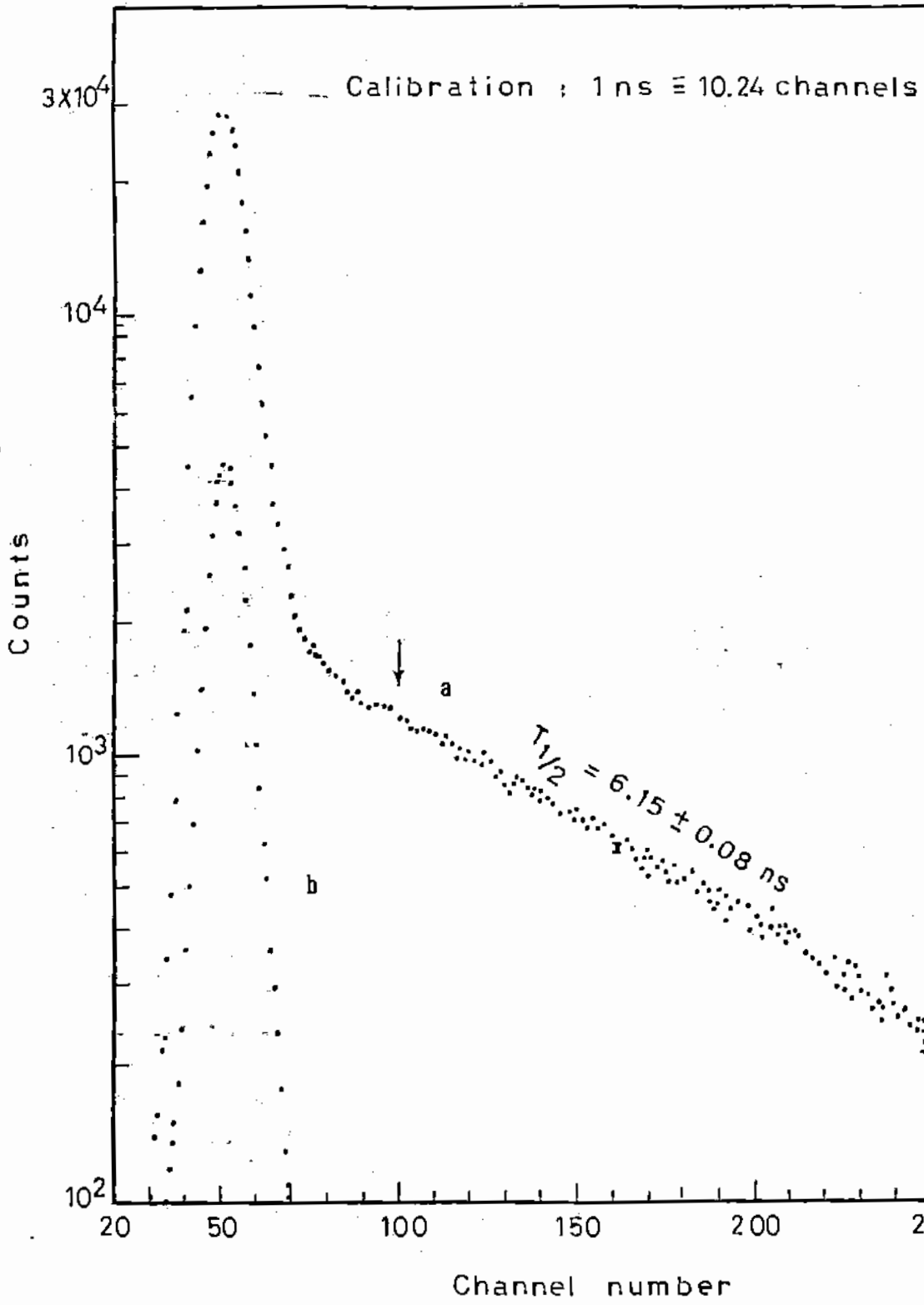
Calibration : 1 ns ≡ 10.24 channels
3X10⁴
10⁴
10³
10²
Counts
a
b
T1/2 = 6.15 ± 0.08 ns
20
50
100
150
200
Channel number

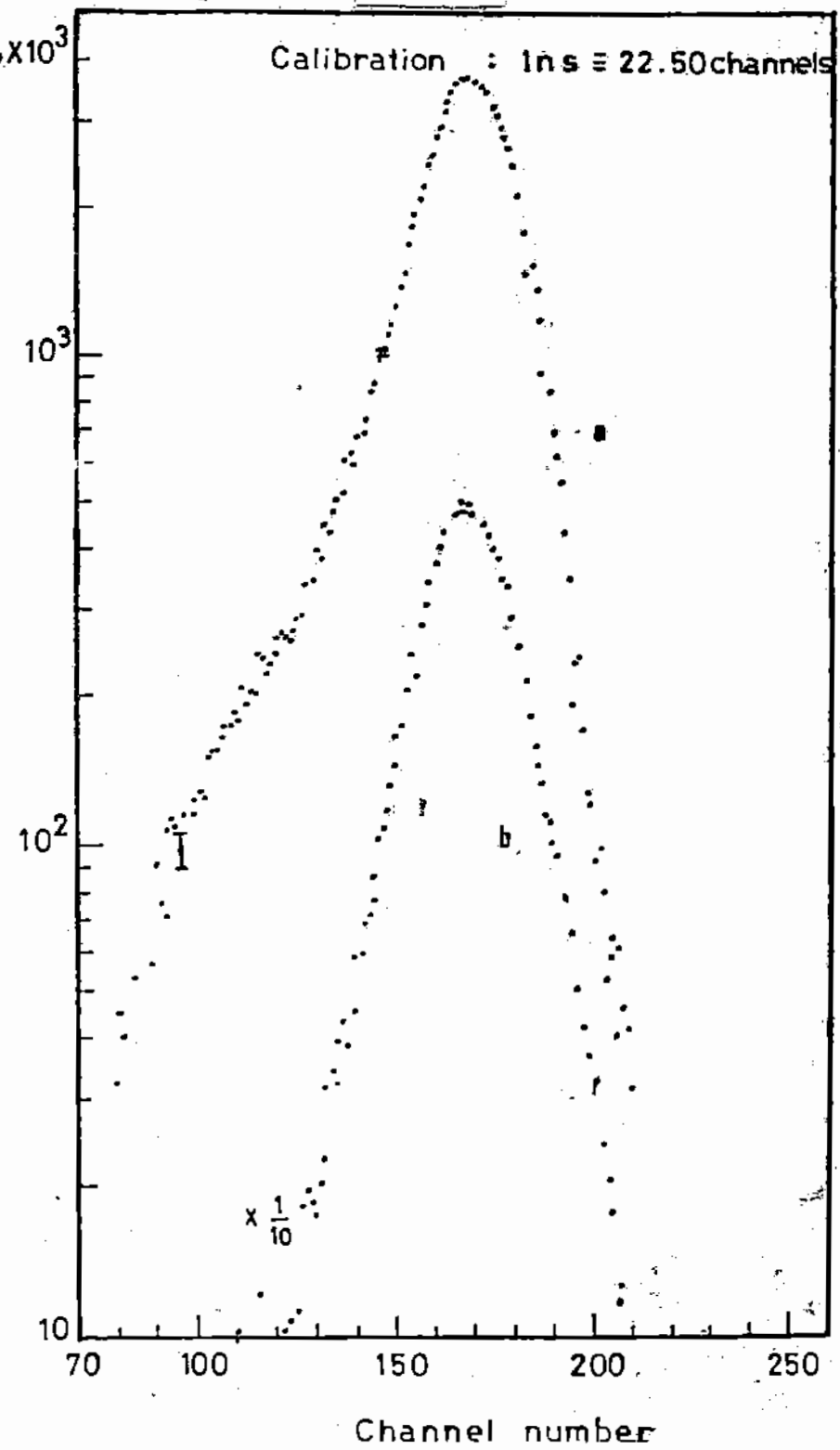
Calibration : 1ns ≡ 22.50channels
X10^3
10^3
10^2
10
70
100
150
200
250
Channel number
X 1/10
a
b

A DWBA analysis of the $^{7}Li(^{3}He,\alpha)^{6}Li$ reaction in the ^{3}He energy range 1.81 to 5.13 MeV

By I.I.Bondouk

Physics Department, Faculty of Science, Tanta University, Tanta, Egypt

Received : 1.1.1979

Abstract

The angular distributions of the α- particles from the reaction $^{7}Li(^{3}He,\alpha)^{6}Li$ measured in the ^{3}He energy range 1.81 to 5.13 MeV were analyzed in terms of the DWBA theory . Zero range DWBA was used without radial cut-off . Absolute spectroscopic factors were obtained and compared with the shell model calculations.

1. Introduction

The angular distributions of the α- particles from the $^{7}Li(^{3}He,\alpha)^{6}Li$ reaction have been measured by different authors in the ^{3}He energy range 1.0 to 27.0 MeV [1 - 7] . DWBA calculationa were carried out at ^{3}He energies between 5.0 and 18.0 MeV [6 , 7] . In the present work, the experimental angular distributions of the α- particles from the $^{7}Li(^{3}He,\alpha)^{6}Li$ reaction measured by P.D.Forsyth et al [2] at ^{3}He energies between 1.81 and 5.13 MeV were analyzed in terms of the DWBA theory.

2. DWBA analysis

DWBA calculations in the usual zero range approximation without radial cut-off were carried out on the Univac 1100 computer of the Institute of Nuclear Physics, Frankfurt, Deutchland-Germany using the code DWUCK due to Kunz [8]. The potential used has the form:

$$V(r) = V_c(r) + V\, f(x) + i\, W\, f(x_i) - V_s \frac{1}{r} \frac{d}{dr} f(x)\, \vec{L}\cdot\vec{S} \qquad (1)$$

$$\text{where } f(x) = \left[1 + \exp \frac{(r - r_o A^{1/3})}{a}\right]^{-1}$$

$$f(x_i) = \left[1 + \exp \frac{(r - r_i A^{1/3})}{a_i}\right]^{-1}$$

The Coulomb potential was assumed to be that of a uniformly charged sphere of radius $R_c = r_c A^{1/3}$. The neutron was assumed to be captured in a potential well of the Saxon - Woods form with the spin-orbit potential of the Thomas type. The well depth parameter was adjusted by the code to give the proper neutron binding energy. The optical model parameters are collected in Table 1. All the previous ^{3}He and the α-particle parameters were tried in the present analysis. It is found however that the results of the analysis are sensitive to the choice of the optical model parameters. Satisfactory fits with reasonable spectroscopic factors were obtained with optical model parameter set BC deduced from the general optical model potentials present in ref. [9]. The results of the analysis are shown in figs. 1, 2, 3. The spectroscopic factors were calculated by using the formula:

$$C^2 S = \frac{1}{N^2} \frac{2(2j+1)}{2s+1} \frac{\sigma_{exp.}(\text{peak})}{\sigma_{DW}(\text{peak})} \qquad (2)$$

where s is the spin of the captured neutron,

j is the total angular momentum of the captured neutron,

$\sigma_{exp.}$ is the experimental reaction cross-section at the peak,

σ_{DW} is the calculated cross-section at the peak,

^{2} is a normalization factor and its value in the case of (^{3}He, α) reactions = 25.o

^{2} = ($T_o t, M_T, M_t \quad T\ M_T$)^2 is the square of the Clebsch-Gordan coefficient for isobaric-^{o}spin coupling [10] , where T_o, T and t are the isobaric- spin quantum numbers of the ^{6}Li final state , ^{7}Li initial state and of the transfered neutron respictively, and M_T , M_T, M_t are their Z - components. In the case of the reaction ^{7}Li(^{3}He, α^o)^{6}Li , C^2 = 1 for T = o states and C^2 = 1/3 for T = 1 states .

he spectroscopic factors are given in Table 2 . Theoritical spectroscopic factors have been calculated by S.Cohen et al [14] and by S.Varma et al [15] . S. ohen et al listed separate components for $1p_{3/2}$ and $1p_{1/2}$ transfers, but S.Varma t al gave only the sum. The experimental spectroscopic factors for 1p transfers btained in the present work were evaluated as though they arose entirely from $p_{3/2}$ transfers or, if allowed entirely from $1p_{1/2}$ transfers. The spectroscopic factors educed in the present work are generally higher than the theoritical predictions.

. Conclusions

le results of the prosent analysis are sensitive to the choice of the optical odel parameters. However, the general formulae of the optical model potentials iven in ref. [9] seem to be applicable to the case of the interactions of ^{3}He ith light nuclei at low energies [11]. The fits obtained in the present work or the different α- groups from the ^{7}Li(^{3}He,α)^{6}Li reaction at the ^{3}He energies under consideration are generally good at forward angles.The lack of obtaining better fits in the case of the α_o and α_2 groups at backward angles is attributed to an exchange mechanism in which the α-particle comes directly from the arget nucleus, the ^{3}He being captured [3], while the lack of obtaining better fits to the case of the α- group may be attributed to the compound nucleus effects.

e author is indebted to professors R.Bass and Th.Elze for helpful discussions. anks are also due to Mr. Th.Weber for help in comutational work.

References

[1] Knudson,A.R., E.A.Wolicki; Direct Interactions and Nuclear Reaction Mechanisms, edited by Clemental,E.,C.Villi, Padua(1963)P.981
[2] Forsyth,P.D.,R.R.Perry: Nucl.Phys.A67(1965)517
[3] Orihara,H.,M.Baba,M.Akiyama,S.Iwasaki,T.Nakagawa,H.Ueno,M.Watanabe:J.Phys.Soc. Japan 29(1970) 533
[4] Mancuso,R.V.,A.R.Knudson,E.A.Wolicki,V.Bluemel: Bull.Am.Phys.Soc.14(1969) 487
[5] Bluemel,V.,M.K.Brussel: Bull.Am.Phys.Soc.11(1966) 10
[6] Linck,I.,R.Bilwes,L.Kraus,R.Seltz,D.Maganac - Valette: J.de Phys.Tome30(1969) 17
[7] Zander,A.R.,K.W.Kemper,N.R.Fletecher: Nucl.Phys.A 173 (1971) 273
[8] [illegible],P.D., : a distorted wave Born approximation program, University of Colorado,1968(unpublished)
[9] Hodgson,P.E., : Direct Interactions and Nuclear reaction Mechaniems, edited by Clemental,E.,C.Villi,Padua(1963) 103
[10] Macfarlane,M.H.,J.B.French : Revs.Mod.Phys. 32(1960) 567
[11] Liu,Y.C.,: Chin.J.Phys. 10 No. 2 (1972) 76
[12] Lüdecke,H.,T.Wan - Tijin, H.Werner,J.Zimmer:Nucl.Phys.A109(1968)676
[13] Bingham,H.G.,K.W.Kemper,N.R.Fletcher: Nucl.Phys.A175(1971)374
[14] Cohen,S.,D.Kurath: Nucl.Phys.A101(1967)1
[15] Varma,S.,P.Goldhammer: Nucl.Phys.A125(1969)193

Figure captions

Fig.1 DWBA fits to the angular distributions of the α_0 - group at the ^{3}He energies 4.36 and 5.13 MeV. Dots are the experimental results taken from ref. [2]. Solid lines are the DWBA calculations in the usual zero range approximation without radial cut-off using the optical model parameter set BC present in Table 1 .

Fig.2 DWBA fits to the angular distributions of the α_1 - group from the reaction ^{7}Li(^{3}He,α)^6 Li at ^{3}He energies between 1.81 and 2.98 MeV. Dots are the experimental results taken from ref. [2]. Solid lines are the DWBA calculations in the usual zero range approximation without radial cut-off using the the optical model parameter set BC present in Table 1.

Fig.3 DWBA fits to the angular distribution of the α_2 - group from the reaction ^{7}Li(^{3}He,α)^{6}Li at $E_{^3He}$ = 4.36 MeV. Dots are the experimental results taken from ref. [2]. Solid line represent the DWBA calculations in the usual zero range approximation without radial cut-off using the optical model parameter set BC present in Table 1 .

Table 1 Optical model [illegible]

Reaction channel	Ref.	V (MeV)	r_o (fm.)	a_o (fm.)	[illegible]	r_i (fm.)	a_i (fm.)	V_s (MeV)	r_s (fm.)	a_s (fm.)	r_c (fm.)
A Helium-3	[12]	140.0	[illegible]	0.47	[illegible]	75	0.75	12.0	1.20	0.70	1.3
B Helium-3	[9]	34.0	1.60	0.65	24.0	1.60	0.65				1.6
C Helium-4	[9]	40.0	1.70	0.65	12.0	1.70	0.65				1.7
D Helium-4	[13]	189.4	1.92	0.60	7.7	1.92	0.60	11.1	1.92	0.60	1.4

Table 2 Spectroscopic factors

E_{He3}	$S_{exp.}$ (pres.work)				$S_{th.}$ [14]				$S_{th.}$ [15]	
(MeV)	α_0 a)		α_1 b)	α_2 c)	α_0 d)		α_1	α_2	α_1	α_2
	J_n=3/2	J_n=1/2	J_n=3/2	J_n=3/2	J_n=3/2	J_n=1/2	J_n=3/2	J_n=3/2		
5.13	1.07 or	1.14			0.43	0.29				
4.36				1.12				0.89		0.75
2.98			1.37				0.55		0.35	
2.50			1.29							
2.14			1.04							
1.81			1.12							

a) α_0 corresponds to the ground state in ^{6}Li with $(J^\pi,T) = 1^+,0$.

b) α_1 corresponds to the excited state of E_x = 2.185MeV in ^{6}Li and $(J^\pi,T) = 3^+,0$.

c) α_2 corresponds to the excited state of E_x = 3.55 MeV in ^{6}Li and $(J^\pi,T) = 0^+,1$.

d) l_n = 1 for all the three α- groups.

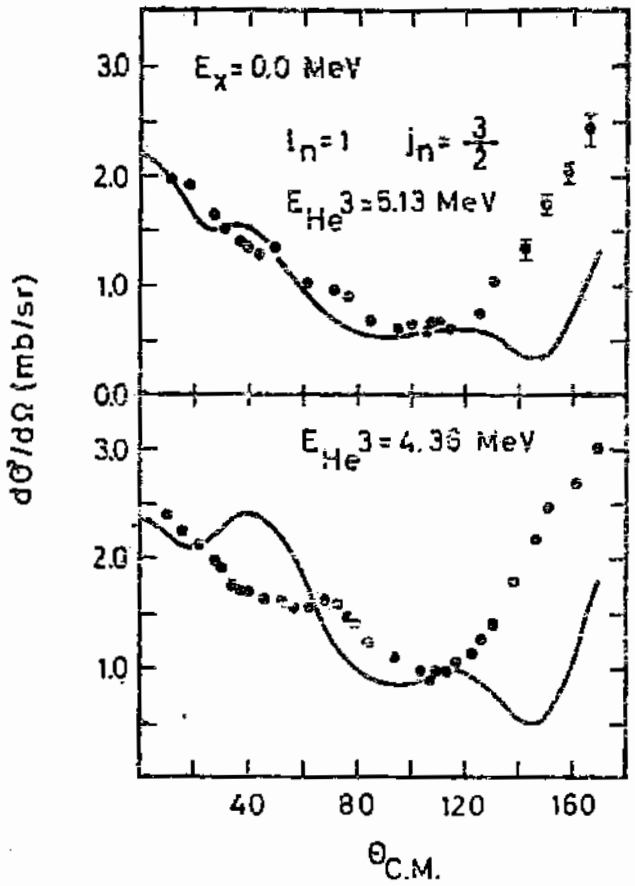
E_x = 0.0 MeV
l_n = 1
$j_n = \frac{3}{2}$
E_{He^3} = 5.13 MeV
E_{He^3} = 4.36 MeV
dσ/dΩ (mb/sr)
3.0
2.0
1.0
0.0
40
80
120
160
$\Theta_{C.M.}$

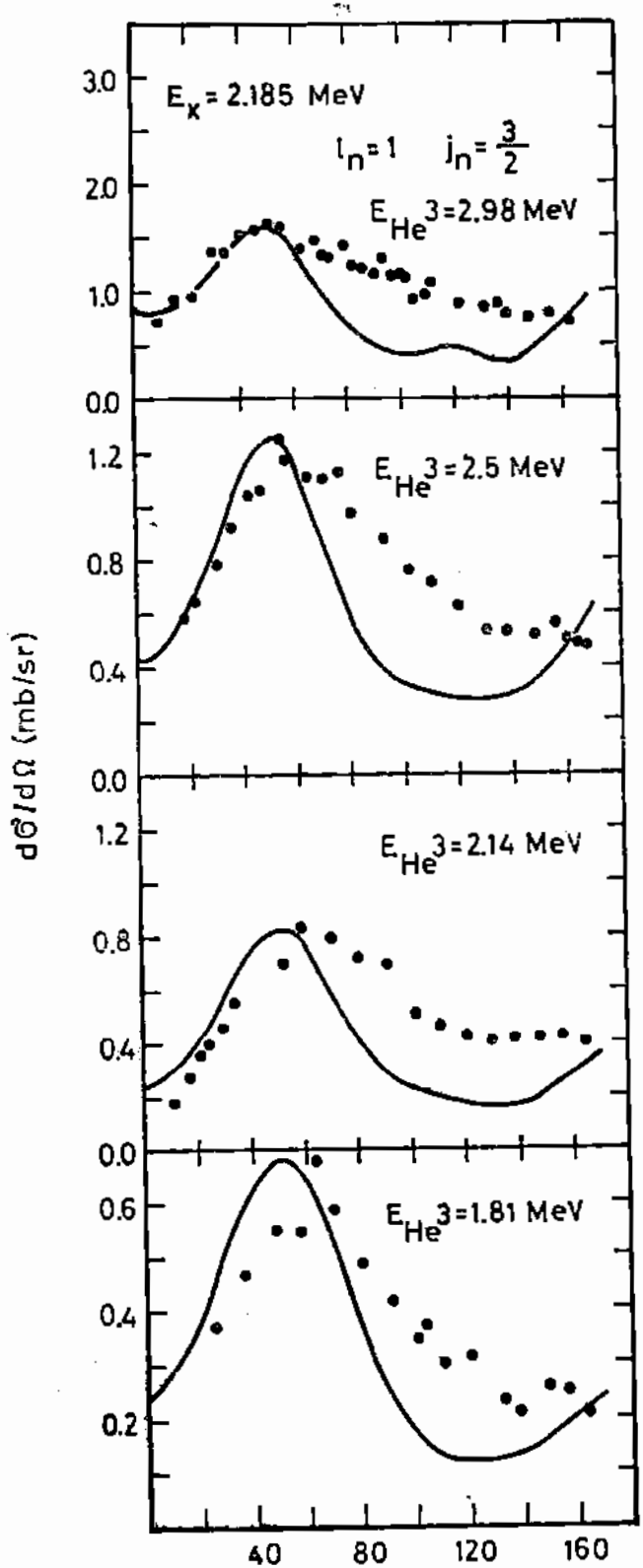
E_x = 2.185 MeV
l_n=1 j_n=3/2
E_{He^3}=2.98 MeV
E_{He^3}=2.5 MeV
E_{He^3}=2.14 MeV
E_{He^3}=1.81 MeV
dσ/dΩ (mb/sr)
3.0
2.0
1.0
0.0
1.2
0.8
0.4
0.0
1.2
0.8
0.4
0.0
0.6
0.4
0.2
40
80
120
160

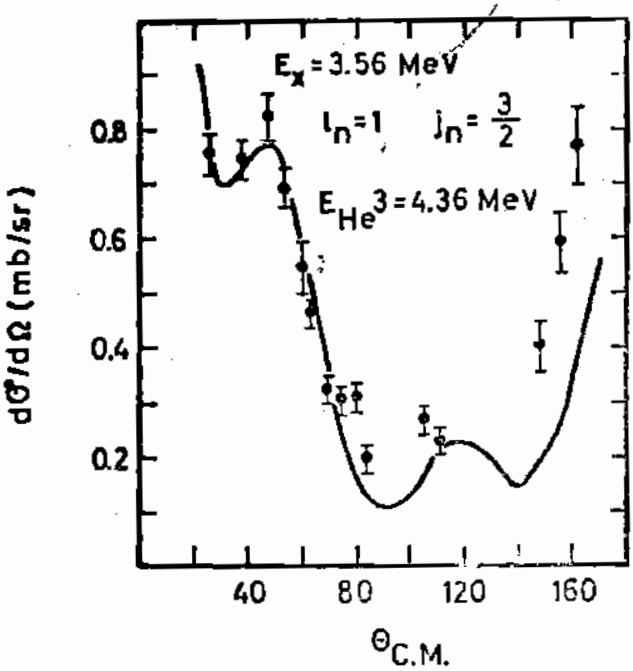
E_x = 3.56 MeV
l_n = 1
j_n = 3/2
E_He3 = 4.36 MeV
dσ/dΩ (mb/sr)
0.8
0.6
0.4
0.2
40
80
120
160
Θ C.M.

تحليل نتائج التفاعل ليثيوم^{7} (هيليوم^{3} ، ألفا) ليثيوم^{6} عند طاقة فترة الطاقه ١٫٨١ الى ١٣٫٠ مليون الكترون فولت باستخدام نظريه الوجه المشوهه.

د. ابراهيم ابراهيم بندق
جامعة طنطا - كليه العلوم - قسم الطبيعه

ملخص:

فى هذا البحث تم تحليل نتائج التوزيع الزاوى لجزيئات الألفا الصادره من التفاعل ليثيوم^{7} (هيليوم^{3} ، ألفا) ليثيوم^{6} والمقاسه عند طاقة الطاقه ١٫٨١ الى ١٣٫٠ مليون الكترون فولت وذلك باستخدام نظريه الوجه المشوهه. واقد أستخدم فى ذلك معاملات ضريبه هيليوم^{3} والألفا. وقورنت النتائج التى تم الحصول عليها من هذا التحليل بالحسابات النظريه.

SPECTROSCOPIC BEHAVIOUR OF TRIETHYLENE-TETRAAMINEHEXAACETIC ACID WITH TETRA AND HEXAVALENT URANIUM IN SOLUTION

By

MOHAMED B. HAFEZ, WAFAA S. HEGAZI[#] and NABIL HAFEZ

Hot Laboratory Center, Atomic Energy Establishment,
Cairo- Egypt.

ABSTRACT

The interaction between triethylenetetraaminehexaacetic acid (TTHA) and tetra and hexavalent uranium is investigated. Evidence is given for the formation of a stable and soluble 1:1 tetravalent uranium chelate. An insoluble 2:1 chelate between uranyl ions and TTHA is formed between pH 2 and 4. Also two soluble 1:1 and 2:1 chelates are formed. Stability constants (log K) of the soluble complexes were calculated to be 15 and 11.8 respectively.

INTRODUCTION

Complex formation between tetra and hexavalent uranium and TTHA has been studied by some workers.[1,2] However, the composition and the stability of the formed complexes were not definitely determined. The probable formation of several uranyl-TTHA chelates

---

University College for Girls, Department of Chemistry, Ain Shams University, Cairo, Egypt.

with different compositions, in the pH range 2–8 was previously reported.[3] Other studies,[4] at low pH, showed that uranyl ions react with TTHA to form only a mononuclear chelate, whose stability varies with the pH and the concentration of the chelating agent. In view of the contradictions in the published data on the uranyl-TTHA chelates, a detailed quantitative study of the equilibria involved in the interaction of tetra and hexavalent uranium ions with TTHA, over a wide range of pH and TTHA concentrations, is undertaken in the present work.

EXPERIMENTAL AND CALCULATIONS

All chemicals used were Analar grade. Tetravalent uranium was freshly prepared by reducing uranyl ions with nascent hydrogen gas using orthochloroplatinic acid as a catalyst.[5] The chelate solutions were prepared by mixing solutions of uranyl ions and TTHA in acidic medium, then adjusting the pH of the mixtures by adding carbonate-free sodium hydroxide solution.

pH-measurements were made using a Pye Unicam Model 292 pH-meter. Spectrophotometric studies were carried out with the aid of a Beckman DU-spectrophotometer, using 1 cm quartz cells.

Formation constants of the chelates were evaluated,[6] and accordingly, the stability constants (log K) were then calculated.[7,8]

RESULTS AND DISCUSSION

I. Chelation of Tetravalent Uranium (U(IV)):

I.1. Absorption spectra of (U(IV)+TTHA) mixture as a function of pH:

The absorption spectrum of $8x10^{-2}$M U(IV) and $3.2x10^{-1}$M TTHA mixture at pH = 1 is identical with that of free U(IV) ions, with absorption maxima at 458, 532, 618 and 645 nm.[4] In the pH range 2.2 - 9.5 the spectrum exhibits characteristic maxima at 464, 538, 622 and 650 nm (Fig.1). This shows that a U(IV)-TTHA complex is formed momentarily within the pH range 2.2 - 9.5. Between pH 2 and 4 the spectra of the mixture did not change for a long period after preparation. However, at pH $\geq$4.5 the U(IV)-TTHA complex changed gradually with time to U(VI)-TTHA.

I.2. Determination of the composition of the formed chelate:

I.2.a) The mole ratio method:

The concentration of U(IV) was kept constant at $8x10^{-2}$M and the [U(IV)] / [TTHA]ratio was varied between 1.00 / 0.25 and 1/4. The pH of the mixture was maintained at 2.2, and the absorbance was measured at 650 nm.

I.2.b) The continuous variation method:

Different concentrations of U(IV) and TTHA were mixed together such that the total concentration was always $1.6x10^{-2}$M. All the solutions were adjusted at pH 2.2 and the optical denisty measurements were made at 650 nm.

Both of the above methods point to the formation of 1:1 chelate, as can be seen from Figs. 2 a) and 2 b). The value of the stability constant of the complex (log K) was calculated to be 20.7 .

II. Chelation of Hexavalent Uranium (U(VI)):

II.1. Absorption spectra of (U(VI)+TTHA) mixture as a function of pH:

The absorption spectra of $8x10^{-2}$M uranyl ions in 0.2N HCl and that of (U(VI)-TTHA) mixtures at different pH values are given in Fig. 3. It was found that at pH=1.5 the spectrum of the mixture is similar to that of free uranyl ions. In the pH range 2-3 a yellow precipitate is formed indicating the formation of an insoluble compound. Between pH 3.5 and 8 a soluble complex is formed as indicated by the increase in the absorbance with increasing pH. At pH >8 the absorbance decreases with increasing pH and uranyl hydroxide is precipitated.

II.2. Determination of the composition of the chelate:

II.2.a) The mole ratio method:

The absorption spectra of mixtures composed of $8x10^{-2}$M U(VI) and various TTHA concentrations ranging from $8x10^{-3}$ to $8x10^{-1}$M at different pH values are given in Fig.4. An insoluble

2U : 1L complex is formed at a pH range 2-3.5. A soluble 2U : 1L complex is observed at 420 nm in the pH range 4.5 -5.5. Between pH 5.5 and 8 a part of uranyl ions was precipitated indicating that the above mentioned complex does not exist at this pH range. Another soluble 1:1 complex is observed between pH 4.5 and 8. At pH = 8.5, however, the uranyl ions undergo hydrolysis yielding the hydroxide.

II.2.b) The continuous variation method:

The total concentration of (U(VI)-TTHA) solution mixtures was kept at 1.6×10^{-2}M and the pH of each solution was adjusted at 4.5. The optical measurements were recorded at 420 nm, from which the formation of two U(VI)-TTHA complexes of mole ratios 1:1 and 2:1 could be concluded. This is in accordance with the results obtained from the mole ratio method.

The values of the stability constants (log K) were found to be 15.0 and 11.8 for the two complexes respectively.

The competition between the oxygen of the uranyl group and the chelate ligand may be a factor which decreases the stability of the formed complex.[9] Similar instability of uranium complexes was also observed with other liganda such as citrates,[10] amines[11] and other polyaminopolycarboxylic acids.[12]

REFERENCES

1. Bhat,T.R. and Krishnamurthy,M.; J. Inorg. Nucl. Chem. 26, 587, 1964.

2. Kozlov, A.G. and Krot, N.N.; J. Inorg. Nucl. Chem. 5, 9, 954, 1960.

3. James,D.B., Poell,J.E. and Spedding,F.H.; J. Inorg. Nucl. Chem.19, 133, 1961.

4. Hafez, M.B.; "Thése de Doctorât es science" CEA-R-3521, 1968.

5. Gogliat,G., De Leone,R. and Lanz,R.; RT/CHI(64), 14 Roma Giugno,196

6. Vosburg and Cooper; J. Am. Chem. Soc. 63, 437 (1941); Sherif and Awad; J. Inorg. Nucl. Chem. 24, 197 (1962).

7. Gel'man, A.D. and Mefod'eva,M.P.; Dok. Akad. Nauk, 124, 815, 1959.

8. Grimes,J.N., Huggard,M.J. and Wilford,S.P; J. Inorg. Nucl. Chem. 25, 1225, 1963.

9. Hafez,M.B. and Mahmoud, K.A.; Isotope and Rad. Res., 6, 2, 1973.

10. Dyatkina,M.E., Markov, V.P., Tsepkina,I.V. and Nikhallov, Yu.N; Russ. J. Inorg. Chem. 6, 5, 293, 1961.

11. Sacconi,L.; Atti. Accad. Nazl. Lincie. Classe. Sci. Fis. Nat.; 8, 6, 639, 1949.

12. Carell, M.J.; Analyst, 77, 859, 1952.

المتراكبات الناتجـــــة من ترابـــط ثلاثى ايثيلين رباعى امين سداسى حمض الخليك مع كل من اليورانيوم الرباعى واليورانيوم السداسى التكافـــــــؤ

محمد بدر الدين حافظ ـ وفاء صلاح حجازى* ـ نبيل حافظ
مـــؤسســـه الطاقـــة الذرية

تم فى هذا البحث دراسة الترابط بين مشتق الحمض الامينى : ثلاثى ايثيلين رباعى امين سداسى حمض الخليك وبين كل من اليورانيوم رباعى التكافـؤ واليورانيوم سداســـى التكافـــؤ لاحتماليه تكوين مركبات متراكبة • وقد دلت النتائج على تكـــوين متراكـــب ثابت وقابل للذوبان فى الماء بنسبة تركيبية ١ : ١ بين اليورانيوم الرباعى وبين مشتـــق الحمض الامينى • كذلك اثبتت النتائج تكوين متراكب غير قابل للذوبان بين شق اليورانيل وبين مشتق الحمض الامينى بنسبة تركيبية ٢ : ١ فى المحاليل ذات الأس الهيدروجينى اكثر من ٢ واقل من (او يساوى) ٤ •

ايضا تم الاستدلال على تكوين متراكبين قابلين للذوبان فى المحلول المائى بنسبـــة تركيبيـــة ٢ : ١ ، ١ : ١ بين شق اليورانيل ومشتق الحمض الامينى على التتالى • وفى جميع الاحوال تم حساب ثوابت الاتـــزان للمتراكبات القابلة للذوبان المذكورة أعـــلاه •

* كلية البنات ـ قسم الكيمياء ـ جامعه عين شمس •

FIGURES

1. Effect of pH on the absorption spectra of (U(IV)+TTHA) mixture; $[U(IV)] = 8\times10^{-2}M$, $[TTHA] = 3.2\times10^{-1}M$; 1) pH = 2.2, 2) pH = 5.5, 3) pH = 7.5, 4) pH = 9.5 and 5) U(IV) only.

2.a) Variation of the absorbance at 650 nm with the mole ratio $[U(IV)] / [TTHA]$ at pH 2.2, $[U(IV)] = 8\times10^{-2}M$,

2.b) Variation of the absorbance at 650 nm for (U(IV)-TTHA) mixtures with mole fraction at pH 2.2, total concentration of the mixtures $1.6\times10^{-2}M$.

3. Effect of pH on the absorption spectra of (U(VI)+TTHA) mixtures; $[U(VI)] = 8\times10^{-2}M$, $[TTHA] = 3.2\times10^{-1}M$.

1) pH = 3.5, 2) pH = 4.5, 3) pH = 5.5, 4) pH = 6.0, 5) pH = 6.5, 6) pH = 7.0, 7) pH = 7.5, 8) pH = 8.0, 9) pH = 9.5 and 10) U(VI) only in 0.2N HCl.

4. Variation of the absorbance at 420 nm with the molar ratio of hexavalent uranium to TTHA; $[U(VI)] = 8\times10^{-2}M$, A) pH = 3.5, B) pH = 4.5, C) pH = 5.5 and D) pH = 7.5.

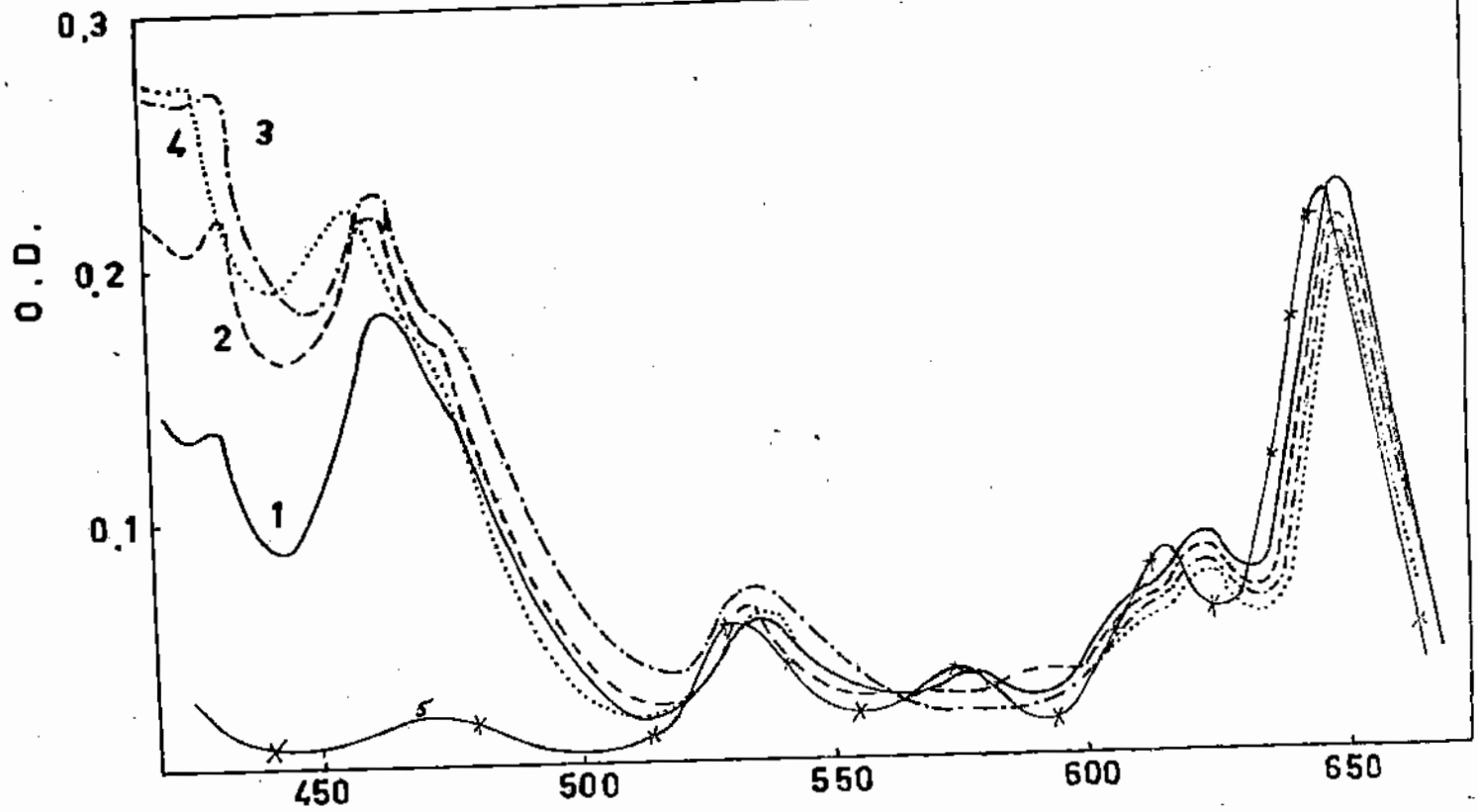

Fig. 1

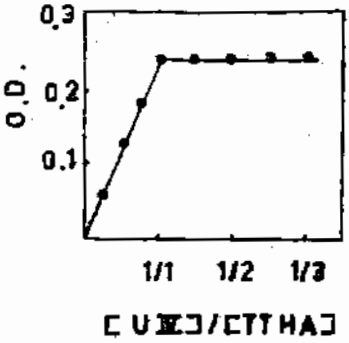

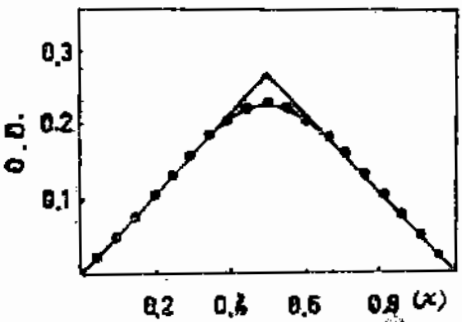

$$x = \frac{[\ \text{U Ⅲ}\ ]}{[\ \text{U Ⅲ}\ ] + [\ \text{TTHA}\ ]}$$

Fig. 2 b

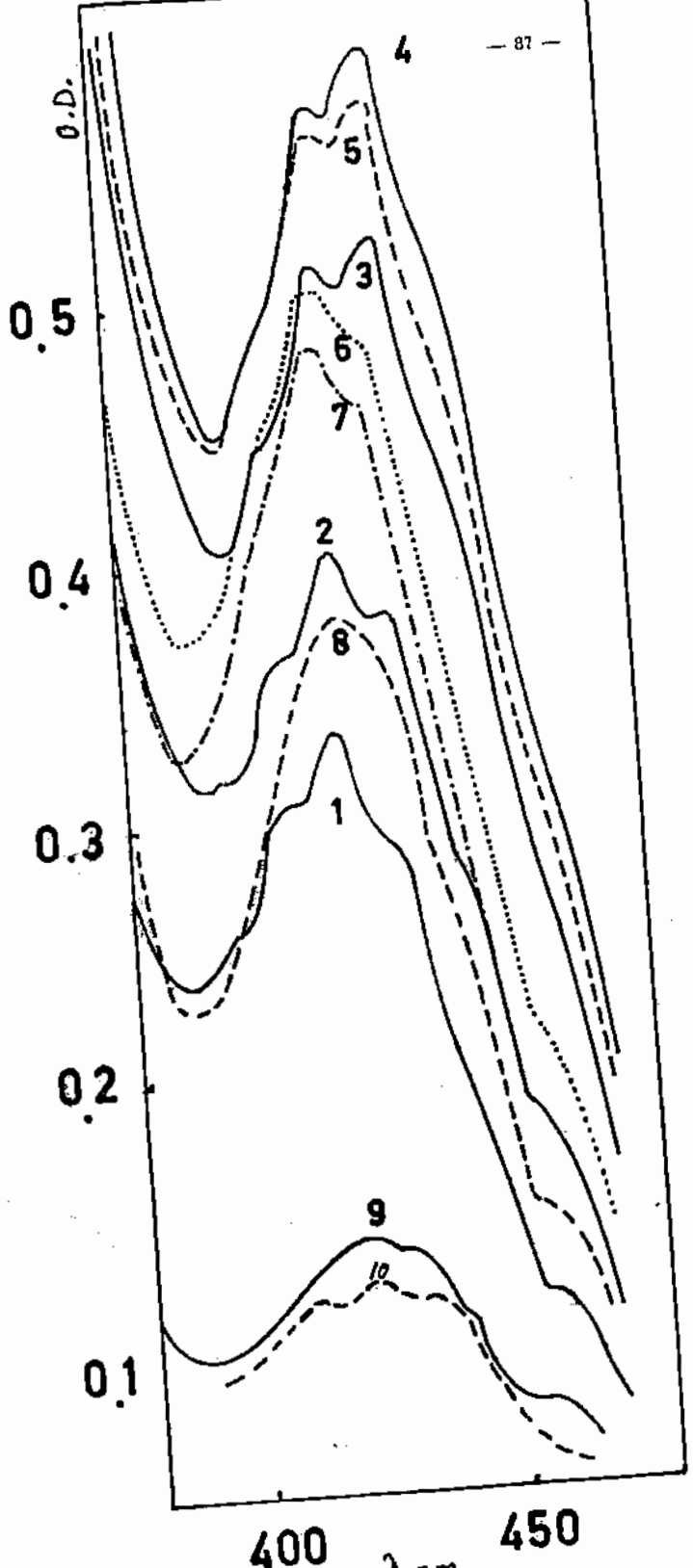

Fig. 3

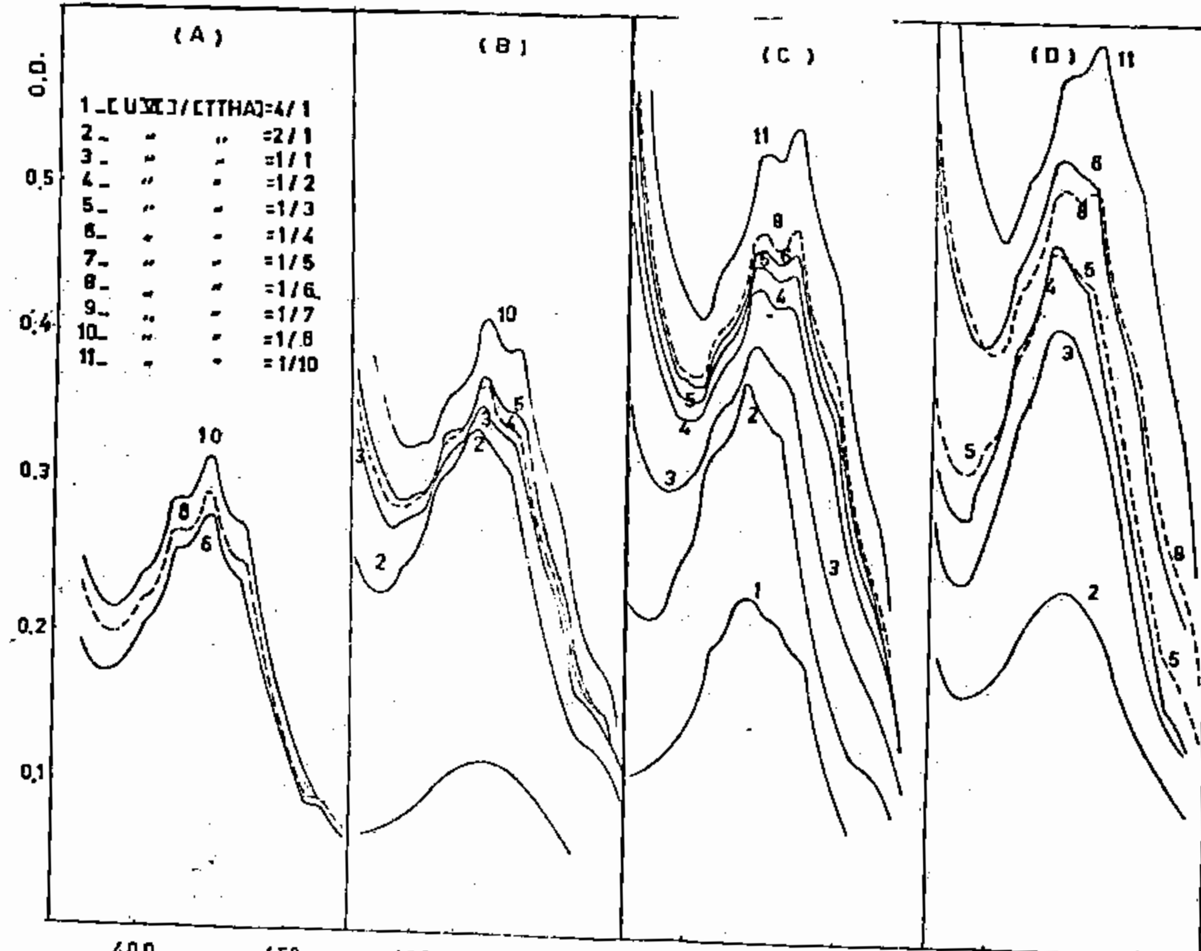
(A)
(B)
(C)
(D)
O.D.
0,5
0,4
0,3
0,2
0,1
1_[UVI]/[TTHA]=4/1
2_ " " =2/1
3_ " " =1/1
4_ " " =1/2
5_ " " =1/3
6_ " " =1/4
7_ " " =1/5
8_ " " =1/6
9_ " " =1/7
10_ " " =1/8
11_ " " =1/10
400
450

EFFECT OF SOLVENTS ON KINETICS OF ESTER AMINOLYSIS.

A.A. Taha and A.S.A. Shawali*

Department of Chemistry, University College for Girls, Ain Shams University, Cairo, Egypt.

n-Butylamine reacts with phenyl dichloroacetate in cyclohexane following third order kinetics only. When the same reaction was carried in cyclohexane-dioxan mixture, the rate of the reaction was found to increase as the percent of dioxan in the mixture is increased. These results suggest that the second order term in the aminolysis of esters in dioxan, reported previously,[1] represents a solvent catalyzed process. The possible mechanisms of such processes are discussed.

Introduction

Satchell and Secomski[2] have claimed that the aminolysis of esters by 1^{ary} or 2^{ary} amines in diethyl ether obeys the rate equation (1) :

$$-d[ester]/dt = k_2[ester][amine] + k_3[ester][amine]^2 \quad \ldots(1)$$

and that added tertiary amines do not accelerate the reaction. It was further argued that these observations rigorously exclude the

* Chemistry Department, Faculty of Science, University of Cairo, Cairo, Egypt.

possibility of the participation of the solvent in a path involving only one amine molecule.

Previously reported results[1] have shown that only 1^{ary}, and not 2^{ary}, amines lead to rate equation (1); 2^{ary} amines have been found to lead exclusively, to an expression first order in amine, as shown in equation (2)[1,3]:

$$-d[ester]/dt = k_2[ester][amine] \quad \ldots\ldots\ldots(2)$$

It was shown in several reports that ester aminolysis is subject to both inter- and intramolecular base catalysis.[1,3,4]

It has been our experience that for the experimental conditions carried for the n-butylaminolysis of p-nitrophenylacetate investigate by Satchell and Secomski[2], third order kinetics may very easily escap detection.[1,5] This sheds doubts on Satchell's conclusions, and we thought it is interesting to investigate the aminolysis of esters in different solvents. The systems investigated in this work include th reaction of phenyl dichloroacetate with n-butylamine in cyclohexane and in cyclohexane-dioxan mixtures. The same aminolysis reaction was reported before in dioxan.[1] Cyclohexane and dioxan were chosen becau they have almost similar dielectric constants, but differ in their ability to interact with the solute molecules. If the solvent plays r role, the kinetics of aminolysis in either solvent or in their mixtur would be expected to be the same.

Experimental

Materials: Cyclohexane and dioxan were Matheson, Coleman and Bell Spectroquality reagents grade solvents. Their purity was checked by i uv and vapor phase chromatographic analysis.

n-Butylamine was purchased from Mathieson, Coleman and Bell . It was rified by storing overnight over sodium hydroxide pellets, then stilled from fresh sodium hydroxide pellets using a 15-in. Vigreux lumn. The fraction having constant b.p. was collected and stored an amber glass bottle over fresh sodium hydroxide pellets. Its degre purity was determined by acid-base titration and checked by vapor ase chromatographic analysis. A clean single peak was obtained, dicating almost 100% purity. Its physical constants agreed with ose in the literature.[6]

Phenyl dichloroacetate was prepared from dichloroacetyl chloride[7] d phenol as described previously.[1] Its physical constants also agreed ith literature value.[6,8]

Kinetics: A Bausch and Lomb Spectronic 505 uv spectrophotometer ith jacketed cell compartment maintained at 25.5 ± 0.1° was used for he kinetic measurements. The reactions were carried out in 1-cm pyrex lass-stoppered fused silica absorption cells. The procedure of following he kinetics of the reactions, and the methods of treating the data are similar to those described previously.[1]

Stoichiometry and Isolation of Products: Authentic samples of -n-butyldichloroacetamide was prepared by independent methods. When he reaction of phenyl dichloroacetate with n-butylamine was carried ut on laboratory scale, the expected amide was obtained in about 8% yield and was identical with the authentic sample.

Results

In all kinetic runs the ester concentration was maintained at .0 x 10^{-4} M, whereas amine concentration was varied in the range .01 to 0.1 M. This excess concentration of amine led to pseudo-

first order disappearance of ester. The reactions were followed by rate of appearance of the phenol peak at 274 mu. The observed first order rate constants, k_{obs}, were calculated from plots of log $(D_\infty - D_t)$ vs. time, where D_∞ and D_t represent the optical densities, at the chosen wave length, at infinite time and at any interval 't', respectively, as explained previously.[1] Values of k_{obs} were normally reproducible to ± 3% or better.

The kinetic data are included in Table 1. For the reaction of phenyl dichloroacetate with n-butylamine in cyclohexane, the following relation was obtained:

$$k_{obs}/[\text{amine}] = k_3 [\text{amine}] \quad \ldots\ldots\ldots\ldots(3)$$

This is illustrated in Fig.1, where a plot of $k_{obs}/[\text{amine}]$ vs. $[\text{amine}]$ gives a straight line, whose slope is equal to k_3.

Results for a series of experiments for the reaction of phenyl dichloroacetate and n-butylamine in cyclohexane-dioxan mixtures are represented in Table 1. In this series, both ester and amine concentrations were held constant and the solvent composition was varied. The data indicate that at constant amine concentration, there is a gradual increase in the rate of the reaction as the ratio of dioxan to cyclohexane in the reaction mixture is increased, then the rate eventually levels off at high concentrations of dioxan, as can be observed in Fig. 2.

Discussion

In a reaction system containing the ester and n-butyl-amine there are three possible pathways that may be considered: (a) the uncatalyzed reaction, (b) base-catalyzed reaction and (c) solvent-catalyzed reaction.

If all three pathways were operating simultaneously, the overall rate expression could be given by:

$$\text{rate} = k_2[E][A] + k_3[E][A]^2 + k_2'[E][A][S] \quad \ldots\ldots\ldots(1)$$

where E, A and S refer to the ester, amine and solvent respectively.

In cyclohexane, the catalytic contribution of the solvent molecules is absent. Accordingly, the rate equation (1) would be reduced to:

$$\text{rate} = k_2[E][A] + k_3[E][A]^2 \quad \ldots\ldots\ldots(2)$$

The available data indicate, however, that only the third order pathway is operating for the aminolysis in cyclohexane. This conclusion is in accordance with Menger's results[9] for the aminolysis of p-nitro phenylacetate in chlorobenzene, where the second order term in amine, is the only term observed. The absence of the second order term when cyclohexane is the solvent suggests that the second order term obtained for the n-butylaminolysis of phenyl esters in dioxan[1] represents a solvent catalyzed reaction. Also, the fact that the overall rate of the reaction of phenyl chloroacetate with n-butylamine increases as the percentage of dioxan increases when the reaction is carried out in cyclohexane-dioxan mixture, substantiates this conclusion.

An alternate explanation for the disappearance of the overall second order term is that in hydrocarbon solvents, such as cyclohexane, the amine exists predominantly in the dimerized form. This is because hydrogen bonding to the solvent itself will be less prominent. Under such conditions, the amine catalyzed pathway becomes the predominant one. This explanation, although seems reasonable, is considered unlikely because the linear relationship of $k_{obs}/[\text{amine}]$ vs. $[\text{amine}]$ (Fig. 1), means that n-butylamine must exist essentially either all

in the monomeric form or in the dimeric form, in the concentration range used. If both monomers and dimers were present in appreciabl amounts in the concentration range used in this study, then a plot $k_{obs}/[amine]$ vs. $[amine]$ would be curved. At lower concentration there would be a lower percentage of reactive dimers in solution than at higher concentration. Nevertheless, the data do not exclud a situation in which there is, for example, 1% monomers and 99% dim This is considered unlikely since it would mean that the true third order rate constant for the reaction of n-butylamine dimer with the phenyl ester in cyclohexane would be larger than that observed in dioxan. The values of k_3 obtained in cyclohexane and dioxan[1] wer found to be 1.30 and 1.65 $molar^{-2}.sec^{-1}$, respectively.

Considering the mechanism of the solvent-catalyzed pathway, it m follow either a concerted mechanism as in scheme I, or a stepwise mechanism according to scheme II

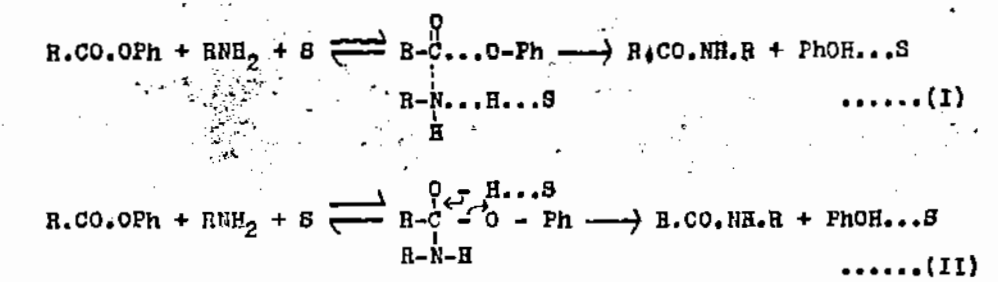

Although the present kinetic data do not provide a direct evidence to exclude completely any of these two possible mechanisms, it is felt that the concerted mechanism (I) is very unlikely, since it ignores the most important addition property of the carbonyl group. The following facts seem also in favor of the stepwise mechanism (I

(1) If the direct displacement mechanism (I) were operative, it

might be anticipated that as the reactivity of the ester increases, the reaction would proceed more through this pathway, since in this way it avoids going though the other multiple equilibrium steps of the base-catalyzed reaction sequence. As a result, the contribution of the latter would be expected to be small for the very reactive esters such as phenyl trichloroacetate and difluoroacetate. Contrary to this, previous kinetic data[1] of the same reaction system in dioxan indicate that the contribution of the third order process to the overall reaction generally increases as the reactivity of the ester increases. (ii) The observed applicability of Taft's relation for the observed second order rate constants for the aminolysis of esters previously reported[1], suggests the possible existence of an addition intermediate by analogy to other reaction series where such a linear free energy relationship holds.[10] (iii) If the transition state (I) is the only one between the reactants (ester and amine) and the products (amide and phenol), it would be difficult to perceive why this transition state would form so much more readily in nucleophilic substitution reactions at the carbonyl-carbon than the corresponding transition state of the displacement of the alkoxyl group in an ether molecule.[4] (iv) A survey of the literature reveals that a direct displacement mechanism has not yet been reported in any nucleophilic substitution reaction at sp^2-hybridized carbon atom.

Based on the foregoing arguments, it is felt that a stepwise mechanism (II), for the second order aminolysis reaction, is more likely than the direct displacement mechanism (I).

References

1- Shawali, A.S. and Blochler, S.S., J. Amer. Chem. Soc., 89, 3020 (1967).

2- Satchell, D.P.N. and Secomski, I.I., J. Chem. Soc., (B) 130 (19

3- Jenks, W.P. and Carriuolo, J., J. Amer. Chem. Soc., 82, 675 (19

4- Bender, M.L., Chem. Rev., 60, 53 (1959).

5- Ross, S.D., J. Amer. Chem. Soc., 80, 5319 (1958).

6- "Tables for Identification of Organic Compounds", 2nd. edition, Supplement to "Handbook of Chemistry and Physics", The Chemical Rubber Publishing Co., Cleveland, Ohio, USA, 1964.

7- Brown, H.C., J. Amer. Chem. Soc., 60, 1325 (1938).

8- Rosen, I. and Stallings, J.P., J. Org. Chem., 24, 1523 (1959).

9- Menger, F.M., J. Amer. Chem. Soc., 88, 3081 (1966).

10- Taft Jr., R.W., J. Chem. Phys., 26, 93 (1957) ; J. Amer. Chem. Soc., 79, 1045, 4016, 4935 (1957) ; ibid., 80, 2936 (1958).

Fig.1. Linear Plot of $k_{obs}/[amine]$ vs. $[amine]$ for the reaction of Phenyl dichloroacetate with n-Butylamine in Cyclohexane at 25.5°.

Fig. 2. Dependence of k_{obs} on percent Dioxan for n-Butylaminolysis of Phenyl dichloroacetate in Cyclohexane-Dioxan mixtures.

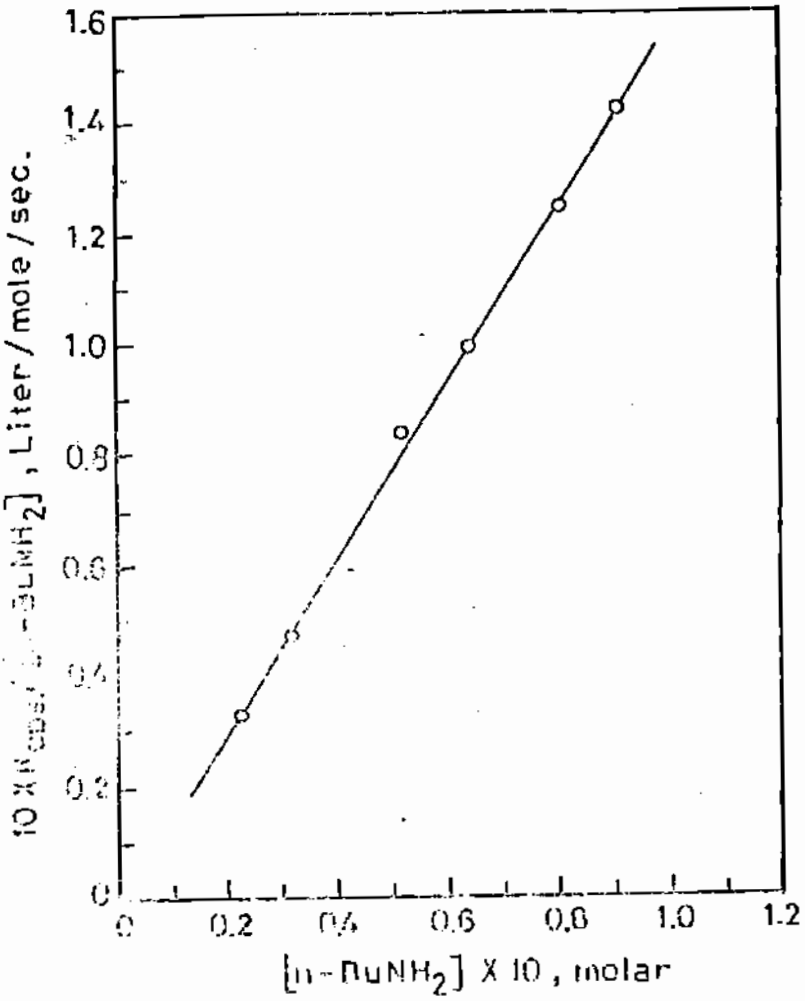
1.6
1.4
1.2
1.0
0.8
0.6
0.4
0.2
0
0
0.2
0.4
0.6
0.8
1.0
1.2
[n-BuNH2] X 10 , molar

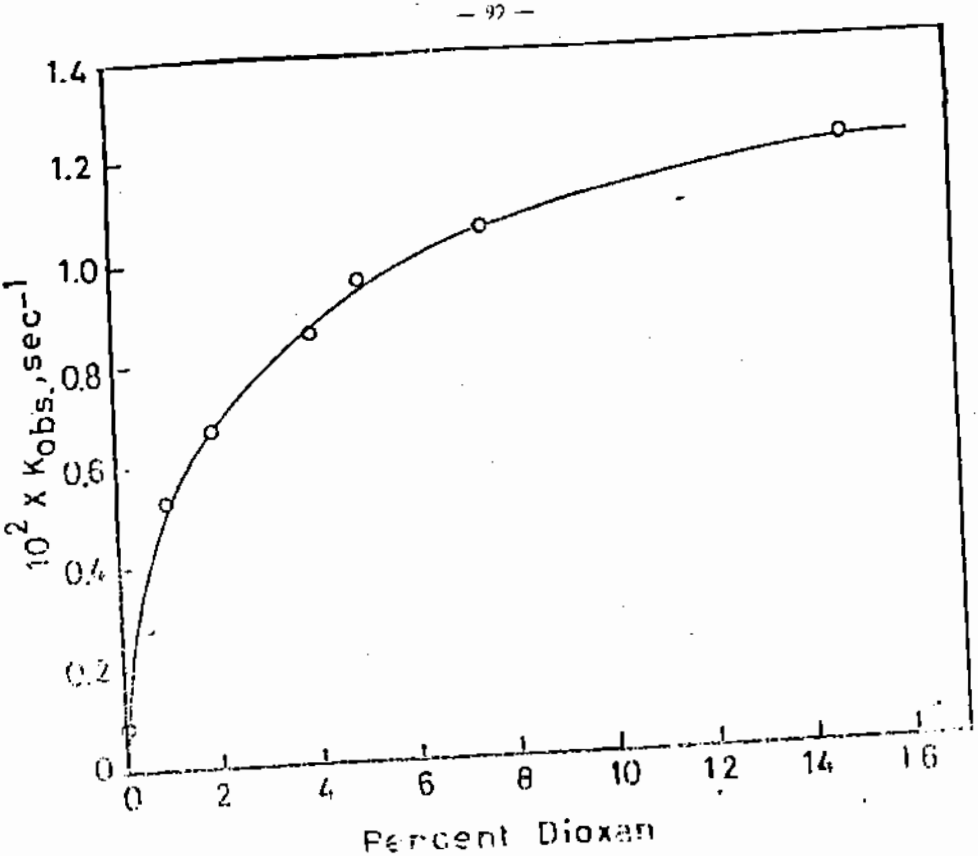
1.4
1.2
1.0
0.8
0.6
0.4
0.2
0
$10^2 \times K_{obs.}, sec^{-1}$
0
2
4
6
8
10
12
14
16
Percent Dioxan

تأثير المذيبات على كينيتيكيه التحلل الامينى للاسـتـرات

احمد عبد الرحيم طه ، احمد سامى الشوالى
قسم الكيمياء كليه البنات جامعه عين شمـس

تم التوصل الى ان كينيتيكيه تفاعل هـ ـ بيوتيل امين مع فينيل ثنائى كلورو الخلات فى الهكسان الحلقى هى من النوع الثانى الرتبه فقط ، وعندما اجرى التفاعل نفسه فى خليط من الهكسان الحلقى والديوكسان ، وجد ان معدل التفاعل يزداد بازدياد النسبه المئويه للديوكسان فى خليط المذيب .

وبناء على هذه النتائج فقد امكن تفسير ان الرتبه الثنائيه التى تم التوصل اليهـا سبقا لكينيتيكيه التحلل الامينى للاسترات فى الديوكسان بمفرده تمثل تفاعلا يدخل فيـه المذيب كعامل حافز .

ويتضمن هذا البحث مناقشه طرق السير (الميكانيكيه) المختلفه التى قد تتم بهـا هذه التفاعلات .

Received : 5·9·1951

Kinetic Study on the Effect of Substituents on the Base-catalysed Darzens'-like Condensations.

by

William I. Awad, Ahmed A. Taha, Wasfi N. Wasef and Soad M. Shindy.
Department of Chemistry, University College for Women, Ain Shams University, Cairo, Egypt.

The kinetics of the base-catalysed condensation of phenacyl chloride, p-methoxy-, p-methyl- and p-chlorophenacyl chlorides with phenanthrenequinone were followed potentiometrically at different temperatures. The condensations follow overall third order kinetics, first order with respect to each reactant. The rate of condensation increases with increasing electron-withdrawing power of the substituents. The rate also increases as the dielectric constant of the solvent increases.

The attempts to achieve acid-catalysed Darzens' condensations failed with phenanthrenequinone and with p-nitrobenzaldehyde.

Introduction

The mechanism of the base-catalysed Darzens' condensation of phenacyl halides with benzaldehyde is generally regarded as being established by Ballester and Bartlett,[1] who reported the absence of any appreciable results in attempted acid-catalysed Darzens' condensations. However, Sipos et al.[2-6] claimed that the condensation of substituted phenacyl halides with substituted benzaldehydes was successfully carried out in different acid media. They reported a mechanism analogous to that of acid-catalysed aldol condensations[7]:

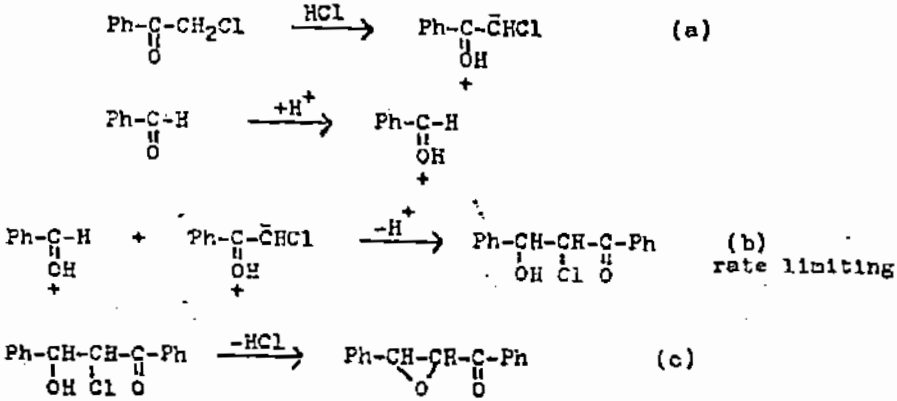

Since the formation of the carbanion in the first step of Darzens' condensation cannot be visualized in acid medium, we doubted the correctness of the results reported by Sipos et al.[2-6] In view of this controversy, we thought it is important to re-investigate the kinetics of Darzens'-like condensations, both in acid and in alkaline media. It is informative to try the condensation between

substituted phenacyl chlorides and phenanthrenequinone, which is as reactive as p-nitrobenzaldehyde.[8]

Our study of the effect of substituents in phenacyl chloride on the rate of condensation was stimulated by our objection to the conclusion reached by Sipos et al.[5,6] They claimed that the rate was decreased by electron drawing substituents in phenacyl chloride.

Experimental

Materials: Phenacyl chloride of analytical reagent grade (m.p. 56-57°)[9] was used. p-methoxyphenacyl chloride (m.p. 98-99°)[10], p-methylphenacyl chloride (m.p. 56-57°)[11], p-chlorophenacyl chloride (m.p. 101-102°)[12] and phenanthrenequinone (m.p. 207-208°)[13] were prepared pure. Peroxide-free dioxan[14] and doubly distilled water were used throughout the study.

Kinetic measurements: The methods adopted for rate measurements were similar to those of Hine et al.[15], and Hanna et al.[16], involving potentiometric titration of the liberated halide ions at different intervals, against $AgNO_3$ using Ag/AgCl-quinhydrone electrode. CARL ZEISS (JENA, D.D.R.) moving scale sensitive galvanometer was employed.

The condensation reactions were carried out in 50, 60 and 70% (v/v) dioxan-water mixtures at 1° (for investigating the effect of the solvent). The runs in 50% aq. dioxan were carried out, in addition, at -3, -7 and -10° (for investigating the effect of the substituents). EIN (Germany) ultrathermostat (-20° to +50° ±0.1°C.) was employed. The reaction was initiated by rapid addition of :

(A) concentrated solution of phenanthrenequinone and phenacyl chloride (or derivative) in dioxan-water mixtures previously cooled to the desired temperature, to (B) a solution of sodium hydroxide in distilled water enough to adjust to the desired molarities, also previously cooled to the desired temperature. At suitable time intervals, equal aliquots of the reaction mixture were pipetted out, quenched with 20 ml 0.1N H_2SO_4 and analysed for free halide ions. The reaction rates were found to be too fast to be followed accurately at temperatures above 1°. In all runs, the reactions were followed up to 75%. Each run was repeated 3 times to check reproducibility.

Isolation of products: The constituents were dissolved in one liter of 50% aq. dioxan previously cooled to 1°. The reaction mixture was kept at 1° for two hours, then at room temperature overnight. Crystallin solids were separated after slow evaporation of the solvent at room temperature, washed with water and crystallized from the suitable solvent to give enol derivatives (i.r. ν_{OH} 3230 cm^{-1}) of spiro (oxirane-2,9'-phenanthrene)[17], of the general form :

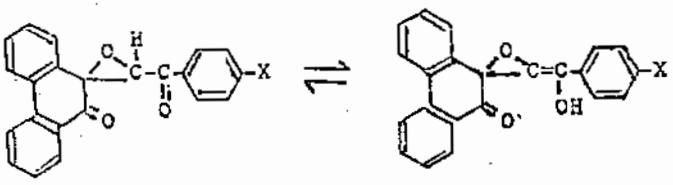

(I)

X = H, Cl, CH_3 or OCH_3

The product obtained from the p-chloro derivative was an exception, where it gave a mixture of 50% keto form and 40% enol form at -3°. Table (1) includes a full survey of the different products obtained.

Acid-catalysed experiments: We repeated the reactions reported by Sipos et al.[5,6] for Darzens' condensation of phenacyl chloride, and its derivatives, with p-nitrobenzaldehyde in acidic media. We tried out the reaction between phenacyl chloride and its derivatives, with phenanthrenequinone and with p-nitrobenzaldehyde in 50% aq. dioxan at 1° in presence of sulphuric or phosphoric acids of concentration ranges from 3-30%. We also attempted the phenanthrenequinone and p-nitrobenzaldehyde condensations in absolute ethanol, using 10% and 30% HCl gas as a catalyst, since Sipos et al. reported that they obtained the best yield in case of 30% HCl.

In all the above cases, no reaction took place, as indicated by the isolation of the reactants unchanged. This is in clear contradiction to the results obtained by Sipos et al.[5,6] When the reaction solution was neutralized, however, solid epoxides separated. These solids were identified by melting points and mixed melting points to be the same as the products obtained from the corresponding base-catalysed condensations. This might indicate that the products obtained by Sipos were not formed in acid medium, but rather, only during neutralization.

Results and Discussion

Kinetics: To permit accurate and reliable determinations of the rates, the molar concentrations of the reactants were not more than 0.001 : 0.001 : 0.01 M of phenanthrenequinone (A) : phenacyl chloride (or substituted phenacyl) (B) : sodium hydroxide, respectively. When higher concentrations were used, the reactions were too fast to follow accurately.

The kinetic results showed that the condensation reaction is an overall third order, first with respect to each component A , B and OH^-. Table (2) includes the rate constants obtained for the different molar ratios employed. Fig. 1 shows the graphical representation of pseudo-second order reactions, using excess of sodium hydroxide (1:1:10). Fig. 2 shows true third order representation when equimolar initial concentrations were used (1:1:1).

Solvent Effect: (Effect of dielectric constant): It was found that the rate of the reaction increases as the dielectric constant of the solvent increases, by increasing the dioxan : water (v/v) ratio. Fig. 3 shows a plot of log k_3 vs. 1/D for phenacyl chloride and its derivatives. The negative slope indicates that the reaction takes place between a negative ion and a dipolar molecule.[18] The employed compositions of the solvent were chosen on the basis that in 40%, or less, aq. dioxan, precipitation took place: and in 80% or higher, aq. dioxan, the solvent became partially immiscible. Hence, only 50, 60 and 70% aq. dioxan mixtures were used.

Effect of Substituents: Table (2) includes calculated values of k_3 at different temperatures. Table (4) includes the different activation thermodynamic parameters calculated from the temperature dependence of the rate constants, and related thermodynamic equations for the different substituted phenacyl chlorides investigated . It is clear from examination of the values in Table (4) that the order of accelerating the reaction is :

$$Cl > H > -CH_3 > -OCH_3$$

This conclusion is also substantiated by the linear relationship of log k vs. σ, showing conformity to the Hammett equation (Fig. 4). A positive value of ρ shows that the rate is enhanced by withdrawal of electron density from the reaction center, and vice versa.

This order of accelaration by the substituents is in clear contradiction to the order claimed by Sipos et al.[5,6], who reported the exact opposite order, with no justification.

Mechanism: Based on all the foregoing discussion of the results, we can propose the following mechanism, which is similar to that given by Ballester[1] :

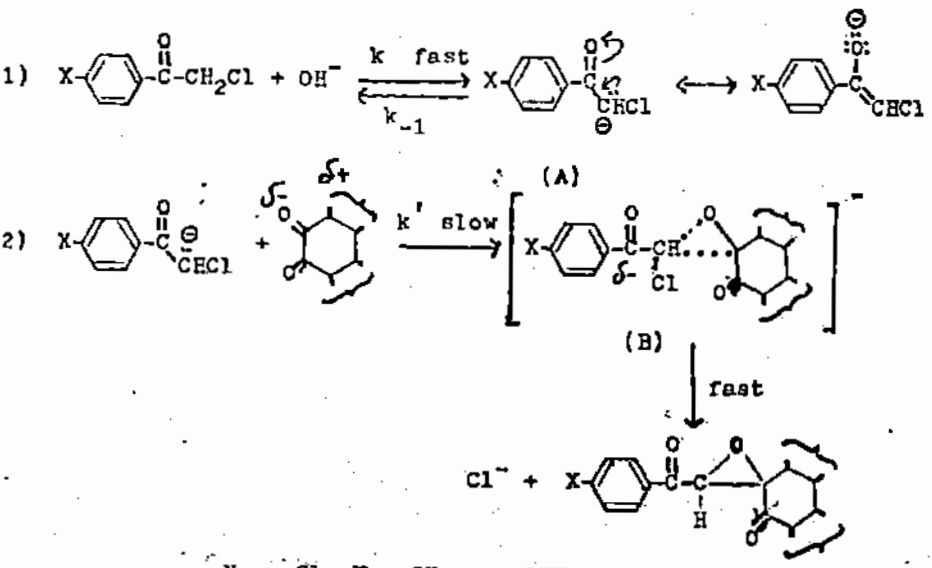

Since the reaction was found to be third order, hence, step (2) is considered to be the rate-limiting step. It can be seen that the formation of the product in step (1) is favoured by electron withdrawal in the indicated direction, thus facilitating the removal of

the H^+ by the OH^- group, and stabilizing the developed negative charge. This can explain the order of reaction acceleration of the different substituents that we report.

REFERENCES

1- M. Ballester and P.D. Bartlett, J. Amer. Chem. Soc., 1953, 75, 2042.

2- Gy. Sipos and R. Szabó, Acta Phys. Chem. (Szeged), 1962, 8, 48.

3- Gy. Sipos, B. Czukar and Z. Dobó, ibid, 1963, 9, 48.

4- Gy. Sipos and F. Sirokman, Nature, 1964, 202, 898.

5- Gy. Sipos and Gy. Schobel, J. Chem. Soc. (C), 1970, 1154.

6- Gy. Sipos, Gy. Schobel and F. Sirokman, J. Chem. Soc., Perkin II, 1975, 805.

7- (a) D.S. Noyes and W.A. Pryor, J. Amer. Chem. Soc. [illegible]

(b) D.S. Noyes and W.L. Reed, ibid, 1958, 80, 5539.

8- W.I. Awad, S. Nashed, S.M. Hassan and H.A. Badawy, Egypt. J. Chem., 1976, 18, 121.

9- D.A. Shirley, "Preparation of Organic Intermediates.", Wiley, New York, 1951, 71.

10- A.L. Wilds and T.L. Johnson, J. Amer. Chem Soc., 1945, 67, 287.

11- P. Kunckell, Ber., 1897, 80, 578.

12- A. Collet, Compt., rend., 1897, 125, 718.

13- Oyster and Adkins, J. Amer. Chem. Soc., 1921, 43, 208.

14- A. Vogel, "Practical Organic Chemistry.", Longmans, Green and Co., 1959, 177.

15- J. Hine and D.E. Lee, ibid, 1951, 73, 22.

16- S.B. Hanna, Y. Iskander and Y. Riad, J. Chem. Soc., 1961, 217.

17- W.I. Awad, Z.S. Salih and Z.H. Aiube, J. Chem. Soc. Perkin I, 1977, 1280.

18- E.S. Amis, "Kinetics of Chemical Change in Solution.", Macmillan Co. of Canada, 1949, 179.

Products from Darzens' reaction of Phenanthrenequinone

with p-substituted Phenacyl chlorides in alkaline medium.

Compound (I)	Formula	Yield %	m.p. °C.	Found C	Found H	Found Cl	Required C	Required H	Required Cl	ν_{max} cm^{-1} OH	ν_{max} cm^{-1} C=O	Solvent of crystallization
X = H	$C_{22}H_{14}O_3$	94.4	197.0	80.5	4.3	-	81.0	4.3	-	3326	1695	2 : 1 gl. acetic:H_2O (v/v)
X = Cl +	$C_{22}H_{13}O_3Cl$ (keto form)	50.0	165	73.0	3.8	9.7	73.2	3.6	9.8	-	1680	methanol
X = Cl	$C_{22}H_{13}O_3Cl$	95.5	210	72.9	3.3	9.9	73.2	3.6	9.8	3220	1695	methanol
X = CH_3	$C_{23}H_{16}O_3$	91.8	176	81.0	5.0	-	81.2	4.7	-	3230	1700	benzene-pet. ether (40-60)
X = OCH_3	$C_{23}H_{16}O_4$	89.9	184	77.7	4.4	-	77.5	4.5	-	3230	1700	benzene-pet. ether (40-60)

+ This compound was obtained when the reaction was carried out at -3° with molar ratio of 1 : 1 : 1 of A : B : OH^- components, respectively: along with 40% enol form.(Initial concentration of phenanthrenequinone 0.001 M)

Table (2)

Rate constants for condensation reactions

at -3° in 50% aq. dioxan.

substituted phenacyl chloride (0.001 M)	molar ratio of A : B : OH^- 1 : 1 : 1 k_3 $l^2/mole^2.sec$	1 : 1 : 10 k_2 l/mole.sec	1 : 1 : 10 k_3 $l^2/mole^2.sec$
p- chloro	1.25×10^2	3.33	3.33×10^2
unsubstituted	0.833×10^2	2.08	2.08×10^2
p-methyl	0.694×10^2	1.37	1.37×10^2
p-methoxy	0.463×10^2	1.14	1.14×10^2

Table (3)

Rate constants at different temperatures

in 50% aq. dioxan

Temp. °C.	k_3 $l^2/mole^2.sec.$			
	p-chloro	unsubstituted	p-methyl	p-methoxy
-10	2.08×10^2	1.14×10^2	0.80×10^2	0.667×10^2
-7	2.50×10^2	1.43×10^2	1.07×10^2	0.864×10^2
-3	3.33×10^2	2.08×10^2	1.37×10^2	1.14×10^2
+1	4.67×10^2	2.67×10^2	1.80×10^2	1.67×10^2

Table (4)

Thermodynamic activation parameters

substituted phenacyl chloride	E^* K. cal/mole	ΔH^* K.cal.	ΔS^* e.u.	ΔG^*_{274} K. cal.
p-chloro	9.15	8.61	-31.70	17.29
unsubstituted	11.44	10.90	-24.46	17.60
p-methyl	12.58	12.40	-21.09	17.82
p-methoxy	13.07	12.53	-19.44	17.85

Fig. 1 Pseudo second order kinetics at -3°. Molar ratios 1:1:1

Fig. 2 True third order kinetics at -3°. Molar ratios 1:1:1

Fig. 3 Dependence of rate constants on dielectric constants of the solvents at 1°

Fig. 4 Validity of the Hammett equation for the different substituents

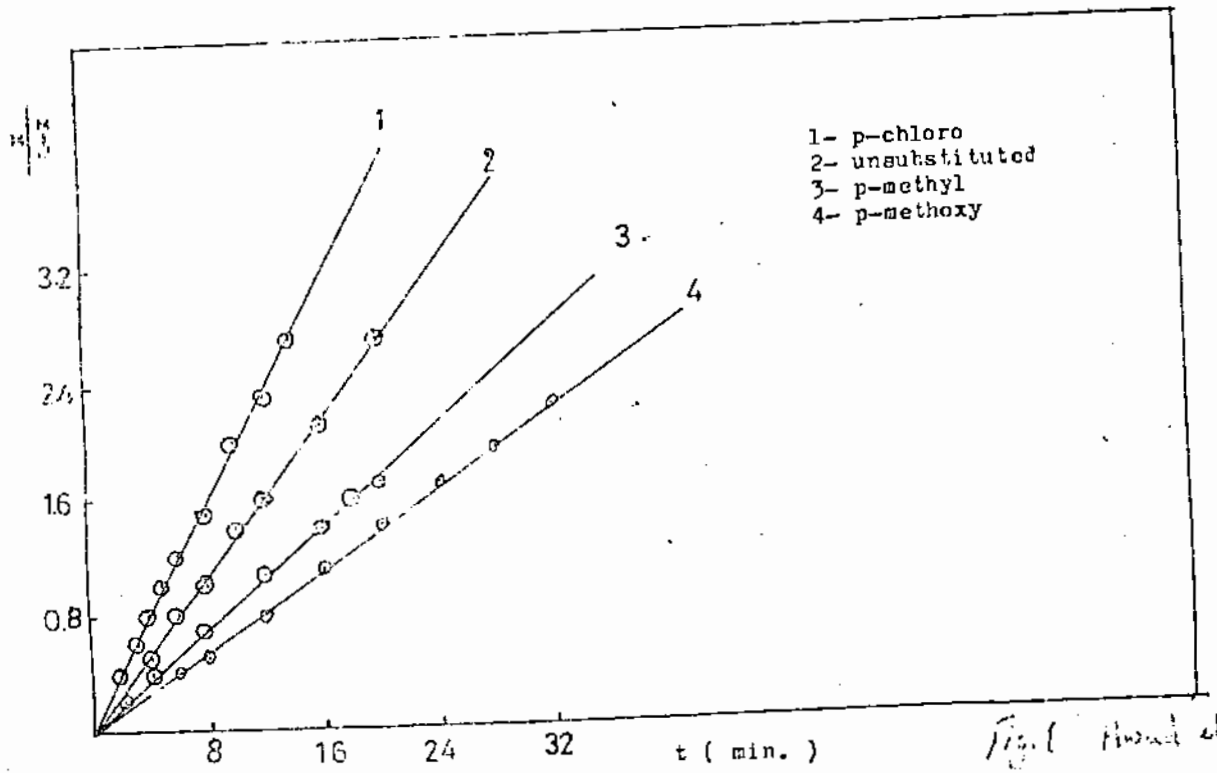
1- p-chloro
2- unsubstituted
3- p-methyl
4- p-methoxy
3.2
2.4
1.6
0.8
8
16
24
32
t (min.)

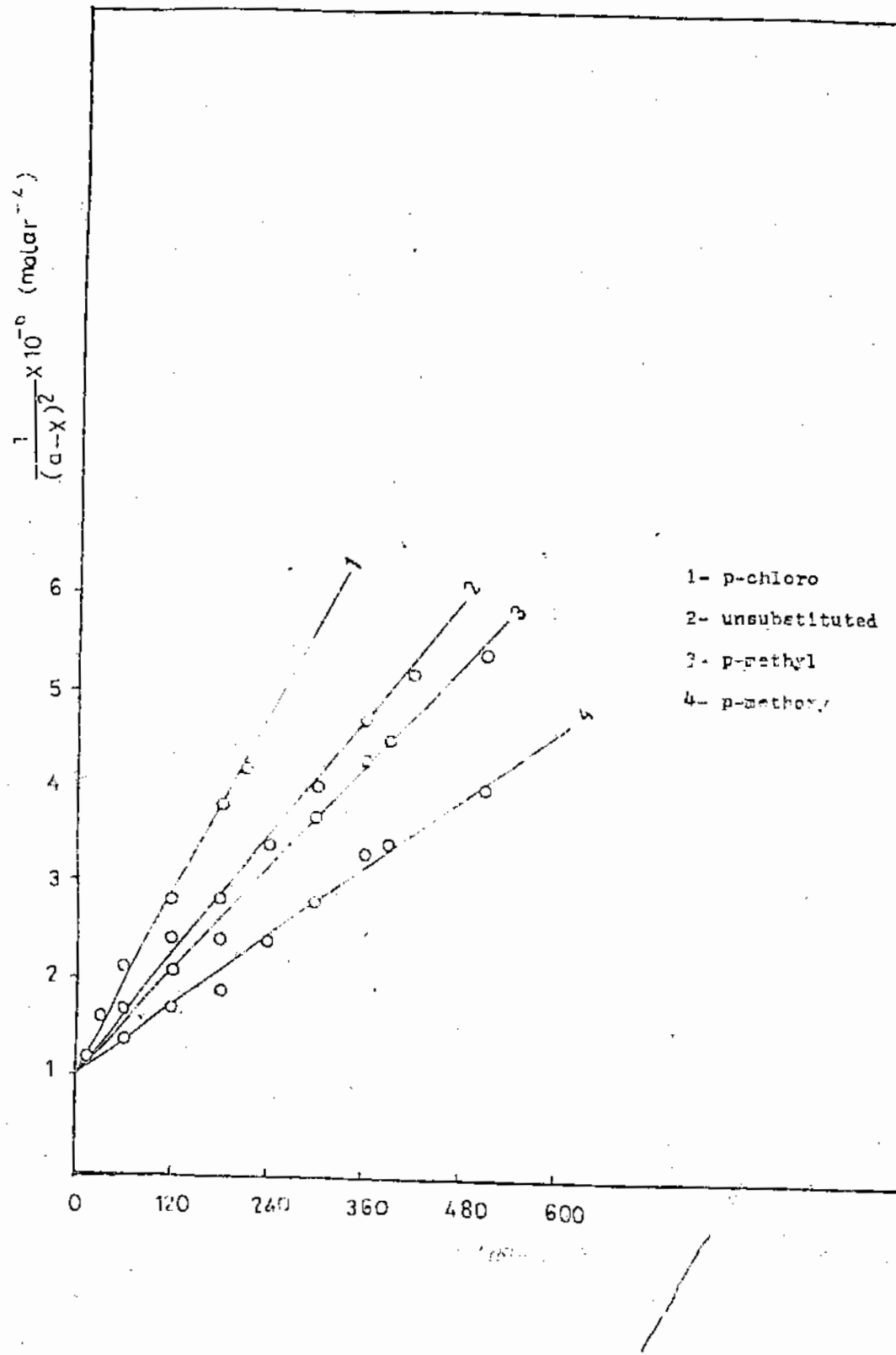
$\frac{1}{(a-x)^2} \times 10^{-6}$ (molar^{-2})
1
2
3
4
5
6
0
120
240
360
480
600
1- p-chloro
2- unsubstituted
3- p-methyl
4- p-methoxy

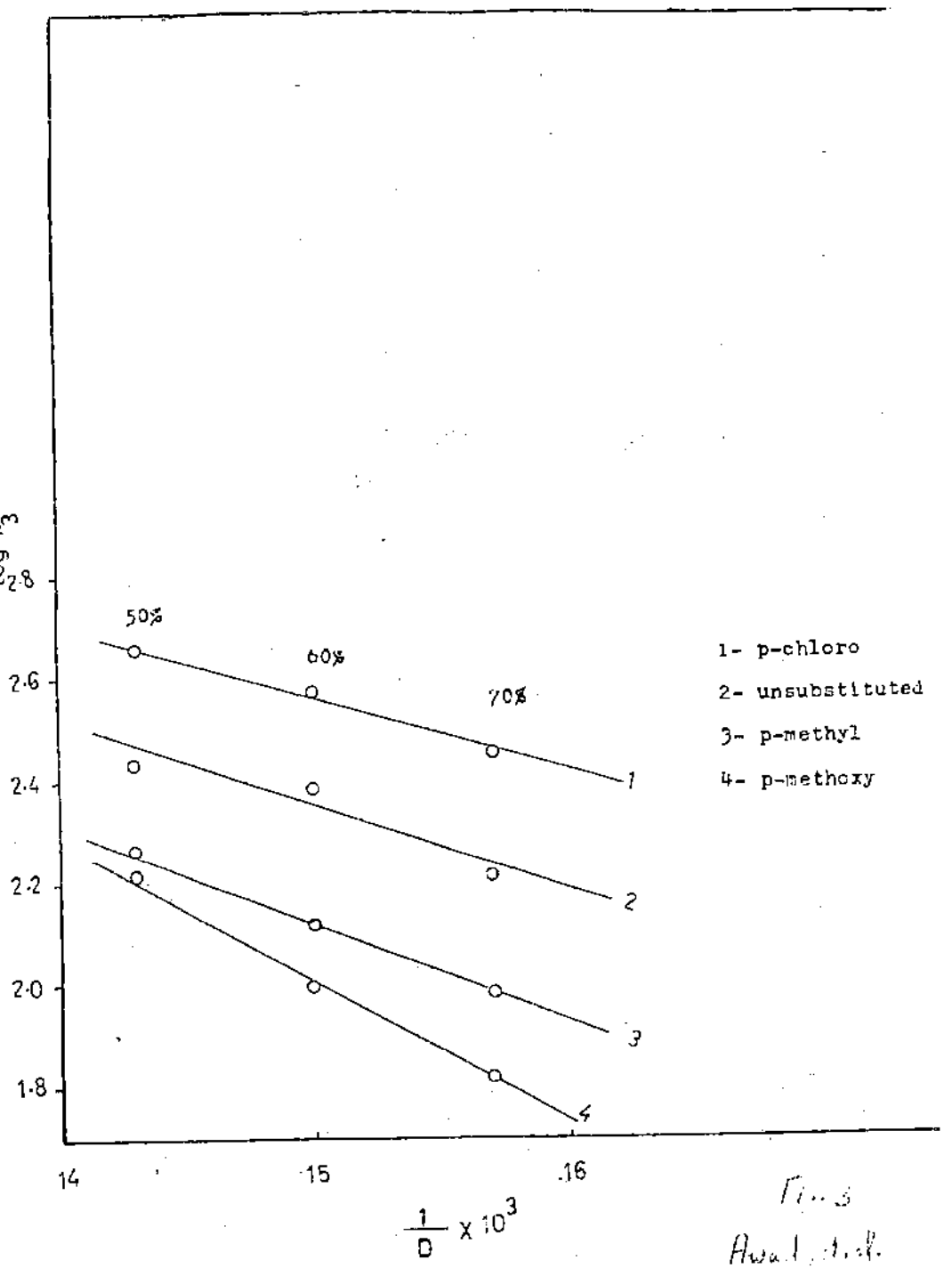
50%
60%
70%
1
2
3
4
1- p-chloro
2- unsubstituted
3- p-methyl
4- p-methoxy
2·8
2·6
2·4
2·2
2·0
1·8
14
15
16
$\frac{1}{D} \times 10^3$

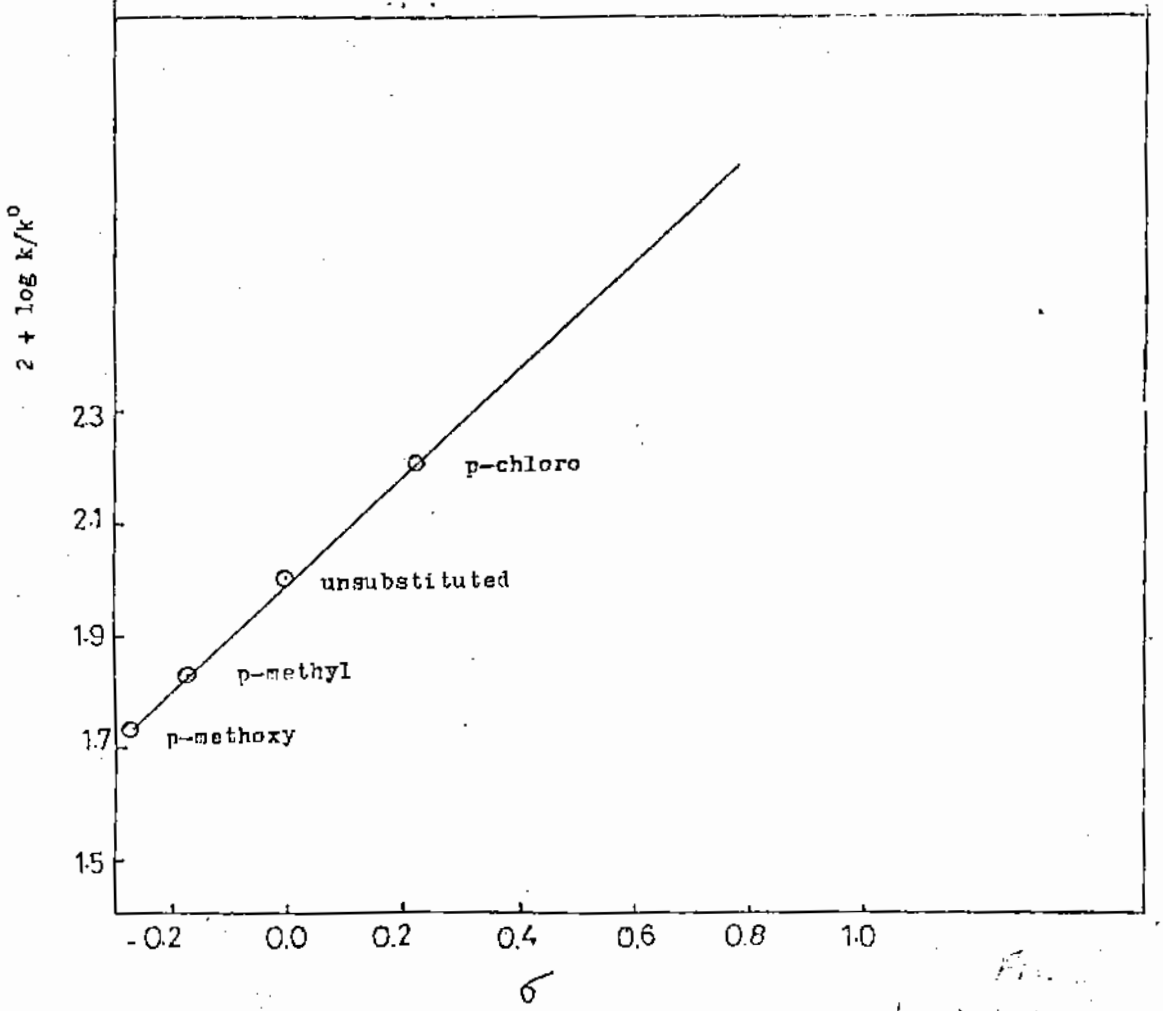
2 + log k/k°
2.3
2.1
1.9
1.7
1.5
p-chloro
unsubstituted
p-methyl
p-methoxy
- 0.2
0.0
0.2
0.4
0.6
0.8
1.0
σ

دراسة كينيتيكية على تأثير المجاميع المستعاضه على تفاعل دارزن الحفزى القاعدى

وليم ابراهيم عوض ، أحمد عبد الرحيم طه ، وصفى نقولا واصف ، سعاد محمد شنودى
قسم الكيمياء - كلية البنات - جامعه عين شمس

تمت فى هذا البحث دراسة كينيتيكية التكثيف الحفزى القاعدى لكل من كلوريد الفيناسيل ، وبارا - ميثوكس ، باراسيتيل ، وبارا - كلوروكلوريد الفيناسيل مع الفينانثرين كينون ، وذلك بدراسة تغير تركيز ايون الكلوريد الى الناتج ، عند درجات حرارة مختلفة .

وقد اظهرت النتائج ان التفاعل من الرتبة الثالثه بصفة كلية ، ومن الرتبه الاولى بالنسبه لكل من المتفاعلات ، المراد المتفاعله .

كذلك اظهرت النتائج ان تفاعل التكثيف يزداد معدله بزياده قدرة المجاميع المستعاضة على سحب الالكترونات . كما ان المعدل يزداد بزيادة قطبية المذيب .

وقد فشلت محاولات تتبع هذا النوع من التفاعل عند اجرائه على اساس حفزى حمضى ، سواء مع الفينانثرين كينون او مع البارا - نيتروبنزالدهيد .

Received: 27.4.1982 (F)

Spectroscopic and Radiolysis Studies on the Interaction of Cobalt with Nitrilotriacetic Acid

by

Wafaa S. Hegazy, Marguerite A. Wassef and Faten M. Zakaria

Department of Chemistry, University College for Women, Ain Shams University, Cairo, Egypt.

Abstract

The stoichiometry and stability of the complexes formed between Co(II) or Co(III) and nitrilotriacetic acid (NTA) were spectrophotometrically investigated. The chelation of the hydrolysed state of Co(III) with NTA was also studied. The behaviour of Co(II)-complex on irradiation with cobalt-60 γ-rays was followed spectrophotometrically.

Introduction:

The interaction between several polyaminopolycarboxylic acids and cobalt ions was extensively studied. The aminopolycarboxylic acid, nitrilotriacetic acid, NTA, was shown to form fairly stable complexes with divalent and tervalent cobalt ions.[1,2] To our knowledge, the study was carried out only potentiometrically and within certain concentration range of both the acid and the metal ions. The present work is concerned with the study of the interaction between cobalt and NTA spectrophotometrically using different concentration ranges. Radiolysis of the formed equimolar Co(II)-NTA complex was carried out using Co-60 γ-rays. According to the results obtained, a radiolytic mechanism was suggested. Such study may be useful in the evaluation of NTA as a decontaminating agent in case of radioactive cobalt contamination of the environment.

Experimental:

All the chemicals used were A.R. reagents. Co^{2+} complexes were prpared by mixing the proper amount of $CoCl_2.6H_2O$ solution with that of

the sodium salt of the acid. Co(III)-chelates were prepared from Co(II)-ones.[3] Aqueous solutions were prepared in carbon dioxide-free double distilled water.

The chelation of the hydrolysed state of Co(II) with NTA was carried out by preparing a series of 4×10^{-2}M solutions of cobaltous chloride adjusted at different pH values and aged for various time periods, followed by the addition of equal volumes of 1.6×10^{-1}M NTA solution, adjusted at the same pH value. Optical densities were measured as a function of pH and standing time.

Spectrophotometric measurements were carried out on Veb Carl Zeiss Jena, Specord UV-Vis spectrophotometer, using 1 cm quartz cells. pH-adjustments were done using TDA, HM-7B pH-meter with a combined glass-calomel electrode.

Irradiations were carried out on 2 ml samples of mixtures of 1×10^{-3}M Co^{2+} and 4×10^{-3}M NTA with γ ^{60}Co-radiation source at a dose rate of 1.66×10^{3} rad./min. The dose rate was determined with the Fricke's ferrous dosimeter. The radiolytic yields were determined spectophotometrically[4] in the UV region.

Results and Discussion:

A. Chelation of each of Co^{2+} and Co^{3+} with NTA:

The interaction between Co^{2+} and Co^{3+}, with NTA was studied spectrophotometrically by the continous variation,[5,6] mole ratio[7] and slope ratio[8] methods. It was found that mixtures of NTA with either cobalt ions obey Beer's law and absorb in the ultraviolet as well as in the visible regions. However, the examination of the spectra in the visible region is restricted only to concentrated solutions because the molar absorption coefficient is relatively low. An obvious shift in wave length due to complexation could be observed. These results are listed in table 1. Co(II)-NTA mixtures having different mole ratios exhibit absorption maxima at λ = 220 and 523 nm between pH 4.5 and 7.5, while Co(III)-complexes show absorption maxima peaks at λ = 250, 400 and 540 nm between pH 7.5 and 9.0.

Applying the continous variation method[5] and its modification,[6]

the results indicated that the shape of a respective curve depends, within certain concentration range, on the total concentration of Co(II)-NTA. For a total concentration of 0.5×10^{-3} M, the representation curve has two maxima at mole fractions 0.5 and 0.66 corresponding to 1:1 and 2:1 complexes, respectively. At higher concentration, the curve has a maximum corresponding to 1:1 complex. This was confirmed by the results obtained by the mole ratio and the slope ratio methods. Guided by these results, the Co^{3+} complexes were studied using concentrated solutions (4×10^{-2}M).

Calculation of the stability constants of both Co^{2+} and Co^{3+} chelates were carried out using Job's equations.[5,6] The values of log K are 10.8 $\pm$ 0.1 and 14.6 $\pm$ 0.2, respectively.

B. Chelation of the hydrolysed state of Co^{2+} with NTA :

The chelation of the hydrolysed state was carried out as a function of pH and standing time. The data obtained are presented in Fig. 1. It was observed that on adjusting the pH of Co^{2+} solution at 7, 8, 9 and 10, a blue precipitate of $Co(OH)_2$ is formed. For all time intervals, the precipitate formed at pH 7 and pH 8 dissolved completely and instantaneously in NTA giving clear pink and brown solutions, respectively. At pH 9 and 10, partial solubility occurs. For such samples separation of the precipitates was carried out by centrifugation directly before recording the spectra. It is to be noted that, all the spectra exhibit maximum absorption at λ = 540 nm. Compared with the optical density-pH curve for fresh solution mixture of Co^{2+} and NTA , it could be concluded that at 48 hours aging time, a remarkable decrease in optical density occured at the pH range from 3 to 7, after which an increase started and reached a maximum value at pH= 8.5, then a sharp decrease occured at pH $\geq$ 9. The general decrease in the optical density could be due to the formation of Co(II) hydroxide, hence lowering the extent of chelation with NTA. However, on increasing the pH from 7 to 8.5, the observed increase in the optical density may be attributed to the oxidation of Co(II) with the oxygen of the air in alkaline medium to give Co(III). These latter species would then interact with NTA forming Co(III)-NTA chelate, as indicated by the maximum absorption at λ= 540 nm and at a relatively high pH value. On the other hand, the solutions aged for one, two and three weeks show a general and gradual increase in the optical density as a function of pH and reached a maximum value at 7.5. This may be explained on the basis,

that as the precipitate, Co(II)-hydroxide is more aged, the process of oxidation of Co(II) to Co(III) become more likely. Accordingly, the pH at which the maximum absorbance occurs is shifted to lower value (7.5) than the case of 48 hours-age time. From figure 1, it is obvious that nearly a constant value of optical density was obtained, in each case, for the pH values 4, 5 and 6. This pH range is characteristic, as reported previously, for the stability of Co(II)-NTA complex. Accordingly, it is supposed that the complete oxidation of Co(II) to Co(III) occurs beyond this pH range. The decrease in the optical density at higher pH values ($>$ 8.5 in the case of 48 hours and $>$ 7.5 in the other cases) may be due to the incomplete solubilization of the precipitate as mentioned before. For the hydrolysed state aged for 4 weeks, a slight decrease in the optical density, at pH values, than that aged three weeks could be shown in Fig. 1. This would mean that as the precipitate is aged longer, some of the hydroxide may change to polymolecular hydrolysed state,[9] which may absorb at a different wave lenghts thus causes the observed decrease in the O.D.

C. Radiolysis of Co^{2+}-NTA complex in aqueous and aerated solution with γ ^{60}Co-radiation:

The irradiation was made on (Co^{2+}-NTA) mixtures, at different pH values, namely 4.5 and 7.5. Plots of the optical density versus the dose absorbed for mixtures of different mole ratios at the two considered pH values are shown in Figure 2.

According to the experimental results, it could be postulated that at pH 4.5 decomposition of the complex occurred, while at pH 7.5 decomposition of the complex occurred, while at pH 7.5 Fig. 2 oxidation of the chelate appears to be the probable process taking place.

The following mechanism for both degradation and oxidation is suggested, which is identical to that discussed before for other cobalt chelates.[10,11]

I. Degradation of the complex:

As the radiolysis is carried out in aered solutions, the reducing species H and $e_{aq.}$ will react with oxygen to give H_2O and O_2^-, respectively:[12,13]

$$H + O_2 = HO_2$$

and

$$e_{aq.} + O_2 = O_2^-$$

The two radicals H_2O and O_2^- react with each other in aqueous solutions as follows:

$$HO_2 + O_2^- \longrightarrow H_2O_2 + O_2 + OH^-$$

Many published work[14,15] have reported that the aminocarboxylic acids were easily attacked via the OH radical, leading to the abstraction of a hydrogen atom from the carbon attached to the carboxylic group. Accordingly, the following reaction may take place:

$$Co^{2+}RNCH_2COO^- + OH = \underset{(I)}{Co^{2+}RNCHCOO^-} + H_2O$$

where $Co^{2+}RNCH_2COO^-$ represents the Co(II)-NTA complex.
In presence of oxygen, the species (I) may add O_2 as follows:

$$Co^{2+}RNCHCOO^- + O_2 = \underset{(II)}{Co^{2+}RNCH(O_2)COO^-}$$

The oxygenated intermediate (II) is unstable and should stabilize itself through the following reaction:

$$Co^{2+}RNCH(O_2)COO^- + H_2O = Co^{2+}RNCH + CH_2O + O_2^- + CO_2$$

The liberated formaldehyde was detected and determined experimentally,[14] its G value was found to be 0.5 ± 0.1. For the 1:1 (Co(II)-NTA) chelate, the G value was determined from the slope of the straight line O.D.-Dose relationship (Fig. 2). It was found to be equal to 3.55 ± 0.2.

According to the above mechanism, the radiolytic degradation of Co(II)-NTA complex may be due only to the OH radical, and thus $G_{Co(II)}$ should be equivalent to G_{OH}. Actually, the experimental value is much higher than that of OH radical. This could be interpreted as being due to oxidation of the complex via H_2O_2 accompanying its degradation. In such a case, the observed G value should be equivalent to the sum of G_{OH} and $G_{H_2O_2}$, which is quite fulfilled.

2. Oxidation of the complex:

The reaction between H_2O_2, as an oxidizing agent, and Co(II)-NTA

chelate during radiolysis, specially in neutral and alkaline media, have to be considered. As a result, the divalent cobalt chelate is converted the corresponding tervalent cobalt one according to :

$$Co^{2+}RNCH_2COO^- + H_2O_2 = Co^{3+}RNCH_2COO^- + OH + OH^-$$

It was found that oxidation varies linearly with the dose absorbed. The G value of the formed Co(III) from the 1:1 Co(II)-Complex was determined from the corresponding curve. It was found to be equal to 1.6 $\pm$ 0.1. Similar results were obtained during the radiolysis of other cobalt chelates.[10,11]

Acknowledgment:

The authors are most indebted to Prof. Dr. Mohamed B. Hafez for his sincere assistance. The authors are also grateful to the facilities provided by the Atomic Energy Establishment lab, in which the radiolysis part of this work was excuted.

References

1. G. Schwarzenbach and E. Freitag, Helv. Chim. Acta, 1950, 34, 1492; b. L. Holleck and Hartinger, Angew. Chem., 1950, 68, 411.

2. K. Agrawal, K. Dwivedi, M. Chandra, V. Agarwala and A. Dey, J. Indian Chem. Soc., 1977, 54, 9[illegible].

3. M. Krishnamurthy, J. Inorg. Nucl. Chem., 1972, 34, 3915.

4. A.J. Swallow, "Radiation Chemistry, an Introduction", 1973, Longman, London, P. 50, 150.

5. Job. Ann. Chim., 1928, (10)9, 113; ibid., 1936. (11)5, 97.

6. F. Sherif and A. Awad, J. Inorg. Nucl. Chem., 1962, 24, 17[illegible].

7. J. Yoe and A. Johnes, J. Anal. Chem., 1944, 16, 111; A. Meyer and G. Ayres, J. Amer. Chem. Soc., 1957, 79, 49.

8. A.B. Hartley and D.L. Manning, J. Amer. Chem. Soc., 1950, 72, 4488.

9. J. Partington, "General and Inorganic Chemistry", 1958, P. 867.

10. M. Hafez, N. Hafez and W. Higazi, Isotopen praxis, 1979, 7, 219.

11. M. Hafez, N. Hafez and W. Higazi, J. Radioanalyt. Chem., 1979, 49, 37.

12. A.Swallow "Radiation Chemistry, An Introduction", Longmen, London, 1973, P. 136 .

13. J. Rabani and G. Stein, Radiat, Res., 1962, 17, 327.

14. S.N.Bhattacharyya, K.P.Kundu,Radiat.Res.,51, 1972, 45.

15. N.Matsuura,N.Shinohara and M.Takizawa,Bull.Chem. Soc.Japan,1967,40,2042.

Table 1

Various values for the molar extinction coefficient, ε, at different $\lambda_{max.}$ for Co(II), NTA and the Complex (Co(II)-NTA)

Species	λ_{max} (nm)	ε $M^{-1}.cm^{-1}$	pH-interval
Co(II)	200, 500	25, 5	
NTA	208	5.5×10^3	
Co(II)-NTA (1:1)	220 and 523	1.9×10^3, 40	4.5 - 7.5
Co(III)	200, 500	1.8×10^2, 7	
Co(III)-NTA (1:1)	250, 400 and 540	4.67×10^2, 125	7.5 - 9

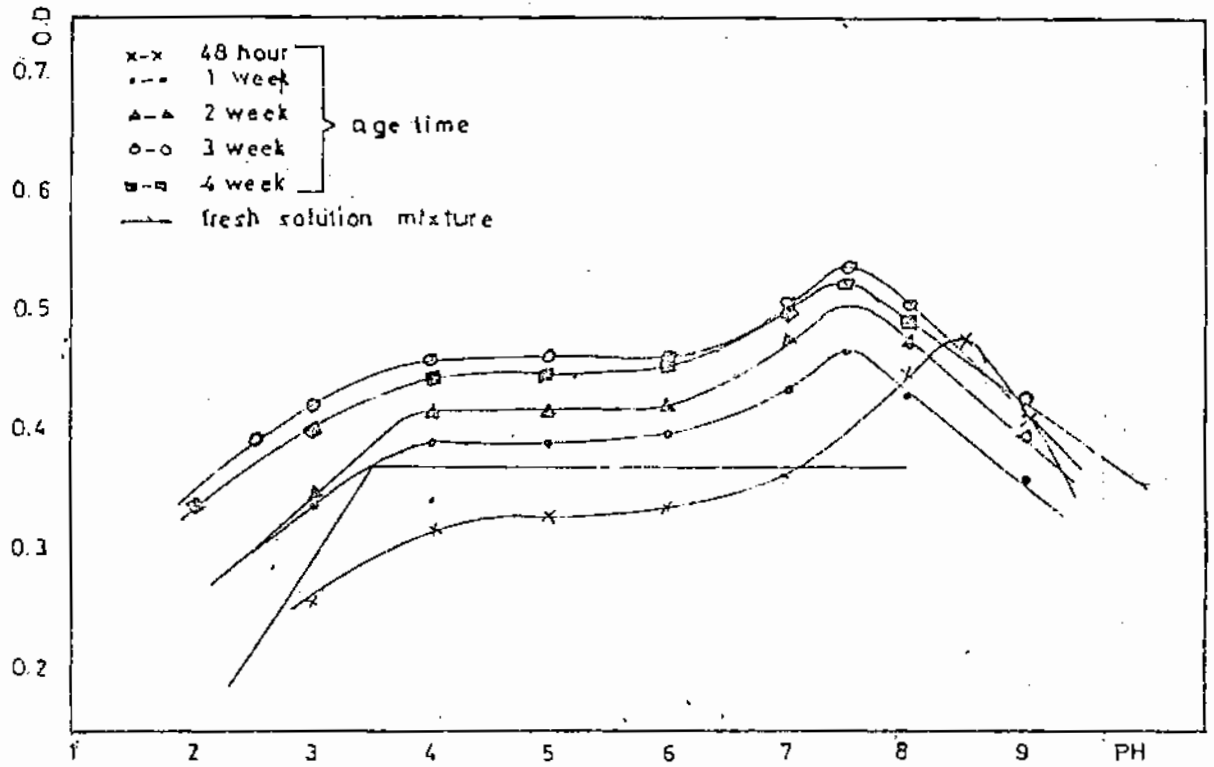

Fig. (7): Variation of the Optical Density of (Co(II)-NTA) Mixtures with pH and Aging Time

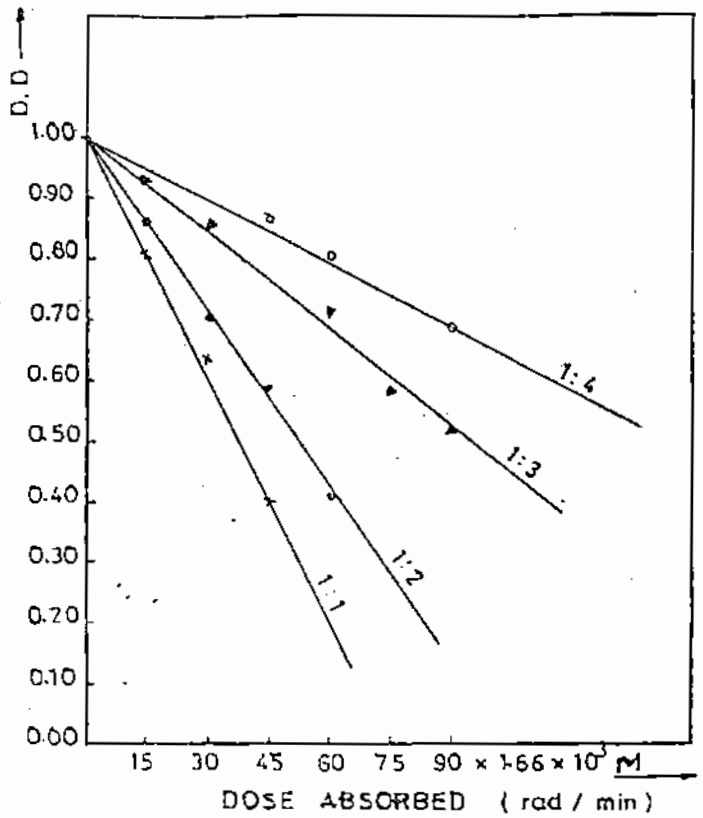

Fig. (2): Gamma radiation induced degradation of 1:1, 1:2, 1:3 and 1:4 Co(II)-NTA mixtures at pH 4.5 at λ = 205 nm.

Formation Constants of the Complexes of Some Prop-2-enoates and Pent-4-enoates with Cu(II)

By

Boshra M. Awad and Nadia R. Guirguis

Chemistry Department, University College for Women, Ain Shams University, Cairo.

Abstract.- This paper deals with the determination of dissociation and stability constants of the Cu(II) complexes of some prop-2- and pent-4-enoates by pH-metric method.

The interaction of Cu^{2+} with substituted benzoic acids has been studied in 50% dioxane-water mixture.[1] Pethe and Mali[2] extended the study for some lanthanides with methoxy substituted benzoic acids. Complexing ability of thiocarboxylic acid has also been studied potentiometrically.[3]

The present work is a continuation of our earlier studies on the complexation of some itaconates and cinnamates with Cu(II) and is undertaken in an attempt to find out whether the aromatic residue has an effect on the complexes formed.[4]

Experimental.- The ligands (E) (naphthyl/COOMe) methyl 2-o-carboxyphenyl-3-(1- and 2-naphthyl)prop-2-enoates I and II, respectively, and (E) 4-methoxycarbonyl-3,3-dimethyl-5(1- and 2-naphthyl)pent-4-enoic acids III and IV, respectively, have been prepared according to the methods adopted in the

literature.[5] Their purity were ascertained from their melting points. The structures of these compounds were established and inferred.[5]

Measurements technique.- A PYE Unicam pH meter Model 290, in conjugation with glass calomel electrode assembly was used for pH measurements. Potassium hydrogen phthalate buffers were used to standardise the pH meter. All the reagents used were Analar, BDH and the titrations were carried out in a thermostated closed cell at 25 ± 0.1°C in a nitrogen atmosphere. Dioxane was purified before use by the standard method.[6] Carbonate-free sodium hydroxide solution was prepared and standardised potentiometrically against standard potassium hydrogen phthalate. The complex solutions were prepared by adding 50 ml of 0.01M solution of the ligand in dioxane to 50 ml redistilled water containing 0.003M copper perchlorate and 0.02931M perchloric acid. 0.5M sodium hydroxide was used for the titration.

The nature of dissociation of the ligands was measured potentiometrically in 50% v/v aqueous dioxane at 25°. From the titration curves the dissociation constants of the ligands pK_L were determined. The values obtained are given in Table 1. The metal-ligand stepwise stability constants have been determined by Bjerrum-Calvin titration technique.[7,

Results and Discussion.

The successive constants are calculated following Poulsen et al.[9] method. From the titration curves, $\bar{n}$,

the average number of lignads bound to the central-metal ion and A, the concentration of the free ligand species in solution could be calculated.

From the titration curves it is observed that the metal-ligand curves are well separated from the ligand titration curves proving that the liberation of protons is due to chelation. The formation curves (Fig. 1) for the complexes formed by Cu(II) with ligands I - IV show two inflection at $n \simeq 1$ and $n \simeq 2$ indicating the stepwise formation of 1:1 and 2:1 molar ratio of L:M. The stepwise formation constants K_1 and K_2 have been determined graphically following the method adopted by Poulsen et al.[9] The values of pK_{LM} were calculated graphically according to the method given by Calvin and Wilson[7] and also by Uitert and Hass[10]. The values of log K_1, log K_2 and pK_{LM} for the complexes at 25° are tabulated in Table 1.

Table 1

Stability Constants of Cu(II)-Ligand Complexes and Dissociation Constants of Ligand at 25°

Ligand	pK_L	pK_{LM}	log K_1	log K_2	$K_{(av)}$
I	6.10	6.00	3.29	3.04	1461
II	6.37	5.88	3.24	2.99	1302
III	7.04	6.59	3.08	2.83	878
IV	6.88	6.47	3.12	2.90	1076

From the results obtained, it is observed that the stability constants of copper complexes of the ligands under

investigation decrease in the order :

$$I > II > IV > III$$

The increase of the stability of the copper complexes of compounds I and II than those of compounds III and IV is attributed to the presence of the electron-withdrawal phenyl group which inhances the capacity of complexation.

Moreover, the coplanarity of the phenyl group makes the metal-ligand ring comparatively more stable than the methyl group. The electron-withdrawing phenyl group pulls electrons from Cu(II) ion, increases its back donation and hence the stability of the complex. This group withdraws electrons away from the proton in the parent acid resulting in a larger dissociation constant. The presence of the electron-donating alkyl groups increases the bond stability between the acid anion and the proton, thus decreases the back donation between the anion and the Cu(II) ion producing a less stable complex a smaller stepwise formation constants. The larger dissociation constant of 1-naphthyl derivative (I) than 2-naphthyl-(II) is in harmony with the naphthoic acids where the dissociation constants of 1- and 2-naphthoic acids are 2.00×10^{-4} and 6.80×10^{-5}, respectively. However, the presence of alkyl group probably makes the dissociation of 2-naphthyl derivative and the complex formed by this ligand larger than the 1-naphthyl derivative. The negative free energies of activation indicates that such complexation takes place spontaneously (Table 2).

Table 2

Free Energies for Stepwise Formation of Cu(II) Ligands at 25°

Ligand	log K_1	$-\Delta G^\circ$	Log K_2	$-\Delta G^\circ$
I	3.29	4.516	3.04	4.1717
II	3.24	4.444	2.99	4.1061
III	3.08	4.2207	2.83	3.8848
IV	3.12	4.2784	2.90	3.9767

The metal-ligands formula is suggested as follows

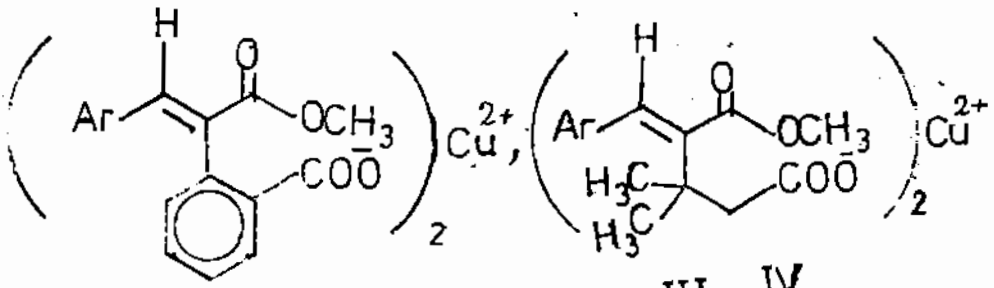

I - II

III - IV

Ar = 1- or 2-Naphthyl

References

1. W.R. May and M.M. Jones, J. Inorg. and Nuclear Chem., 24, 511 (1962).
2. L.D. Pethe and B.D. Mali, Indian J. Chem. Soc., 55, 846 (1978); 55, 364 (1978).
3. K.P. Dubey and M.K. Puri, Rev. Chem. Miner., 12(3), 255 (1975).
4. B.M. Awad and N.R. Guirguis, Egypt.J.Chem., 23(5),287 (1980).
5. S.M. Abdel Wahhab, B.M. Awad, N.R. Guirguis and T.H. Salem, Egypt.J.Chem., 23(1), 47(1980); ibid, 23(2),137(198
6. A.I. Vogel "A Text Book of Practical Organic Chemistry", Longman Green and Co., p. 177 (1956).
7. M. Calvin and K. Wilson, J. Amer. Chem. Soc., 67, 2003 (1945).
8. J. Bjerrum, "Metal amine formation in aqueous solution", Hease, Copenhagen, 1941.
9. K.G. Poulsen, J. Bjerrum and J. Poulsen, Acta Chem. Scand., 8, 921 (1954).
10. L.G. Van Uitert and C.G. Haas, J. Amer. Chem. Soc., 75, 451 (1953).

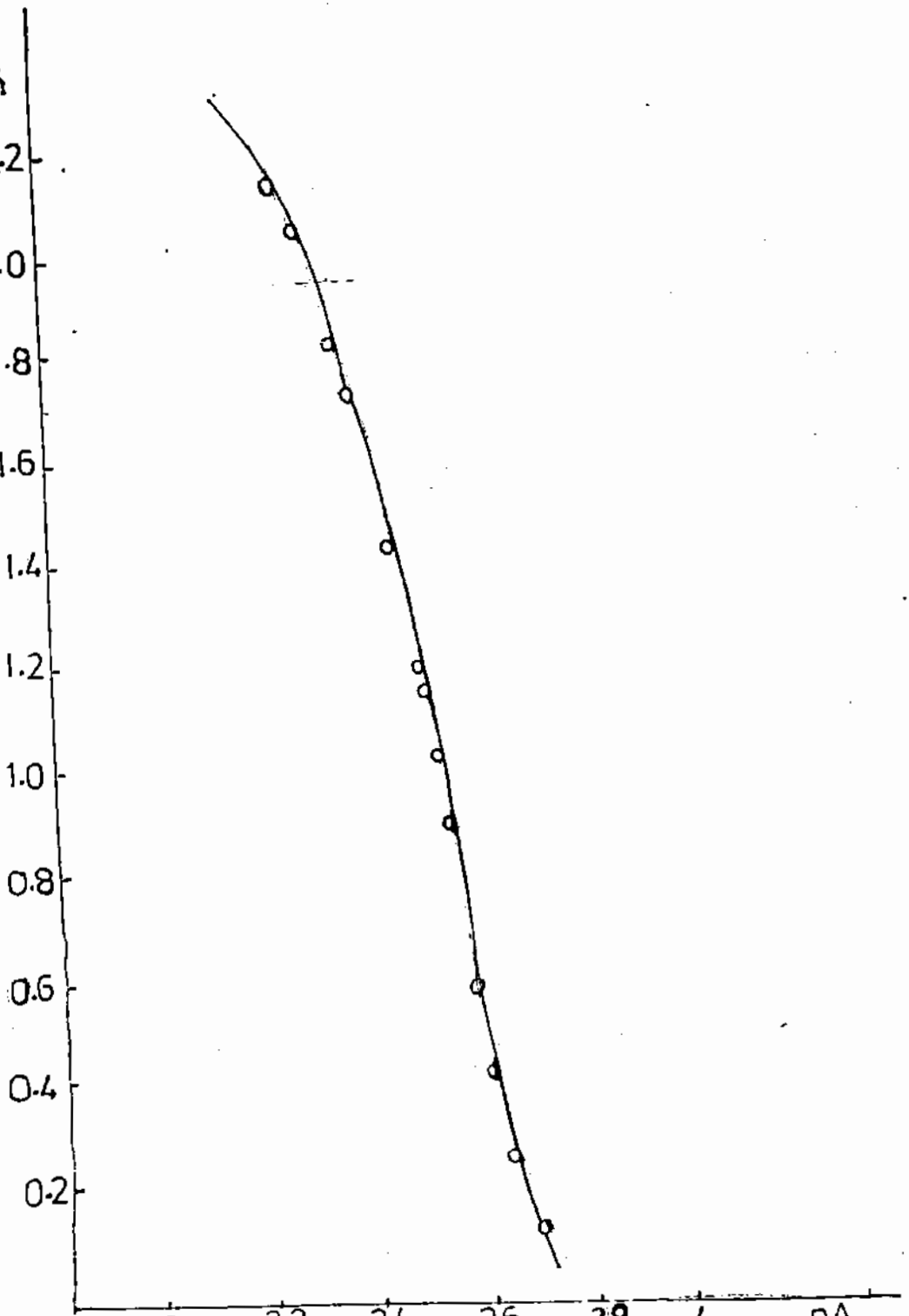

Fig 1

Corrosion Behaviour of Iron in Phosphate Solutions

By
Kh. M. Kamel, A.A.Kassab and O.R.Khalifa
Chemistry Department, University College for Girls,
Ain-Shams University, Heliopolis, Cairo
Egypt

Introduction:

Few studies have been carried out on theelectrochemical behaviour of metals in phosphate solutions. The results obtained for lead[1] and tin[2] showed that the nature of the phosphate film and the concentration ranges within which the electrode exhibits reversible behaviour depend on the electrode material and the solution pH. In case of zinc[3], no thermodynamic behaviour was observed. In addition to given information regarding the charac teristics of metals as phosphate electrodes, these studies help to clarify the mechanism by which phosphate ions inhibit the corrosion of metals. In continuation to our work in this field. We investigate the behaviour of iron.

Experimental:

The potential of the iron electrode was measured as a function of time within a period of four hours in aqueous phosphate solutions of concentration varying between 5×10^{-4} and 1 M. In order to prevent any variation

in potential due to pH changes, the phosphate solutions were adjusted to definite pH values. Various series of solutions covering the pH range 2-11 were used; the composition of these has already been given[1]. The pH values were checked with the hydrogen electrode and when possible, with the quinhydrone electrode.

The electrodes were prepared from Analar iron rods 3 mm in diameter (B.D.H. England). Before use, the electrode was abraded successively to 00 finish, degreased with acetone and then washed thoroughly with water. Each experiment was carried out with a newly polished electrode and with fresh portion of the solution. A saturated calomel electrode was used as a reference electrode and the potentials are corrected to the normal hydrogen scale. The potential ws measured with the aid of a Cambridge potentiometer readible to 0.5 millivolt. The results were reproducible to $\pm$ 5 millivolts.

Determination of the corrosion rate was also carried out using the weight-loss technique. Experiments were performed on iron pieces measuring 5 x 10 cm and 0.8 mm. thick, cut from Analar iron sheet. The test pieces were first degreased with acetone and then etched in a solution containing 15 g/l $Na_3 PO_4$ + 20 g NaOH at 80-85^{o} for 1 min. They were then washed with conductivity water, dried in alcohol and ether and then weighed. Corrosion tests were carried out in a wide 200 ml jar,

in which the specimen was suspended for 2 hours in the test solution. The specimen was then removed, rinsed with conductivity water and finally dried and weighed. All corrosion tests were carried out in aerated unstirred solutions. — Results were duplicated and the mean was computed.

The chemicals used in all experiments were of Analar grade. All measurements were carried out at $30^{o}C$ in an air thermostat controlled to $\pm$ 0.5 .

Results and Discussion:

Corrosion of Iron in Acid Phosphate Solutions:

The steady state potentials obtained four hours after immersion in 0.001 - 1 M H_3PO_4 are plotted as a function of the logarithm of the molar acid concentration; and the curve is shown in Fig. I. As evident from this curve the potential increases with the acid concentration. The increase amounts to 90 mv/unit log C. The potential tends to a more or less constant value at about one molar acid. These results cannot be attributed to the behaviour of the metal as a metal oxide electrode, because the persistence of oxides is not possible in these acid media. We therefore concluded that the observed potentials are corrosion potentials, rather than thermodynamic values.

Comparison of the results obtained in these acid solutions with those observed by Brasher in neutral solutions [4] reveals that corrosion promotion is not necessarily accompanied by a negative slope for the potential - log C relation. Brasher's equation might be understood on the basis that the anions promote the anodic reaction whereas the cathodic reaction is not affected by the anions. Thus, if the concentration of the cathodically reduced entities (H^+ or O_2 molecules) remains constant, equality of the anodic and cathodic reactions rates is brought about through the shift of the corrosion potential to more negative values. In acid solutions, the rate of the cathodic reaction increasees with increase of H^+ ion activity. Thus, if the increase of the cathodio reaction rate is larger than the increase of the anodic reacton rate, the corrosion potential increases. The results of the present investigation indicate that cathodic acceleration predominates.

In order to test whether the increase in the corrosion rate is due only to the increase of H^+ ion activity or the anions contribute in the promotion of corrosion, the corrosion behaviour was studied at constant pH value, ca. pH2. Hence, the corrosion rates were measured in equimolar NaH_2PO_4 -H_3PO_4 mixtures, within the range 0.001-0.2M. The results are shown in Fig. (2). It is clear that $H_2PO_4^-$ ions promote

the corrosion of the metal. This behaviour is important because it indicated that the primary phosphate ion exhibits corrosive action. In this respect the results agree with Brasher's theory[4] . However this ion did not show inhibitive action at higher concentrations as required by Brasher theory[4] for neutral solutions.

Corrosion Inhibition with Phosphate Ions in Neutral and Alkaline Solutions:

Potential-time curves were also constructed for the iron electrode in sodium phosphate solutions of different pH values. The steady state potentials obtained four hours after immersion, are plotted as a founction of the logarithm of the molar concentration. Different relations were obtained depending on the solution pH (cf. Figs. 3 and 4). In none of the solutions studied within the pH range 4.6-13 did the electrode potential show a linear logarithmic decrease with phosphate concentration, indicating that, at least under our experimental condition, iron does not behave as a reversible metal/metal phosphate electrode.

Generally speaking it is clear from these curves that the potential increases with the phosphate concentration till it reaches a maximum value, and then decreases again with further increase of concentration. The maximum concentration C_{max} for the different series are given in the following table.

Series	pH	max	C_{max}
NaH_2PO_4(in acetic acid sodium acetate buffer)	4.6	- 0.408 V	0.005 M
NaH_2PO_4 + Na_2HPO_4	6.5	- 0.394 V	0.01 M
Na_3PO_4	9.4-12.9	- 0.136 V	0.02 M
Na_2HPO_4 + Na_3PO_4	10.96	- 0.094 V	0.05 M
Na_3PO_4 + 0.01N NaOH	11.2 - 13	- 0.083 V	0.02 M

As mentioned above, the increase of potential with phosphate concentration shows that iron does not behave as metal/metal phosphate electrode. The results indicate also that the electrode potential is not governed by an oxide layer. This is because the solutions of a given series are adjusted at a constant pH value, and hence, the potential should have remained constant in the different solutions of each series. The behaviour observed in these solutions is not probably ascribed to the inhibitive effect of phosphate ions on the corrosion of iron. The mechanism of corrosion inhibition and the phenomenon of potential maximum are discussed here below from the stand-point of the rates of the various electrode reactions.

The heterogenity of the surface, in the sense that some sites are anodic and others are relatively

cathodic, is now a well established fact. At a metal corroding in aerated solutions, the probable reactions expected to proceed are:

i) Anodic dissolution of the metal from the anodic areas

$$M \rightleftharpoons M^{2+} + 2e \quad \ldots\ldots(1)$$

ii) Cathodic deposition of the metal ions at the cathodic areas.

$$M^{2+} + 2e \rightleftharpoons M \quad \ldots\ldots(2)$$

iii) Cathodic reduction of oxygen at the cathodic areas

$$O_2 + 2H_2O + 4e \rightleftharpoons 4\ OH^- \text{(in alkaline solutions)} \quad (3)$$

iv) and finally, the anodic evolution of oxygen at the anodic areas.

$$4\ OH^- \rightleftharpoons 2H_2O + O_2 + 4e \quad \ldots\ldots(4)$$

The rates of these reactions are represented, respectively by:-

$$V_1 = K_1 (x) \exp\left[\frac{2\alpha EF}{RT}\right] \quad \ldots\ldots(5)$$

$$V_2 = K_2(M^{2+})(1-x)\exp\left[\frac{-2(1-\alpha)EF}{RT}\right] \quad \ldots\ldots(6)$$

$$V_3 = K_3(O_2)(1-x) \exp\left[\frac{-4\beta EF}{RT}\right] \quad \ldots\ldots(7)$$

$$V_4 = K_4(OH)(x) \exp\left[\frac{4(1-\beta)EF}{RT}\right] \quad \ldots\ldots(8)$$

Where K_1, K_2, K_3 and K_4 are the rate constants, x is the anodic fraction of the surface and (1-x) the cathodic fraction; α and β are the fractions of the electrode potential, E, which accelerate the metal dissolution and reduction of oxygen, respectively, and $(1-\alpha)$ and $(1-\beta)$ correspond to the reverse reactions.

Under stationary conditions, the metal corrodes at a rate V_{corr}, equal to the net rate of metal dissolution, which is also equal to the net rate of reduction of oxygen;

thus

$$V_{corr} = V_1 - V_2 = V_3 - V_4 \quad \ldots\ldots\ldots\ldots\ldots (9)$$

The reduction of oxygen is often very slow compared to the metal dissolution. Thus $(V_1 - V_2) \simeq 0$, with the result that $V_1 \simeq V_2$. This means that the potential approaches the reversible value of the metal/metal ion or metal/metal compound when a precipitating anion is present, For noble metals, on the other hand, reduction of oxygen proceeds at a higher rate than metal dissolution Hence, $(V_3 - V_4) \simeq 0$ and accordingly $V_3 \simeq V_4$. The potential approaches, therefore, the reversible value of the oxygen electrode in the given solution. In many other cases, metal dissolution and reduction of oxygen proceed at comparable rates; the electrode thus acquires a potential which is appreciably more positive than that of the metal/metal ion system, and appreciably more negative than that of the oxygen electrode in the given solution. In this case the reverse rections, i.e. the deposition of metal ions and the anodic evolution of oxygen, are neglected, and

$$V_1 \simeq V_3 = V_{corr} \quad \ldots\ldots\ldots\ldots\ldots\ldots\ldots (10)$$

The potential acquired by the metal in this case satisfies the equality of the anodic and cathodic reaction rates, and is called "corrosion potential".

In view of the above argument we can proceed to explain the experimental results. Thus, in solutions of pH 4.6-13 containing phsophate ions, the anodic areas of the metal surface are covered with a persisting layer of iron oxide or iron phosphate. The shift of potential to less negative values on inoreasing the phosphate concentraton shows that the rate of the anodio reaction, viz., the metal dissolution is being subjected to a decelerating effect, which is possibly the decrease of the ionic conductivity of the iron oxide or iron phosphate layer. In analogy to lead[1], tin[2] and zinc[3], this can be attributed to the adsorption of phosphate ions on the iron oxide or iron phosphate layer, in a highly polymerised form. The interface between the iron phosphate layer and solution acquires a semi-glassy constitution rather than an ionic or crystalline structure, and hence, inhibits the transfer or iron ions to the solution. In order that the equality between the rate of metal dissolution and that of cathodic reduction of oxygen

is restored, the potential rises. This leads to decrease of the rate of the cathodic reaction V_3 , and consequently to diminution of the corrosion rate (of equations 7 and 10).After reaching to a certain maximum, the potential decreases with further increase of concentration. This shift of potential to the active side might be taken as indication to increased corrosion rate, on the basis that some complex compounds might form at high phosphate concentrations.

We therefore measured the corrosion rates in some representative solutions. The results given in fig (5). reveal that the corrosion rates at concentrations higher than C_{max} are generally smaller than the rates at lower concentratons. This means that although the potential decrease the corrosion rate is further diminshed.

The decrease of potential after reaching a maximum value is explained on the basis that further increase of concentration permits adsorption on the cathodic sites of the metal surface. The area available for cathodic reduction of oxygen, (1-x), decreases, and hence, the rate of reduction V_3 , should decrease as equation (7) implies. Accordingly, the potential decreases so that the equilibrium between the anodic and cathodic reaction is again restored. If follows

that v_1 and consequently the corrosion rate is once more diminished (Cf. equation (5) and (10).

Summary:

The potential of the iron electrode in aqueous phosphate solutions was measured at 30° C as a function of pH and electrolyte concentration.

In pure phosphoric acid solutions as well as in phosphoric acid-primary phosphate mixtures having constant pH value, corrosion of iron is promoted as the concentration is increased. This is possibly due to acceleration of the metal dissolution by adsorbed ions on the bare anodic areas.

In solutions of pH 4.6-13, the potential increases with phosphate concentration, and after reaching a maximum value, it decreases again on further increase of concentration. The corrosion rate was always decreasing as the phosphate concentration was increased. A mechanism for corrosion inhibition is proposed, based on the adsorption of phosphate ions, on the surface of a persisting phosphate or oxide layer, in a highly polymerised form. The film/solution interface acquires, therefore, a sami-glassy structure, which hinders the transfer of iron ion to the solution,

[illegible] The decrease of potential after reaching a maximum value was attributed to the adsorption of phosphate ions on the bare cathodic areas of the electrode surface. This leads to the deceleration of the cathodic reduction of oxygen, and results in further inhibition of corrosion.

REFERENCES

1. S.A.Awa[illegible].A. El-hady, J. Electronal. Chem., 20, 79 (1969).
2. S.A. Awad and A. Hassab, J. Electronal. Chem., 20, 203 (1969).
3. S.A.Awad and Kh. M. Kamel, J. Electronal. Chem., 24, 217 (1970).
4. D.M. Brasher, Nature, Lond., 193, 868 (1962).

السلوك التآكلى للحديد فى محاليل الفوسفات

تم قياس جهد قطب الحديد فى المحاليل المائيه للفوسفات عند درجه ٣٠° مئويه كدالة للرقم الايدروجينى وتركيز الالكتروليت.

وقد وجد انه فى محاليل حمض الفوسفوريك وكذلك فى مخاليط من حمض الفوسفوريك واحادى فوسفات الصوديوم المثبته عند رقم ايدروجينى معين يزداد معدل تآكل الحديد مع زياده التركيز. وقد فسر ذلك على اساس ادمصاص الانيونات على المناطق الصعديه المعراه.

اما فى الفوسفات ذات الرقم الايدروجينى ٤٫٦ ــ ١٣ فقد لوحظ زياده الجهد مع زياده تركيز الفوسفات حتى قيمه معينه ، ثم ينقص الجهد مع زياده التركيز.

اما عن معدل التآكل فقد وجد انه ينقص مع زياده تركيز الفوسفات وقد نسبت زياده الجهد الى تكوين طبقه غير منفذه نتيجه ادمصاص الانيونات على سطح طبقه من اكسيد الحديد او فوسفات الحديد.

وعند التراكيز العاليه فانه يتم ادمصاص الانيونات على المناطق المهبطيه للفلز ، مما يؤدى الى نقص معدل اختزال الاكسجين ، وهذا يؤدى الى نقص الجهد.

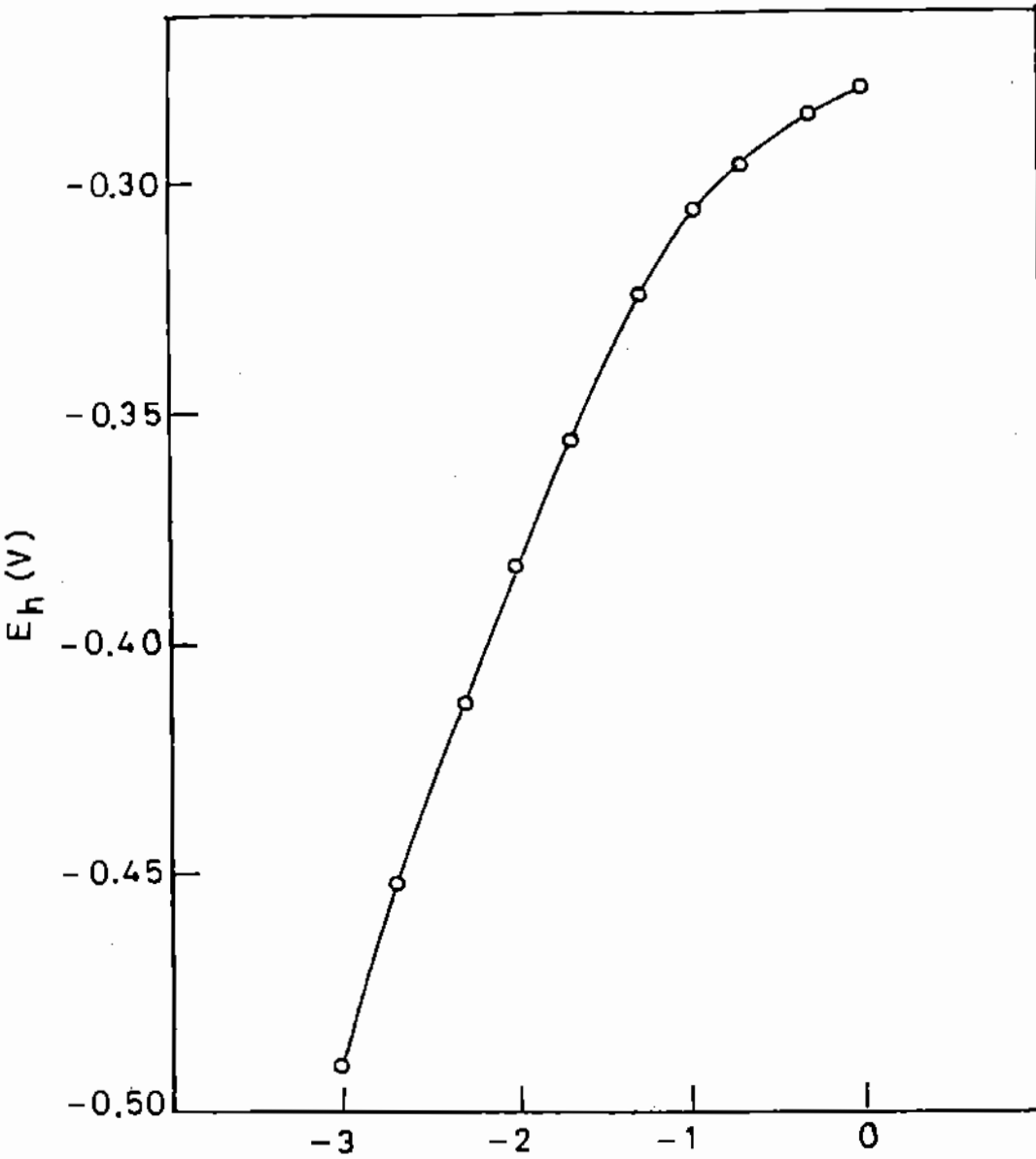

Fig (1)

Effect of Concentration of H_3PO_4 o

the Potential of Iron.

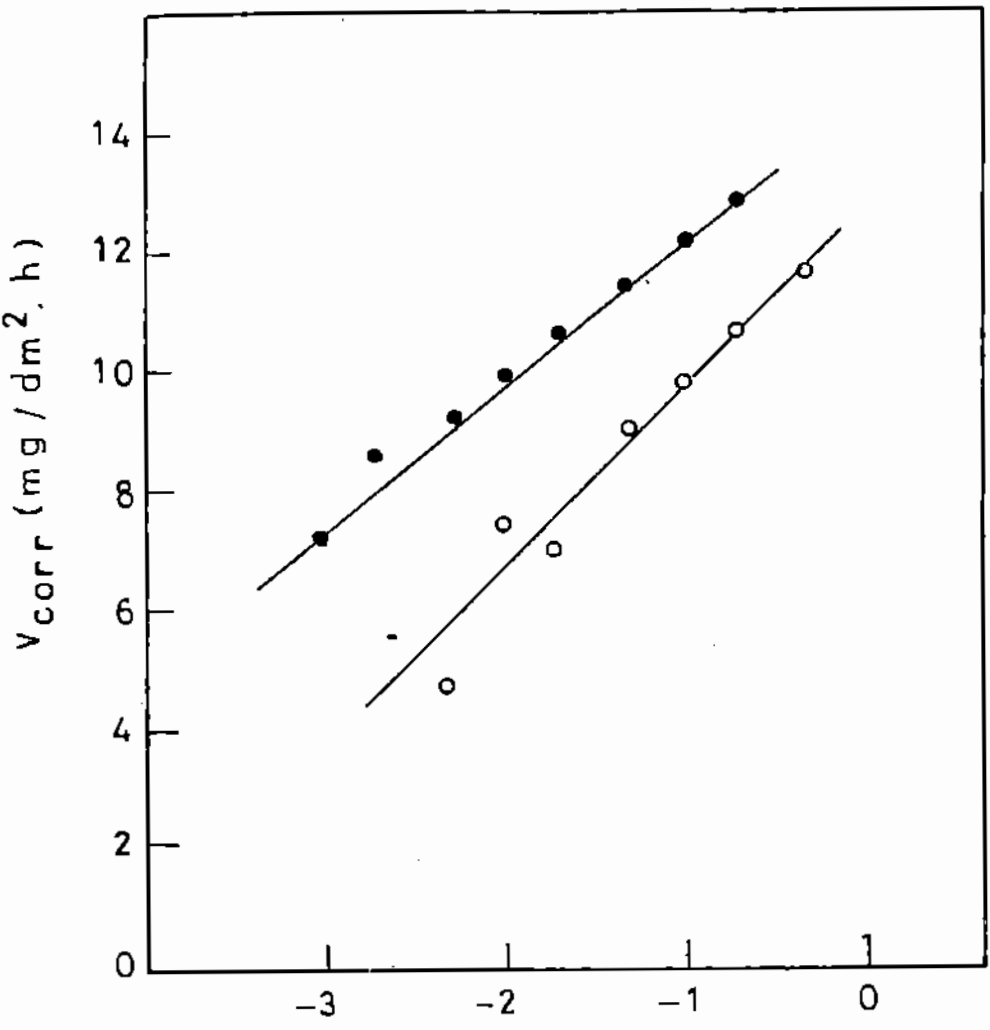

Fig (2)

Rate of Corrosion of Iron in:

- • $NaH_2PO_4 + H_3PO_4$
- o H_3PO_4

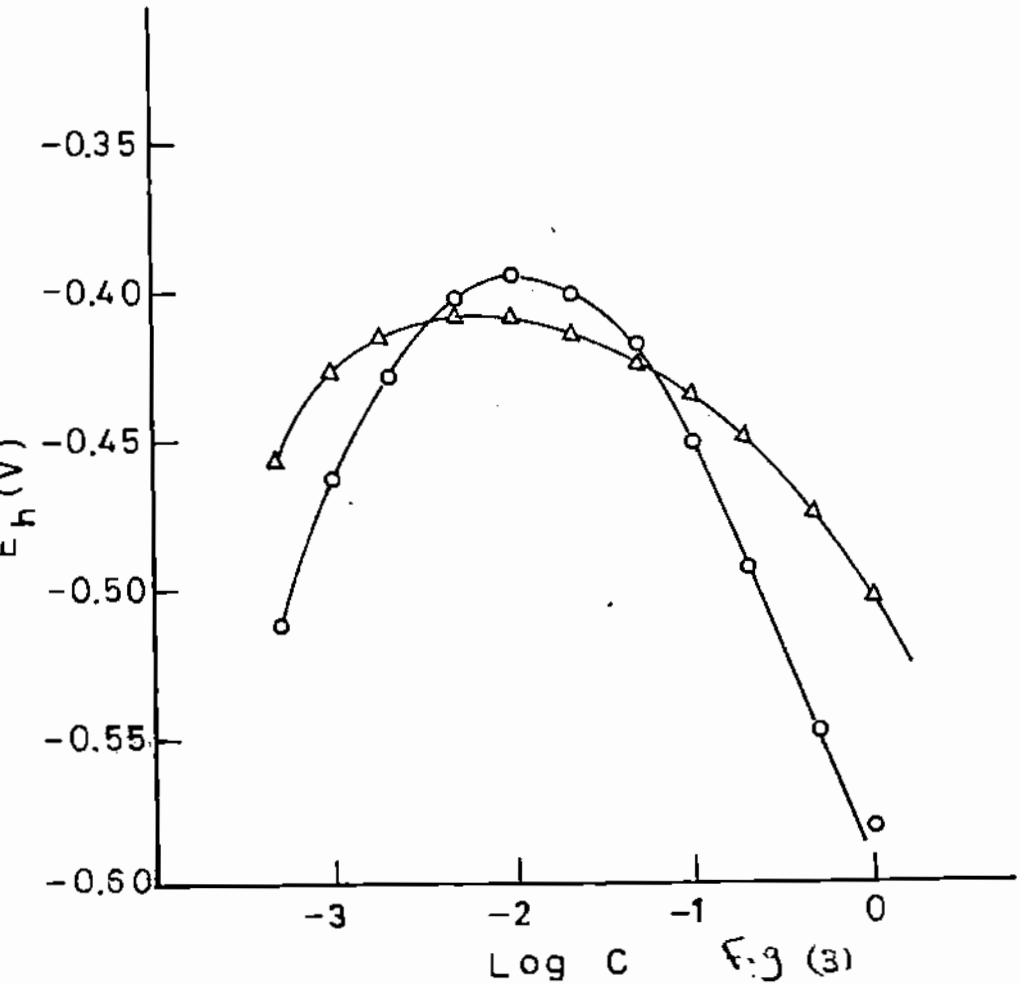

Fig (3)

Effect of Concentration of Simple NaH_2PO_4 and of ($NaH_2PO_4 + Na_2HPO_4$) mixture on the Potential of Iron

o ($NaH_2PO_4 + Na_2HPO_4$)

Δ (NaH_2PO_4) in (Na acetate + acetic acid) Buffer soln.

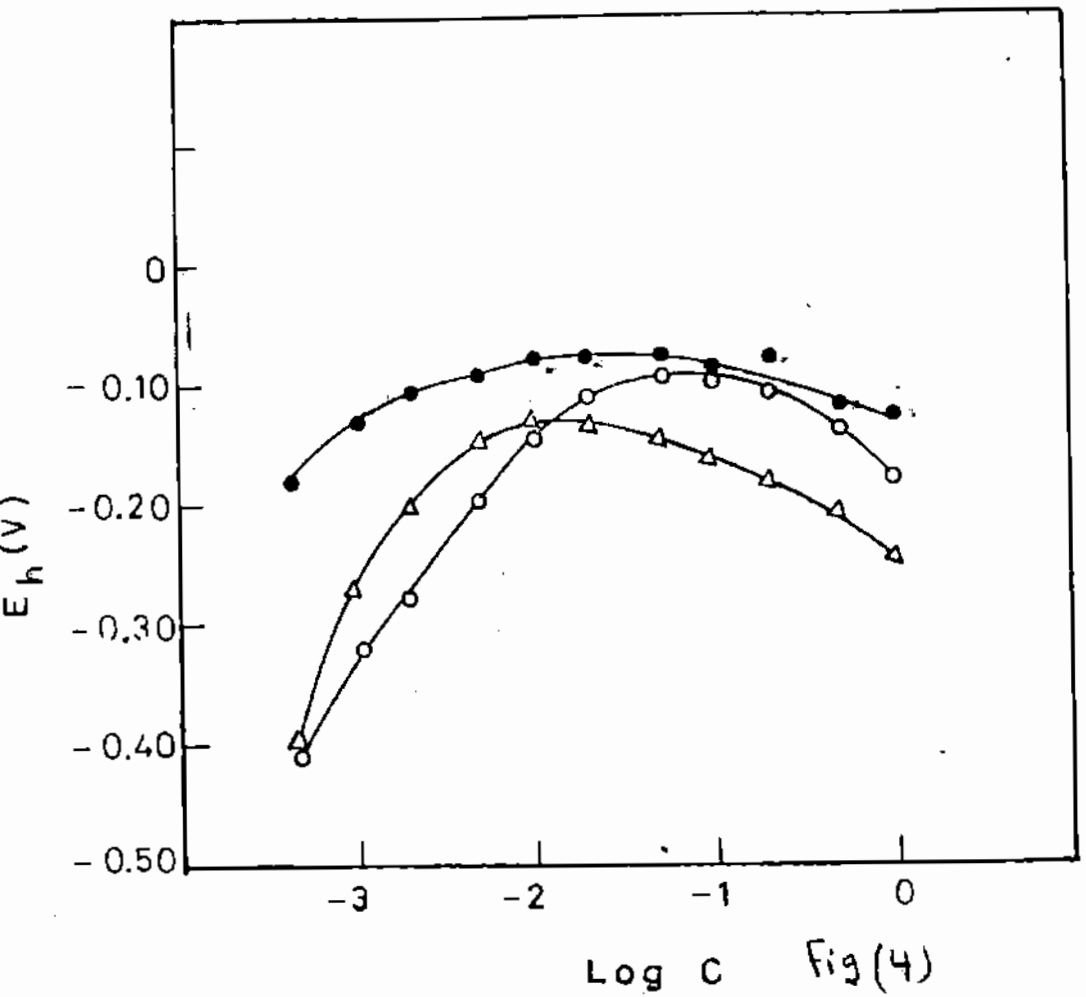

Fig (4)

Effect of Concentration on the potential of Ir

- ● Na_3PO_4 in 0.01 N NaOH
- △ Na_3PO_4
- ○ $Na_2HPO_4 + Na_3PO_4$

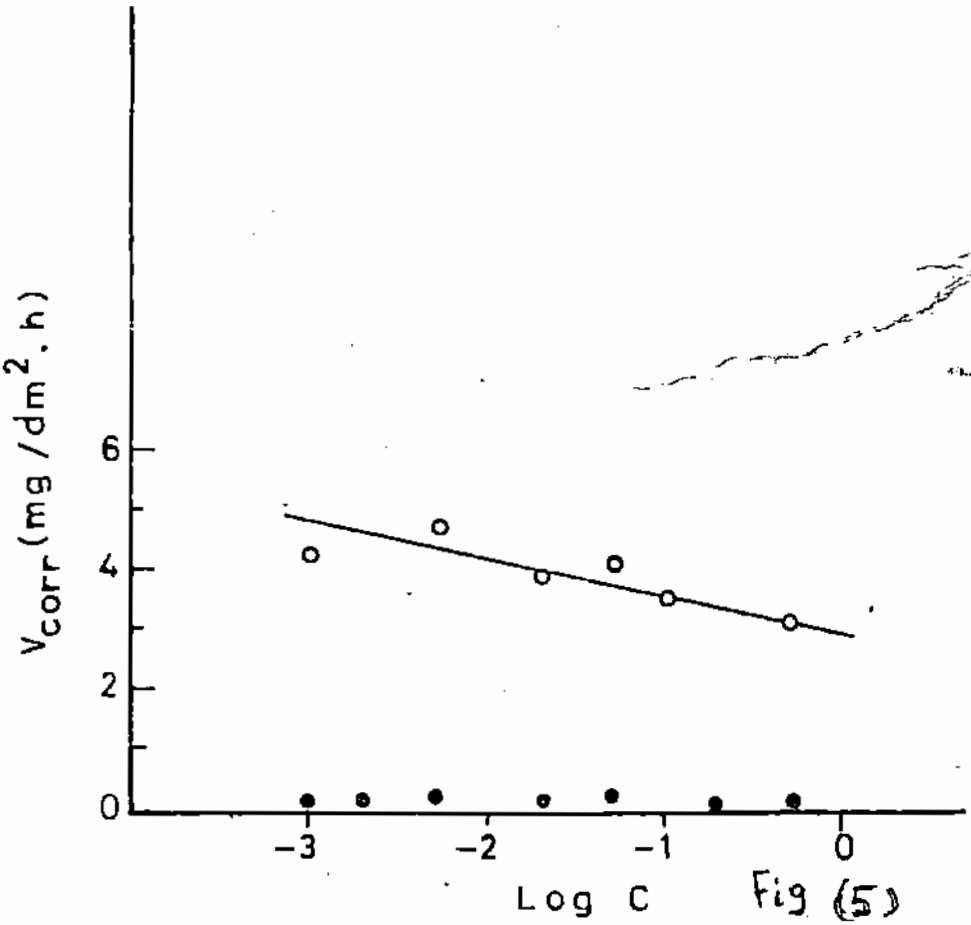

Fig (5)

Corrosion of Iron in:- o NaH_2PO_4 + Na_2H

• Na_3PO_4 Free

Kinetics of Methoxymercuration of trans-Cinnamic Acid and Methyl Cinnamate

William I. Awad, Boshra M. Awad, Nadia R. Guirguis and Afaf A. El-Beih

Department of Chemistry, University College for Women, Ain Shams University, Heliopolis, Cairo, Egypt.

The rates of methoxymercuration of trans-cinnamic acid and methyl cinnamate are determined by following up the change of concentration of the liberated acetic acid. The overall order of reaction is found to be a second order kinetics being first order with respect to each of the alkene and mercuric acetate. The reaction proceeds via three consecutive steps in which $[H^+]$ first increases with time, then decreases and finally increases again. The rate of the reaction is also determined by following up the change of the concentration of the inorganic mercury which represented only the formation of methoxymercuric acetate. The energies of activation are calculated.

It is well established that the reaction of mercuric salts in a protic solvent with an alkene affords an oxymercurial.[1-3] Many mechanisms have been suggested for methoxymercuration of alkenes which are (a) an ionic mechanism via an alkene mercurinium ion,[4] (b) a non-ionic mechanism,[5,6] or (c) a free radical mechanism.[3] Schrauth et al.[7] have shown that mercuric acetate adds to methyl cinnamate to give methyl β-methoxy-α-acetoxymercuric-hydrocinnamate.

Most of the kinetic studies for the methoxymercuration of different alkenes were carried out by following the change of the concentration of inorganic mercury.[3,8-12]

Adopting a different procedures in this investigation, it is planned to study the kinetics of methoxymercuration of alkenes with known geometrical configuration which are trans-cinnamic acid and methyl cinnamate by following up the change of $[H^+]$ due to liberation of acetic acid during the reaction.

EXPERIMENTAL AND RESULTS

Preparation of Methoxymercuric Acetate .- Dissolution of mercuric acetate (5 g) in absolute methanol,[13] then removal of the free acetic acid and excess methanol under vacuum gave methoxymercuric acetate,[5,9] (90% yield).

Procedures of Rate Measurements :

(a) Change of the Concentration of H^+ .- The rate of methoxymercuration of trans-cinnamic acid (0.001 M) with mercuric acetate (0.0125 M) was studied at 26° by following the change of the concentration of the liberated acetic acid, at different intervals of time by means of pH meter (PYE UNICAM), and also by titration of aliquots of 5 ml of the reaction mixture against standard (0.05 N) sodium carbonate solution using phenolphthalein as indicator. It was found that, on plotting either the pH values or the mls of carbonate at different intervals against time t, curves with three consecutive stages were obtained, in which $[H^+]$ increases, then decreases and finally

increases again. In each case a blank experiment with 0.001 M cinnamic acid was carried out. On repeating the measurements of the pH for solvolysis of mercuric acetate (0.0125 M) in methanol (i.e., without addition of alkene), the plot of pH values against time gave a straight line parallel to the first stage of the pH-time curve for the reaction (Fig. 1). The titration method was used throughout all the experiments.

Kinetic Measurements .- In every experiment, the required weight of the alkene was dissolved quantitatively in absolute methanol. The reaction flask was kept in a thermostat type [(EIN), -50° to $+30^{\circ} \pm 0.01^{\circ}$, Germany] adjusted at the required temperature. After attaining the thermal equilibrium, the appropriate weight of mercuric acetate was added and thoroughly mixed. Immediately, after mixing, a sample of 5 ml of the reaction mixture was withdrawn, placed in a conical flask containing 10 ml redistilled water, previously immersed in an ice-salt cooling mixture and then titrated against the standard titrant. This reading is considered as the zero reading. Samples of 5 ml of the reaction mixture were withdrawn at suitable intervals of time until at least 75% of the reaction was completed. The final reading was taken after sufficient time depending on the temperature and the alkene. Each run was repeated at least twice.

Order of the Reaction .- On using equimolars of both the alkene (0.001 M) and mercuric acetate (0.001 M) at 26°, the reaction was found to be of a second order kinetics overall,

first order with respect to each of the alkene and mercuric acetate; the molecular concentration of alcohol being considered constant. Thus, on using a relatively high molecular concentration of mercuric acetate (0.0125 M), the rate of the reaction became pseudo-first order with respect to the alkene. Hence, plotting log $\frac{a}{a-x}$ vs time (t) gave curves with three intercepting lines showing an increase of log $\frac{a}{a-x}$, followed by a decrease and then increases again. From these curves three velocity constants designated as k_1, k_2 and k_3 could be calculated, representing the three consecutive stages, respectively. This reaction was repeated at three different temperatures, 25°, 30° and 35°. Plotting log k for each stage against $\frac{1}{T}$ gave straight lines from which energies of activation could be calculated and from which the enthalpies and entropies of activation were conventionally calculated. The results obtained are given in Table 1.

Methoxymercuration with Prepared Methoxymercuric Acetate.- Studies of the rate of methoxymercuration of cinnamic acid (0.001 M) with prepared methoxymercuric acetate (0.001 M and 0.0125 M) at 23° in methanol show that with 0.001 M of mercuric salt, the reaction is of a second order kinetics; being first order with respect to each component. Plot of $(\frac{a}{a-x})$ against time (t) gave a curve with two intercepting straight lines. In the second case when 0.0125 M mercuric salt was used, plot of log $\frac{a}{a-x}$ vs (t) gave a curve with only two stages in which log $\frac{a}{a-x}$ decreases by time, then increases. Calculation of the velocity constants for this curve gave values of k_2 and

Table I. Velocity Constants and Activation Parameters for Methoxymercuration of trans-Cinnamic Acid and Methyl Cinnamate

	trans-Methyl Cinnamate			trans-Cinnamic Acid			
Temp. ^{o}C	k_1 min^{-1}	k_2 min^{-1}	k_3 min^{-1}	Temp. ^{o}C	k_1 min^{-1}	k_2 min^{-1}	k_3 min^{-1}
25	9.28×10^{-3}	5.70×10^{-2}	6.67×10^{-3}	20	5.62×10^{-3}	9.39×10^{-3}	4.31×10^{-3}
35	2.08×10^{-2}	8.48×10^{-2}	1.48×10^{-2}	26	9.71×10^{-3}	1.56×10^{-2}	6.14×10^{-3}
40	3.07×10^{-2}	1.03×10^{-1}	2.15×10^{-2}	36	2.33×10^{-2}	3.45×10^{-2}	1.07×10^{-2}
$E^{\#}$ k cal. $mole^{-1}$	14.9	7.3	14.5		16.1	14.5	10.1
$\Delta H^{\#}_{25^{o}}$ K cal $mole^{-1}$	14.4	6.7	13.9	$\Delta H^{\#}_{26^{o}}$	15.5	13.9	9.5
$-\Delta S^{\#}_{25^{o}}$ cal $degree^{-1}$	16.66	38.90	19.90	$-\Delta S^{\#}_{26^{o}}$	16.98	21.26	37.58

k_3 which are in accordance with the results obtained on using cinnamic acid and mercuric acetate in methanol under the same conditions. The results obtained are given in Table II. This fact indicates that the first step in the reaction with mercuric acetate represented the prior formation of methoxymercuric acetate.

Table II. Reaction of Cinnamic Acid (0.001 M) with Mercuric and Methoxymercuric Acetate (0.0125 M) at 23°.

Mercuric salt	k_2 min^{-1}	k_3 min^{-1}
Mercuric acetate	1.22×10^{-2}	5.16×10^{-3}
Methoxymercuric acetate	1.21×10^{-2}	5.05×10^{-3}

(b) Change of Inorganic Mercury Concentration.- The rate of methoxymercuration of cinnamic acid (0.001 M) was also followed up by measuring the change of concentration of the inorganic mercury by its titration at different time intervals against standard KCNS solution using ferric alum as an inidicator.[3] Different molecular concentration of mercuric acetate (0.001, 0.0125 and 0.035 M) were used. For equimolars, the reaction was found to be of a second order kinetics overall; being first order with respect to each component. Hence, using relatively high molecular concentration of mercuric acetate, the reaction became pseudo-first order with respect to the alkene. Plotting log $\frac{a}{a-x}$ against time (t) gave straight lines with only one stage from which the velocity constant k was calculated

On using 0.0125 M mercuric acetate, it was found that, under the same conditions, the value of k obtained was nearly equal to the value of k_1 representing the first stage when sodium carbonate was used as titrant, within a small range of experimental error. These results indicated that thiocyanate solution represents only the first step of this reaction in which the inorganic mercury is consumed to form methoxymercuric acetate. The results are given in Table III.

Table III. Comparison Between Titrations Using Sodium Carbonate and Potassium Thiocyanate as Titrants.

Titrant	Sodium Carbonate	Potassium Thiocyanate
Temp. °C	k_1 min^{-1}	k_1 min^{-1}
23	7.38×10^{-3}	7.55×10^{-3}
26	9.71×10^{-3}	1.00×10^{-2}
36	2.33×10^{-2}	2.49×10^{-2}
$E^{\#}$ Kcal $mole^{-1}$	16.09	16.70

(c) Other Procedures .- When the rate of this reaction was followed up by its titration against HCl in butanol using thymol blue as an indicator, it was found that, whatever the millilitres taken from the reaction mixture and at any interval, the colour of the indicator changes from red to yellow[14] after the addition of the same amount of HCl in butanol. The same result was also obtained on using a solution of indicator in methanol. It seems that the change in colour is produced as a result of the change of the pH of the solution from 2.8 to

1.2 by the addition of HCl. The same result was obtained by following the dithiazone method.[10,12]

DISCUSSION

The data obtained reveal that the kinetic studies of methoxymercuration of alkenes by following the liberated acetic acid give s more detailed ides about the different steps involved in this reaction and the role of the proton. In all cases, a pH-time curve with three stages obtained indicating that methoxymercuration of cinnamic acid and methyl cinnamate takes place via three consecutive steps. The first step in which $[H^+]$ increases is attributed to the formation of methoxymercuric acetate which is formed by prior solvolysis of mercuric acetate by the alcohol.[5] This step is also represented by potassium thiocyanate and by change of the pH of the solvation of mercuric acetate in methanol with and without the alkene. This step is reversible whereby its rate is decreased by increasing the acidity of the medium. Wright and his coworkers[5] found that addition of acetic acid during methoxymercuration retarded the reaction, whereas removal of the free acetic acid from solution by some means accelerated it. They attributed it to further solvolysis. The first step can be represented as :

$$MeOH + Hg(OAc)_2 \underset{k_{-1}}{\overset{k_1 \text{ fast}}{\rightleftharpoons}} Me\text{—}\ddot{O}\text{—}Hg\text{-}OAc + H^+ + {}^-OAc$$

In the second step, the $[H^+]$ decreases, i.e., an uptake of protons occurs that becomes detectable around a critical

pH (viz. pH .5.7). This step is also reversible and the velocity constant of this step is represented as k_2. The rate of this step increases by decreasing the $[H^+]$ of the medium. This means that protonation enhances the reaction and must play an important role. If the proton is taken by the formed methoxymercuric acetate, the rate will be independent on the alkene used which is not the case. Here we have to differentiate between the methoxymercuration of ordinary olefins and that of α,β-unsaturated carbonyl compounds. In the case of ordinary olefins, e.g. stilbene,[8] 1- and 2-pentenes[15] the reaction is generally very slow and not accelerated by acids,[8] and cis-form reacts faster than the trans-one. However, α,β-unsaturated carbonyl compounds[16] react much more rapid with a regiospecific entrance of the Hg- atom at the α-carbon atom.

The compounds investigated here are of the latter type and protonation (uptake of proton) can take place on the lone pair of electrons of the oxygen which is conjugated with the double bond. This clearly increases the polarity of the double bond and highly facilitates methoxymercuration. This step is substantiated by the fact that no reaction occurs with the prepared methoxymercuric acetate in aprotic solvent (dioxane) except after protonation with formic acid. This step can be represented as follows :

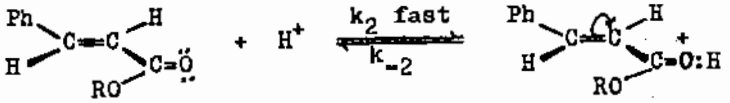

R = H or CH_3 Protonated complex

The idea of the association of polarity with the increase in rate of reaction can also interpret why cis-isomers (more polar) react faster than trans-ones[8,15] (less polar).

The third step which is slow and the rate determining step is irreversible one. Its rate is represented as k_3. Since the reaction is a second order overall, first order with respect to both of the alkene and methoxymercuric acetate, it is convenient to propose a transition state containing these two species. In this step $[H^+]$ increases indicating that the addition of methoxymercuric acetate to the activated protonated complex takes place with the liberation of the proton. This is supported by the fact that this step is accelerated by decreasing the $[H^+]$ of the medium and this may explain why the energy of activation in case of cinnamic acid is lower than that for methyl cinnamate in this stage. This step is a concerted process ($2\pi + 2\sigma$ cycloaddition reaction) going through a four-membered transition state. The low entropies of activation favours this mechanism. This is in accordance with that mechanism suggested by Wright et al.[3,7,10] for methoxymercuration of cyclohexene. The third step can be represented as follows:

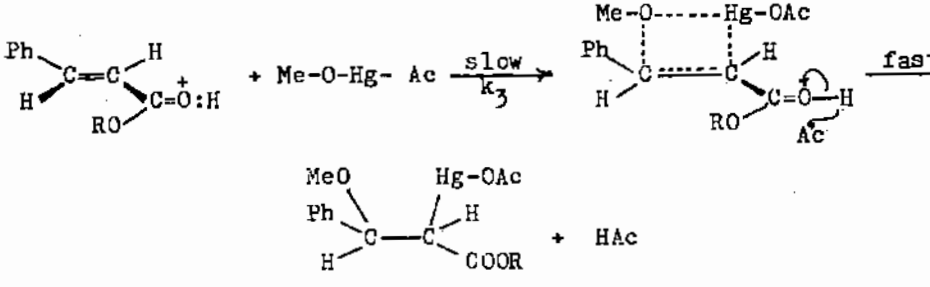

REFERENCES

1. L.T. Sandborn and C.S. Marvel, J. Amer. Chem. Soc., 48 1409 (1926).

2. W. Schrauth, W. Schoeller and R. Struenser, Ber., 43, 695 (1910).

3. G.F. Wright, J. Amer. Chem. Soc., 57, 1993 (1935).

4. M.L. Lucas, F.R. Heper and S. Winstein, J. Amer. Chem. Soc., 61, 3102 (1939).

5. A. Rodgman and G.F. Wright, J. Org. Chem., 17, 988 (1953), J. Amer. Chem. Soc., 69, 797 (1947).

6. W. Manchat, Ber., 53, 984 (1920).

7. W. Schrauth, W. Schoeller and R. Struenser, Ber., 44, 1048 (1911).

8. A.M. Birks and G.F. Wright, J. Amer. Chem. Soc., 62, 2412 (1940).

9. W.H. Brown and G.F. Wright, J. Amer. Chem. Soc., 62, 1991 (1940).

10. J. Romeyn and G.F. Wright, J. Amer. Chem. Soc., 69, 687 (1947).

11. G.F. Wright, Cand. J. Chem. Soc., 33, 1002 (1955).

12. M.L. Mallik and M. Nadas, J. Amer. Chem. Soc., 82, 4269 (1960).

13. A.I, Vogel, "Practical Organic Chemistry", Longmans Green Co., p. 167 (1948).

14. I.M. Kathoff and E.B. Sandell, "Text Book of Quantitative Inorganic Analysis", New York, MacMillan Co., p. 541 (1967).

15. H.C. Brown and P.J. Geoghegan Jr., J. Org. Chem., 37, 1937 (1972).

16. A.J. Blood Worth and R.J. Bunce, J. Chem. Soc. (D) 753 (1970).

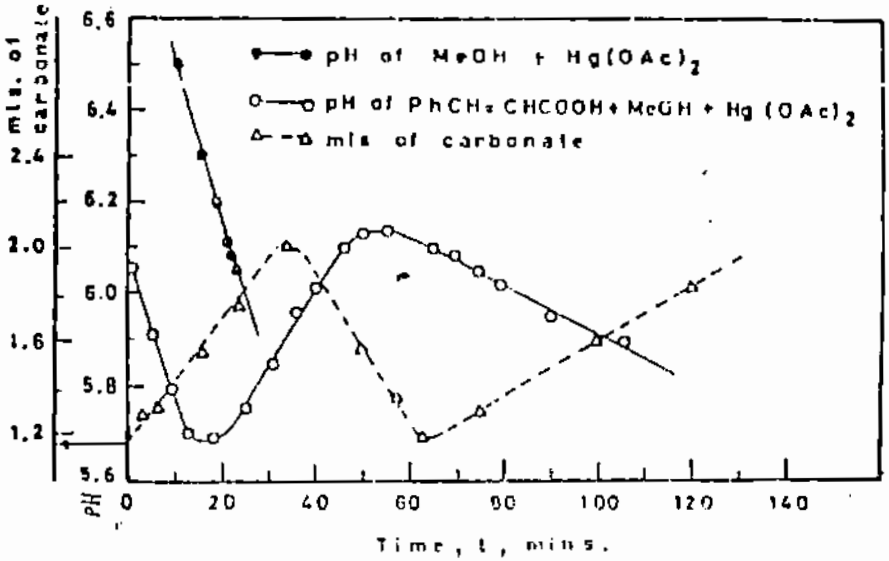

Fig. 1

Change of $[H^+]$ with time

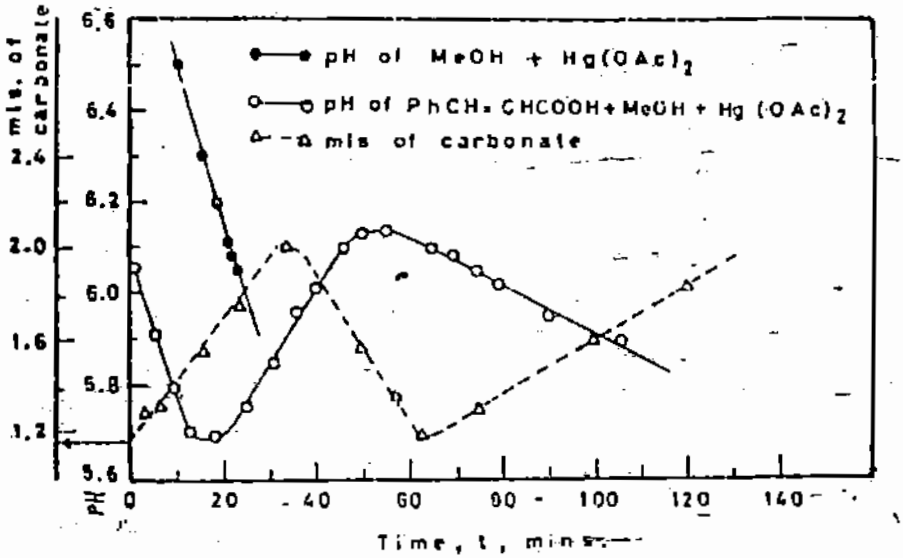

Fig. 1

Change of $[H^+]$ with time

MECHANISM OF ANODIC DISSOLUTION OF LEAD IN SODIUM HYDROXIDE SOLUTIONS

By

S. A. AWAD, Z. A. EL-HADI and K. M. KAMEL

Chemistry Department, University College For Women, Ain-Shams University, Heliopols, Cairo, Egypt.

INTRODUCTION:

From studies on the anodic dissolution of tin in alkaline solutions[1], it was suggested that the surface tin atoms exist as diatomic molecules, a suboxide (Sn_2O) is first formed, which undergoes self oxidation to stannous oxide.

The study is now extended to lead. Although much work has been published on the electrochemical behaviour of Pb in acid solutions, its behaviour in alkaline solutions has received, relatively little attention. Jones et al[2] found that lead anodes dissolved in 1N KOH first as plumbite and then passivated by a film of PbO_2. On the other hand, Khamudkhamova[3] found that lead anodes dissolved directly in KOH solutions with the formation of $HPbO_2^-$ and PbO. After complete covering of lead surface with oxides, the potential increased, the formation of PbO_2 began and O_2 evolved.

The electrochemical behaviour of PbO in deaerated NaOH solutions has been studied by Abdul Azim et al[4]. They observed that the porosity of the initially formed PbO_2 is maximal in 2N NaOH.

It was observed that no mention is made in the literature of the kinetics of the anodic reactions of lead. In the present investigation, the mechanism of its anodic dissolution in alkaline solutions is examined.

EXPERIMENTAL:

Polarisation measurements on the lead anode were carried out in a cell (constructed from the arsenic-free hard borosilicate glass, Hysil) which permitted the rigorous purification of the solutions under investigation through anodic pre-electrolysis[5]. For this purpose a platinum anode (2 cm.^{2} platinum sheet welded to a platinum wire sealed to glass.

The electrodes were prepared from extra pure lead rods, 3 mm in diameter (Schering-Kahlbaum Company). The electrodes area was 1 cm.^{2}. Each run was carried out with a new electrode. All solutions were prepared from A.R. materials.

Before each run, the cell was cleaned with a mixture of nitric and sulphuric acids (A.R.), and thorough washed with conductance water. The test solution was then introduced into the pre-electrolysis compartment of the ce and pre-electrolysis was conducted at 10^{-3} - 10^{-1} A cm.$^{-2}$ for 30 h. The lead electrode was then introduced into the anode compartment of the cell and adjusted to touch the Luggin capillary which lid, via a salt bridge, to a satura ed calomel electrode. Some of the pre-electrolysed soluti was then transferred to the anode compartment, and the Taf line was determined from low to high current densities and then downwards again. After each overpotential run, the concentration of the electrolyte was determined analytical

All measurements were carried out in an air-thermostat, the temperature of which was kept constant wit ± 0.5 °C. The current density value was calculated using apparent surface area. All potentials are recorded on the normal hydrogen scale.

RESULTS AND DISCUSSION:

The potential of the lead anode was measured 30 °C in 0.1 - 10 N NaOH as a function of the current dens

within the range of 10^{-6} - 10^{-1} A cm.$^{-2}$. At any current density the potential was constant within few minutes. In each solution, six potential-current density relations (on six electrodes and solutions) were measured; the results were reproducible to ± 5 mV. At very low anodic polarisation, the anodic potential did not change with current, and a stationary potential was measured in each of these solutions. These stationary potentials are given in Table (1) together with the pH values of the different solutions.

1. Nature of anode reaction:

The stationary potentials represent, or at least closely approach, the reversible potentials for the reaction taking place at the anode. We can, therefore, define the nature of this reaction by comparing the experimentally observed stationary potentials with the theoretical values for all possible reactions involving lead in alkaline solutions.

The following oxidation reactions have been suggested as being the most probable to occur on the surface of the lead anode,

	E_B^o (at pH 14 and 25 °C) V (NHE)	
$Pb + 2\ OH^- \longrightarrow Pb(OH)_2 + 2\ e$	-0.562	(1)
$Pb + 2\ OH^- \longrightarrow PbO + H_2O + 2\ e$	-0.580	(2)
$Pb + 3\ OH^- \longrightarrow HPbO_2^- + H_2O + 2\ e$	-0.540	(3)
$Pb + 4\ OH^- \longrightarrow PbO_2 + 2\ H_2O + 4\ e$	-0.166	(4)

The standard potentials E_B^o for the above reaction, at unit hydroxyl ion activity, are calculated from the standard free energy of formation[6] of the different products, OH^- and H_2O.

Since the standard potentials are little affected by temperature[7], the above values may be taken as the standard potentials at 30 °C. In Fig. (1), the observed potentials are plotted as a function of the pH value of the solution. The dotted lines represent the theoretical potential / pH relations

of the oxidation reactions suggested above. These are drawn on the basis that the potential varies with pH by the same gradient as that for the hydrogen electrode (60 mV at 30 °C). It is clear from Fig. (1) that the experimental potential / pH relation coincides with that of the Pb / PbO couple, indicating that the anode reaction is represented by equation (2). The oxide dissolves as plumbite through the action of OH^- ions, with the result that the electrode surface remains active.

2. Mechanism of anode reaction:

The discussion made so far indicates that the overpotential (difference between the potential measured at a given current density and the stationary potential) at the lead anode is associated with the formation of PbO. The mechanism of the reaction can be elucidated from the observed parameters and characteristics of overpotential. These are summerized below:

(a) Slope of overpotential-log current density relations:

The mean values of overpotential, η, were plotted against the logarithm of the current density; some representative relations (which are usually called Tafel lines) are given in Fig. (2). It is clear that the Tafel lines exhibit a linear logarithmic part. The mean values of the slopes of these parts amount to 28-34 mV (see Table 1).

(b) The electron number:

This is the number of electrons required to complete one act of the rate-determining step. This parameter is calculated from the exchange current of the Tafel line, i_o, and the slope of the overpotential-current density relation at low values of η; the expression for the electron number, λ, is:

$$\lambda = (RT/i_o F)(\partial i/\partial \eta)_{\eta \to o} \qquad (5)$$

Examples of the relations between η and current density at low anodic polarization are shown in Fig. (3). The slopes of such relations, together with the exchange current for the different Tafel lines and the calculated values for the electron number, are given in Table (1).

It is obvious from Table (1) that the experimental values of λ are very near to 4. This value is peculiar, since on the basis of the stationary potentials, the oxidation to the tetravalent state is excluded.

Reconciliation between the dissolution of lead as plumbite and the doubled value of the electron number can be made by assuming that the surface lead atoms exist (or at least participate in electrochemical reactions) as diatomic molecules. An analogous assumption has accounted satisfactorily for the cathodic[8] and anodic[9] behaviour of tellurium and tin[1].

(c) Effect of pH on overpotential:

One of the important means which help to distinguish between the different possible mechanism is the dependence of overpotential, at a constant current density and temperature, on the pH of the solution. The overpotential of lead anodes was found to be almost independent of the alkali concentration, as is clear from Table (1), in which the values of at 10^{-3} A cm.$^{-2}$ are given. This behaviour will give an indication as to whether the suboxide is oxidised anodically:

$$Pb_2O + 2\ OH^- \longrightarrow 2\ PbO + H_2O + 2\ e \qquad (6)$$

or undergoes a self-oxidation process:

$$2\ Pb_2O \longrightarrow 2\ PbO + Pb_2 \qquad (7)$$

(d) Effect of neutral salts on overpotential:

Neutral salts affect the structure of the double layer at the anode-solution interface, and hence they affect the concentration of OH^- at that interface. It follows that they affect the velocity of the anode reaction. The effect

of neutral salts can thus exist in elucidating the proper reaction mechanism. The overpotential was measured in 0.1 and 0.3 N solutions which contain excess (1 M) Na_2SO_4. The results indicated that the Tafel line is not affected by neutral salts, for instance, the overpotentials at 10^{-3} a. cm.$^{-2}$ are the same as for the corresponding pure solutions (see Table 1). We concluded that the expression for η does not include the zeta potential (ζ).

On the basis of the above mentioned features of overpotential, the mechanism of anodic dissolution of lead in alkaline solutions was formulated as follows:

$$\text{Step I:} \quad Pb_2 + OH^- \overset{V_1}{\underset{V_1'}{\rightleftharpoons}} Pb_2OH + e \qquad (8)$$

$$\text{Step II:} \quad Pb_2OH + OH^- \overset{V_2}{\underset{V_2'}{\rightleftharpoons}} Pb_2O + H_2O + e \qquad (9)$$

$$\text{Step III:} \quad Pb_2O \xrightarrow{V_3} Pb_2 + 2\,PbO \qquad (10)$$

Reaction (10) is the rate-determing step, since it requires 4 electrons. To confirm this mechanism, the Tafel line slope is theoretically deduced and compared with the experimentally observed values. The velocities of the different steps in the anodic direction are refsrred to as V_1, V_2 and V_3, and V_1' and V_2' repreaent the velocities of the first two step in the cathodic direction. Since the velocity of the reverse of reaction (10) is negligible, the general expression for the overall rate is:

$$V_1 - V_1' = V_2 - V_2' = V_3 \qquad (11)$$

It is assumed that in the anodic direction, step II is faster than step I, and hence, reaction (9) is governed by reaction (8). It follows that:

$$V_2 = V_1 \qquad (i)$$

On the other hand, step II is assumed to be slower than step I in the cathodic direction. Thus, reaction (8) is governed by reaction (9), and accordingly:

$$V_1' = V_2' \qquad (ii)$$

Substituting V_1' by V_2' (cf. condition ii), or V_2 by V_1 (cf. condition i), equation (11) reduces to:

$$V_1 - V_2' - V_3 = 0 \qquad (12)$$

It is important to mention that if reaction (9) is sufficiently fast in the anodic direction, Pb_2OH is rapidly converted into Pb_2O, with the result that the surface concentration of Pb_2OH is neglected. On the basis of a symmetrical energy barrier, the rate V_1, which represents the rate of the anode formation of Pb_2O, is given by:

$$V_1 = k_1(1-x)[OH^-]_{d.l.}\exp(\Delta\phi F/2RT) = a_1(1-x) \quad (13)$$

where k_1 is the specific reaction rate, a_1 is the electrochemical rate constant, x is the fraction of the surface covered with Pb_2O, (1-x) is the bare fraction of the metal surface, $[OH^-]_{d.l.}$ is the activity of hydroxyl ions in the outer Helmholtz double layer; and $\Delta\phi$ is the potential difference between the electrode and this Helmholtz layer. The rate V_2', which represents the rate of cathodic reduction of Pb_2O, is given by:

$$V_2' = k_2'(x)\exp(-\Delta\phi F/2RT) = a_2'(x) \quad (14)$$

The rate of the self-oxidation process (reaction 10) is:

$$V_3 = k_3(x^2) = a_3(x^2) \quad (15)$$

The steady state corresponding to a constant coverage, current and potential, is represented by equation (12). The self-oxidation process governs the dissolution of lead under the condition[10]:

$$(a_1 + a_2') > 10\, a_3 \quad (16)$$

From equations (12) - (16), the total surface coverage becomes:

$$x = a_1 / (a_1 + a_2') \quad (17)$$

Under conditions when a_1 is much smaller than a_2',

$$x = a_1 / a_2' = k_1 / k_2'[OH^-]_{d.l.}\exp(\Delta\phi F/RT) \quad (18)$$

The net anodic current is given by:

$$i = 4FV_3 = 4Fk_3(k_1/k_2')^2[OH^-]^2_{d.l.}\exp(2\Delta\phi F/RT) \quad (19)$$

The tafel line slope according to equation (19) is 0.03 V at 30 °C, in agreement with the experimental values.

Equation (19) satisfies also the requirement that the overpotential is independent of the alkali concentration. This is revealed by substituting $[OH^-]_{d.l.}$ by $[OH^-]\exp(\zeta F/RT)$,

(where $[OH^-]$ is the OH^- concentration in the bulk of solution), and $\Delta\phi$ by $(\Delta\phi_r + \eta - \zeta)$, (where $\Delta\phi_r$ is the reversible potential in the given solution). Thus:

$$i = k[OH^-]^2 \exp(2\zeta F/RT) \exp(2(\Delta\phi_r + \eta - \zeta)F/RT) \quad (20)$$

and hence,

$$\eta = \text{const.} + (RT/2F)\ln i - (RT/F)\ln[OH^-] - \Delta\phi_r \quad (21)$$

Since $\Delta\phi_r = E_B - (RT/F)\ln[OH^-]$, it is clear that at a constant current density, η = constant.

The absence of ζ from equation (21) accounts also for the fact that addition of neutral salts brings about no effect on the overpotential.

Derivation of the rate equation on the basis that the suboxide is oxidised anodically (reaction 6), leads to the expression:

$$\eta = \text{const.} + (RT/2F)\ln i - (1.5RT/F)\ln[OH^-] - \Delta\phi_r \quad (22)$$

This relationship requires that addition of excess neutral salt (which causes ζ to approach zero), the overpotential decrease 30 mV for ten-fold increase of the alkali concentration. Experiment showed that η remained practically constant in 0.1 and 0.3 N NaOH containing excess neutral salts (cf. Table 1). This result supports the self-oxidation mechanism.

3. Heat of activation:

The heat of activation, $\Delta H^{\neq}$ of the anode reaction at the reversible potential can be evaluated from the effect of temperature on the exchange current; the expression being:

$$d\log i_o/d(T^{-1}) = -\Delta H^{\neq}/2.303R \quad (23)$$

The overpotential was, therefore, measured at 20, 30, 40 and 50 °C in 0.5, 5 and 10 N solutions. Fig. (4) shows the Tafel lines at different temperatures for the 10 N solution. The values of $\log i_o$ for the different solutions are plotted against 1/T in Fig. (5). It is obvious that the exchange current is almost unaffected with temperature; this means that the heat of activation is equal to zero. This result can be understood in the light of the theory of absolute reaction

rates, which shows that the parameter that determines the reaction rate is the free energy of activation ΔG^*, and not ΔH^*. Since $\Delta G^* = \Delta H^* - T\Delta S^*$, the value of ΔH^*, and consequently, the temperature effect on i_o, depends on the value of ΔS^*. In the case under consideration, ΔS^* is evidently negative, and its numerical value is such that $T\Delta S^*$ compensates for ΔG^*, i.e., $\Delta G^* = -T\Delta S^*$, and accordingly $\Delta H^* = 0$. It is reasonable that the formation of the activated complex $(Pb_2O)_2$ from two Pb_2O entities is accompanied by decrease in the order of the system, and hence, ΔS^* is negative, Table (2).

4. Passivity of lead:

When the current density is such that the rate of formation of plumbous oxide exceeds the rate of its chemical dissolution, the potential was found to rise rapidly, showing a tendency towards passivity. The current density at which passivity occured, increased as the concentration of the alkali hydroxide was increased.

SUMMARY:

The potential of the lead anode was measured as a function of current denaity in 0.1 - 10 N NaOH solutions at 20 - 50 °C.

The overpotential is independent of pH in pure solutions as well as in solutions containing excess neutral salts. From the electron number value (4), it was suggested that the surface lead atoms exist as diatomic molecules. A suboxide (Pb_2O) is first formed, which undergoes self-oxidation to PbO. This latter step governs the overall reaction rate. The effect of temperature was also investigated. The exchange current is almost unaffected with temperature; this means that the heat of activation is equal to zero.

REFERENCES:

1. S. A. Awad and A. Kassab, J. Electroanal.

Chem., 26, 127, 1970.

2. P. Jones, H. R. Thirsk and W. F. K. Wynne-Jones, Trans. Faraday Soc. 52, 1003, 1956.

3. SH. Z. Khamudkhamova, Trudy Tashkent, Farm. Inst. 1, 359, 1957.

4. A. A. Abdul-Azim and K. M. EL-Sobki, Corrosion Science, 12, 207, 1972.

5. S. A. Awad, Electrochem. Acta, 7, 677, 1962.

6. W. M. Latimer, Oxidation Potential, Prentice-Hall, Englewood Cliffs, N. J., 2nd. Ed., pp. 39 & 149, 1952.

7. A. J. De-Bethune, T. S. Licht and N. Swendeman, J. Electrochem. Soc., 106, 616, 1959.

8. S. A. Awad, J. Electrochem. Soc., 109, 865, 1962.

9. S. A. Awad, Electrochem. Acta, 13, 925, 1968.

10. J. O'M. Bockris & E. C. Potter, J. Electrochem. Soc., 99, 169, 1952.

Table 1

Stationary potentials and parameters of overpotential for lead anodes in different solutions at 30 °C.

$[NaOH]/_{-1}$ mol l^{-1}	pH	Stationary potential/V NHE	Tafel slope/ mV	i_o A $cm.^{-2}$ 10^{-5}	$(\partial\eta/\partial i)_{\eta=2} \rightarrow \infty$ / VA^{-1} $cm.^{-2}$	λ	η /mV at 10^{-3} A $cm.^{-2}$ Pure soln.	Soln. containing 1 M Na_2SO_4
0.1	12.89	-0.521	32	7	80	4.65	33	34
0.3	13.32	-0.532	32	17.85	36.6	3.99	32.5	33
0.5	13.54	-0.548	30	15.85	36.7	4.48	23	
1	13.83	-0.570	31	19.95	31.7	4.12	20	
2	14.15	-0.591	28	17.78	36.7	3.99	21	
5	14.68	-0.636	27	12.95	53.3	3.88	24	
10	15.04	-0.655	28	7.5	96.7	3.60	29	

Table 2

Effect of temperature on the exchange current for lead anodes in different NaOH solutions.

Temperature T	Log. i_o 0.5 N	5 N	10 N	ΔS^*
20	-3.8	-3.95	-4.10	-0.0/40
30	-3.8	-3.90	-4.125	-0.0/36
40	-3.75	-3.90	-4.14	-0.0/32
50	-3.75	-3.85	-4.14	-0.0/28

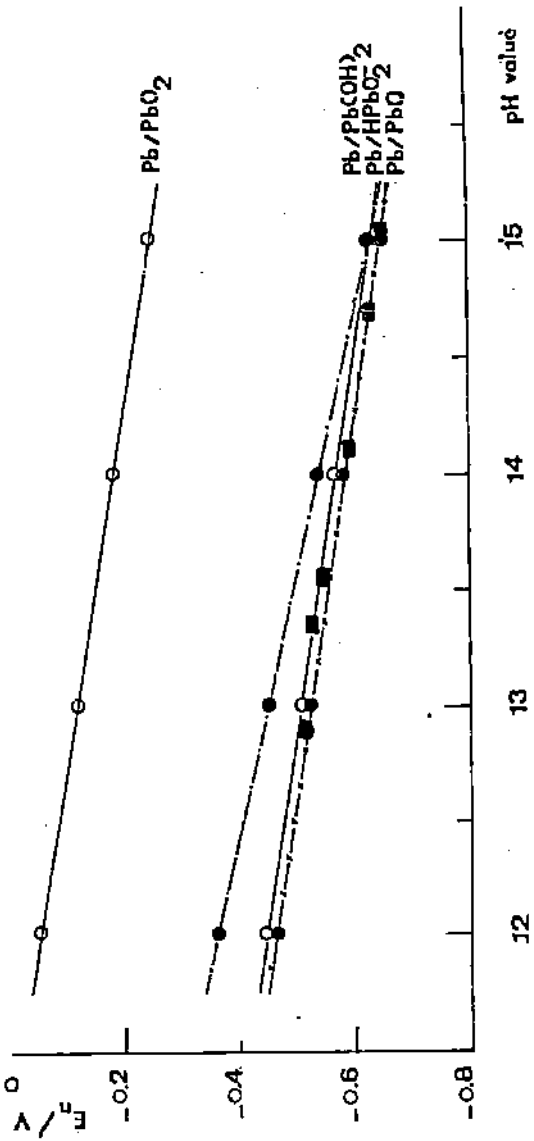

Fig (1): Effect of pH on the reversible potential of lead anodes.

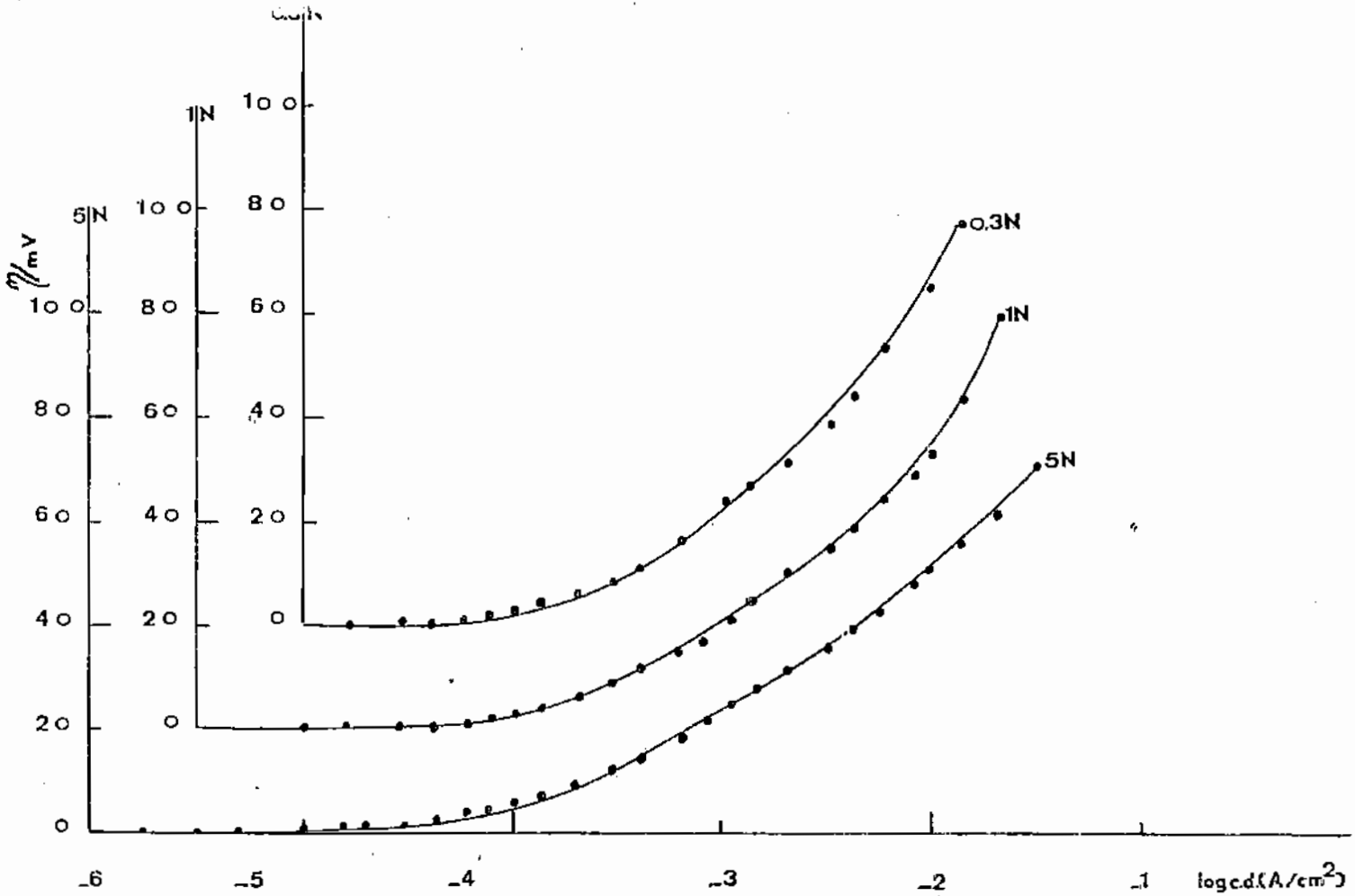

Fig.(2): Tafel lines for lead anodes in NaOH solutions at 30°C.

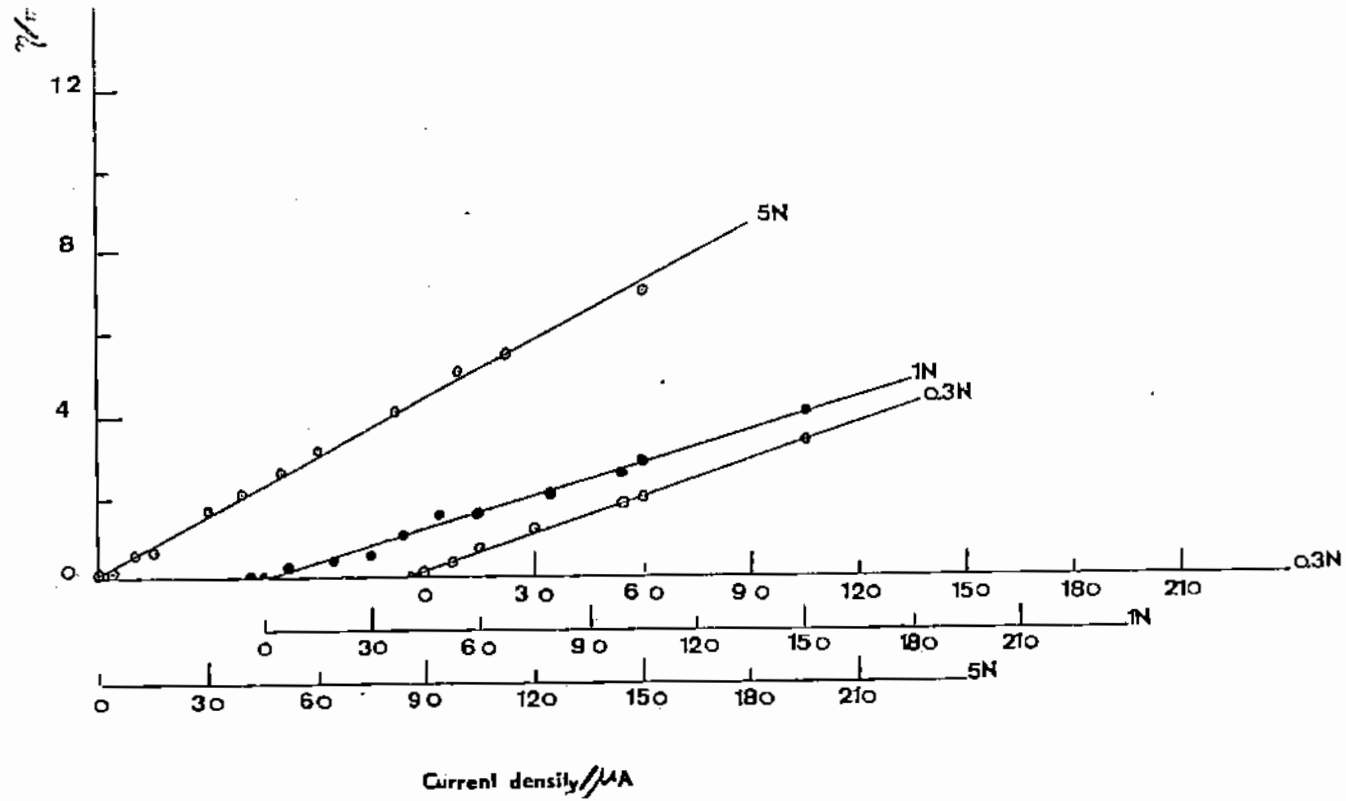

Fig (3): Relation between current density and overpotential at low anodic polarisation of lead.

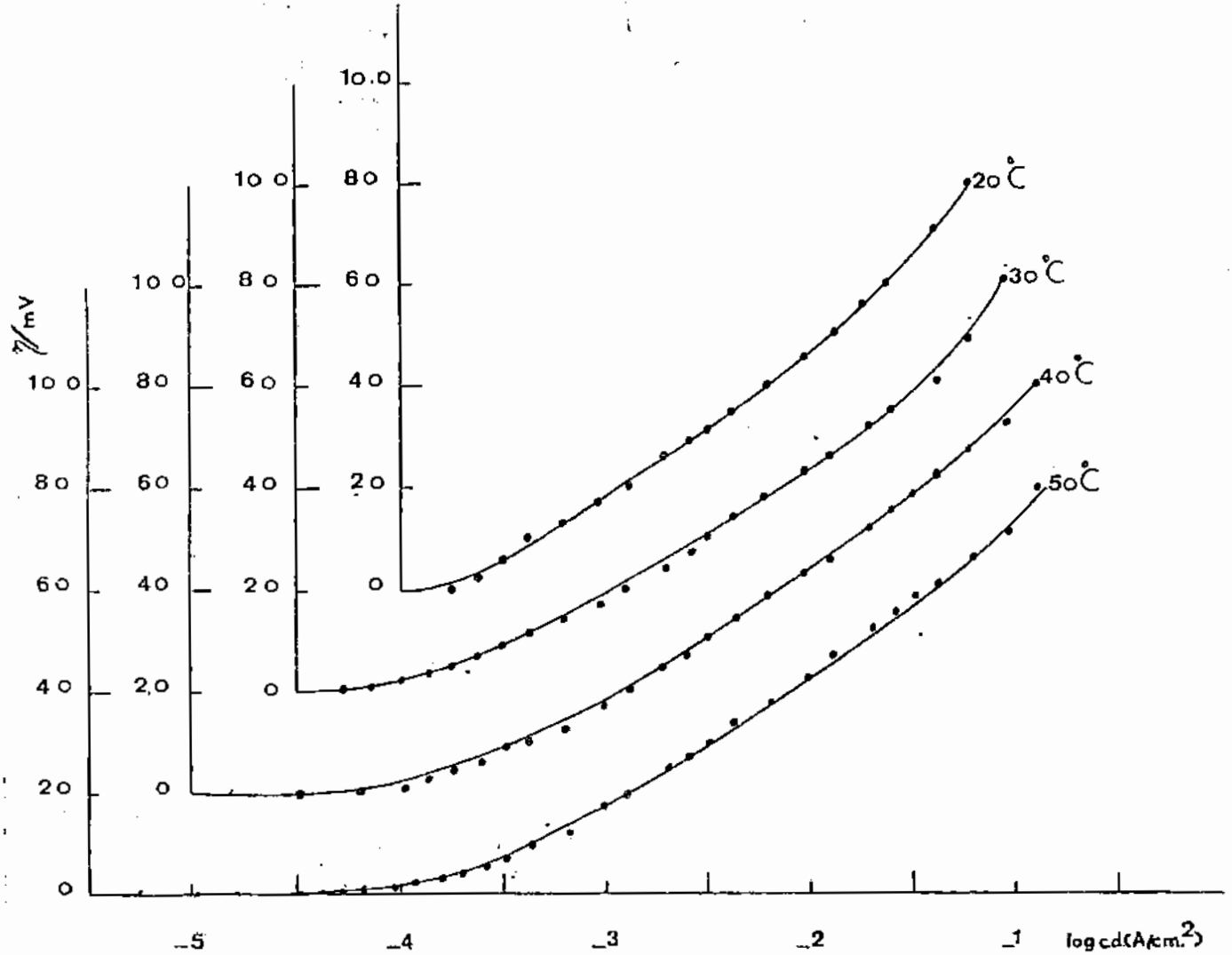
η/mV
10.0
8.0
6.0
4.0
2.0
0
20°C
30°C
40°C
50°C
-5
-4
-3
-2
-1
log cd(A/cm.²)

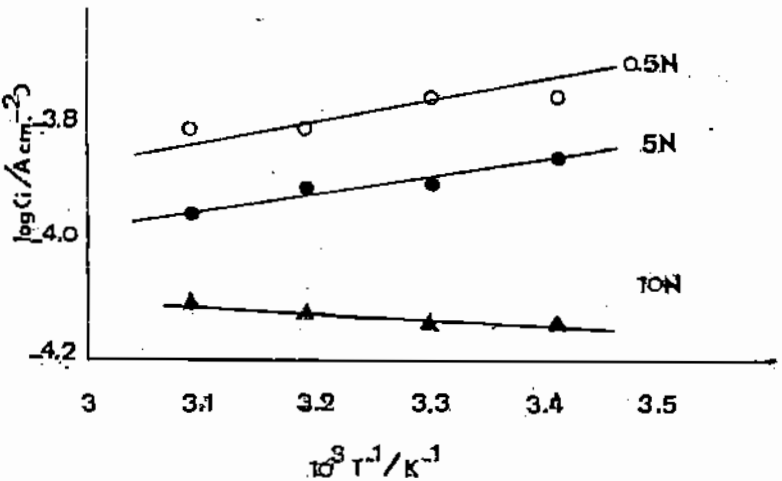

Fig (5): Effect of temperature on the exchange current for lead anodes in different NaOH solutions.

INTERACTION BETWEEN SOME HIGHER PLANTS AND AZOTOBACTER CHROCOCCUM

Zeinab Y.M., Abo Bakr and Fatma A. Helemish
Botany Dep., Women's College, Ain Shams University,
Cairo, Egypt.

Abstract

The interaction between four higher plants and Azotobacter chroococcum was studied in soil extract solution under sterile conditions. Cell counts of the test organism increased in the solution and on the rhizoplane. Incoulation with bacteria increased the dry weight of the test plants and their length. In addition it increased the nitrogen content of these plants and that of soil extract solutions. The extent of nitrogen fixation depends on the plant type.

Introduction

The beneficial effects of Azotobacter chroococcum on plant growth in soil of low fertility are well documented since long time ago (Mishustin and Naumova 1962; Jackson et al., 1964; Rovira 1965 and Denarié and Blacheré 1966). Recent work by several authors (Monib et al, 1979; Mahmoud et al. 1984; Kumar et al. 1984 and Barbash and Lozhikina 1985) have shown the beneficial effects of associative symbiosis between Azotobacter and certain higher plants.

Some authors assumed that bacteria utilize root exudates and provide the plants with nitrogenous compounds they secrete during N_2-fixation. However, Clark (1969) showed that different sugars, organic acids and amino acids were detected in root secretion

ov various plants. The role of organic matter in the interaction of higher plants and microorganisms in artificial ecosystem was studied by Golovko et al. (1984) who found that root exudates of cabbage and stubble root remains produce an increased in the quantity of certain microbial groups and they also found that perlite cultivation results in the accumulation of amino acids (64.1-120 mg per 100 g of dry perlite).

Brown (1982) thouth that the beneficial effects result from absorption by the plant roots of growth regulator substances produced in the bacterial culture used as inoculum, and from production of such substances in rhizosphere rather than from nitrogen fixation by the bacteria in the soil.

The present work was carried out to test the ability of a strain of Azotobacter chroococcum to colonize on the root system of some higher plants (wheat, barley, lupine and fenugreek) grown in soil extract solution under sterile conditions. The effect of interaction between plants and the test organism was evaluated by recording the change in dry weight of plants, length and nitrogen content as well as nitrogen content in soil extract solution.

Material and Methods

Barley, wheat, lupine and fenugreek were grown in soil extract culture to examine their response to inoculation with

Azotobacter. For each type of plant, seeds were chosen similar in size and weight and surface sterilized with 95% alcohol and 0.1% HgCl$_2$ solution (Rovira 1956). Seeds were then placed in petridish on sterile cotton wool, impregnated with distilled water and kept at 25°C till root emergence. Soil extract solution was distributed after sterilization in conical flasks (100 ml capacity) at the rate of 50 ml, plugged with cotton wool and resterilized. A batch of conical flasks was prepared for each type of seed, two thirds of which were inoculated with 1 ml of Azotobacter suspension of known cell density, prepared by growing the organism on nitrogen-deficient agar plates for 5 days at 30°C, then suspended in sterile distilled water and the one-third was left without inoculation as a control. Three seedlings aseptically placed on sterile thin cloth and tightly wrapped with threads and fine holes in the centre to permit downward movement of the root. Another set of conical flasks, inoculated with Azotobacter but without plants, was used as a second control. Conical flasks were kept in a room, exposed to day light after wrapping the bottom with paper to protect the roots from light.

Examination were carried out at weekl, intervals. For each type of plant, three of the inoculated conical flasks as well as three of the uninoculated ones were taken at random to estimate plant length, dry weight and nitrogen content of plants and soil extract solution. Bacteriological analysis was made on some other three conical flasks. Soil extract solution was made up to the original volume with distilled water before analysis. Control conical flasks were treated similarly.

Bacteriological and chemical analysis. For the determination of Azotobacter viable counts on the rhizoplane, 50 ml of sterile water and glass beads were added to the bottle containing the roots, while in solution, glass beads were placed in the original cultures. After mechanical shaking for 5 min. 10-fold dilutions were prepared and five tubes of nitrogen-deficient agar medium were inoculated from each dilution each tube was poured in petridish and incubated at 30°C for 15 days, then counted.

For chemical analysis, plants were dried at 100°C to constant weight and pulverised. Total nitrogen in plants as well as in soil extract solution was determined using the kjeldahl method (Jackson 1958).

Results

Effect of bacterization on plant growth

The effect of inoculating plants with Azotobacter was assessed by the determination of plant length and dry weight, nitrogen content of plant and soil extract solution. The favourable effect of bacterization was noticed after two weeks where inoculated plants were heavier and longer than uninoculated ones, but the response to bacterization varied from one plant to another (Tables 1, 2 and 3). At the end of the experiment, the percentage increase resulting from inoculation was varied from 16.00 to 25.68 for dry weight of shoot, from 12.50 to 33.33 for dry weight of root and from 14.28 to 20.38 for height of shoot of the tested plants (Table 4). The

effect of inoculation is also indicated by the increase in nitrogen content in plant tissue and in soil extract solution. Big amounts of nitrogen were found due to the interaction between plants and Azotobacter but type of plant plays an important role in that respect, barley and wheat gave higher amounts, while lupine and fenugreek gave lesser amounts during the five weeks of experiment. At the same time soil extract solution was found to contain big amount of nitrogen which had fixed by the bacteria. It was found higher in barley and wheat soil extract solution and lower in lupine and fenugreek (Table 5). It is evident that no significant changes in nitrogen were noticed in system devoid of Azotobacter, indicating that no nitrogenous compounds e.g. NH_3 were introduced in the system during the period of the experiment. As a result of the association between the tested plants and the N_2-fixer microorganisms all systems invariably showed positive results.

Effect of plant type on the development of Azotobacter.

It is clear from (Table 6) that all root system harboured population of Azotobacter within the first week ranging from 1.0 - 2.9 x 10^4 /root. Changing in microbial density thereafter depended on the plant type. In case of barley and wheat progressive increase was noticed at the end of the experiment while in case of lupine and fenugreek slight increase was noticed. Counts of graminaous plants were ranging from 4.6 - 6.2 x 10^4/root, while of leguminous plants, counts were ranging from 3.0 - 3.9 x 10^4/root.

Regarding the changing in bacterial counts of soil extract solution, it is clear that Azotobacter could survive for relatively long periods in soil extract solution lacking carbon source since the change in counts in the control was remain more or less constant, no change in nitrogen content of soil extract was recorded. Azotobacter counts ranging from 2.0 - 3.9 x 10^4/flask within the first week for the tested plants reaching from 5.9 - 6.1 x 10^4/flask for graminaous plants and from 4.6 - 5.9 x 10^4/flask for leguminous plants at the end of the experiment. Since the product of root exudates are not identical for different plants, the effect on the propagation of Azotobacter is vary according to the plant involved. Wheat followed by barley seemed to be the most favourable plant in that respect. Fenugreek and lupine followed wheat and barley. Bacterial count of graminaous plants increased 10-12 fold in whole system, while leguminous plants increased 8-9 fold at the end of the experiment comparable to the initial bacterial count at the begining of the experiment.

Discussion

The beneficial association between higher plants and Azotobacter has been extensively studied from different points of view. This relationship which could not be regarded as symbiosis is still obscure in its nature. Since many years ago several authors had suggested that Azotobacter probably influene the development of plants by producing growth regulating substance (Burger and Bukatsch 1958;

Brakel and Hilger 1965; Vancura and Macura 1960; Burlingham 1964; Hennquin and Blacheré 1966 and Brown and Barlingham 1968). While others have reported that beneficial effects are due to root secretion (Clark 1969). Moreover Berestetskii and Kravchenko (1980) showed that volatile organic compound which found in germinating wheat, corn, pea and lupine seeds were used as energy source for soil microorganisms.

For rhizobacteria to exert physiological effects on plant growth the bacteria must first effectively colonize the root surface, Douglas et al (1985). It was found in this investigation that all root systems harboured population of Aotobacter witin the first week, while microbialdensities changed thereafter depending on the plant type It was higher in presence of wheat and barley and lower in presence of lupine and fenugreek. The results reported herein were in full agreement with those obtained by Monib et al (1979) who found that microbial propagation depended on the type of plant being much higher in presence of wheat, followed by barley, maize, broad bean and cotton, while in presence of fenugreek and lentil lower rates of multiplication were recorded.

Microbial propagation depends not only on the type of plant but also on the variety of the same plant, however kumar et al. (1984) found that the rhizosphere of cotton variety H14 harboured significantly higher population of bacteria, actinomycetes, fungi and Azotobacter than variety P 5-10. Contrary, Mahmoud et al. (1984) noticed that total microbial flora of tomato and common

bean plants decreased slightly during the growth season in soil and rhizosphere. The R/S ratio were positive depending on plant species and ages. There was destinct relation between stages of plant development and the densities of total microbial flora. Densities of Azotobacter seemed to be contstant in their low count in the rhizosphere.

Inoculation of plants with bacteria increased their dry weight length and nitrogen content in plants and in soil extract solution. However, Monib et al. (1979) found that dry weight of plants increased by 5-12% and length by 3-18% in addition to increase nitrogen content of plants and nutrient solution.

Recent work by Azcon et al. (1978); Bagyaraj and Menge (1978) and Carr (1981) has shown that if an inoculum of Azotobacter chroococcum is added with the endophyte, plants grow better than if inoculated with endophyte only. Azotobacter chroococcum alone has been used for many years as a bacterial inoculant to improve plant growth, but only occasionally yields have been increased significantly (Brown 1974). Thus dual inoculation may prove to be more benificial in soil of low fertility than inoculation with either organism alone (Brown and Carr 1984). In this respect further studies were needed using dual inoculation for increasing soil fertility and crop yield.

REFERENCES

- Azcon, R., Azcon, G., De Aguilar, C. and Barea, J.M. (1978): Effect of plant hormones present in bacterial cultures on the formation and responses to VA endomycorrhiza. New Phytologist 80, 359-364.

- Bagyaraj, D.J. and Menge, J.A. (1978): Interactions between a VA mycorrhiza and Azotobacter and their effects on rhizosphere microflora and plant growth. New Phytologist 80, 567-573.

- Barbash, O. Yu and L.A. Lozhkina (1985). Effect of variously aged Azotobacter culture on cucumber root system. Mikrobiol ZH 47:17-20.

- Berestetskii, O.A. and L.V. Kravchenko (1980). Volatille organic compounds in germinating seeds as an energy source for soil microorganisms S-KH Biol 15: 878-881.

- Brakel, J. and Hilger, F. (1965): Etude qualitative et quantitative de la synthése de substances de nature auxinique par Azotobacter chroococcum in vitro. Bull. Inst. agron. Stns. Rech. Gembloux 33, 469.

- Brown, M.E. and Burlingham, S.K. (1968): Production of plant growth substances by Azotobacter chroococcum. Journal of General Microbiology 53:135-144.

- Brown, M.E. (1974): Seed and root bacterization. Annual Review of Phytopathology 12, 181-197.

- Brown, M.E. (1982): Nitrogen fixation by free-living bacteria associated with plants-fact or fiction. In Bacteria and plants ed. Rhodes-Roberts, M.E. and Skinner, F.A. pp.26-41. Society for applied Bacteriology Symposium Series No. 10 London: Academic Press.

- Brown, M.E. and Carr, G.R. (1984): Interaction between Azotobacter Chroococcum and vesicular-arbuscular mycorrhiza and their effects on plant growth. Jour. Appl. Bact. 56, 429-437.

- Burger, K. and Bukatsch, F. (1958): Über die Wuchsstoff synthese in Boden Freilebender, stickstoff bindender Backterien. Zentbl. Bakt. Parasitkde Abt. II, III, I.

- Burlingham, S.K. (1964): Growth regulators produced by Azotobacter in culture media. Ann. Rep. Rothamsted Exp. Stat. P. 92.

- Carr, G.R. (1981): Interaction of soil microorganisms in the rhizosphere of crop plants. Ph.D. Thesis, University of London.

- Clark, F.E. (1969). Ecological association among soil microorganisms In: Soil Biology Reviews of Research, UNESCO. Natural Resources Research IX, Paris, 125.

- Douglas, J.W. Jr.; Suslow, T.V. and Steinback, K.E. (1985): Relationship between rapid, firm adhesion and long-term colonization of roots by bacteria. Appl. Environ Microbiol 50:392-397.

- Denarié, J. and blachére, H. (1966): Inoculation de graines de vegétaux cultivé à l'aide de souches bacteriennes. Ann/s Inst. Pasteur, Paris III, Suppl. to No. 3, 57.

- Golovko, e.A., Gorobets, S.A. and Mazorchuk. (1984): The role of organic matter in the interaction of higher plants and microorganisms in artificial ecosystems. Fiziol Biokhim Kuet Rast 16:273-279.

- Hennequin, J.R. and blachére, H. (1966): Recherches sur la synthése de phytohormones et de composés phenoliques Par Azotobacter et des bactéries de la rhizosphere. Annls. Inst. Pasteur, Paris III, Suppl. to No. 3, 89.

- Jackson, M.L.. (1958): Soil Chemical Analysis, Constable and Co., London.

- Jackson, R.M., Brown, M.E. and Burlingham, S.K. (1964): Similar effects on tomato plants of Azotobacter inoculation and application of gibberellin Nature, 203: 851.

- Kumar, K, Agrawal, R.A. and Gaur, A.C. (1984). Systemic granular insecticides and rhizosphere microflora of cotton. J. Entomol Res. (New Delhi) 8: 168-192.

- Mahmoud, S.A.Z., Thabet, F.M., Ramadan, E.M. and Khater, T. (1984): Microbial and biochemical changes in soil and rhizosphere of tomato and common bean plants. Zentral Bl. Mikrobiol., Vol. 139, No. 4, pp. 219-226.

- Monib, M.; Abd-el-Malek, Y.; Hosny, I. and Fayez M. (1979). Associative symbiosis of Azotobacter chroococcum and higher plants. Zbl. Bakt. II. Abt. 134: 133-139.

- Mishustin, E.N. and Naumova, A.N. (1962): Bacterial fertilizars, their effectiveness and mechanism of action. Microbiologiya 31:543.

- Rovira, A.D. (1965). Effect of Azotobacter, Bacillus and Clostridium on the growth of wheat. Plant Microbe Relationships,

Symposium on Relationships between Soil Microorganisms and Plant Roots, Prague, 1963, P. 193.

- Rovira, A.D. (1956). Plant root excretions in relation to the rhizosphere effect. I. The nature of root exudate from oats and peas. Plant and Soil 7:178.

- Vancura, V. and Macura, J. (1960): Indole derivatives in Azotobacter cultures. Folia microbiol., Praha 5:293.

Table 1: Dry weight of shoot (mg) at different periods (weeks) (mean of three shoots) .

Plants		1	2	3	4	5
Barley	A	39	39	42	51	67
	B	46	48	55	62	82
Wheat	A	28	29	32	45	87
	B	48	50	50	54	103
Lupine	A	437	484	521	535	545
	B	516	521	530	547	685
Fenugreek	A	27	28	42	60	100
	B	59	61	74	78	116

A uninoculated with Azotobacter
B inoculated with Azotobacter

Table 2 : Dry weight of root (mg) at different periods (weeks) (mean of three roots) .

Plants		1	2	3	4	5
Barley	A	12	19	22	26	32
	B	14	22	24	29	36
Wheat	A	11	13	24	35	47
	B	13	16	30	39	50
Lupine	A	54	[illegible]7	75	82	88
	B	68	[illegible]	84	95	107
Fenugreek	A	9	[illegible]	[illegible]	17	27
	B	11	[illegible]	[illegible]	21	36

A uninoculated with [illegible]

B inoculated with Azotobacter

Table 3 : Height of shoot (cm) at different periods (weeks) (mean of three shoots).

Plants		1	2	3	4	5
Barley	A	6.55	7.00	8.11	8.16	8.20
	B	6.91	7.83	9.27	9.35	9.50
Wheet	A	5.22	5.44	5.75	6.44	7.00
	B	6.55	6.77	7.00	7.30	8.00
Lupine	A	12.33	13.96	15.00	16.77	15.50
	B	12.55	15.05	15.16	16.83	18.66
Fenugreek	A	2. 77	2. 77	3. 66	6. 00	11.66
	B	3. 05	3.72	5. 77	8. 50	13.33

A uninoculated with Azotobacter
B inoculated with Azotobacter

Table 4 : Percentage increase over control of dry weight (mg) of shoot, root and height of shoot (cm) after five weeks (mean of three readings)

Plants	Dry Weight of shoot			Dry weight of root			Height of shoot		
	A	B	%	A	B	%	A	B	%
Barley	67	82	22.30	39	36	12.5	8.20	9.50	15.8
Wheat	87	103	18.30	47	50	27.6	7.00	8.00	14.28
Lupine	545	685	25.68	88	107	21.5	15.50	18.66	20.38
Fenugreek	100	116	16.00	27	36	33.33	11.66	13.33	14.32

A uninoculated with Azotobacter

B inoculated with Azotobacter

Table 5 : Nitrogen content of plants and soil extract solution of the different periods

Plants		In plants(mg / 100 mg dry weight)					In solution (mg /100 ml)				
		Weeks					Weeks				
		1	2	3	4	5	1	2	3	4	5
Barley	A	1.80	2.30	2.80	2.80	2.90	1.2	1.2	1.3	1.4	1.60
	B	1.90	2.30	2.60	3.50	3.70	1.60	5.00	8.40	11.00	13.10
Wheat	A	1.90	2.50	2.90	3.10	3.30	3.30	3.40	3.50	3.60	3.60
	B	2.70	3.00	3.40	4.50	4.30	3.4	5.40	8.80	11.5	14.60
Lupine	A	6.4	7.6	7.70	8.60	8.90	4.60	4.60	4.40	4.20	4.20
	B	7.6	8.4	9.6	9.60	10.6	3.60	3.60	5.80	6.40	7.20
Fenugreek	A	1.80	3.10	4.00	4.40	4.50	2.60	2.81	3.70	3.75	3.83
	B	3.40	3.40	3.50	4.40	5.50	3.8	4.1	4.28	4.92	5.50

A uninoculated with Azotobacter
B inoculated with Azotobacter

extract solution :

Plants	*Azotobacter* counts in rhizoplane x 10^4					*Azotobacter* counts in soil extract solution x 10^4				
	Weeks					Weeks				
	1	2	3	4	5	1	2	3	4	5
Barley	1.0	1.2	1.8	3.1	4.6	2.0	2.3	4.2	5.0	5.9
Wheat	2.9	3.1	3.3	5.3	6.2	3.9	5.0	5.1	5.5	6.1
Lupine	1.9	2.5	2.8	3.4	3.9	3.9	4.0	4.1	4.3	4.6
Fenugreek	1.4	1.5	1.7	2.1	3.0	3.0	3.3	4.9	5.7	5.9

Intial *Azotobacter* count was 1.5×10^4 in whole system .

العلاقة بين بعض النباتات الراقيه وبين نوع معين من الميكروبات الدقيقة

زينب يوسف أبو بكر فاطمه عبد الوهاب حليمش
قسم النبات — كلية البنات — جامعة عين شمس — القاهره

ملخص

يهدف هذا البحث الى معرفة علاقة النباتات الراقيه بنوع معين من الميكروبات الدقيقه هو الازوتوباكتر كروكوكم فى مستخلص التربه المعقم على مدى خمس اسابيع من بداية التجربة . لذلك تم تعيين كل من الوزن الجاف للساق والجذر وطول الساق والمحتوى النيتروجينى لكل من النبات ومستخلص التربه وكذلك عد البكتيريا الموجوده على الجذر والموجوده فى محلول مستخلص التربه هذا وقد اوضحت النتائج ما يلى :

١— كانت هناك زيادة محسوسه فى الوزن الجاف لكل من الساق والجذر وكذلك زيادة فى طول الساق وذلك نتيجة للعلاقة التى نشأت بين النبات الراقى وبين الكائن الدقيق حيث كانت هذه الزيادة تختلف باختلاف نوع النبات .

٢— النباتات النجيلية كانت اكثر استجابة لهذه العلاقة عن النباتات البقولية .

٣— زاد المحتوى النيتروجينى لنبات القمح والشعير بنسبة اكبر من نبات الترمس والحلبه وزاد المحتوى النيتروجينى فى مستخلص التربه للقمح والشعير عنه فى الترمس والحلبه .

٤— اعداد البكتريا على جذر نبات القمح والشعير كانت اكبر من اعدادها على جذر نبات الترمس والحلبه واعداد البكتريا فى مستخلص التربه كان اعلى فى النباتات النجيلية عنه فى النباتات البقولية . بينما كانت اعداد البكتريا على الجذور عموما اقل من اعدادها فى مستخلص التربه .

GAMMA RADIATION INDUCED FUNGICIDE-SENSITIVE MUTANT OF PEANUT RHIZOBIUM STRAINS

F.A. HELEMISH and S. Abd El AAL*

Botany Dep., Women's College, Ain Shams University, Cairo, Egypt.

ABSTRACT

Two fast growing Rhizobium strains of peanut (Arachis hypogea) A.V. and 169 were subjected to increasing doses of γ-radiation. Dose response curve and sublethal dose were determined. Effect of the fungicide (Tilt) on the survival of the most radioresistant bacterial isolates was alsoexamined.

Results showed that the dose response curve of both strains was of the exponential type and the sublethal dose for 169 strain was 50 k rad while that for A.V. strain was 75 k rad.

Interaction of the most radioresistant bacterial isolates and the fungicide (Tilt) with different doses of 2.5, 5, 7.5, 10, 20, 25 and 30 ppm showed that γ-rays induced a fungicide sensitive isolates more than the wild type.

INTRODUCTION

Some authors (Jordan, 1952a; Dygdala, 1962, 1963; Russell and Jones, 1973; El-Zawahry, 1976; Srivastava et al., 1980 and Barend and Henri, 1981) have studied the effect of radiation on growth and survival of the bacteria responsible for soil fertility through symbiotic association, such as the symbiotic nitrogen fixing bacteria belonging to the genus Rhizobium.

The use of pesticides has become an integral and economically essential part of agriculture. Because of concern about possible side effects the attention of soil microbiologists has been focused on the effects of pesticides on non target soil microorganisms such as Rhizobium.

---

* Atomic Energy Establishment, Cairo, Egypt.

Pareek and Shidu (1978) reported that the phenoxy herbicide 2,4-D reduced the growth of R. meliloti, R. trifolii and Rhizobium sp., oxygen suptake was stimulated though endogenous respiration was not affected.

Janos et al., (1979) studied the effect of the urea herbicide chlorobromuron and its hydrolysate product, chlorobromaniline, on R. meliloti and found that chlorobromuron inhibited growth at a concentration of 10 mg/L. However chlorobromaniline stimulated the growth of R. meliloti.

Kao and Wang (1981) studied the interaction between herbicides and Rhizobium in pure culture. They found that the fast-growing type rhizobia were more sensitive than the slow-growing ones in presence of the same herbicide dosage, however linuron with the dosage of 50 ppm was decomposed by Rhizobium-leguminosarum and Rhizobium japonicum (Cowpea strain) individually, and 2,4-D of 50 ppm was also decomposed by Rhizobium lupini. Mutants of R. meliloti, R. phaseoli and cowpea rhizobia that were resistant to the fungicides thiram, phygon and spergon have been isolated by Odeyemi and Alexander (1977a,b). These fungicide resistant mutants were able to destroy the pesticides and were highly effective on their host plants. So, these fungicide resistant mutants considered as better inoculants than their parental strains when applied to legume seeds that had been treated with these fungicides.

The present investigation aimed at the response of two strains of Peanut to increasing doses of γ-radiation as well as the effect of the fungicide (Tilt) on the survival of the most raioresistant bacterial isolates.

MATERIAL AND METHODS

Bacterial strains: Effective strains were obtained from the Microbiology Research Center, Ministry of Agriculture, Cairo, two strains were used A.V. and 169. Cultures were grown and maintained on yeast extract mannitol medium (YMA) (Allen, 1957) of the following composition: Mannitol, 10g; Nacl, 0.1g: $MgSo_4$. 7 H_2O, 0.2g; K_2H PO_4, 0.5g: yeast extract, 0.5g; $CaCl_2$, 0.1 g, distilled water 1000 ml. The pH of the medium was adjusted to 7.2 using NaOH. Fifteen grams of Difco agar were added when desired.

Irradiation techniques:

Source of Gamma radiation: The used source of radiation was cobalt 60 (commercial Gamma cell Atomic Energy of Canada Limited, Located in the Physics Department of the Egyptian Atomic Energy Establishment), giving a dose of 15 rads per second at time of experiment.

Irradiation of the wild type Rhizobium strains A.V. and 169:

The adopted method was that recommended by Dygdala (1963), Schwinghamer (1969) and Russell and Jones (1973). The wild strains

of Rhizobium A.V and 169 were allowed to grow individually untill the late log phase on yeast extract mannitol liquid medium. At the end of the growth period, the cells were hervested by centrifugation. The harvested cells were then washed with phosphate buffer at pH 7.0 for three times and finaly resuspended in the buffer to a concentration of 10^7 - 10^8 cells/ml. The bacterial suspension was divided under aseptic condition into 5 ml aliquots in sterile test tubes. Duplicate tubes of the above bacterial culture were exposed to increasing doses of γ-radiation (10, 20, 30, 40, 50, 75 and 100 Krad) at room temperature. Control culture tubes (of non irradiated culture) were kept at room temperature. Viable count for each of the irradiated and the control cultures were determined by the dilution plate (pour agar plate) method on yeast extract mannitol agar medium. Incubation of the agar plates continued for one week at 28°C before they were counted. Dose response curve was constructed by plotting log N/No VS: the irradiation dose where No and N were the intial and final viable count for each irradiation dose.

Isolation of the most radioresistant bacterial isolates:

Bacteria at the sublethal dose were subcultured three times on petridish containing yeast extract mannitol agar medium.

Effect of the fungicide (Tilt) on the survival of the most radioresistant bacterial isolates:

The effect of the fungicide "tilt" on the survival of the most radioresistant bacterial isolate of the wild type A.V and 169 strains was investigated. Bacteria were incoulated separately

in yeast extract mannitol broth medium supplemented with tilt at concentrations of 2.5, 5, 7.5, 10, 15, 20, 25 and 30 ppm of active ingredient per ml medium. Cultures were prepared in 100 ml conical flask containing 50 ml of medium incoulated with 0.2ml of a culture of the bacteria (about 10^6 cells/ml) in yeast mannitol liquid medium and incubated at 28°C on a rotary shaker. Viability of the bacteria was monitored by plating on yeast extract-mannitol-agar.

Pesticide:

One comercially available pesticide was used in this investigation.

The fungicide (Tilt), a product of (GIBA-GEIGY) Switzerland. The active ingredient is 1-[2-(2,4 dichlorophenyl)-4-propyl-1,3-dioxolan-2-yl methyl]-1H-1,2,4 triazole.

It is available as an emulsifiable concentrate with 25% active ingredient, and 0.25% recommended field application (Hussain, 1985).

RESULTS

Response of Rhizobium of Peanut A.Y. and 169 strains to increasing doses of γ-radiation.

This experment was conducted to measure the resistance of Rhizobium of Peanut strains to the following doses of γ-radiations 10, 20, 30, 40, 50, 75 and 100 K rad. The number of viable cells after irradiation was taken as criterion for resistance as compared with non irradiated control.

Fig. (1) and Table (1) show the effect of different doses of γ-radiation on the number of viable cells of the wild type of Rhizobium of Peanut 169 strain. These results suggested that this Rhizobium strain was highly sensitive to γ-radiation. Dose response curve is of the exponential type as the viable count decressed with the increase of γ-radiation. Vaible count begins with 1.3×10^8 and ends with 1.3×10^3 at non irradiated control and dose of 50 k rad respectively. No growth was recorded at 75 k rad. A dose of 50 k rad was estimated as the sublethal dose. It was found that a dose of 50 k rad reduced the number of survival cells by 5 log cycle.

Fig. (2) and Table (2) show the effects of different doses of gamma radiation on the number of viable cells of the wild type of Rhizobium of Peanut A.V. strain. The results suggested that this Rhizobium strain was less sensitive to γ-radiation. Dose response curve is of the exponential type because the viable count decreased with the increase of γ-radiation. Non irradiated control begins with 6.9×10^8 and reaches 3.1×10^2 at the dose of 75 krad. No growth was recorded at the dose of 100 k rad. A dose of 75 k rad was estimated as the sublethal dose and it reduced the viable count by 6 log cycle.

Effect of the fungicide (Tilt) on the survival of the most radio-resistant bacterial isolates of A.V. and 169 strains and their wild type.

Addition of the fungicide (Tilt) at different concentrations varying from 2.5 to 30 ppm to the yeast extract mannitol broth

together with the most radioresistant bacterial isolate and its parent (Table 3) during the log phase results in an increase in viable count of the wild type of strain 169. Survival percentage increased gradually from 2.5 to 20 ppm then decreased at 25 and 30 ppm. Highest survivors recorded at 20 ppm. Survival percentage of the most radioresistant isolate increased at the lower doses of fungicide, while it decreased at the higher dosage. Highest survivors recorded at 7.5 ppm then it decreased gradually after that (Table 3).

Table (4) shows that survival of Rhizobium of Peanut A.V. in yeast extract mannitol medium supplemented with different doses of the fungicide (Tilt)-increased with the increase of the fungicide concentration from 2.5 to 7.5 ppm then decreased from 10 to 30 ppm. Highest survivors recored at 7.5 ppm. It was found that at this concentrations of the fungicide, the survivors increase 4-fold over that of the control. Survivors of the most radioresistant isolate increased gradually at the lower fungicide concentration from 2.5 to 7.5 then it decreased in presence of 7.5 to 30 ppm. Highest survivors recorded at 7.5 ppm.

It is clearly shown that the most radioresistant bacterial isolate either from 169 strain or from A.V. strain produced fungicide sensitive mutants while the wild type produced fungicide resistant mutants.

DISCUSSION

Many leguminous plants have been infected by certain fungi articulary Peanut (Arachis hypogea).

Aspergillus flavus, the common soil fungus may infest products uch as Groundnut and dried foods and produced a toxin called aflaoxin known to induce diseases to man and animals (Wogan 1965).

The purpose of this investigation was to manifest the effect of gamma radiation and the fungicide "Tilt" on the survival of the Peanut (Groundnut) Rhizobium strains for finding a fungi-cide resistance mutant used as an inoculant of Groundnut seeds as for the protection from Aspergillus flavus and other filamentous soil fungi.

Rhizobium strain 169 was foundmore sensitive to gamma radiation as the viable count was decreased with the increase of gamma radiation doses, thus it exihibited a simple exponential response curve with most radioresistant bacterial isolate at 50 k rad dose (Table 1). El-Zawahry (1976) found that radioresistant strains could be developed if the wild type of Rhizobium leguminosarum strain is subjected to different doses of gamma rays.

Rhizobium strain A.V. was found less sensitive to gamma radiation and it exihibited a simple exponential dose response curve with most radioresistant isolate at 75 k rad (Table 2). Barend and Henri (1981) studied the effect of gamma rays on the growth and

survival of Peanut Rhizobium strain in peat culture and they found that the Rhizobium strain is not sensitive to gamma rays and it is not affected byincreasing the dose from 25 to 50 KGY.

As "Tilt" is a fungicide of many agriculture plants, it would be useful to have resistant strains to be used as inoculants. Tilt induced a fungicide resistant mutant with the wild type of Rhizobium strains and 20 ppm fungicidal concentration induced survival increase 3-fold over that of control (Table 3) in 169 strain while 7.5 ppm fungicidal concentration induced survival increase 4-fold in A.V. strain (Table 4).

The fact that pesticides inhibited and/or stimulated Rhizobium strains, many authors have suggested that it might be due to a lack of energy for cell synthesis because the pesticides acts as an uncoupling agent of oxidative phosphorylation (Pareek and Shidu 1978). While Odeyemi and Alexander (1977a,b) and Kao and Wang (1981) have suggested that the fungicide resistant mutants were able to destroy the pesticide.

The most radioresistant isolate did not induced a fungicide resistant mutants as all the fungicidal concentrations induced survival decrease in viable count of cells, survivals decreased with the increase of fungicidal concentrations (Tables

3 and 4). Since the most radioresistant isolate of 169 strain was achieved at 50 K rad and the most radioresistant isolate of A.V. strain was achieved at 75 K rad; survivors of 169 strain were more than those of strain A.V., they were 88% and 48% at the same level of fungicidal concentration (7.5 ppm) respectively (Tables 3 and 4).Golebiowska et al., (1967) reported that Rhizobium strains showed different sensitivities to the fungicide thiuram. They also reported that subculturing bacteria in media containing thiuram did not increase the fraction of thiuram resistant mutants in most Rhizobium strains. However the frequency of bacteria resistant to thiuram was increased among survivors of U.V. irradiation indicating that resistance could be induced by mutation. Ruiz-Sainz et al. (1984) studied the effect of the fungicide captafol on the survival and symbiotic properties of Rhizobium trifolii and they found that captafol resistant mutants lost the smallest plasmid responsible for nodulatin and nitrogen fixation, hence it is not necessary that a fungicide resistant mutants form good nodulation and nitrogen fixation. Curley and Burton (1975) have made a similar suggestion in a report in which they found that although captan was less toxic for Rhizobium japonicum than PCNB (pentachloronitrobenzene) the former was more inhibitory to nodulation when they were used as seed protectants for inoculated soybean.

If comparing the effect of certain chemicals and the effect of radiation on Rhizobium survival and activity, Khare et al. (1982)

found that mutagency by radiation was more pronounced than chemical mutagency in Cicer arietnum Rhizobium strains. The mutant produced different from their parents in that the mutant colony size was bigger and gelatinase activity was higher, the number of nodules and its size were also higher.

Many studies have been done on the effect of pesticides on Rhizobium in which the measurment of the viability of a culture after a pesticide treatment has been the main method used to determine whether the assayed pesticides were harmful for Rhizobium or not (Ruiz-Sainz et al., 1984). Further work is needed to determine the effect of the fungicides on the survival and symbiotic properties of the Rhizobium strains.

ACKNOWLEDGEMENT

The authors are grateful to professor Dr. H. Roushdy, Director of NCRRT for the facilities provided to carry out this work.

REFERENCES

1. Allen, O.N. (1957) Experiments in soil Bacteriology. 3rd ed. Minneapolis.

2. Barend, W.S. and Henri, J.V.R. (1981): Effect of steam sterilization and gamma irradiation of peat on quality of Rhizobium inoculants, Applied and Environmental Micobiology, 41(6), 1344-1347.

3. Curley, R.L. and Burton, J.C. (1975). Compatibility of R. japonicum with chemical seed protectants. Agronomy Journal 67, 807-808.

4. Dygdala, K. (1962). Morphological and cytological changes of Rhizobium as influenced by gamma rays and radiometric substances. Bull. Acad. Polon. Sci, Ser. Biol., 10, 381.

5. Dygdala, K. (1963). Morphological and cytological observations on gamma rays irradiated Rhizobium leguminosarum. Acta Micr. Pol., 12, 237.

6. El-Zawahry, Y.A. (1976). Study on the effect of gamma radiation on growth and activity of Rhizobium leguminosarum Ph.D. Thesis, Cairo University. Egypt.

7. Golebiowska, J., Kaszubiak, H. and Pajewska, M. (1967). Adaptation of Rhizobium to thiuram. Acta microbiologica polonica, 16, 153-158.

8. Hussain, A.A. (1985). Studies on the effect of some pesticides on the chemical composition of some yeasts. Ph.D. Thesis. Women's College, Ain Shams University. Egypt.

9. Janos, E., Cserhati, T. and Kecskes, M. (1979). Xenobiotics and soil micrbiota affected by xenobiotic interactions. Chlorobromuron and its breakdown product inhibiting the growth of different microorganisms. Acta microbiological academiae scientiarum, hungaricae, 26, 301-309.

10. Jordan, D.C. (1952a). Studies on the legume root nodule bacteria. II, The production and behavior of colonial mutants produced by X-ray; irradiation. Cand. J. Botany, 30, 125-130.

11. Kao Te-chen and Chi-chu wang (1981): Studies on the effect of herbicides on growth of Rhizobia and development of root nodules III. The interaction between herbicides and Rhizobia in pure culture. Journal of the Agricultural association, 114, 45-66.

12. Khare, A.K., Shinoe, D.A. and Nayak, M.L. (1982). Comparative effeciency of chemical and radiation mutagens on 2 Cicer-arietnum rhizobial strains.

13. Odeyemi, O. and Alexander, M. (1977a). Resistance of Rhizobium strains to phygon, speryon and thiuram. Applied and Environmental Microbiology, 33, 784-490.

14. Odeyemi, O. and Alexander, M. (1977b). Use of fungicide-resistant rhizobia for legume inoculation. Soil Biology and Biochemistry, 9, 247-251.

15. Paresk. R.P. and Shidu, B.S. (1978). Uncoupling of phosphorylation in Rhizobium spp. by 2, 4-dichlorophenoxy acetic acid and Taficide-80. Indian Journal of Microbiology, 18, 97-100.

16. Ruiz-Sainz, J.E.; Beringer, J.E. and Gutierrez-Navarro, A.M. (1984). Effect of the fungicide captafol on the survival and symbiotic properties of Rhizobium trifolii. Journal of Applied Bacteriology, 57, 361-367.

17. Russell, J.A., and Jones, D.G. (1973). The effect of ultra violet light on the symbiotic effectiveness and some physiological characteristics of four strains of Rhizobium trifolii J. Appl. Bact., 36, 567.

18. Schwinghamer, E.A. (1969). Mutation to auxotrophy and protatrophy as related to symbiotic effectiveness Rhizobium leguminosorum and R. trifolii. Cand. J. Microbiol. 15, 611.

19. Srivastava, R.C.; Mukerji, D.; Chandra, G. and Mathur, S.N. (1980). Radiation induced changes in the nitrate reductase activity in Rhizobium culture, leaves and nodules of Black-Gram (Vigna mungo (L) Hepper). Annual meeting of the American society of plant physiologists and the phytochemical society of North America.

20. Wogan, G.N. (ed.) (1965): Mycotoxins in foodstuffs. 291 pp. Cambridge, Mass.: M.I.T. Press.

Table (1) : Effect of different doses of Gamma radiation on the survival of Rhizobium of Peanut (Arachis hypogea) 169 strain .

Irradiation dose (Krad)	Number of surviving cells	Log number of surviving cells	Log surviving fraction ($\log \frac{N}{N_0}$)
Control	1.3062×10^8	8.116	0
10	1.6443×10^7	7.215	- 0.900
20	1.5601×10^6	6.193	- 1.922
30	2.0057×10^5	5.302	- 2.813
40	1.5520×10^4	4.190	- 3.925
50	1.3172×10^3	3.119	- 4.996
75	No growth	-	-
100	No growth	-	-

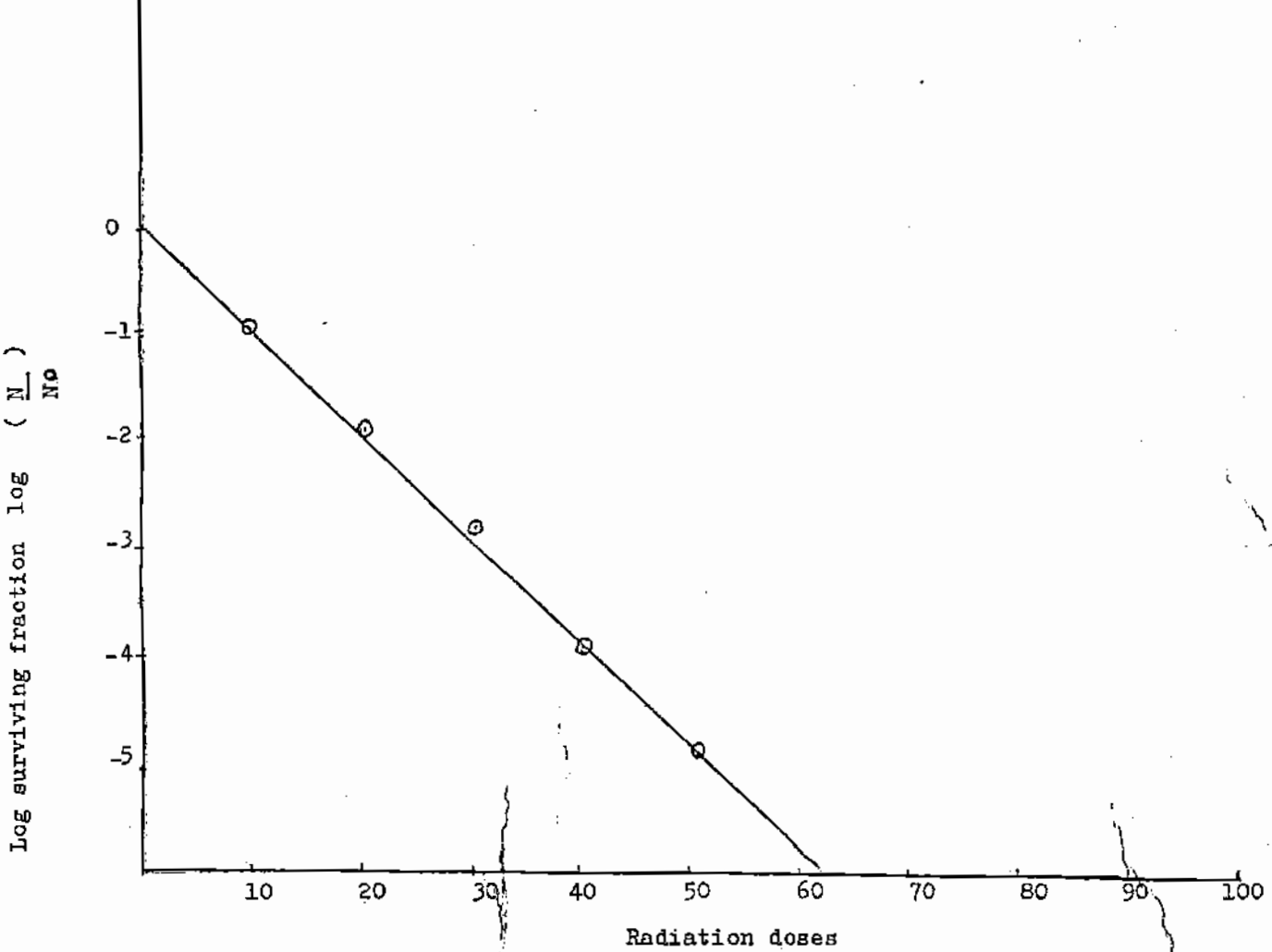

Fig (1) Dose response curve of peanut Rhizobium strain 169

Table (2) : Effect of different doses of Gamma radiation on the survival of Rhizobium of Peanut (Arachis hypogea) A.V strain

Irradiation dose (Krad)	Number of surviving cells	Log number of surviving cells	Log surviving fraction (log $\frac{N}{N_0}$)
Control	6.9155×10^8	8.839	0
10	6.3480×10^7	7.802	- 1.037
20	4.4016×10^6	6.643	- 2.196
30	2.5259×10^5	5.402	- 3.437
40	2.689×10^4	4.422	- 4.410
50	3.1155×10^3	3.493	- 5.346
75	3.1020×10^2	2.491	- 6.348
100	No growth	-	-

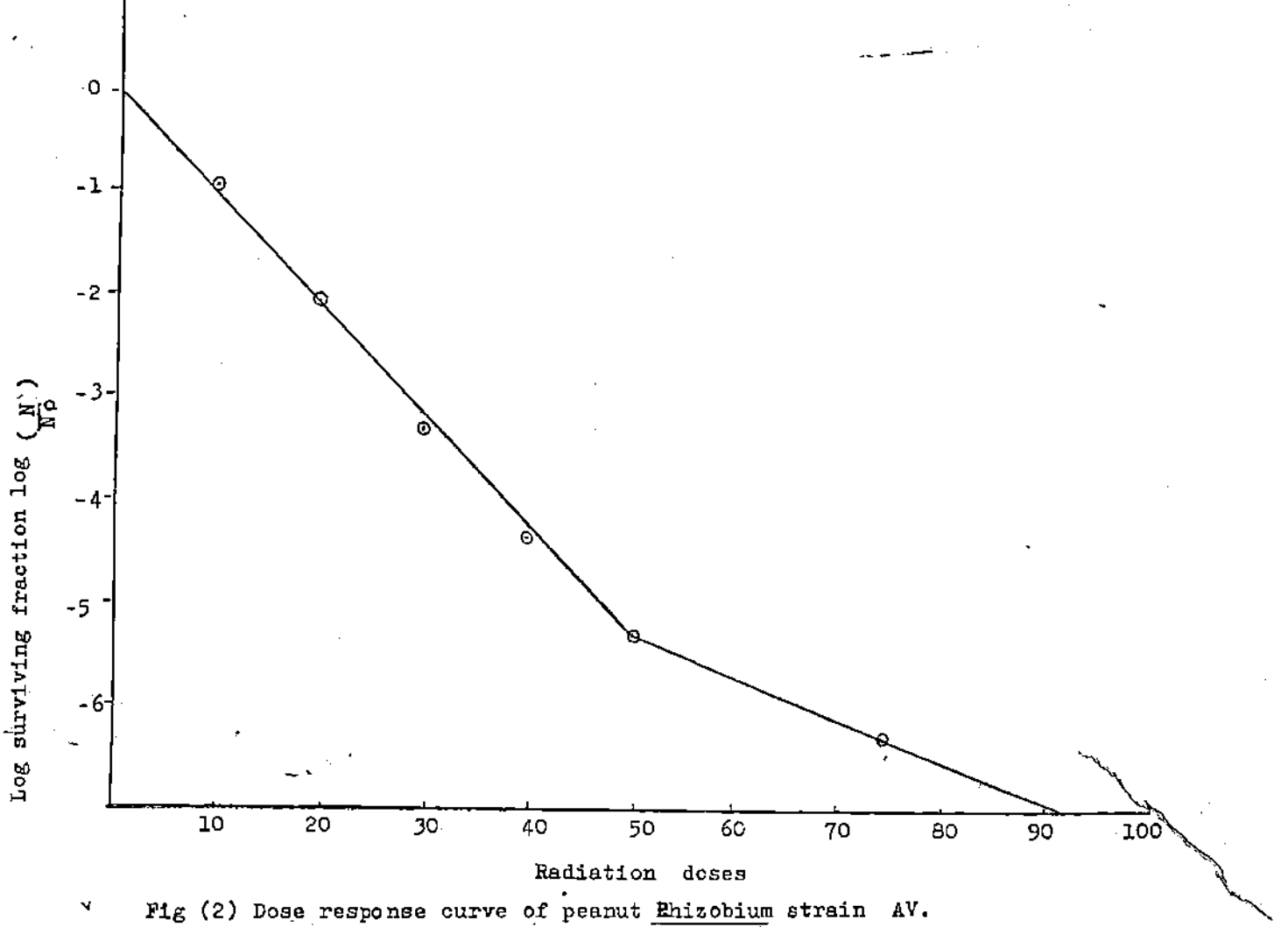

Fig (2) Dose response curve of peanut Rhizobium strain AV.

Table (3) : Survival of Rhizobium of peanut 169 strain in yeast extract mannitol medium supplemented with different concentrations of the fungicide tilt.

Conc. of fungicide (ppm)	Wild type		Most radioresistant isolate	
	Viable count (Cells/ ml)x 10^8	Survival (%)	Viable count (Cells/ ml) x 10^8	Survival (%)
Control	1.0635	100	0.8050	100
2.5	0.5140	48.33	0.4636	57.59
5	0.8281	77.86	0.6173	76.68
7.5	1.1708	110.08	0.7156	88.89
10	1.4277	134.24	0.6752	83.87
15	1.8764	176.43	0.5762	71.57
20	2.8433	267.35	0.4852	60.27
25	2.0688	194.52	0.3312	41.14
30	1.7188	161.61	0.2900	36.02

Table (4) : Survival of Rhizobium of peanut A.V strain in yeast extract mannitol medium supplemented with defferent concentrations of the fungicide tilt

Conc . of fungicide (ppm)	Wild type		Most radioresistant isol ate	
	Viable count (cells / ml) $x10^8$	Survival (%)	Viable count (cells/ml) $x\ 10^8$	Survival (%)
Control	1.2902	100	1.0300	100
2.5	0.9657	74.84	0.0570	5.53
5	3.1825	246.66	0.2489	24.16
7.5	5.6755	439.89	0.4991	48.45
10	4.4005	341.07	0.4911	47.67
15	1.9220	148.96	0.3251	31.56
20	1.4531	112.62	0.2483	24.10
25	1.4658	113.61	0.2478	24.05
30	1.2562	97.36	0.2310	22.42

انتاج سلاله حساسه لمبيد فطرى من سلالات ريزوبيم الفول السودانى بواسطة الاشعاع الجامى

* فاطمه عبد الوهاب حليمش و سعاد عبد العال **
* قسم النبات ـ كلية البنات ـ جامعة عين شمس ـ القاهره
** قسم البيولوجيا الاشعاعيه ـ مؤسسه الطاقه الذريه المصريه ـ القاهره

ملخص

استهدف هذا البحث تعريض سلالاتين من ريزوبيم الفول السودانى متميزه بالنمو السريع الى جرعات متزايده من اشعة جاما وقد تم تعيين منحنى الاستجابه وكذلك الجرعه تحت المميته ثم دراسة تاثير المبيد الفطرى (تلث) على نمو السلالات المقاومه لاكبر جرعه من اشعة جاما والتى يتوقف النمو بعدها تماما . هذا وقد اوضحت النتائج ما ياتى :

١ـ سلالات الفول السودانى ١٦٩ ، A.٧ ذات حساسيه عاليه لاشعة جاما ومنحنيات تجاوب الجرعه من النوع (ا) وكانت الجرعه تحت المميته ٥٠ كيلو راد بالنسبه للسلاله ١٦٩ ، و ٧٥ كيلو راد بالنسبه للسلاله A.٧ .

٢ـ عندما تعرضت السلاله المقاومه لاكبر جرعه من اشعة جاما والتى يتوقف نموها تماما الى جرعات متزايده من المبيد الفطرى (تلث) وجد ان هذه السلاله كانت حساسه للمبيد الفطرى وان نسبة عدد الخلايا الحيه يقل بازدياد جرعاته بعد التركيز (٧,٥ جزء فى المليون) وقد اعطت هذه الجرعه من المبيد الفطرى اعلى نسبه من عدد الخلايا الحيه (٨٨,٨٦) بالنسبه للسلاله ١٦٩ بينما كانت (٤٨,٤٥) بالنسبه للسلاله A.٧ .

٣ـ كانت السلالات المتطرفه من ١٦٩ ، A.٧ اكثر مقاومه لجرعات متزايده من المبيد الفطرى وقد وجد ان نسبة عدد الخلايا الحيه يزداد بازدياد تركيز المبيد الفطرى وحتى تركيز (٢٠ جزء فى المليون) وقد اعطى هذا التركيز اكبر نسبه من عدد الخلايا الحيه بالنسبه للسلاله ١٦٩ بينما اعطى التركيز (٧,٥ جزء فى المليون) اكبر نسبه من عدد الخلايا الحيه بالنسبه للسلاله A.٧ .

Received : 15.10.1982

Cytological effects of dimethylformamide, dimethylacetamide and dimethylsulphoxide on root tips of Allium cepa

By

A . S . Shehab

Botany Department, Faculty of Girls

Ain - Shams University, Cairo

Introduction

Dimethylformamide (DMF), dimethylacetamide (DMAC) and dimethylsulphoxide (DMSO) are used as common solvents for industrial organic chemicals such as polymers and dye stuffs. They are extremely powerful solvents; DMSO being the most powerful. They are aprotic solvents being capable also of certain kinds of chelation They are totaly miscible with water; DMSO being even hygroscopic. Moreover, they are fat soluble,

The aim of this investigation was to study the mitotic effect of DMF, DMAC and DMSO on root tips of Allium cepa as ateet plant .

Material and Methods

Allium cepa bulbs were grown in tap water, in the dark and at r om temperature. When the roots were 2-3 cm in length; water was replaced by the experimental solutions.

The different concentrations used from DMF, and DMSO were 1,3,5 and 7 %. The time of treatment was 3 hourse. After each treatment, the roots were cut, fixed in carnoy's fixative (1 : 3 acetic-alcohol) for 24 hours, then stored in 70% alcohol under refrigeration.

Observations were made from leuco-basic fuchsin stained slides.

Mitotic index was calculated as the average number of dividing cells from 10 different root tips, for each treatment 10,000 cells were counted.

Results and Disussion

The three chemicals used have a mild effect on mitosis of Allium cepa, the inhibition of mitotic index was obvious in the higher concentrations (Table I). They also affected the mitotic phasses. Aslight increase in the number of prophases was noted in 1 and 5% DMAC. While slight increase in metaphases was observed in 3 and 5% DMSO. It is also apparent from Table I that the number of ana-telophases was higher than the other phases in 1 and 5% DMF and 7% DMSO.

The percentage of aberrant cells was proportional to the concentration of the chemicals (Tablr 2).

Most of the abnormalities scored were in the metaphase stage, Table 2. This means that the three chemicals used act as stathmokinetic agents. Accumulation of prophases and metaphases may refer to a delay in the spindle formation and not to the blocking of mitosis at metaphase.

The presence of multipolar spindles indicate that the chemicals used were mero-stathmokinetic agents.

The most dominant abnormality is the disturbed type(Table). Disturbed prophases (Fig I) were observed in nearly all treatments but in small peecentages. Fig 2 shows prophase metaphase which is a sign of stathmokinesis. This abnormality was dominant in 5% DMAC. While figs 3,4,5 show different forms of disturbed metaphases. Figs 6 show a somatic reduction of chromosomes, in which the metaphase chromosomes were seperated into two unqual groups. Disturbed ana-telophases and multi-polar spindles (Figs7,8 and 9) were also observed.

Agents such as acetone (Kaharity I966), folidol (Ravindran I97I), Sevin (Amer et al I97I) and Rogar (Amer and Farah I974) were also known to produce disturbed meta and ana-telophases.

Polyploidy (Fig. IO) was noted in I and 3% DMAC only and in 6 (Table 3). Ennis et al. (I948) atributed polyploidy to the impairment of the action of the spindle.

Surpassing chromosomes (Fig. II), Iagging chromosomes (Fig. I2), anaphase bridges (Fig. I3), c-metaphase (Fig. I4) and c-anaphase (Fig. I5) were less dominent abnormalities. Micronucleated (Fig. I7) and binucleate of interphase cells (Fig. I8) were also observed in small percentages.

Super contraction of metaphase chromosomes (Fig. 6 and I6) was an abnormality observed after treatment with the three chemicals. This abnormality was also seen by Reib (I975) after treating Allium Cepa roots with the mycotoxin diacetoxyscirpeno

SUMMARY

The effect of dimethylformamide, dimethylacetamide and dimethylsulphoxide on root mitosis of Allium Cepa was studied.

The three chemicals had amild effect on the mitotic index. They also affected the mitotic phases. Their effect was on the spindle. The observed abnarmalities were : disturbed metaphases and ana-telophases, lagging chromosome, bridges, c-metaphase, c-anaphase and polyploidy. Super contracted chromosomes were eminent after treatment with the chemicals used.

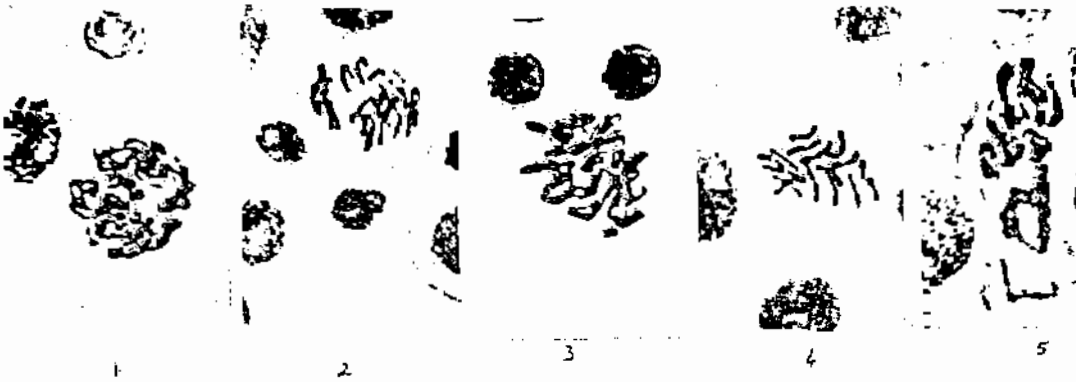

Fig I abnormal prophase (3% D M F)

Fig 2 prophase metaphase (5% D M A C)

Fig 3,4 and 5 Disturbed metaphase (3% DMSO nad DMAC)

Fig 6 Somatic reduciton (5 and 7% D M F)

Fig 7,8 and 9 multipolar spindles (5 and 7% D M F)

Fig IO polyploid metaphase (3% D M A C)

11

12

13

14

15

16

17

18

Fig 11 Surpassing chromosomes 5% D M F

12 Lagging chromosome and bridge 5% D M F

13 Multibridged anaphase. 5% D M S O

14 C-metaphase 1% D M S O

15 C-anaphase 3% D M F

16 Contracted metphase chromosomes (3% D M S)

17 Micro-nuclei. (1% D M S)

18 Binucleate cell (5% D M F)

Mitotic index and percentage of mitotic phases in treated Allium cepa roots

Agents	Total No of Div. cells	Prophase		Metaphase		Ana-telophase		M.I. o/oo
		No	%	No	%	No	%	
Control	650	302	46.46	126	19.38	222	34.15	65
D M F								
1%	570	132	23.16	154	27.01	284	49.82	57
3%	518	206	39.76	106	20.46	206	39.76	51.8
5%	580	218	37.58	110	18.96	252	43.44	58
7%	490	208	42.44	112	22.85	170	34.69	49
D M A C								
1%	564	296	52.48	128	24.82	140	24.82	56.4
3%	434	184	42.39	98	22.58	152	35.02	43.4
5%	424	250	58.96	70	16.5	104	24.5	42.4
7%	420	206	49.04	74	17.61	140	33.33	42
D M S O								
1%	680	280	41.17	76	11.17	234	34.41	68
3%	604	208	34.43	168	27.81	228	37.74	60.4
5%	462	170	36.79	120	25.92	178	37.22	46.2
7%	430	184	42.79	70	16.27	176	40.93	43

Table 2

Total percentage of abnormalities and percentage of abnormalities in each phase

Agents	NO of abn. cells	% of abn. cells	Prophase		Metaphase		Ana-telophase	
			NO abn. cells	abn. % cells	NO abn. cells	abn. % cells	NO abn. cells	abn. % cells
Control	20	3.07						
D E F								
I %	52	9.I2	-	-	38	73.07	I4	26.92
3 %	76	I3.5I	I0a	I4.28	40	57.I4	20	28.57
5 %	I86	32.06	4	2.I5	90	48.38	92	49.46
7 %	I92	39.I8	I8	9.37	I00	52.08	74	38.54
D A C								
I %	72	I2.76	8	II.II	46	63.88	I8	25
3 %	66	I5.2	2	3.03	52	78.78	I2	I8.I8
5 %	II8	27.63	52	44.06	62	52.54	4	3.38
7 %	I06	25.23	I8	I6.98	58	54.7I	30	28.30
D M S O								
I %	44	6.47	-	-	28	63.6	I6	36.36
3 %	86	I4.23	I2	I3.95	52	60.46	22	25.58
5 %	80	I8.6I	20	23.25	38	47.78	28	32.55
7 %	I20	27.90	6	5.0	50	4I.66	64	53.33

Percentages of the different abnormalities in treated Allium cepa roots

Agents	Dist.	Lag.	Brid.	c.m.	c. anap	Polyploidy
D M F						
1%	26.92	19.23	11.53	42.3	-	-
3%	88.57	2.85	-	-	8.57	-
5%	87.09	7.52	1.07	-	4.3	-
7%	82.29	9.34	-	-	8.33	-
D M A C						
1%	83.33	-	-	5.55	-	11.11
3%	86.11	2.7	-	-	-	2.7
5%	98.36	1.69	-	-	-	-
7%	92.45	7.5	-	-	-	-
D M S O						
1%	68.18	9.09	9.09	13.63	-	-
3%	81.39	4.65	2.32	11.62	-	-
5%	81.39	6.97	11.62	-	-	-
7%	78.33	13.33	8.33	-	-	-

References

Amer, S., Hammouda, M.A., and Farah, O.R. 1971
Cytological and morphological effects of the insecticide N-methy-1-naphthyl carbamate "Sevin" Flora 160, 433 -439.

Amer,S. and Farah, O.R. 1974.
Cytological effects of pesticides.
VI Effect of the insecticide "Roger" on the mitosis of Vicia faba and Gossypium barbadense
Cytologia 39 (3) : 507 - 514.

Ennis. W.B. Jr., Fish. El. and Graber, L.F. 1948
Nuclear and celluar responses of certain plants to iso-propyl -N- phenyl carbamate.
Amer. J. Bot. 35 :808.

Kabority, A. 1966.
Induction of multipolor spindles in the meiosis of Triticum aestivum as affected by acetone.
Cytologia 31 : 457 - 460

Ravindran, P.N. 1971 Cytological effects of folidol.
Cytologia 36 : 504.

Reib, J. 1975 Mycotoxin poisoning of Allium cepa root tips. II Reduction of mitotic index and cytological abnormalities by patulin, rubratoxin and diacetoxyscirpenol.
Cytologia 40 : 700 - 708.

التأثيرات السيتولوجية لثنائى ميثيل فورماميد وثنائى ميثيل اسيتاميد وثنائى ميثيل سلفوكسيد على جذور نبات البصل

أمـــال شهـــاب

قسم النبات ـ كلية البنات ـ جامعة عين شمس

درس تأثير ثنائى ميثيل فورماميد وثنائى ميثيل اسيتاميد وثنائى ميثيل سلفوكسيد على الانقســـام الغير مباشر لجذور البصل •

وجد أن الثلاث مواد المستعملة لها تاثير بسيط على معدل الانقسام وكذلك تؤثر على معـــدل الاطـوار • وقد وجد أن تأثيرها يكون على المغزل • وأنواع الشذوذ المختلفة هى اضطراب المغـزل فى الطور الاستوائى والانفصالى والكروموسوم المتلكى• والقناطر والاستوائى الكولشيـينى والانفصـــالى الكولشيـينى والتضاعف • وقد وجدت الكروموسومات القصيرة جدا فى جميع المعاملات بالثـــــلاث كيماويات المستعملة •

"THE EFFECT OF GROWTH MEDIUM ON LEVELS OF FATTY ACIDS IN SOME YEASTS "

Mohamed I.H. Mahmoud, Mehreshan T. El Mokadem and Zeinab H. Khairalla.

Department of Botany, Women's College Ain Shams University, Helipolis, Cairo.

SUMMARY

Saccharomyces cerevisiae and the osmotolerant yeasts S. rouxii and Debaryomyces hansenii were aerobically and anaerobically grown in presence of increasing concentrations of sodium chloride from zero to 15% (w/v). Levels of both saturated and unsaturated fatty acids in the yeast cells were estimated using gas liquid chromatography. Palmitic and stearic acid constituted the major component of saturated fatty acids in the three test organisms. However, palmitoleic, oleic and elaidic were the major components of unsaturated fatty acids.

No linear correlation was found between levels of sodium chloride in the culture medium and levels of either saturated or unsaturated acids in the yeast cells. Levels of total unsaturated fatty acids were higher in aerobically grown cells of S.rouxii and

D. hansenii than those grown anaerobically, although their levels were indifferent in S.cerevisiae. Also, levels of total saturated fatty acids in S. rouxii were lower than their levels in both D. hansenii and S. cerevisiae. However, levels of unsaturated fatty acids in S. rouxii were higher than those of D.hansenii or S. cerevisiae.

INTRODUCTION

The lipid composition of yeasts is very responsive to changes in the chemical and physical properties of the environment. White and Werkman (1948) reported an increase in the lipid content of Saccharomyces cerevisiae following the growth in presence of sodium chloride. Combs and Pisano (1968) found that on increasing the concentration of sodium chloride from zero to 10%, the lipid content as well as levels of the unsaturated palmitoleic fatty acid in Candida albicans increased. Mahmoud et al (1981) found that levels of both total lipids and phospholipids in S. rouxii, Debaryomyces hansenii and S. cerevisiae decreased with the increase of sodium chloride concentration.

The aim of the present study was to show the effect of sodium chloride on the levels of both saturated and unsatuarated fatty acids in the osmotolerant yeasts S. rouxii and D. hansenii in comparison with those of S. cerevisiae.

MATERIALS AND METHODS

Test Organisms

Saccaromyces rouxii was isolated from a sample of dried Egyptian dates, while Debaryomyces hansenii was isolated from a sample of an Egyptian cheese brine commonly called (Mesh). Both organisms were isolated and identified by Mahmoud (1978). S. cerevisiae, however, was isolated from a sample of commercial compressed yeast, a local product of the Egyptian " Starch Products and Yeast Co.".

Growth Medium

The test organisms were grown in 100 ml fractions of a medium containing the desired concentration of sodium chlorids, and dispensed in 250 ml capacity Erlenmeyer flasks. The glucose-yeast extract broth medium of Crabtree and Hindstill (1974) was used with slight modifications. It has the following composition (g. %): 0.5 peptone, 0.3 yeast extract, 1.0 glucose, 0.2 KH_2PO_4 and 0.05 $MgSO_4.7H_2O$ (initial pH 6.5).

Sodium chloride was added as gram per cent (w/v). However, the final readings of the water activity of the growth medium were measured using a Beckman Hygroline recorder, model SMT . Each measurement was taken until the recorder was stable for 30 minutes to one hour.

Inoculated flasks were shaken at 30°C using a rotary shaker. For anaerobic growth, however each flask aseptically received 10 ml of sterile paraffin oil, and incubated (unshaken) at 30°C. The incubation period varied between 2-15 days for reaching the early stationary phase of growth. This depended upon the test organism as well as the concentration of sodium chloride.

Washing of cells:

After the proper incubation period, the yeast cells were harvested and washed three times using distilled water by centrifugation at 2400 r.p.m.

Extraction of Lipids

Free lipids were extracted from the yeast cells according to the method presented by Letters (1968) with slight modifications. Yeast cells were disintegrated by mechanical shaking with glass beads, and the broken

cell preperation was extracted with neutral and acid solvents as follows: 20 ml portions of 80% (v/v) aqueous ethanol at 80°C were added to samples of broken cells, each corresponding to 100-130 mg dried yeast cells. The suspension was maintained at 80°C for 15 minutes, then filtered through Whatman No. 44 paper. The extract together with other two ethanol washings were combined, and the antioxidant (BHT) was added at a final concentration of 0,005%. Samples were then stored at - 20°C. The residue samples were shaken with 50 ml of 95% ethanol-ethyl ether (1:1 v/v) for 24 hrs at 30°C. The solvent phase was separated by filtration and added to the ethanol extract. The residue was reextracted twice with chloroform. Bound lipids were extracted according to Letters (1966) by subjecting the residue from ethanol-ethylether and chloroform treatments to digestion in acidic mixture (chloroform-methanol-hydrochloric acid 124:65 : 1 (v/v/v) for 5 hrs. at 50°C . The extract was then neutralized using 2N Na OH. Two extractions were done, the first was with 95% ethanol-ethylether 1 : 7 (v/v), and the second with chloroform. Each extraction rested for 24 hrs. Finally, all extracts were combined and the solvents were removed in vacuum.

Seperation of Neutral Lipids

The solvent partition system described by Galanos and Kapoulas (1962) was adopted.
The lipid extracts dissolved in 15 ml of petroleum ether were transferred to a separatory funnel containing 45 ml of both petroleum ether and 95% aqueous ethanol. After shaking and seperation of layers, the lower layer which contains the phosphlipids was transfered to a second funnel. The neutral lipids in the first funnel were then washed twice by shaking with 12 ml portions of 95% aqeous ethanol to ensure complete separation of phospholipids.

Gas liquid chromatography

Analysis of free fatty acids was done using gas-liquid-chromatography according to Lipsky et al (1959) and Hunter and Rose (1971). All samples of neutral lipids were analyzed using a Perkin-Elmer 910 GLC-type Flame ionization detector after complete estrification of fatty acids. The fetty acid-methylesters were seperated on 10% diethylglycol adipate (DEGA) supported on 35-80 mesh chromosorb w, and packed in a stainless steel column of 6 ft 0.25 inch.

The (DEGA) Column was maintained at 195°C with nitrogen flow rate of 50 ml/min and the detector at 195°C. All samples injected to the column (1.5 ul) were dissolved in 1 ul dimethylether. For statistical analysis of data, the paired-sample t-test was used according to Campbell (1974).

RESULTS AND DISCUSSION

Tables 1, 2 and 3 represent levels of fatty acid esters of the three test organisms, aerobically and anaerobically grown in the presence of increasing concentrations of sodium chloride. In case of aerobically grown cells of Saccheromyces rouxii palmitic acid (16 : 0) and steeric acid (18: 0) were the major components of the saturated fatty acids. In anaerobically grown cells, the fatty acids N-nonoic (9:0), capric (10: 0), undecanoic (11: 0) as well as pentadecanoic (15:0) practically disappeared. While stearic acid disappeared also in presence of sodium chloride, where palmitic acid (16:0) became the major component and its levels were significantly higher than those under aerobic conditions.

In Debaryomyces hansenii , levels of stearic acid in anaerobically grown cells were higher than those grown aerobically, in contrast to palmitic, myristic (14:0) and tridecanoic (13:C), since their levels did not show any statistically significant difference in the aerobically and anaerobically grown cells.

In S. cerevisiae, levels of the fatty acid lauric (12:0) in the aerobically grown cells were higher than in those anaerobically grown, contrary to stearic acid. However, levels of the rest of saturated fatty acids did not show any significant difference in the aerobically and anaerobically grown cells. In both S. rouxii and D. hansenii palmitic acid constituted the major component of saturated fatty acids, while palmitic and stearic acids were dominant in S. cerevisiae.

Palmitoleic (16:1), oleic (18:1), and elaidic (18:2) constituted the unsaturated fatty acids in the three test organisms. Levels of oleic acid in aerobically grown cells of S. rouxii were higher than in the anaerobically grown cells contrary to levels of both palmitoleic and elaidic. Levels of elaidic acid were higher in the aerobically grown cells of D. hansenii then in those anaerobically grown and contrary to the rest of other acids. In S. cerevisiae, however, levels

of palmitoleic and oleic acids did not show any difference in aerobically over anaerobically grown cells. Hunter and Rose (1971) found that levels of palmitoleic acid were higher than oleic in S. cerevisiae when the cells were grown anaerobically at 30°C. In the present study, levels of palmitoleic were higher than oleic in S. cerevisiae (aerobically or anaerobically). However, levels of oleic acid in both S. rouxii and D. hansenii were higher than levels of palmitoleic acid whether the cells were grown aerobically or anaerobically.

As a response to the presence of sodium chloride in the medium, no linear correlation could be found between levels of the fatty acids and salt concentration. However, levels of tridecanoic acid (13:0) in S. cerevisiae aerobically increased and anaerobically decreased in response to salt concentration, although its levels did not show any significant difference in D. hansenii. Levels of palmitic acid showed a decrease in aerobically grown cells of S. rouxii but not under anaerobic conditions. Also, its levels were indifferent in D. hansenii. In S. cerevisiae, however, its levels increased aerobically and decreased anaerbbically with the increase of solute concentration.

Combs and Pisano (1968) found that when Candida albicans was grown in presence of zero to 10 % sodium chloride, levels of palmitoleic acid increased, while levels of oleic acid decreased with the increase of solute concentration. In the present study, levels of palmitoleic acid showed a significant increase in response to sodium chloride under aerobic and anaerobic conditions. Levels of oleic acid in S. rouxii decreased in cells grown under either conditions, although they decreased aerobically and increased anaerobically in S. cerevisiae. However, its levels were indifferent in D. hansenii.

Two general processes for the formation of unsaturated fatty acids have been discussed by Erwin (1973). Introduction of unsaturation into yeast fatty acids appeared to be restricted to oxygen-dependent desaturase systems. Also, he postulated the presence of an alternate anaerobic pathway for the introduction of unsaturation. In the present study, levels of total unsaturated fatty acids were higher in aerobically grown cells of S. rouxii and D. hansenii than in those grown anaerobically. However, their levels were indifferent in aerobically and anaerobically grown cells of S. cerevisiae.

As a response to increasing concentration of sodium chloride, levels of total saturated fatty acids decreased in S. rouxii (aerobically or anaerobically) although they increased in S. cerevisiae grown under both conditions. On the other hand, levels of unsaturated fatty acids increased in S. rouxii (aerobically or anaerobically) but decreased in aerobically grown S. cerevisiae and increased under anaerobic conditions. In D. hansenii, however, levels of both total saturated and unsaturated fatty acids did not show any statistically significant difference in aerobically and anaerobically grown cells as a response to increasing concentration of sodium chloride.

Jollow et al (1968), and Bulder and Reinink (1974), found that when baker's yeast cells were grown anaerobically, the content of unsaturated fatty acids decreased. In the present study, in absence of sodium chloride, levels of total unsaturated fatty acids were higher in aerobically grown cells. However, on increasing the salt concentration, their levels decreased in the aerobically grown cells and increased in the anaerobically cultivated cells.

Demel et al (1967) and Koh (1975) working on the fatty acid composition of an obligate osmophilic mutant of S. rouxii, reported that the changes of the ratios of

saturated palmitic and the unsaturated palmitoleic and oleic acids might cause changes in the cell membrane. The increase in the content of unsaturated fatty acids could also result in increasing the fluidity of the yeas cell membrane. In the present study , increasing the concentration of sodium chloride decreased the levels of palmitic and oleic in aerobically or anaerobically grown cells of S. rouxii. however, levels of palmitoleic and elaidic acids increased in the aerobically cultivated and decreased in the anaerobically grown cells.

Generally, levels of total saturated fatty acids in aerobically and anaerobically grown cells of S. rouxii were lower than their corresponding levels in D. hansenii and S. cerevisiae, where their levels did not show any difference. However, levels of total unsaturated fatty acids in S. rouxii were higher than those of D. hansenii and S. cerevisiae, where their levels were indifferent.

REFERENCES

Bulder, C.J., and M. Reinink (1974)
Unsaturated fatty acid composition of wild type and respiratory deficient yeasts after aerobic and anaerobic growth.
J. Microbiol. Serol., 40, 446.

Campbell, R.C. (1974):
"Statistics for biologists" p. 159.
Cambridge University Press (Publ.)
London.

Combs, T and M. Pisano (1968)
The effect of sodium chloride on the lipid content and fatty acid composition of Candida albicans.
Mycologia 60, 1232.

Crabtree; K., and R. Hindstill (1974)
In "Fundamental Experiments in Microbiology". P. 340. W.B. Saunders (Publ.), Philadelphia, U.S.A.

Demel, R., L. Van Deenen, and B.A Pethica (1967).
Monolayer interactions of phospholipids and cholesterol.
Biochim. Biophys. Acta, 135, 11.

Erwin, J. (1973)
Comparative biochemistry of fatty acids in eukaryotic microorganisms. In " Lipids and biomembranes of eukaryotic microorganisms. Erwin, J. (ed.) p. 41. Academic Press Inc., New York, U.S.A.

Galanos, D., and V. Kapoulas (1952)
Thin layer chromatography of phosphatides and glycolipids.
J. Lipid Res. 3, 134.

Hunter, K., and A. Rose (1971):
Lipid composition of Saccharomyces cerevisiae as influenced by growth temperature.
Biochim. Biophys. Acta, 260, 639.

Jollow, D., G. Kellerman and A. Linnane (1968)
The biogenesis of mitochondria. III-
The lipid composition of aerobically and anaerobically grown Saccharomyces cerevisiae as related to the membrane systems of the cell.
J. Cell Biol. 37, 221.

Koh, T.Y. (1975).
The isolation of obligate osmophilic mutants of the yeast Saccharomyces rouxii.
J. Gen. Microbiol. 88, 184.

Lellers, R. (1966).
Phospholipids of yeasts. II extraction, isolation, and characterization of yeast phospholipids.
Biochim. Biophys. Acta, 116 , 489.

Letters, R. (1968)
Phospholipids of yeasts. P. 303.
in "Aspects of Yeast Metabolism"
Blackwell Press, Oxford. London.

Lipsky, S., R. Landowne and J. Lovelook (1959)
Separation of lipids by gas liquid chromatography.
Anal. Chem. , 31, 852.

Mahmoud, M.I. (1978)
The effect of the water activity of the milieu on rates of glucose uptake by the osmophilic yeasts Saccharomyces rouxii and Debaryomyces hansenii.
Zbl. Bakt. Abt. B.d., 133, 726.

Mahmoud, M.I., M.T. El Mokadem, and Z.H. Khairalla (1981)
The effect of growth medium on the levels of lipids in some yeasts. (Submitted for publication)

White, A.G., and C. Werkman, (1948)
Fat synthesis in yeast.
Arch. Biochem. 17, 478.

Table 1

Levels of Fatty acids in Saccharomyces rouxii (mg/g neutral lipids)

Sodium Chloride%(w/v)		0%	1.7	3.4	6.5	9.8	15.3	0	1.7	3.4	6.5	9.8	15.3
Final water activity		0.998	0.992	0.98	0.96	0.932	0.89	0.998	0.992	0.98	0.96	0.932	0.89
		Aerobic Growth						Anaerobic Growth					
N-Nonoic	9:0	-	3.0	1.5	0.5	traces	3.4	-	-	-	-	-	-
Capric	10:0	2.2	2.2	4.5	1.8	--	-	-	-	0.6	-	-	-
Undecanoic	11:0	-	-	9.0	1.8	1.3	0.8	-	-	-	-	-	-
Lauric	12:0	0.2	0.2	9.0	1.1	1.3	2.1	0.7	0.2	0.5	-	-	-
Myristic	14:0	4.5	4.0	3.0	3.8	4.0	4.7	2.7	-	8.6	-	-	-
Pentodecanoic	15:0	0.3	9.8	1.5	1.1	1.9	2.6	-	-	0.6	-	-	-
Palmitic	16:0	133.9	123.9	124	103.7	87	81.3	183.3	241.8	186.7	187.9	151.8	111.9
Palmitoleic	16:1	105.9	190.4	216.5	212.2	180.1	142.2	45.5	121.7	232.2	257.2	300.3	382.8
Heptodecanoic	17:0	0.8	-	-	-	-	-	-	-	-	-	-	-
Stearic	18:0	21.4	11.1	12.1	13.1	33.0	40.1	74.0	-	-	-	-	-
Oleic	18:1	614.0	530.2	542.1	575.6	564.6	582.7	510.8	489.8	431.3	405.2	396.9	378.4
Elaidic	18:2	107.0	119.5	72.3	82.1	127.1	135.4	169.2	136.5	121.5	112.6	89.7	69.7
Saturated	(Total)	163.3	154.2	164.6	126.9	125.5	135	260.7	242.0	198	187.9	151.8	111.9
Unsaturated	(Total)	826.9	840.1	830.9	869.9	871.8	860.3	725.5	748	785	765	785.1	830.9

Table 2

Levels of Fatty acids in *Debaryomyces hansenii* (mg/g neutral lipids)

Sodium Chloride % (w/v)		0	1.7	3.4	6.5	9.8	15.3	0	1.7	3.4	6.5	9.8	15.3
Final water activity		0.998	0.992	0.98	0.96	0.932	0.89	0.998	0.992	0.98	0.96	0.932	0.89
		Aerobic Growth						Anaerobic Growth					
Capric	10:0	0.6	-	-	0.3	-	-	-	-	0.3	-	-	-
Undecanoic	11:0	0.9	-	-	3.1	4.6	0.8	-	-	1.5	-	2.0	2.5
Lauric	12:0	-	-	-	-	-	-	2.4	0.2	0.3	0.3	3.2	3.0
Tridecenoic	13:0	4.6	11.2	14.7	1.5	traces	traces	1.8	1.8	2.0	1.7	5.9	5.9
Myristic	14:0	1.7	16.4	14.7	6.7	2.2	1.1	1.2	1.5	4.2	5.1	5.5	4.8
Pentadecanoic	15:0	-	-	10.7	4.9	3.3	1.1	-	-	2.7	3.3	3.9	6.7
Palmitic	16:0	215.8	252.6	225.2	95.6	140.4	177.1	267.7	221.8	182.5	184.4	234.6	348.0
Palmitoleic	16:1	46.1	51.8	83.7	98.3	148.9	218.9	36.4	83.9	107.6	87.6	80.9	71.2
Heptadecanoic	17:0	10.1	-	-	-	-	-	-	-	-	-	-	-
Stearic	18:0	10.4	15.5	10.7	17.0	61.7	62.9	109.5	150.1	136.2	140.8	134.4	117.0
Oleic	18:1	520.7	502.4	486.3	463.8	298.3	225.2	481.5	469.0	496	412.4	442.9	349.7
Elaidic	18:2	152.2	100.1	84.9	258.6	230.9	185.9	72.8	31.7	48.3	30.8	22.1	17.3
Saturated	(Total)	244.1	295.7	276	129.1	212.4	243	382.6	372.1	329.7	335.6	389.5	487.9
Unsaturated	(Total)	719	654.3	654.9	820.7	678.1	630	590.7	587.9	651.9	590.8	545.9	438.8

Table 3

Levels of Fatty acids in Saccharomyces cerevisiae (mg/g neutral lipids)

Sodium Chloride % (w/v)		0	1.7	3.4	6.5	9.8	15.3	0	1.7	3.4	6.56	9.8	15.3
Final water activity		0.998	0.992	0.98	0.96	0.932	0.89	0.998	0.992	0.98	0.96	0.932	0.89
		Aerobic Growth						Anaerobic Growth					
Capric	10:0	-	-	-	-	-		-	0.7	0.9	-		
Undecanoic	11:0	2.2	-	-	1.4	-		4.3	7.0	1.8	10.9		
Louric	12:0	2.4	2.9	3.2	8.2	1.4		23.3	30	40	70		
Tridecanoic	13:0	0.3	2.0	2.0	1.4	2.5		5.0	1.6	traces	traces		
Myristic	14:0	1.3	-	-	-	-	GROWTH	26.5	24.6	21.8	61.3	GROWTH	GROWTH
Pentadecanoic	15:0	0.5	-	-	-	-		1.4	3.5	3.0	2.7		
Palmitic	16:0	71.8	133.1	163.9	203.3	214.9		284.8	166.7	178.7	137.8		
Palmitoleic	16:1	278.8	397.6	425.6	444.3	450.1		343.2	405.6	407.3	386.2		
Heptadecanoic	17:0	10.4	18.4	16.3	2.2	traces		-	-	-	-		
Stearic	18:0	110.7	144	130	111.0	110		37.2	44.3	27.6	16.2		
Oleic	18:1	480.0	211.6	215.2	201.7	191.7		273.6	313.0	300.3	298.5		
Elaidic	18:2	1.6	49.4	38.3	24.4	28.5	NO	-	-	-	-	NO	NO
Saturated (Total)		199.6	300.4	315.4	327.5	328.5		381.5	272.3	273.8	298.9		
Unsaturated (Total)		760.4	658.6	679.1	670.4	670.3		616.8	718.6	707.6	684.7		

تأثير بوشنة النمو على مستويات الاحماض الدهنية في بعض قطريات الخميرة

دكتور / محمد ابراهيم حسن محمود ، دكتوره / مهرشامه طه المقدم
والدكتوره / زينب حسن خير الله

قسم النبات — كلية البنات — جامعة عين شمس

ملخص

في هذه الدراسة نبت كل من قطريات الخميرة "سكارومايسزروكسي" و "ديبهاريومايسزهانسنى" و "سكارومايسز سيرفيسى" تحت ظروف هوائية و لا هوائية عند تركيزات متزايدة من كلوريد الصوديوم تتراوح بين صفر و ١٥٪

فوجد ان حمض الباالميتيك و حمض الاستياريك يكونان الحجم الاكبر من كمية الاحماض الدهنية المشبعة في الخمائر تحت الاختبار . أما الاحماض الدهنية بالميتوليك و الايديك فكانت اساس الاحماض الدهنية غير المشبعة في الخلايا .

كما وجد أن مستويات الاحماض الدهنية غير المشبعة في خلايا كل من "سكارومايسز روكسي" و "ديبهاريومايسزهانسنى" النامية هوائيا كانت أعلى من مستوياتها تحت الظروف اللاهوائية ، ولكن لم يلاحظ اى فرق بين مستوياتها في الخلايا النامية و تلك النامية لا هوائيا في خميرة "سكارومايزسيرفيسى" .

كما وجد ايضا ان مستويات الاحماض الدهنية المشبعة في خميرة "سكارومايسزروكسي" منخفضة عن نظائرها في كل من خميرتى "ديبهاريومايسزهانسنى" و "سكارومايسزسيرفيسى" ولكن وجد ان مستويات الاحماض الدهنية غير المشبعة في خميرة "سكارومايسزروكسي" اعلى من نظائرها في كل من خميرتى "ديباروماسزهانسنى" و "سكارومايسزسيرفيسى" .

Notes on the aquatic habitats of macrohydrophytes and associated algae in various regions in Egypt. 3- Governorates of Giza, Cairo, Qalyubia and Sharkia

by

Wafaa S. Abou El-Kheir and Gahiza H. Ismail

Botany Department, Girls College, Ain Shams University, Egypt.

Introduction

Abou El-Kheir and Ismail (1980) and Abou El-Kheir et al. (1986) studied the association between algae and macrohydrophytes in various regions in Egypt including; Fayum, Ismailiya and neighbouring places. In these two mentioned publications the authors reviewed relevant earlier works on the relationship between algae, macrohydrophytes and other organisms. The present study represents the third part on the same subject and is concerned with the regions: Giza, Cairo, Qalyubia and Sharkia.

Material and Methods

Thirty-six samples, were taken from 16 sites, at Giza, Maadi, Delta Barrage and Benha-Zagazig road (see Fig. 1). The samples were collected from irrigation streams, irrigation canals, drains and River Nile (see table 1). Some physical factors were measured such as pH, water temperature and water current velocity (table 1). Chemical analysis of the 36 water

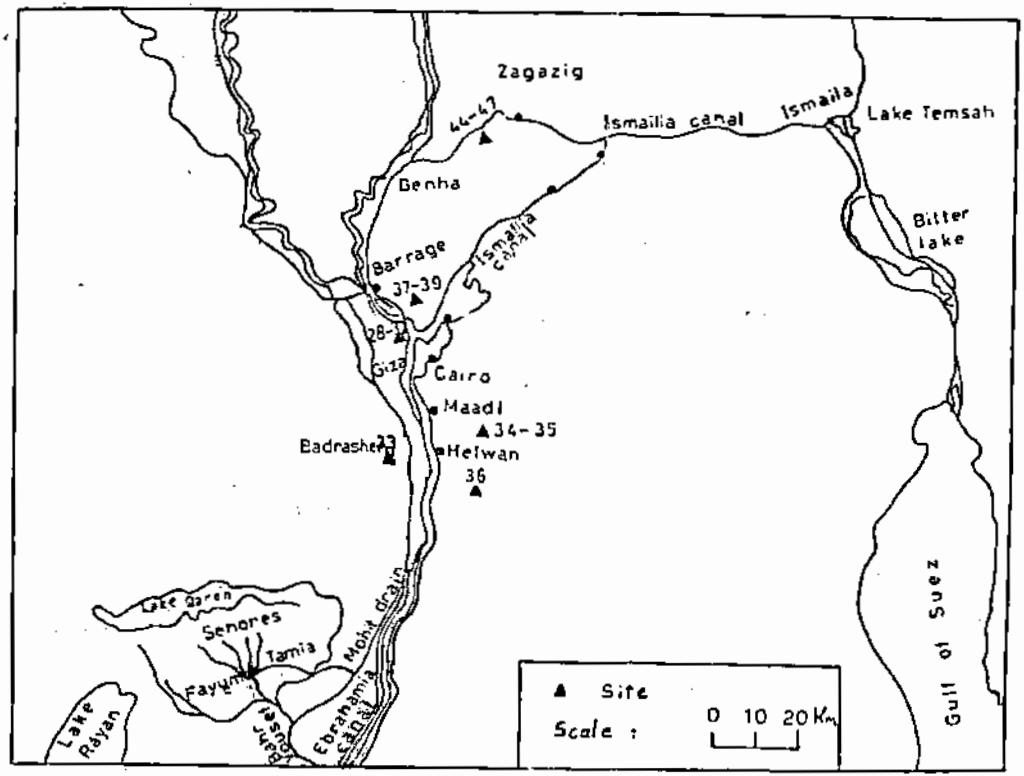

Map showing sites of collection

samples have been done and data are given in table 2. Algal taxa present in all samples were investigated and identified. Natural photos of 21 of these algal taxa are given on plates 1 and 2. The numbers given to the sites and samples in the tables are their registration numbers given to them at the time of collection.

Results and Observations

Description of habitats, characters of macrohydrophyte communities, the main associated algal flora in the studied sites are presented in table 1. It is clear from this table that:

1- Giza region: Maryotia canal (site 28) showed slow flowing water and dominance of Potamogeton nodosus at middle with some common phytoplankton (Cyclotella ocellata, Cocconeis placentula, Melosira granulata and Synedra ulna splendens), while at edge Typha domingensis and Lemma gibba dominated with some of the previously noted phytoplanktons. Eichhornia crassipes and Potamogeton nodosus extended to 10 km. from site 28c, and were also associated with the same planktoner Synedra ulna splendens. Gizawia irrigation canal (site 33) with faster flow at middle than Maryotia canal did not show dominance of macrohydrophytes or algae at middle of the canal, while Eichhornia crassipes and Panicum repens dominated inner to canal side.

Four drains in the region (sites 29-32) showed dominance of Lemna gibba and Ceratophyllum demersum associated with dominant Oedogonium capilliforme. In addition to this association some diatoms were found common in the two drains (sites 29 & 30) with moderately flowing water but none in the two drains (sites 31 & 32) with almost quiet water.

2- Maadi region (Cairo Governorate): River Nile at Maadi (site 35) showed dominance of Eichhornia crassipes in a 10 meter belt at bank, and Phragmites australis at bankside, while the river showed a wide open water surface inwards, with fast flowing water. No domirant algal taxa associated the macrohydrophytes.

Khashab irrigation canal (site 34) showed, however, Cladophora glomerata as dominant and Cyclotella ocellata and Oscillatoria tenuis as common with macrohydrophytes.

A drain near Torra (site 36) showed dominance of macrohydrophytes: Eichhornia crassipes, Typha domingensis and Phragmites australis but no dominant algal taxa were encountered.

3- Delta Barrage region: An irrigation canal in Barrage region showed domination of Phragmites australis and Panicum repens with slight association of algae at site 37. While under Lemna gibba and Ceratophyllum demersum association of Rhopalodia gibba was observed at site 38.

Table (1) : Habitat, Macrohydrophyte communities and Main algal flora.

Site No.	Date of collection	Habitat & locality	Flowing velocity	Temperature	pH	Macrohydrophyte plant community		Dominant and common algae	
28	11/6/79	Maryotia canal east Giza Pyramids (fresh water) w; 20 m	0.4 m/sec	25°C (11:0 a.m.)	7.8	a: Potamogeton nodosus	d	Bacillariophyta:	
								Cyclotella ocellata	c
								Cocconeis placentula	c
								Melosira granulata	c
								Synedra ulna splendens	c
						b: Typha domingensis	d	Bacillariophyta:	
						Bank plants:			
						Imperata cylindrica		Cocconeis placentula	c
						Cyperus alternifolius		Synedra ulna splendens	c
						c: Lemna gibba	d		
						d: Eichhornia crassipes	d	Bacillariophyta:	
						Potamogeton nodosus (10 km from site 28c)	d	Synedra ulna splendens	c
29	"	Drain parallel to Maryotia canal east of Giza Pyramids.	0.6 m/sec.	27.5°C (11:10 a.m.)	7.8	a: Lemna gibba	d		
						Panicum repens	d		
						Phragmites australis			
						b: Cyperus alternifolius		Bacillariophyta:	
								Cyclotella ocellata	c
								Synedra ulna biceps	c
								S. ulna amphirhynchus	c
						c: Lemna gibba	d		
30	"	Drain east Maryotia canal w: 4m, de: 1m.	0.7m/sec.	27.5°C (11:20 a.m.)	7.0	Eichhornia crassipes	d		
						Panicum repens	c		
						Phragmites australis	c		
31	"	Drain at Faifela village. w : 2m	Almost quiet	28°C (11:30 a.m.)	7.8	a: Lemna gibba	d	Chlorophyta:	
						Ceratophyllum demersum	d	Oedogonium capilliforme	d
						b: Panicum repens	d		
						Phragmites australis	d		
						Drain side plants.			
						Imperata cylindrica			
32	"	Drain near Faifela village Pyramid region w: 4 m.	Almost quiet	27°C (12:0 N)	7.7	Lemna gibba	d		
						Phragmites australis	c		

Table (1) Cont.

Site No.	Date of collection	Habitat & locality	Flowing velocity	Temperature	pH	Macrohydrophyte plant community		Dominant and common algae	
33	17/12/79	Gizawia irrigation canal at Badrasheen, 26 km from Cairo (fresh water) (w: 20m	Almost quiet near bank and fast flowing at middle (1.4m/Sec.)	17°C (11:30 a.m.)	6.7	Bank plants: Polygonum salicifolium Panicum repens Eichhornia crassipes	d d d		
34	17/12/79	Khashab irrigation canal Mandi's road (fresh water)	Almost quiet	15.5°C (11:30 a.m.)	6.5	Lemna gibba Ceratophyllum demersum Phragmites australis Eichhornia crassipes Canal side plants: Cynodon dactylon	d d d c	Bacillariophyta: Cyclotella ocellata Chlorophyta: Cladophora glomerata Cyanophyta: Oscillatoria tenuis	c d c
35	"	River-Nile Mandi (fresh water)	Almost quiet near bank Fast flowing at middle.	17°C (12:0 N)	6.9	a: Eichhornia crassipes (w:10 m. de; 1 m) b: Panicum repens Ceratophyllum demersum Phragmites australis Bank plants: Polygonum salicifolium Open water	d d c c d		
36	"	Drain near Torra Mandi road 100% plant cover.	Almost quiet	16°C (12.30 N)	6.7	Eichhornia crassipes Typha domingensis Phragmites australis Drain side plant: Imperata cylindrica.	d d d		

Table (1) Cont.

Site No.	Date of collection	Habitat & locality	Flowing velocity	Temperature	pH	Macrohydrophyte plant community		Dominant and common algae	
37	26/1/80	Irrigation canal (fresh water) w:4 m, de: 50 cm	Almost quiet	17°C (12:0 N)	6.9	Panicum repens Phragmites australis canal side: Polygonum salicifolium	d e		
38	"	The same irrigation canal (fresh water) w: 4m, de: 50 cm 5 k from site 37	quiet	17°C (12:10 p.m.)	6.5	Lemna gibba Ceratophyllum demersum	d d	Bacillariophyta: Rhopalodia gibba var ventricosa	c
39	1/3/80	Irrigation canal (fresh water) Barrage garden w: 4m, de: 1m	Almost quiet	21°C (1:0 p.m.)	7.0	Nymphaea coerulea Potamogeton nodosus Eichhornia crassipes Phragmites australis	d d c c	Bacillariophyta: Achnanthes minutissima Cyclotella ocellata Navicula cryptocephala Nitzschia frustulum Rhopalodia gibba var ventricosa. Chlorophyta: Cladophora glomerata Spirogyra varians	d c c c c d d
	30 /6/80		Almost quiet	29°C (1:0 p.m.)	6.5	a: Nymphaea gerulea b: Potamogeton nodosus c: Open water d: Phragmites australis e: Nymphaea coerulea 25 m from site 39 f: Eichhornia crassipes	d d d d d		
44	9/2/80	Irrigation stream (fresh water) w: 1-1.5 m.	Almost quiet	17°C (2:0 p.m.)	6.6	Potamogeton crispus Lemna gibba Typha domingensis Phragmites australis Stream side plant: Polygonum salicifolium	d c c	Chlorophyta: Spirogyra varians	d
45	26/11/80	Irrigation stream (fresh water) w: 3m, de:50 cm Zagazig Benha road	45:a,b,d,e almost quiet 47c:1m/sec	17°C (11:0 a.m.)	6.5	a: Eichhornia crassipes b: Open water c: Nymphaea coerulea d: Lemna gibba e: Phragmites australis	d d d d		
46	"	Irrigation stream (fresh water) w:2m, de:30 cm	46a: almost quiet b: 0.4m/sec	17°C (11:30 a.m.)	6.5	a: Nymphaea coerulea b: Open water	d		
47	"	Irrigation stream (fresh water) w:2 m, de:50 cm	Almost quiet	17°C (12:0 N)	6.5	a: Nymphaea coerulea b: Open water c: Eichhornia crassipes	d d		

Table (2): Water analysis in the thirty-six collected samples.

Site No.	MINERALS (mg/l)						
	Cl	PO_4	NO_3	Ca	Mg	Na	K
28a	106.5	10.0	1.3	44.0	24.0	8.2	3.5
b	183.4	9.0	4.2	75.0	37.8	11.5	10.5
c	106.5	9.2	5.5	126.0	72.0	15.4	12.4
d	136.1	6.2	1.9	60.0	29.4	11.5	2.3
29a	76.9	1.1	2.6	44.0	26.4	11.5	4.3
b	213.0	9.6	5.6	70.0	28.2	11.5	22.6
c	88.7	7.0	1.1	66.0	26.4	9.2	15.6
30	53.8	7.2	0.2	62.0	90.0	6.9	2.7
31a	153.	3.6	0.8	32.0	7.8	11.5	3.5
b	165.7	10.0	1.4	89.0	28.2	20.7	2.3
32	76.9	6.0	7.7	50.0	8.4	34.5	11.3
33	41.4	5.6	0.3	50.0	13.8	4.6	7.4
34	82.8	11.2	0.2	69.0	11.4	4.6	1.1
35a	65.1	8.0	0.4	50.0	1.8	6.9	3.1
b	65.1	6.0	0.1	54.0	16.8	4.6	3.9
36	100.6	6.2	1.9	72.0	15.6	9.2	1.5
37	165.6	5.6	1.60	54.0	32.8	50.6	10.1
38	88.7	11.6	0.12	109.0	312.0	43.7	3.1
39	59.6	8.4	0.38	60.0	17.4	4.6	0.9
a	47.3	7.4	-	59.0	13.2	2.3	0.4
b	47.3	4.4	0.01	50.0	24.0	4.6	0.4
c	53.2	0.8	-	60.0	6.0	9.2	2.0
d	47.2	3.8	0.02	48.0	18.6	4.6	0.8
e	47.2	3.6	-	38.0	18.6	4.6	1.2
f	35.5	3.6	0.02	28.7	31.2	25.3	1.2
44	59.2	8.0	0.10	55.0	11.4	25.3	2.0
45a	59.6	12.8	-	20.0	19.2	9.2	5.9
b	106.5	16.2	0.10	54.0	18.0	4.6	4.2
c	47.3	3.0	-	40.0	15.6	6.9	0.8
d	59.6	5.6	-	43.0	15.0	4.6	1.2
e	59.6	10.0	0.02	42.0	10.2	4.6	8.6
46a	53.2	0.4	-	43.0	15.0	4.6	1.2
b	53.2	0.8	0.02	42.0	13.2	4.6	1.2
47a	59.6	2.2	0.04	45.0	9.0	4.6	1.2
b	59.6	3.8	0.05	45.0	15.6	4.6	1.2
c	59.6	8.4	0.02	48.0	15.0	4.6	1.8

Another irrigation canal in Barrage garden (site 39) showed Nymphaea coerulea and Potamogeton nodosus as dominant with rich algal flora of Cladophora glomerata, Spirogyra varians, Achnanthes minutissima as dominants and Cyclotella ocellata, Navicula cryptocephala, Nitzschia fruatulum v. perminuta and Rhopalodia gibba as common.

4- Benha-Zagazig road region: At site 44 (irrigation stream) Potamogeton crispus dominated and was associated with Spirogyra varians. At sites 45-47 (all irrigation streams), dominant macrohydrophytes were associated with a few algae (table 1).

Concluding Remarks

It is clear from table 1 that Phragmites australis, Eichhornia crassipes, Lemna gibba, and Typha domingensis are wide spread in the studied regions since they are present in almost all investigated regions. Potamogeton nodosus, Panicum repens and Ceratophyllum demersum were moderately spread, while Nymphaea coerulea, Potamogeton pectinatus and P. crispus showed a narrower range of distribution.

Occurrence of the macrohydrophytes is noticed to be controlled by factors of the aquatic environment including spacial and flowing characteriatics. Zonation of the macrohydrophytes is a typical phenomenon. It occurs in accordance with depth of

water, along-side the banks of the water channel, stream or other habitat. In shallow waters are present swamp reeds while in deeper water submerged and free floating macrohydrophytes.

It is also noticed that with the gradual change of habitat characters with zonation, the pattern of the macrohydrophyte changes and this is simultaneously accompanied with a change in the algal flora associated with these macrohydrophytes.

A marked difference exists between quiet or stagnant waters where a lentic habitat exists, characterized by plants such as Lemna gibba and lotic water habitats with faster flowing water characterized contrastly by plants such as Nymphaea coerulea.

The most common species and varieties of diatoms that are found in association with the studied hydrophytes are: Achnanthes minutissima, Cocconeis placentula, Cyclotella ocellata, Melosira granulata, Navicula cryptocephala, Nitzschia frustulum, Rhopalodia gibba ventricosa, Synedra ulna genuina, S. ulna biceps, S. ulna amphirhynchus and S. ulna splendens.

The number of taxa of green algae was not high in almost all sites. In certain sites, however, there was an extensive growth of Cladophora glomerata, Spirogyra varians, Oedogonium capilliforme and Selenastrum gracile. The best qualitative

representation of Chlorophyceae was in the majority of the samples of the Barrage region, where Chlorophyceae comes on top of Cyanophyceae. This may be explained to be due to the relatively low pH value, and agrees with the works of Knudson (1954), Roa (1955) and Jorgensen (1957) who mentioned that water with low pH value is suitable for the growth of green algae.

Oscillatoria tenuis is the only taxon recorded dominant concerning Cyanophyceae.

The drain near Torra (site 36) showed dominance of macrohydrophytes Eichhornia crassipes, Typha domingensis and Phragmites australis with 100% plant cover which resulted in absence of dominance of algae which could be ascribed to be due to decreased illumination caused by the dense higher plant cover. Similarly El-Nayal (1935) and Talling and Rzoska (1967) noticed that high turbidity of the Nile water with the silt during the flood season decreased light penetration and consequently the algal flora decreased.

Variation in algal taxa and macrohydrophytes under the different studied habitats including fresh water of rivers, canals, drains and streams, has been noticed and this is dependent on various ecological factors of ecosystems (see Fig. 2).

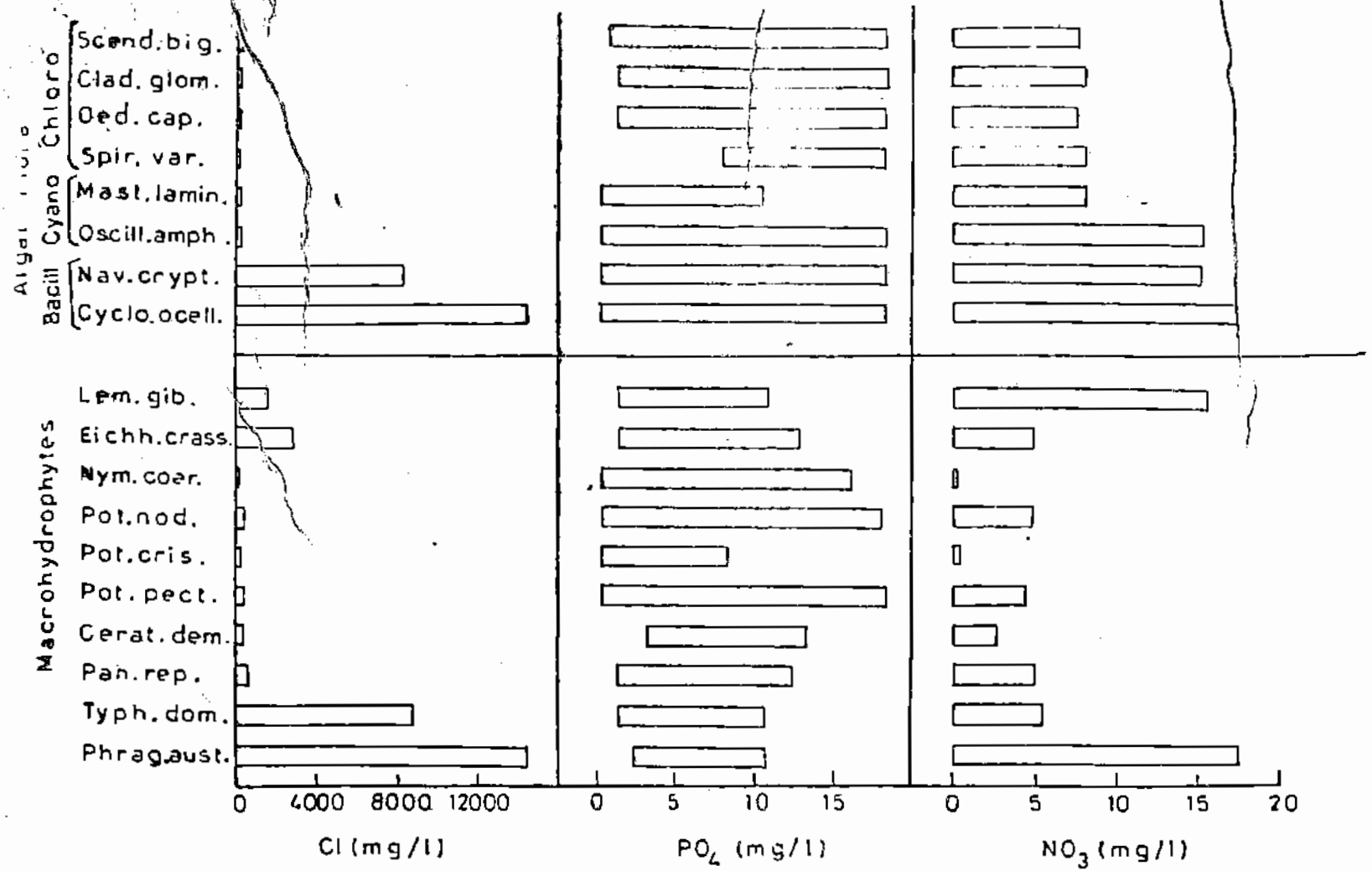

Fig. 2 . Ecological amplitude of the studied macrohydrophytes and some

It is clear from the present study on the distribution of algal flora that the diatoms contributed the greatest number of taxa. This observation agrees with the works of Luchini (1974), Harlin (1975), Ballantin and Harold (1975) and Nassar (1980). It is clear also that the abundance of algae at different sites is affected by the ecological characters including the chemical and physical properties of water.

Summary

Thirty-six samples were collected from 16 sites at Giza, Maadi, Qalyubia and Sharkia. The association between algae and macrohydrophytes was studied in the 36 collected samples. The study revealed certain associations between some algae and the common macrohydrophytes. Reduced algal flora was noticed unde dense water plant cover and in fast flowing waters. A marked difference exists between lentic habitat (quiet or stagnant waters) and lotic ones (fast flowing water).

Acknowledgement

The authors wish to express their deepest gratitude to Dr. Mohamed A. Hammouda, Professor of Botany at Ain Shams University for kind help and illuminating criticism.

References

Abou El-Kheir, W.S. and Ismail, G.H. (1986). Notes on the aquatic habitats of macrohydrophytes and associated algae in various regions in Egypt. 1- El-Fayum region. Phytologia 60: 469-482.

————————' Hammouda, M.A., and Ismail, G.H., (1986). Notes on the aquatic habitats of macrohydrophytes and associated algae in various regions in Egypt. 2- Ismailia canal and nearby water bodies from Cairo to Ismailia city. Ain Shams Sci. Bull. 28. (accepted).

Ballantine, D. and Harold, J.H., (1975). Benthic algae of the Anclote estuary: 1- Epiphytes of sea-grass leaves. Flasci 38 (3): 150-162.

El-Nayal, A.A., (1935). Egyptian fresh water algae. Bull. Fac. Sc. 4: 1-146.

Harlin, M.M. (1975). Epiphyte-host relations in seagrass communities. Aquat. Bot. 1 (2): 125-131.

Jorgensen, E.G., (1957). Diatom periodicity and silicon assimilation. Dansk Bot. Ark. 18: 1-54.

Knudson, B.M., (1954). The ecology of the diatom genus Tabellaria in English lake District. J. Ecol. 42: 345-355.

Luchini, L., (1974). Epiphytic diatoms and macrophytes (Prov. Chubut.) Physis Secc. B. Aguas Cont. Org. 33 (86): 127-139.

Nassar, A.H., (1980). Studies on algal flora of certain habitats in the vicinity of Cairo. M.Sc. Thesis, Fac. Sci., Ain Shams Univ.

Roa, C.B., (1955). The distribution of algae in a group of six small ponds. Part 11. J. Ecol. 43: 291-308.

Talling, J.F. and Rzoska, J., (1967). The development of plankton in relation to hydrological regime in the Blue-Nile, J. Ecol. 55: 637-662.

Explanation of Plate I

Fig. 1. Rhopalodia gibba genuina X 1000.

Fig. 2. Epithemia zebra proboscidea X 1000.

Fig. 3. Cymatopleura solea X 1000.

Fig. 4. C. solea subconstricta f. minor X 1066.

Fig. 5. Pinnularia viridis intermedia X 1000.

Fig. 6. Melosira granulata X 1000.

Fig. 7. Navicula viridula genuina X 1000.

Fig. 8. Gomphonema gracile major X 1143.

Fig. 9. G. montanum acuminatum X 1143.

Fig.10. Cocconeis placentula euglypta X 1250.

Fig.11. Grammatophora oceanica X 1556.

Fig.12. Amphora ovalis typica X 1000.

Fig.13. Cyclotella meneghiniana X 1902.

Plate 1

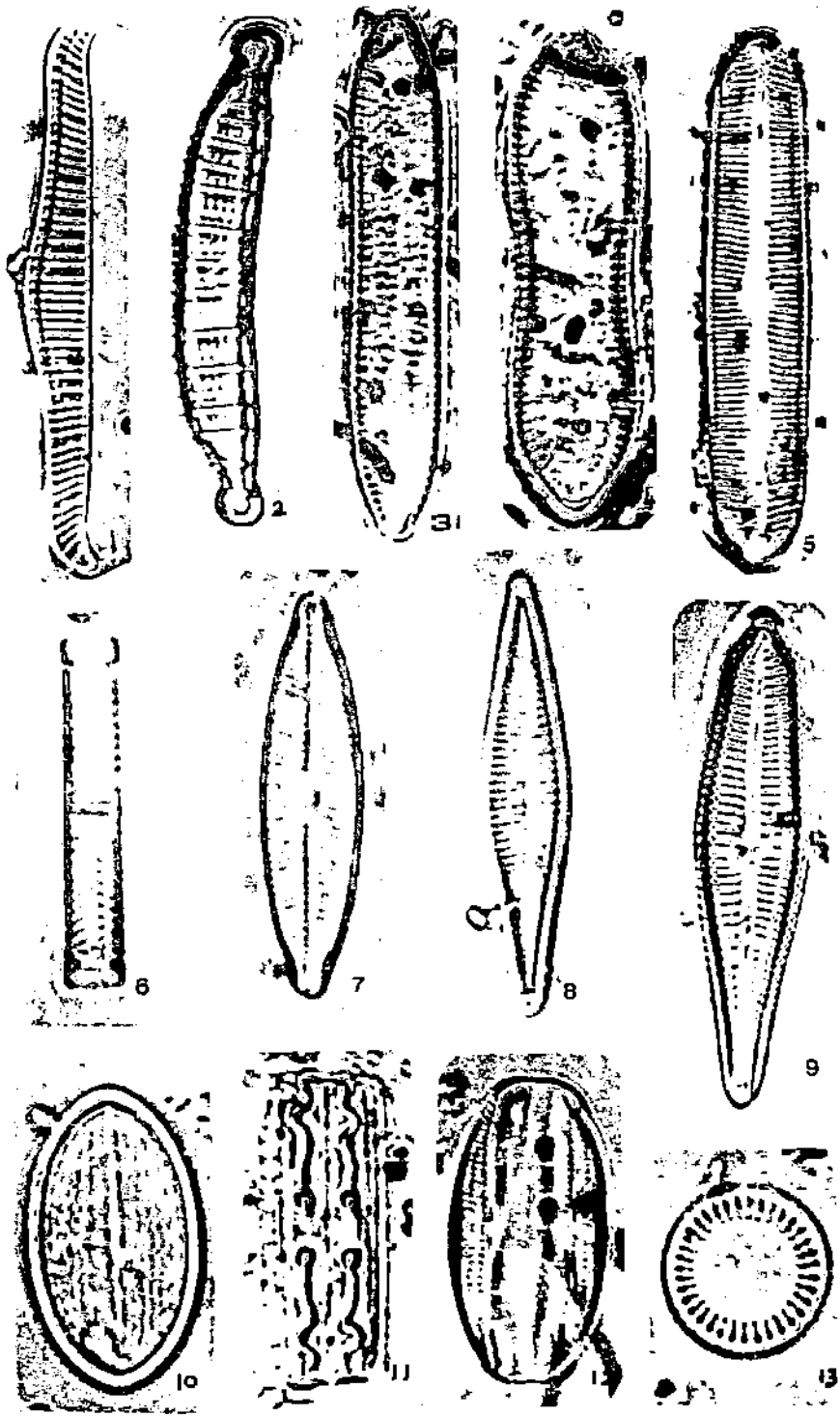

Explanation of Plate II

Fig. 1. Chlorococcum humicola X 1250.

Fig. 2. Spirogyra varians X 250.

Fig. 3. Scenedesmus armatus X 1000.

Fig. 4. Pediastrum borganum X 1000.

Fig. 5. Cosmerium laeve X 1000.

Fig. 6. Tetraedron minimum X 2727.

Fig. 7. Anabaena oscillaroides X 1000.

Fig. 8. Spirulina subsalsa X 1000.

Plate 2

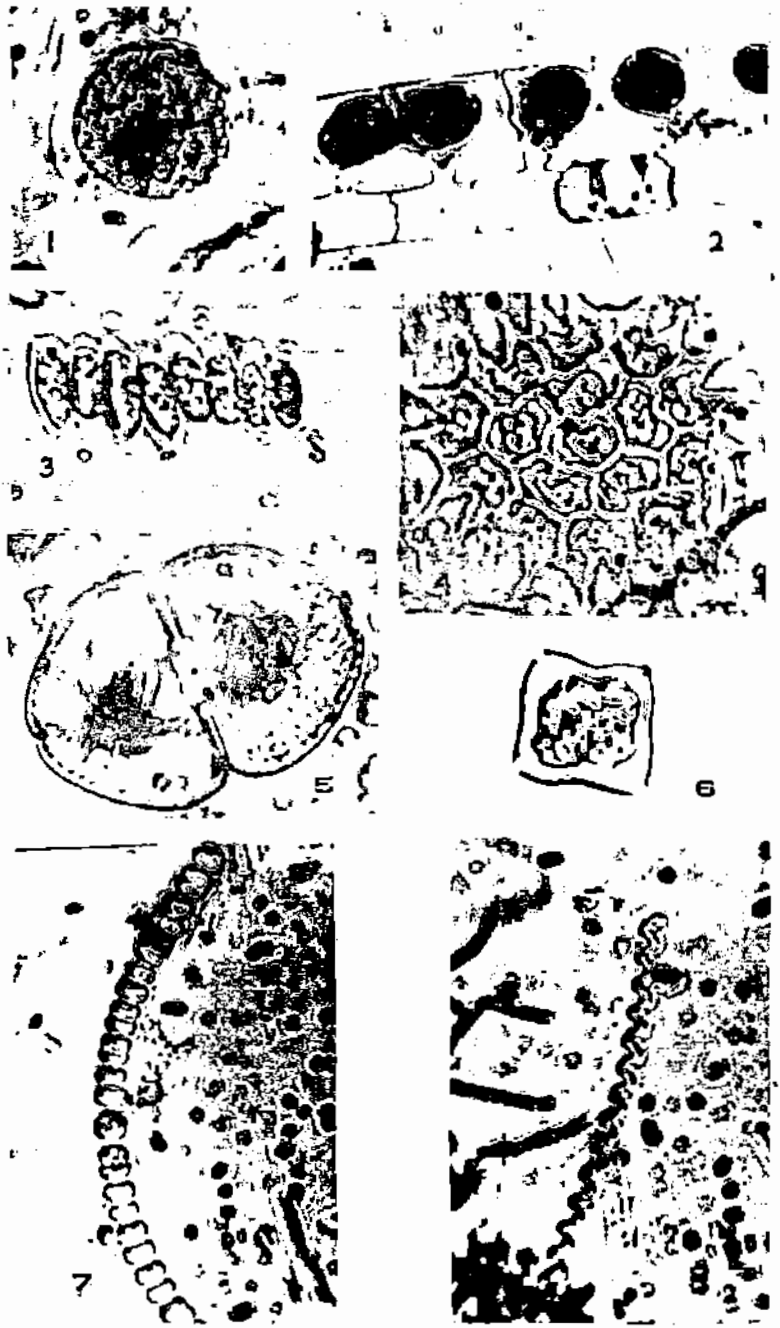

ملاحظات على البيئات المائية للنباتات المائية الكبيرة وما يصاحبها من فلورا طحلبية فى مناطق مختلفة من مصر ٣ ــ محافظات الجيزة والقاهرة والقليوبية والشرقية

الدكتورة وفاء صبحى أبو الخير ــ الدكتورة جهيزة عبد الحكيم اسماعيل

يهدف البحث الحالى الى دراسة الفلورا الطحلبية المصاحبة للنباتات المائية المنتشرة فى بيئاتها الطبيعية فى ٣٦ عينة جمعت من محافظة الجيزة (الجيزة) والقاهرة (المعادى) والقليوبية (القناطر الخيرية) والشرقية (منطقة الزقازيق) اتضح من الدراسة وجود مصاحبة بين بعض الطحالب والنباتات المائية فى العينات المدروسة . لوحظ نقص الفلورا الطحلبية تحت الغطاء النباتى الكثيف للنباتات المائية وفى المياه سريعة الجريان ــ كما لوحظ وجود اختلاف بين البيئات ذات المياه سريعة الجريان والبيئات ذات المياه الراكدة .

Studies on algal floras inhabiting different water sources in Egypt.

3- Waste-water bodies (drains and swamps)

by

Wafaa S. Abou El-Kheir and Laila E. Mekkey
University College for Girls, Ain Shams University, Egypt.

Introduction

Publications dealing with the Egyptian marine algal flora are: Ghazzawi (1939), Aleem (1948, 58, 78a, b, 80 and 81), Nasr and Aleem (1949), Mohamed and Halim (1952), Salah (1960), Kaleafah (1964), Motwalli (1966), Nasr et al. (65-66), Nasr and Ibrahim (67 & 68), Abdel Fattah and Hussein (1970), Nasr and Bekheet (1970), Nosseir and Abou El-Kheir (1970a), Mohsen and Shaalan (1971a & b), Salem et al. (1971), Abdel Fattah and Edress (1977), Kobbia (1981), Shaaban et al. (1983), Abou El-Kheir and Mekkey (1986a). However, a few studies had been carried out on the Egyptian fresh and brackish algal floras: El-Nayal (1931, 35 & 37), Abdin (1948 a & b), Nosseir and Abou El-Kheir (1970b, c & 1972), Abou El-Kheir and El-Shimi (1976), Ramadan et al. (1976), El-Naggar (1977). Nassar (1980), Shaaban and El-Habibi (1978), Shaaban et al. (1980a, b, c & 82), Abou El-Kheir and Ismail (1986), Abou El-Kheir et al. (1986) and Abou El-Kheir and Mekkey (1986b).

In Egypt most of the work in the field of water algal ecology, whether marine, fresh or brackish, is related to lakes,

seas, springs, rivers, irrigation canals, ponds, pools and ditches. The present investigation is aimed to extend the algal survey (see Abou El-Kheir and Mekkey, 1986a & b) to some other water sources namely drains and swamps. Physical and chemical properties of the water were determined, to find out their effect on the algal flora.

Material and Methods

Excursions were made to three localities; Helwan, Maadi and Ismailia, during the period 9/3/79-17/12/79. Fourteen brackish water samples were collected: 7 from Helwan, 4 from Maadi and 3 from Ismailiya (Table 1). The chlorides content of the samples ranged between 150-250mg/L. Temperature and pH of water were measured. Determination of dissolved nutrients (Table 2) was carried out by different methods (see Mekkey, 1984). Identification of algal taxa in the 14 samples was done using the inverted microscope. Natural photographs of some algal taxa are shown on plates 1 and 2.

Table (1) Details concerning Region, kind and source of water, date of collection and the number of samples taken.

Region	Date of collection	Source & Kind of water	No. of samples taken
Helwan	9/3/1979	Brackish water:	
		stagnant swamps	2
		a running swamp	1
		running drains	3
		a stagnant drain	1
Ismailia	30/3/1979	Brackish water:	
		drains	3
Maadi	17/12/1979	Brackish water:	
		drains	3
		a swamp	1

Table (2) Values of pH, temperature and nutrients in the three localities of collection. Values of nutrients are given as p.p.m.

Locality		Sample No.	pH	Temp. °c	No_3	Po_4	Cl	Na	Ca	Mg	K	Co_3	HCo_3
Helwan	S	1	7.5	23	4.0	0.8	1495	1725	2.4	1.1	46.8	-	213
		2	9	16	-	1.4	11168	1150	10.1	6.2	23.4	-	15
		3	7.3	17	-	1.6	1663	2530	2.3	0.9	39	-	172
		4	7	26	-	-	2345	552	2.2	1.5	[illegible]	-	203
	D	5	7	27	-	1.3	1867	1897	2.6	1.3	46.8	-	71
		6	10	22	0.7	5.5	292	676	0.2	0.5	42.9	30	772
		7	7.8	22	4.0	-	1619	285	1.2	1.4	23.4	-	38
Maadi	S	8	7	16	13.4	2.8	168	184	0.5	0.2	23.4	-	244
		9	6.7	16.5	0.7	4.6	168	172	0.8	0.4	31.2	-	305
	D	10	6.8	16	2.0	2.8	221	213	0.6	0.4	54.6	-	213
		11	6.5	16	-	12.2	5549	161	3.7	5.6	74.1	-	167
Israilia	D	12	5.8	22	1.3	1.2	201	253	0.5	0.3	3.9	-	406
		13	6	24	66.5	7.5	247	696	0.6	1.0	31.2	-	30
		14	6.5	26	102.5	26.6	442	28.7	1.1	0.3	2[illegible].4	-	111

S = Swamp D = Drain

Results

Table 3 shows that members belonging to Bacillariophyceae occur in the 14 studied samples, collected from 10 drains and 4 swamps. The number of taxa representing Bacillariophyceae is 138, Chlorophyceae: 24, Cyanophyceae: 19, Euglenophyceae: 2 and Xanthophyceae: 2. Although the samples were taken from similar sources of stagnant waste water, yet, Bacillariophyceae was best represented in Ismailia, Chlorophyceae in Maadi and Cyanophyceae in Helwan. Tolerant diatom species existing in both drains and swamps in the three localities are Achnanthes brevipes intermedia, Cyclotella meneghiniana genuina, Melosira fennoscandica, Navicula cryptocephala subsalina, N. cryptocephala exilis, Nitzschia apiculata, Gomphonema parvulum genuina and G. exillissium. While those representing Cyanophyceae also in the three localities are Oscillatoria amphibia, O. elegans and O. tenuis. Although Chlorophyceae did not exhibit such tolerance, yet some of its members were predominant or dominant in certain samples of a single locality. Thus Enteromorpha flexuosa and Mougeotia sp. were predominant in 3 samples in Helwan, Cladophora sp. and Spirogyra sp. were predominant and dominant respectively in 2 samples in Maadi and Ankistrodesmus spirales fasciculatus was dominant in one sample in Ismailia.

The highest values of NO_3 and PO_4 were recorded in sample no. 14 from Ismailia and of chlorides in sample no. 2 from Helwan (see table 2).

Table (3) The recorded algal taxa in the 14 collected samples.
c = common, d = dominant, p = predominant, H = Helwan,
M = Maadi, I = Ismailia.

Algal taxa	H							M				I		
	1	2	3	4	5	6	7	8	9	10	11	12	13	14
Bacillariophyceae														
1 Biddulphia polymorpha (Grun.) Woll.	+			+										+
2 Cyclotella comensis Grun.														+
3 C. meneghiniana genuina A.Cl.	+	+	+						+		+		+	+
4 C. meneghiniana plana Frick.												+		
5 C. meneghiniana pumila Grun.														+
6 C. ocellata Pant.		+	+						+			+	+	+
7 C. operculata.												+		
8 C. striata bipunctata Frick.	+													
9 Melosira fennoscandica.	+		+	+			+		+			+	+	+
10 M. granulata angustissima O.M.	+			+			+					+	+	+
11 M. granulata typica A.Cl.									+					
12 M. islandica typica A.Cl.			+				+							
13 M. jurgensii bothnica (Grun.) A.Cl.	+		+						+					

	Algal taxa	H.							M.				I.		
		1	2	3	4	5	6	7	8	9	10	11	12	13	14
14	Achnanthes brevipes angustata (Grev.) Cl.			+							+				
15	A. brevipes intermedia Kz.	+		+	+	+		+	+	+	+				+
16	A. brevipes parvula Kz.			+	+	+				+	+				
17	A. exigua heterovalvate Krasske.														+
18	A. lanceolata genuina May.							+						+	
19	Amphora acutiuscula Kz.		+			+									
20	A. coffaeiformis boraelis.		+	+		+									
21	A. coffaeiformis salina (W. Sm.) A.Cl.	+	+	+				+			+				
22	A. libyca typica A.Cl.									+				+	+
23	A. maxicana major (Cl.) A.Cl.			+											
24	Bacillaria paradoxa Gerl.	+			+			+		+					+
25	Caloneis amphisbaena fenzlii (Grun.)Cl.													+	+
26	C. amphisbaena genuina A.Cl.														+
27	C. permagna (Bail.) Cl.	+													
28	C. silicula limosa diminuta A.Cl.														+

Table 3, Cont.

	Algal taxa	H.							M.				I.		
		1	2	3	4	5	6	7	8	9	10	11	12	13	14
29	Cocconeis lineata A.Cl.												+	+	
30	C. placentula intermedia (H. & P.) Hust.			+				+							
31	C. placentula lineata f. major														+
32	C. placentula lineata f. trilineata														+
33	Cymatopleura elliptica angulata f. imperfecta.														+
34	C. solia genuina Frick.														+
35	C. solia eubconstricta O.M.												+		
36	C. solia subconstricta f. minor.														+
37	Cymbella cisluta hebetata (Pant.) Cl.														+
38	Diatoma elongatum tenua f. normalis.	+				+	+								
39	Diploneis decipiens typi a A.Cl.													+	
40	D. elliptica genuina f. minor.	+		+	+	+		+							
41	Epithemia argus protracta May												+		
42	E. turgida capitata Fricke.														+
43	E. turgida granulata (E.) Grun.												+		

	Algal taxa	H.							M.				I.		
		1	2	3	4	5	6	7	8	9	10	11	12	13	14
44	Fragilaria capucina arctica A.Cl.							+	+	+	+				
45	F. construens genuina f. typica.														+
46	F. striatula Lyn.	+													
47	F. virescens lanceola.						+								
48	Frustulia saxonica laticeps.														+
49	Gomphonema constrictum capitatum.							+							
50	G. dubravicense Pant.														+
51	G. gracile genuinum May.				+										
52	G. gracile hybridum A.Cl.	+		+	+	+									
[illegible]	G. gra[illegible] navi[illegible]loides W. Sm.	+								+					
[illegible]	G. lar[illegible]atum pe[illegible]num A.Cl.			+				+		+	+			+	+
[illegible]	[illegible]												+		
[illegible]	[illegible]										+				
[illegible]	[illegible]												+		
[illegible]	[illegible]												+		

Table (3) Cont.

	Algal taxa	H.							M.				T.		
		1	2	3	4	5	6	7	8	9	10	11	12	13	14
59	G. parvulum exillissimum Grun.		+	+	+			+		+	+			+	+
60	G. parvulum genuina May	+			+	+							+		+
61	G. subclavatum Grun.										+	+	+		+
62	G. truncatum capitatum.										+				
63	Gomphonitzschia ungeri Grun.							+				+			
64	Gyrosigma acuminatum gallicus.			+	+	+								+	+
65	G. acuminatum lacustre (W. Sm.) A.Cl.														
66	G. distortum marinuna A.Cl.	+													+
67	Hantzschia amphioxys densestriata (Font.) Cl.			+											
68	Mastogloia braunii Grun.			+											
69	M. lacustris amphicephala (Grun.) A.Cl.			+											
70	M. lacustris genuina A.Cl.	+											+		
71	Navicula arenaria formis Pant.													+	
72	N. avenaceae													+	
73	N. cincta typica A.Cl.														

Table (3) Cont.

	Algal taxa	H.							M.				I.		
		1	2	3	4	5	6	7	8	9	10	11	12	13	14
74	N. crucigere subhuyalina.	+		+	+										
75	N. cryptocephala exilis Grun.	+	+	+	+	+		+							
76	N. cryptocephala genuina A.Cl.							+							
77	N. cryptocephala subsalina Hust.	+	+	+	+	+	+	+							
78	N. cuspidata ambigua (E.) Cl.	+		+	+										
79	N. gastrum genuina A.Cl.							+		+					
80	N. graciloides May.									+					
81	N. inflata genuina A.Cl.			+											
82	N. paramutica.												+		
83	N. pygmaea Kz.		+	+											
84	N. rhyncocephala amphiceros (Kz.) V.H.												+		
85	N. viridula capitata May.	+		+				+		+		+		+	
86	N. viridula capitata f. minor.														+
87	Nitzschia affinis Grun.												+		

Table (3) Cont.

	Algal taxa	H.							M.				I.		
		1	2	3	4	5	6	7	8	9	10	11	12	13	14
88	N. angustata antiqua (Sch.) A.Cl.		+												
89	N. apiculata (Greg.) Grun.	+		+	+	+		+							
90	N. dissipata genuina A.Cl.														
91	N. gothlandica.									+					
92	N. granulata Grun.														
93	N. hantzschiana tenuior A.Cl.	+			+	+									
94	N. hungarica genuina Grun.													+	
95	N. kutzingiana genuina A.Cl.	+			+	+									
96	N. laevissima Grun.									+					
97	N. lanceolata minima Grun.														+
98	N. latestriata major A.Cl.						+	+							
99	N. nathorstii Brun.												+		
100	N. obtusa scalpelliformis Grun.	+													
101	N. obtusa schweinfurthii Grun.	+		+	+	+		+		+					+
102	N. obtusa vulgaris Grun.			+											
		+						+		+				+	

Table (3) Cont.

	Algal taxa	H.							M.				I.		
		1	2	3	4	5	6	7	8	9	10	11	12	13	14
103	N. obtusa nana Grun. .												+		+
104	N. paradoxa genuina Grun.												+	+	
105	N. palea genuina A.Cl.								+						
106	N. parvula Lewis.														+
107	N. pellucida faeminores											+			
108	N. punctata curta Grun.										+				
109	N. sigma clausii (Htz.) Grun.				+			+		+					
110	N. sigma claussii f. major .	+		+	+										
111	N. sublinearis Hust.							+							
112	N. thermalis intermedia Grun.	+	+	+		+					+	+			
113	N. tryplionella debilis (Arn.) May														+
114	N. tryplionella genuina Grun.									+		+			+
115	N. tryplionella suborbicularis A.Cl.									+					
116	N. vermicularis genuina A.Cl.			+							+	+			

Table (3) Cont.

	Algal taxa	H.							M.				I.		
		1	2	3	4	5	6	7	8	9	10	11	12	13	14
117	N. vermicularis lamprocampa (Kz.) V.H.	+			+									+	+
118	N. vitrea genuina Grun.													+	
119	Pinnularia laticeps spherocephala			+						+					+
120	P. parvula (Ralf) A.Cl.														+
121	P. rostrata A.Cl.	+			+	+	+								
122	Pleurosigma elongatum genuinum A.Cl.	+													
123	P. elongatum kerianum (Grun.) A.Cl.	+													
124	P. formosum genuinum A.Cl.										+				
125	Rhoicosphenia curvata genuina A.Cl.														+
126	R. curvata marina (W. Sm.) Grun.													+	
127	Rhopalodia gibba genuina Grun.			+											
128	R. gibba ventricosa (Kz.) O.M.						+						+		+
129	R. gibberula constricta (W. Sm.) A.Cl.	+		+						+					
130	R. gibberula minuens O.M.														

Table (3) Cont.

Algal taxa	H.							M.				I.		
	1	2	3	4	5	6	7	8	9	10	11	12	13	14
131 Surirella ovalis Breb											+			
132 S. patella Neupausri (Pant.) A.Cl.	+			+	+									
133 Synedra tabulata affinis (Kz.) A.Cl.		+			+									
134 S. ulna biceps Sch.							+							
135 S. ulna danica f. continua			+						+					
136 S. ulna genuina f. typica										+				
137 S. ulna splendens (Kz.) A.Cl.													+	+
138 S. ulna subaequalis Grun.												+		
Chlorophyceae														
1 Ankistrodesmus convolutus													+	
2 A. radiatus				+										
3 A. spiralis									+				+	
4 A. spiralis fosciculatus													+	
5 Chlamydomonus gloeocystiformis										c				

Table (3) Cont.

	Algal taxa	II.							III.				I.		
		1	2	3	4	5	6	7	8	9	10	11	12	13	14
6	Chlorococcum humicola	+							+						
7	C. infusionum				+	+									
8	Cladophora revularis									+					
9	C. sp.														+
10	Coelastrum sp.													+	
11	Cosmerium sp.														+
12	Enteromorpha flexuosa		F			P									
13	Mougeotia sp.				P	P									
14	Oedogonium patulum									+					
15	Rhizoclonium sp.									+					
16	Scendesmus abundance									+					
17	S. bijuanatus														+
18	S. quadricauda									+					
19	Spirogyra sp.												G		G
20	Staurastrum gracile												+		

Table (3) Cont.

	Algal taxa	H.							M.				I.		
		1	2	3	4	5	6	7	8	9	10	11	12	13	14
21	Tetraedron minimum f. apiculatum									+					
22	Ulothrix fenuissima				+										
23	U. pearsonii									+					
24	Uronema confervicolum									+					
	Cyanophyceae														
1	Chroococcus minutas						+								
2	Lyngbya martensiana						+								
3	L. majuscula				+										
4	Merismopedia elegans			c						c				c	
5	M. tebermalis					+	+								
6	Oscillatoria amphibia				c						c			c	
7	O. animalis			+	+										
8	O. brevis					+				p					
9	O. geminata			+											

Table (3) Cont.

	Algal taxa	M.							M.				I.		
		1	2	3	4	5	6	7	8	9	10	11	12	13	14
10	O. numidica				+		+								
11	O. ornata	+			+		+								
12	O. planctonica			+											
13	O. sancta			+											
14	O. subtilissima		+		+										
15	O. tenuis		r	r		+									r
16	O. terebriformis				+										
17	Phormedium vesiculosa					r									
18	Placoma vesiculosa					r									
19	Schizothrix arenaria vermiformis					r									
	Xanthophyceae														
1	Koliola sp.				+										
2	Vaucheria sessilis													r	

Table (3) Cont.

Algal taxa	H.							M.				I.		
	1	2	3	4	5	6	7	8	9	10	11	12	13	14
Euglenophyceae														
1 Phacus anomala									+					
2 P. longicauda									+					

Discussion

In 1935 El-Nayal mentioned that Hydrodictyon sometimes forms extensive growths in drains, and it is generally associated with Cladophora. He stated also that they may form intricate masses that block the drains and hinder their courses. In the present study Cladophora was found predominant in one sample taken from a drain at Maadi, while Hydrodictyon did not show up in any of the 10 drain samples.

Paul (1977) stated that the accumulation of important quantities of fertilizers (nitrates and phosphates) in lake Geneva has resulted in a considerable increase of phytoplankton, with appearance of species not formerly reported from the lake. Similar results were obtained here since, samples 13 and 14 collected from Ismailia, were rich in nutrients especially nitratee and phosphates and contained the largest number of diatom taxa. However,no obvious effects of either NO_3 or PO_4 or both were observed in the present study, except in these two mentioned samples.

Prescott (1969) stated that planktonic blue-greens and diatoms are abundant in water with high pH (7.4-9.0). Durrell (1964) and Nassar (1980) as well found that diatoms and blue-greens were more characteristic to alkaline waters. Similar results were obtained here concerning blue-greens; members of which were numerous and well represented in alkaline water

samples (pH 7-10) from Helwan. However, concerning diatoms they were found flourishing in alkaline water samples (pH 7-10, Helwan) as well as in acidic ones (pH 5.8-6.5, Ismailia).

It may be said in conclusion that, although, the samples were all collected from brachish waters (brackish drains and brackish swamps) yet it has been found that the samples from Helwan (drains and swamps) were generally characterised by the presence of copious masses of blue-greens followed by diatoms. At Maadi (drains and a swamp) greens were best represented followed by blue-greens, while at Ismailia (drains) diatoms were dominant whereas greens and blue-greens were poorly represented. These results seem to be correlated with pH since it ranged from 7.0-10.0 in Helwan samples, from 6.5-7.0 in Maadi samples and from 5.8-6.5 in Ismailia samples. It must be mentioned also that differences concerning elements of the algal floras are more pronounced between localities than between sources of water, being drains or swamps (see table 3). In other words each of the three localities has its distinct algal flora for example concerning diatoms, only 35 out of 138 recorded taxa occur in more than one locality. This observation holds also true for blue-greens and greens (see table 3). Again this may be explained as due most probably to pH.

Summary

Excursions were made to three localities: Helwan, Maadi, and Ismailia Fourteen brackish water samples were collected from 10 drains and 4 swamps. 185 algal taxa belonging to Bacillariophyceae, Chlorophyceae, Cyanophyceae, Xanthophyceae and Euglenophyceae were identified. Blue greens were best represented in Helwan, greens in Maadi, while diatoms in Ismailia These results seem to be correlated with pH. No obvious effects of No_3 or Po_4 were observed.

Explanation of Plate I

Fig. 1. Cymbella cistula hepetata X 1077.

Fig. 2. Fragilaria virescans genuina X 1093.

Fig. 3. Grammatophora marina X 1120.

Fig. 4. Rhoicosphenia curvata fracta X 1714.

Fig. 5. Rhoicsphenia curvata marina X 1809.

Fig. 6. Rhopalodia gibbaventricosa X 1050.

Fig. 7. Gomphonema parvulum exilissimum X 1330.

Fig. 8. Caloneis silicula limosa genuina X 938.

Fig. 9. Melosira varians X 900.

Fig.10. Lyngbya majuscula X 1000.

Fig.11. Lyngbya martensiana X 1000.

Fig.12. Phacus curvicauda X 1000.

Fig.13. Phacus sp. X 1000.

Fig.14. Scenedesmus abundans X 1000.

Plate 1

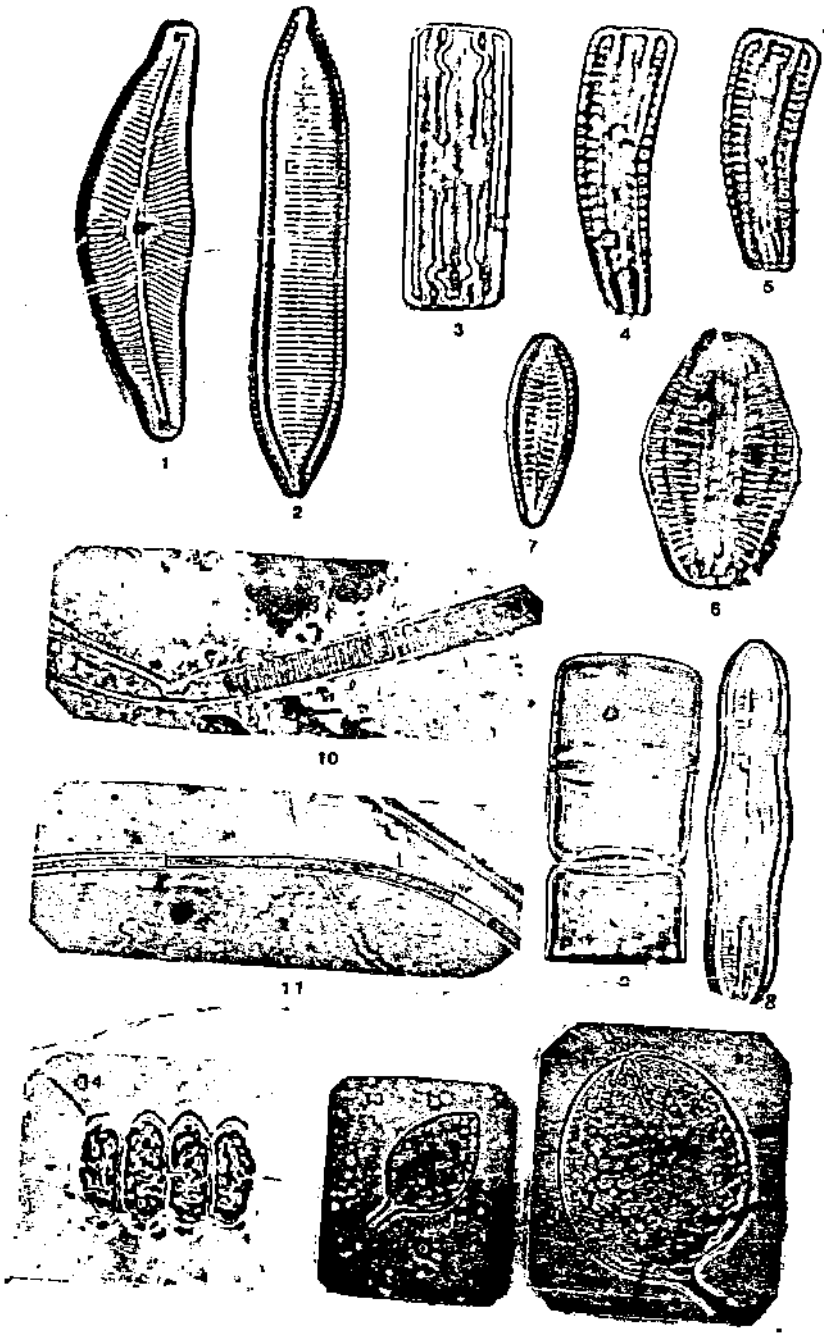

Explanation of Plate II

Fig. 1. Enteromorpha flexuasa X 1000.

Fig. 2. Oedogonium sp. X 1000.

Fig. 3. Cladophora sp. X 1000.

Fig. 4. Spirogyra sp. X 1000.

Fig. 5. Staurastrum gracile X 1000.

Fig. 6. Vaucheria sessilis. X 1000.

Fig. 7. Oedogonium sp. X 1000.

Plate 2

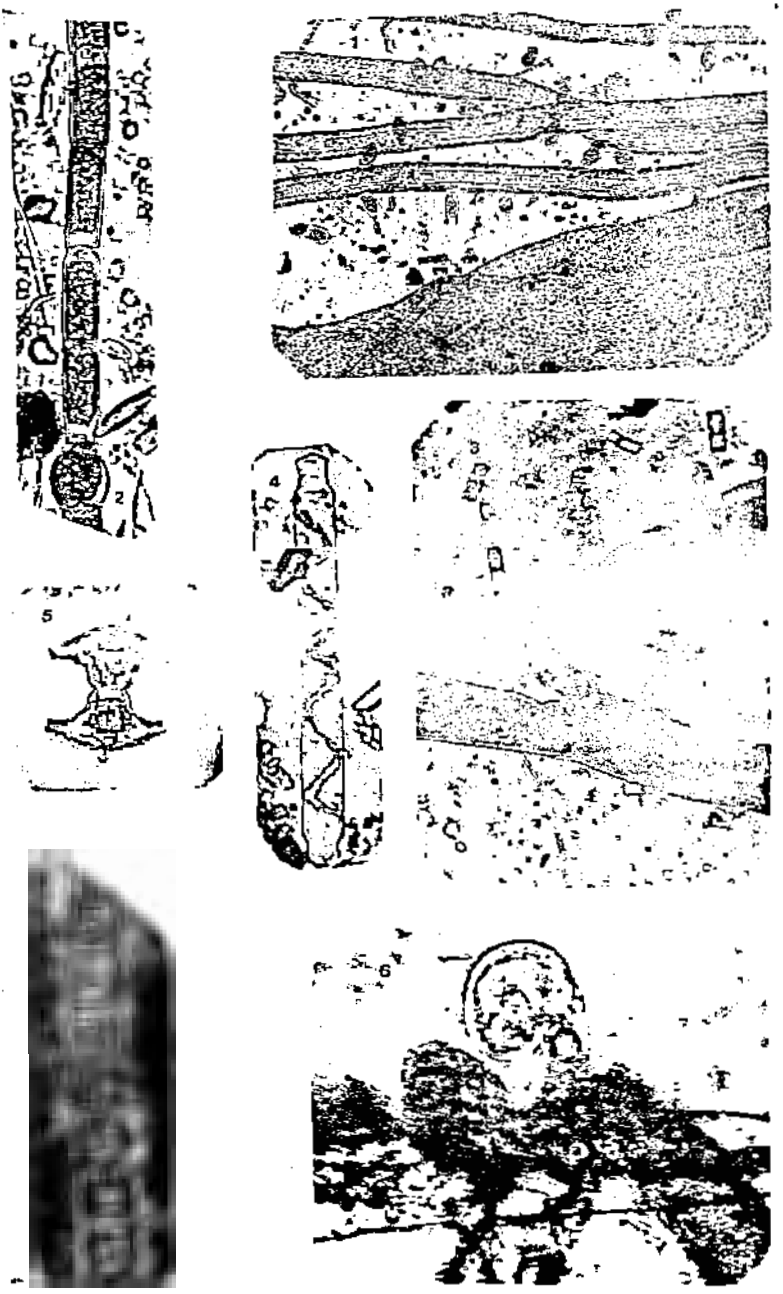

References

Abdel-Fattah, A.F. and Hussein, M.M. (1970). Composition of some brown algae as influenced by seasonal variations Phytochem. 9, 721.

———————— and Edress, M. (1977). Carbohydrates of the brown seaweed Padina pavonia. Phytochem. 16, 939.

Abdin, G. (1948a). Physical and chemical investigation relating to algal growth in the River Nile. M.Sc. Thesis, Fac. of Sc., Cairo Univ..

———— (1948b). Condition of growth and periodicity of the algal flora of Aswan Reservoir. Bull. of Fac. Sc. Cairo Univ., 27: 157-176.

Abou El-Kheir, W.S. and El-Shimi, A.A. (1976). The effect of some dissolved nutrients on the distribution and periodicity of Chlorophyceae and Cyanophyceae in El-Zomor and El-Mansoriya canals, Giza, Egypt. Univ. Coll. for Girls Ann. Rev. No. 9. Ain Shams Univ. press.

———————— and Ismail, G.H. (1986). Notes on the aquatic habitats of macrohydrophytes and associated algae in various regions in Egypt. 1- El-Fayum region Phytologia 60: 469-482.

————————, Hammouda, M.A., and Ismail, G.H. (1986). Notes on the aquatic habitats of macrohydrophytes and associated algae in various regions in Egypt 2- Ismailia canal and nearby water bodies from Cairo to Ismailia city. Ain Shams Sci. Bull. 28. (accepted).

——————— and Mekkey, L.E. (1986a). Studies on algal floras inhabiting different water sources in Egypt. 1- River Nile and its derivatives. Ain Shams Sci. Bull. 28. (accepted).

——————————————— (1986b). Studies on algal floras inhabiting different water sources in Egypt. 2- Lakes and Springs. Phytologia 61, No. 5.

Aleem, A.A. (1948). The recent migration of certain Indo-Pacific algae from the Red Sea into the Mediterranean. The New Phytologist, 88-96.

——————— (1958). A taxonomic and paleoecological investigation of the diatom-flora of the extinct Fayum lake (Upper Egypt). Bull. Fac. of Sc. Alex. Univ., Vol. 2: 217-245.

——————— (1978a). Contribution to the study of the marine algae of the Red Sea: 1- The algae in the neighbourhood of Al-Ghardaga, Egypt (Cyanophyceae, Chlorophyceae, and Phaeophyta). Bull. of Fac. of Sc., King Abdulaziz Univ. Jeddah Vol. 2: 73-87.

——————— (1978b). Contribution to the study of the marine algae of the Red Sea: II- The algae in the neighbourhood of Al-Ghardaga, Egypt (Rhodophyta). Bull. of Fac. of Sc., King Abdulaziz Univ., Jeddah Vol. 2: 89-97.

——————— (1980). Contribution to the study of the marine algae of the Red Sea: IV- The algae and seagrasses inhabiting the Suez Canal (Syptematic part). Bull. of Fac. of Sc., King Abdulaziz Univ., Vol. 4: 31-89.

———————— (1981). Compsopogon aegyptiacus Nov. sp. Red Algae from the Manzala, Egypt, with notes on the taxonomy of the genus. Bull. of the Fac: of Sc., King Abdulaziz Univ., Jeddah Vol. 5: 1-49.

Durrell, L.W. (1964). Algae in relation to soil fertility. Bot. Rev., 30 (1): 92-128.

El-Naggar, M.E., (1977). Studies on the algas in Dakahlia area. M.Sc. Thesis Fac. Sc. Mansoura Univ.

El-Nayal, A.A. (1931). An enumeration of Egyptian Chlorophyceae and Cyanophyceae. Extrait de la Revue Algologique pp. 177-195.

———————— (1935). Egyptian freshwater algae. Bull Fac. Sc. No. 4: 1-106.

———————— (1937). On some new freshwater algae from Egypt. Bull. Fac. Sc. No. 13: 5-15.

Ghazzawi, F.M. (1939). A study of the Suez Canal plankton, the phytoplankton. Hydrob & Fish-Directorate, Notes & Memoires No. 24, Egypt.

Kaleafah, A.F. (1964). Ecology of algae in lake Mariut. M.Sc. Thesis. Fac. Sc. Alex. Univ.

Kobbia, I.A. (1981). Seasonal vartions of phytoplankton in the salt marshes of Egypt. J. Bot. Vol., 24 (3): 191-201.

Mekkey, L.E. (1984). Studies on the algal flora of different water sources in Egypt. M.Sc. Thesis, Girls Coll. Ain Shams Univ.

Mohamed, A.F. and Halim (1952). Agar from Egyptian seaweeds. Am. J. Bot. 9: 689.

Mohsen, A.F. and Shaalan, S.H. (1971a). Studies on the brown alga Halopteris scoparia (Kütz). Saur. at Abu-Qir locality. Part I: Effect of some hydrographic factors on the growth characteristics. Bull. Fac. Sci. Alex. Univ. 11, 177.

——————————— (1971b). Studies on the brown alga Halopteris scoparia (Kütz). Saur. at Abu-Qir locality. Part IV: Epiphytic pattern, Morphological and anatomical features and algal associations. Bull. Fac. Sci. Alex. Univ. 11, 235.

Motwalli, A.M. (1966). M.Sc. Thesis, Alex. Univ. (cited from Shaaban et al. (1983). Egypt. J. Bot. 24 (3): 179-190).

Nasr, A.H. and Aleem, A.A. (1949). Ecological studies of some marine algae from Alexandria. Hydrobiol. 1, 251.

————————, Mohsen, A.F.A. and Bekheet I.A. (1965-1966). Agar production from Egyptian Agarophytes. Bull. Fac. Sci. Alex. Univ. 7, 99.

———————— and Ibrahim R.K. (1967). An electrochromatographic investigation of the amino acid pattern of some marine algae from Alexandria. Hydrobiol. 29, 80.

——————————— (1968). The effect of different nitrogen and carbon sources on amino acid synthesis in Ulva, Dictyota and Pterocladia. ibid. 31, 7.

———————— and Bekheet, I.A. (1970). Effect of certain trace elements and soil extract on some marine algae. ibid. 36, 53.

Nassar, A.H. (1980). Studies on algal flora of certain habitats in the vicinity of Cairo. M.Sc. Thesis, Bot. Dept. Fac. Sc. Ain Shams Univ.

Nosseir, M.A. and Abou El-Kheir, W.S. (1970a). Effect of dissolved nutrients on the distribution of algal flora in selected lakes of U.A.R. 1- lake Qarun. Ann. Rev. Univ. Coll. Girls. Ain Shams Univ. No. 6: 15-24.

——————————————— (1970b). Effect of dissolved nutrients on the distribution of algal flora in selected lakes of U.A.R. II- Lake Nasser. Ann. Rev. Univ. Coll. Girls. Ain Shams Univ. No. 6: 33-47.

——————————————— (1970c). Distribution and periodicity of algal flora in El-Khashab canal during winter and spring months. Ann. Rev. Univ. Coll. Girls Ain Shams Univ. No. 6: 49-68.

——————————————— (1972). Fluctuation and periodicity of the algal flora found in El-Khashab canal throughout the year 1968-1969. Ann. Rev. Univ. Coll. Girls. Ain Shams Univ. No. 7: 59-66.

Paul, M. (1977). Phytoplankton of lake Geneva. SAUSSUREA, 6: 325-328.

Prescott, A. (1969). The algae A Review, New York.

Ramadan, F.M., Shehata, S.A. and Roushdy, H. (1976). Symposium on Nile water and lake Dame projects. Sessions: Water quality and pollution held at the National Rec. Cent. Dokki, Cairo, Egypt. 4: 38.

Salah, M.M. (1960). The phytoplankton of lake Maruit and lake Edku with a general contribution to the Halobian system. Hydrob. Dep. Alex. Inst. Hydrob. Notes and Mem. No. 57: 1-15.

Salem, H.M., Abdel-Fattah, A.F. and Hussein, M.M. (1971). Structural investigation on the alginic acid of the Egyptian brown algal species Cystoceira barbata. Phytochem. 10: 1059.

Shaaban, A.S. and El-Habibi, A. (1978). The algal flora of Egyptian Oases. 1-The algal flora of Kharga oasis. Bull. Inst. Dest. Vol. 28, 1.

Shaaban, A.S., Younis, M.E., El-Habibi, A. and El-Naggar, M. (1980a). The algal flora of Dakahlia area (A.R.E.). 1- Seasonal variations in the phytoplankton from Damietta branch of the River Nile. Delta Jour. Sci. Tanta Univ. 4: 1.

(1980b). The algal flora of Dakahlia area (A.R.E.). II. Studies on the phytoplankton of El-Sahil Canal. Delta Jour. Sci. Tanta Univ. 4: 19.

(1980c). The algal flora of Dakahlia area. III. The phycoflora of El-Tawila drain. Bull. Fac. Mans. Univ. (in press).

———————, Ghazi, S.M. and Hassan, N. Sh. (1982). Ecological studies of algae in Zagazig area, (A.R.E.). Proc. Egypt. Bot. Soc. 3 (Mansoura Conf.) 135.

———————, El-Habibi, A.M. and El-Naggar, M.E. (1983). Algal vegetation of the Mediterranean coast of Egypt. J. Bot. Vol., 24 (3): 179-190.

دراسات على الفلورا الطحلبية التى تعيش فى مصادر مياه مختلفة فى مصر ٣ ـ المياه المهملة (مصارف ومستنقعات)

للدكتورة وفاء صبحى أبو الخير ـ والماجستير ليلى الحسينى مكى

يهدف البحث الحالى الى دراسة الفلورا الطحلبية فى مياه المصارف والمستنقعات ومدى تأثر تلك الفلورا بالعوامل الكيميائية والطبيعية المختلفة . تم جمع ١٤ عينة من عشرة مصارف وأربعة مستنقعات من أماكن مختلفة فى حلوان والمعادى والاسماعيلية . وقد تم التعرف على ١٨٥ وحدة تصنيفية (تاكسونا) من الطحالب تنتمى الى الدياتومات والطحالب الخضراء والخضراء المزرقة والصفراء واليوجلينية . وقد أزدهرت الطحالب العصوية (الدياتومات) فى الاسماعيلية والخضراء المزرقة فى حلوان والخضراء فى المعادى . ويبدو أن تلك النتائج ترتبط بالرقم الايدروجينى فى تلك الأماكن . أظهرت النتائج عدم أهمية النترات والفوسفات للفلورا الطحلبية فى تلك المصادر .

SILICIFIED ROOT FRAGMENTS OF TAMARIX L. FROM THE PLEISTOCENE OF EL-FAYUM

BY

W. E. EL-SAADAWI, AFAF A. BADAWI, and A.A.EL-AWAMRI

Botany Department, Faculty of Science, Ain Shams University, Cairo

Received : 10.3.1979

SILICIFIED ROOT FRAGMENTS OF TAMARIX L. FROM THE PLEISTOCENE OF EL-FAYUM

By

W. E. EL-SAADAWI, AFAF A. BADAWI, and A. A. EL-AWAIRI

Botany Department, Faculty of Science, Ain Shams University, Cairo

INTRODUCTION

Literature on the geology (e.g. Blanckenhorn, 1901 ; Gardner, 1927) and geography (Butzer, 1959) of Egypt includes reference to the occurrence of fossil Tamarix in various places in the country especially in Pleistocene deposits of El-Fayum. This, however, is the first botanical work on fossil remains of Tamarix collected from that Province.

LOCALITY

Specimens of silicified roots of Tamarix were collected a few years ago from the Pleistocene diatomaceous earth at Dimai (Dimê), north of Lake Qarun in El-Fayum (see the Map in Fig. 1). The fossil roots were associated with silicified fragments of shoots of Phragmites (El-Saadawi et al 1975). Fossil diatoms also occur in the fossiliferous area (El-Saadawi et al 1979) which represents shore-line deposits of the old fresh water Pleistocene Moeris Lake (see the Map in Fig. 1).

PLATE III


1


3


2

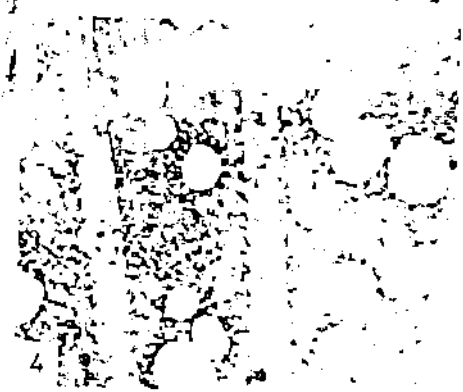
4

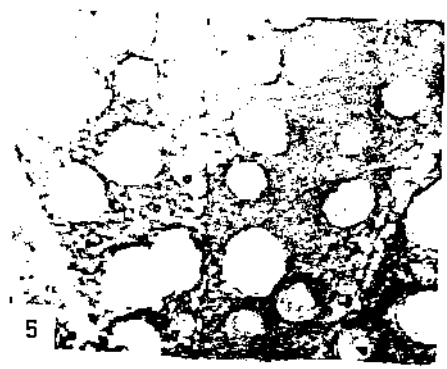
5

PLATE II

obtained are : T. amplexicaulis Ehrenb., T. aphylla (L.) Karst., T. arborea Bunge, T. nilotica (Ehrenb.) Bunge, and T. tetragyna Ehrenb. Transverse and tangential sections of roots of these species were prepared and stained as usual with living plant material.

DESCRIPTION AND COMPARISON

The fossil root fragments are small being a few centimeters long and about half a centimeter in diameter (Pl. II, Fig. 3). They are of whitish colour and radial vascular rays and feeble annual rings were easily seen by naked eye in transversely cut faces of the root fragments.

Data concerning the main anatomical features of the secondary xylem of roots of all Tamarix species studied are given in Table 1. Figures illustrating these main features of vessels and rays of secondary xylem of all species concerned are given on Plates II - IV. Reference to specific figures of each species is given also in the table.

The table shows that the anatomical features of the fossil root specimens are different from those of all other species. However, the extent of difference varies and is least toward the extant species T. aphylla. Concerning the dead specimens the least difference lies between them and the extant species T. nilotica . This means also that the fossil and dead specimens, though collected from one locality, yet they might belong to two different species.

TABLE 1

CHARACTERISTIC FEATURES OF ROOT SECONDRY XYLEM RECORDED FROM FOSSIL, DEAD, AND FIVE OF THE EXTANT TAMARIX SPECIES.

No.	Tamarix spp. / Features	Fossil Tamarix	Dead Tamarix	T.aphylla	T.nilotica	T.arborea	T.amplexicaulis	T.tetragyna
1-	No. of vessels per sq. mm.	30 - 33	20 - 22	24 - 34	19 - 22	25 - 33	35 - 40	35 - 42
2-	Shape of vessels in transverse sections	circular &oval	circular, rarely oval	circular, rarely oval	circular, sometimes oval	oval& circular	oval & circular	circular & oval
3-	Arrangement of vessels	alternate and opposite	opposite&alternate or in single rows	alternate rarely opposite	alternate, sometimes opposite	alternate and opposite	alternate and opposite	alternate
4-	Radial diameter of vessels	36 - 127 µ	54 - 373 µ	36 - 108 µ	55 - 182 µ	36 - 109 µ	36 - 109 µ	36 - 73 µ
5-	Vessels union: free	common	common	common	common	common	common	common
	united in 2	very rare	very rare	very rare	present	common	common	common
	united in 3	very rare	absent	absent	present	common	rare	common
6-	Seriation of rays	multiseriate (2-6)	multiseriate (2-6)	multiseriate (2-5)	multiseriate (2-10)	multiseriate (2-10)	multiseriate (2-5)	uni,&multiseriate (1-7)
7-	No. of xylem rays per sq.mm.	4 - 5	4	3 - 5	3 - 7	4 - 5	5 - 7	6 - 8
8-	Ray height in T.L.S.	0.45-1.73 mm.		.90-1.62 mm.	0.364-0.91 mm.	1.092-2,184 mm.	0.364-0.91 mm.	0.45-0.91 mm.
9-	Ray width in T.L.S	36 - 91 µ (Pl. II, Fig.4; Pl.IV, Fig.1)	36 - 73 µ (Pl.II, Fig.2; Pl.IV, Fig.2)	36-91 µ (Pl.II, Fig. 1; Pl.IV, Fig.4)	54 - 182 µ (Pl.II, Fig.5; Pl.IV, Fig.3)	36 - 182 µ (Pl.III, Fig.4)	36 - 91 µ (Pl. III, Figs. 1,5)	18 - 127 µ (Pl.III, Figs. 2,3)

DISCUSSION AND CONCLUSION

The comparisons show that neither the fossil nor the dead specimens are identical with any of the studied extant species. This, however, does not mean that two new species should be erected for the fossil and dead plants because the comparison is incomplete for the two following reasons :

1. Some of the extant species of Tamarix that grow in Egypt (T. effusa Ehrenb. and T. passerinoides Del. ex Desv.) have not been included in the comparison.

2. The range of variation of each of the studied characters should be verified by recording the extent of character variation in relation to changes in natural habitat conditions for each species.

Although many specimens of Tamarix (shoots and roots in each case) have been collected from various places in Cairo, Giza, and El-Fayum Provinces yet none of them proved to belong to T. effusa or T. passerinoides though carefully looked for. These two species are among the rare Egyptian Tamarix species Täckholm (1956, 1974). Herbarium specimens of these rare species, and indeed of all Tamarix species, include only parts of the shoot system but not the root.

It must be mentioned also that our present state of knowledge of the extant Egyptian species of Tamarix is far from complete and Täckholm (1974) stated that the whole genus is in need of a thorough revision. For example in 1889 Ascherson and Schweinfurth reported 8 species of Tamarix from Egypt, so also did Täckholm in 1956 but in 1974 she mentioned only 5 species and incorporated some of those mentioned earlier by her and by Ascherson & Schweinfurth in some others. For example T. arborea and T. nilotica which were first treated as two distinct species were later

treated as synonyms. The present study, however, shows that these two species, though close together yet they, are not identical concerning the studied root features. This means that they should perhaps be kept as two distinct species or as two varieties of a single species. The final answer to this, however, requires further investigations in the morphological and anatomical features of the various organs of these two plants. This in fact applies to all other species of the genus.

The above mentioned publications of Ascherson & Schweinfurth and Täckholm show also that there is controversy concerning the geographical distribution of the various Tamarix species within the Egyptian territory. Further collection and investigation of new and old collections is therefore still required.

It may be said in conclusion that although the present study has thrown more light on the extent of the problem of the taxonomy of the genus Tamarix yet it did not solve it and indeed it might have added to its complexity by introducing two new plants (fossil and dead) that still require taxonomic treatment. A more extensive study of the extant Egyptian species of Tamarix should, therefore, be started. A similar extensive study of the fossiliferous area at Dimai and elsewhere in Egypt, in search for more instructive remains of the fossil Tamarix, should also begin to find out whether the fossil Tamarix plant belongs to one of the extant species or to an extinct one.

ACKNOWLEDGEMENT

Thanks are due to Prof. Vivi Täckholm for kind permission to examine herbarium specimens of Tamarix deposited at the Botany Department of Cairo University.

SUMMARY

Anatomical features of silicified root fragments of Tamarix collected from Pleistocene diatomaceous earth in El-Fayum are described. Root specimens of dead Tamarix collected from the same locality and root specimens of five extant Tamarix species collected from various localities in Egypt are also described anatomically. Comparisons showed that the fossil specimens are not identical with any of the studied species. Further work on fossil and extant species of the genus is required to reach more definite conclusions.

REFERENCES

Ascherson, P. et Schweinfurth, G. 1889 : Illustration de la flore d'Égypte. Mém. Inst. Egypt. tome II, première partie.

Blanckenhorn, M. 1901 : Geologie Ägyptens, Führer durch die geologische Vergangenheit Ägyptens von der Steinkohlenperiode bis zur Jetztzeit.- Berlin.

Butzer, K. W. 1959 : Environment and human ecology in Egypt during Predynastic and Early Dynastic times. Bull. Soc. d'Égypte 82.

El-Awamri, A. A. 1976 : Studies on some Egyptian fossil plants. M. Sc. Thesis, Ain Shams University, Cairo.

El-Saadawi, W. E., Badawi, A. A., and El-Awamri, A. A. 1975 : On silicified rhizome fragments of Phragmites communis Trin. from the Pleistocene of El-Fayum, Egypt. Palaeontographica, Abt. B. 154 : 172-178.

———, ———, Shaaban, A. A., and El-Awamri, A. A. 1979 : Pleistocene diatoms from El-Fayum. (accepted for publication in "Proc. Egypt. Acad. Sci." on 6.3.1979).

Gardner, E. W. 1927 : The recent geology of the northern Fayum desert. Geol. Mag. (Great Britain) 64 : 386-410.

Joy, K. W., Willis, A. J., and Lacey, W. S. 1956 : A rapid cellulose peel technique in palaeobotany. Ann. Bot., N. S. 20 : 635-637.

Lacey, W. S. 1963 : Palaeobotanical techniques : View Points in Biology. (Editors J. D. Carthy and C. L. Duddington) 2 : 202-243.

Sass, J. E. 1940 : Elements of botanical microtechnique. First Edition pp.101.

Täckholm, V. in collaboration with Drar, M. and Fadeel, A. A. 1956 : Students' Flora of Egypt, Cairo.

----- 1974 : Students' Flora of Egypt. Second Edition, Beirut.

EXPLANATION OF PLATES

PLATE I

Fig. 1. *Tamarix* shrubs growing in desert area near Cairo.

Fig. 2. *Tamarix* shrubs fringing a small shallow pond thickly inhabited by *Phragmites*, in desert area near Cairo.

PLATE II

Fig. 1. Portion of a transverse section of root of *Tamarix aphylla*. x 130.

Fig. 2. Portion of a transverse section of dead root branch of *Tamarix*. x 60.

Fig. 3. Fragments of silicified root branches collected from Dimai area. x 1.

Fig. 4. Portion of a transverse section of a silicified root branch . x 140.

Fig. 5. Portion of a transverse section of root of *Tamarix nilotica* showing free and united xylem vessels. x 60.

PLATE III

Fig. 1. Portion of a tangential section of root of *Tamarix amplexicaulis*. x130.

Fig. 2. Portion of a tangential section of root of *Tamarix tetragyna* showing uni- and multiseriate rays. x 100.

Fig. 3. Portion of a transverse section of root of *T. tetragyna* showing free and united vessels. x 140.

Fig. 4. Portion of a transverse section of root of *Tamarix arborea* showing free and united vessels. x 125.

Fig. 5. Portion of a transverse section of root of *T. amplexicaulis* showing free and united vessels. x 120.

PLATE IV

Fig. 1. Portion of a tangential section of a silicified root branch. x 125.

Fig. 2. Portion of a tangential section of dead root of *Tamarix* sp. x 60.

Fig. 3. Portion of a tangential section of root of *T. nilotica*. x 80.

Fig. 4. Portion of a tangential section of root of *T. aphylla*. x 100.

PLATE I

1

2

Dry dead stumps of Tamarix trees and basal portions of Phragmites culms were observed, near the site of collection, projecting from sand in position of growth.

MATERIAL AND METHODS

The material investigated here includes not only the fossil root specimens but also (and for the purpose of comparison) specimens of roots of the dead Tamarix collected at the locality and specimens of roots of five of the extant Tamarix species collected where they grow wild in desert areas in Cairo (Pl. I, Figs. 1, 2), Giza, and El-Fayum. The dead and living root specimens were chosen from portions of the root system of the corresponding plants that are of similar size to the collected fossils.

Figure 3 of Plate II shows some of the many silicified fragments of Tamarix roots that were found loose at the locality. The specimens were examined superficially and by preparation of thin-ground transverse and tangential sections according to the method devised by Nicol and Sanderson and described by Lacey (1963) and El-Awamri (1976). Peel sections were less successful than thin-ground sections in showing fine details of root structure.

Specimens of dead Tamarix roots were resuscitated by boiling in soapy water for 3-5 minutes. Transverse and tangential sections from these specimens were prepared and stained according to the method described by Sass (1940).

The five extant species of Tamarix from which root specimens were

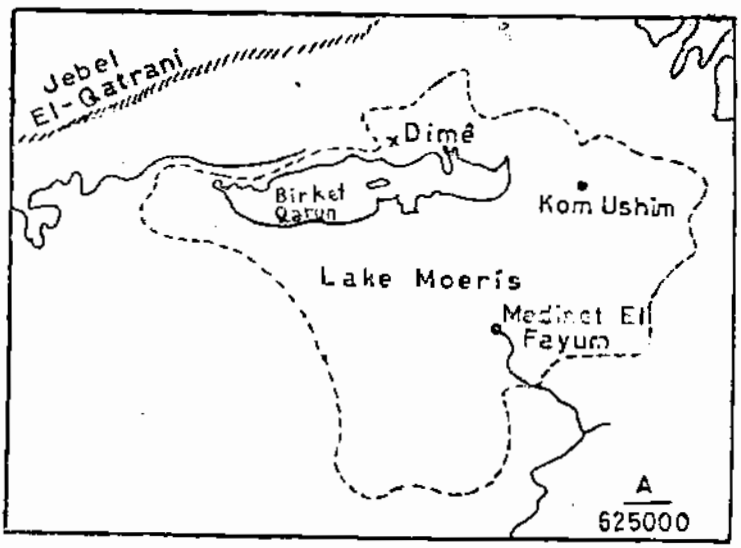

Fig. 1. Map of El-Fayum showing Lake Moeris, Lake Qarun and Dimê fossiliferous locality. After Beadnell, 1905.

PLATE IV

أجزاء من جذور أثل متحجرة من العصر البليستوسيني من الفيوم

للدكتور/ وجيه السعداوي ، الدكتورة/ عفاف بدوي ، السيد/ أحمد العزامي

ملخص

تم في هذا البحث وصف تشريحي لجذور نبات أثل متحجرة تم جمعها من أرض الهايتومات التي تنتمي إلى العصر البليستوسيني وكذلك تم وصف التركيب التشريحي لجذور مماثلة لنوع من نبات الأثل الميت الجاف من نفس المنطقة كما تم وصف التركيب التشريحي لجذور خمسة أنواع مختلفة من جنس الأثل التي تعيش حاليا بمصر . وأثبتت المقارنة أن جذور النوع الحفري تختلف عن الجذور الأخرى وأنه لاستكمال البحث في أنواع هذا الجنس الحفرية والحية ضروري للوصول إلى نتائج أكثر تحديدا .

Effects of Anti - histaminic Drugs on Meiosis of *Vicia faba* and *Allium cepa*

Amal, S.; Shehab and Zakia, A, Abo-El-Khier
Botany Department, Faculty of Girls, Ain-Shams University
Cairo.

The effects of promethazine hydrochloride and chlorpheniramine maleate (anti-histaminic drugs) on mitosis of *Vicia faba* and *Allium cepa* roots have been studied by Shehab and Abo-El-Khier 1983'.

In completion of such study, the present investigation was undertaken to elucidate the effects of these anti-histaminic drugs on meiosis and pollen viability of *Vicia faba* and *Allium cepa*.

Materials and Methods

Vicia faba (var. Giza 1) and *Allium cepa* (var Giza 6) flower buds were treated for 3 hours with the different concentrations of the drugs (20 and 40 ppm), using a piece of cotton soaked with the drug solution. The treated flower buds were collected 24 and 48 hours after treatment (recovery test), at random from 20 plants for each treatment. Tap water was used for control in the same manner.

Fixation of buds (treated and non-treated) in acetic alcohol 1 : 3 was followed by aceto-carmine squash preparations.

For determination of pollen viability, pollens which proved to be abnormal, shrunken and could not stained with aceto-carmine were considered abortive.

RESULTS AND DISCUSSION

The data gathered in tables 1 and 2 show that treatments with the two drugs induced a high percentage of anomalies in the two utilized plants.

It was also evident that the total percentage of anomalies has a negative correlation with concencentration after the two recovery periods in treated Vicia PMCs, (Table 1).

The effect of promethazine HCl on Vicia PMCs was temporary, since the percentage of abnormalities decreased with lapse of time of recovery. On the other hand, chlorpheniramine maleate has a permanent effect on the same plant, (Table 1).

No correlation could be traced between the concentration of the used drugs and the percentage of the induced abnormal PMCs in Allium cepa plants (Table 2).

Also, no trend was observed between the percentage of anomalies and time of recovery in Allium cepa.

After 24 and 48 hours recovery, the highest percentage of abnormalities was mostly observed in the 1st division of Vicia faba and Allium cepa plants treated with the two drugs. It may be mentioned also that the highest percentage of abnormalities was mostly observed in the metaphase stages (Tables 1 & 2).

Different types of abnormalities were observed in the two treated plants. Stickiness was the most prominent abnormality in the two plants and after the two recovery periods (Figs 1 & 3 and Table 3).

Another interesting abnormality was the disturbed type (disturbed metaphases and ana-telophases). Treatments with chlorpheniramine maleate gave a considerable percentage of this abnormality in the two plants (Fig 2 and Table 3). It was also evident that chlorphineramine maleate induced multipolarity (Figs 3 & 6 and Table 3). A phenomenon may be due to the disturbance of the extrachromosomal mechanism (merokinetic) leaving the intrachromosomal process to proceed normal, (Kabarity 1966). This phenomenon was also observed in the root tip cells of Vicia faba and Allium cepa after treatment with the same drug (Shehab and Abo-El-Khier 1983). Amer and Farah (1976) observed multipolarity in AII and T II

of Vicia faba PMCs treated with " Rogor ", IPC, and " Duphar ". They concluded that these cells gave rise to an aggregate of cells instead of the usual tetrad stage.

Bridges were also observed in most treatments but in a small percentage. Most of the observed bridges were sticky ones. Another type of bridges (structural) were also met with (Fig 4), which may be the result of breakage followed by reunion of the broken ends.

In addition to the above mentioned abnormalities lagging chromosomes (Fig 3), breaks and fragments, (Figs 2 & 4) were also observed. Breaks and fragments were more obvious in the 1st division than in the 2nd one and after 24 h recovery. Dempong (1972) attributed this phenomenon to differential susceptibility of the heterochromatic regions to the chromosome breaking action of the antibiotic mitomycin C.

Despiralization, Fig 5, was observed in treated Vicia PMCs with the two drugs after 24 hour recovery only. This may be an indication that these drugs cause complete dissolution of the matrix substance (Shehab 1983).

From table 4, it was clear that the two drugs were not effective pollen sterilizers.

SUMMARY

In this work, the effect of promethazine hydrochloride and chlorpheniramine maleate (antihistaminic drugs) on flower buds of Vicia faba and Allium cepa were studied.

Treatments with the two drugs induced a high percentage of abnormalities in Vicia faba and Allium cepa plants. Most of the abnormalities were observed in the 1st division. The highest percentage of abnormalities was mostly observed in the metaphase stages.

Different types of abnormalities were met with, stickiness, disturbed metaphases and ana-telophases, multipolarity, lagging chromosoms, bridges, breaks, and fragments. Despiralization was noted in treated Vicia PMCs only.

The two drugs were not effective pollen sterilizers.

REFERENCES

Amer, S.M. and O.R. Farah 1976 Cytological effects of Pesticides. VIII Effects of the carbamate pesticides " IPC " " Rogor", and " Duphar " on Vicia faba.
Cytologia 41 : 597 - 606.

Dempon[illegible], M.A. 1972 Mitomycin. C induced subchromatid and chromatid aberrations in Vicia faba pollen mother cells.
Bull. Torrey. Bot. club 99 (3): 113 - 118.

Kabarity, A. 1966. Induction of multipolar spindles in the meiosis of Triticum aestivum as affected by acetone.
Cytologia 31 : 457 - 460.

Shehab, A.S. 1983 Mitotic effects of some cyanine dyes.
Cytologia 48 : 157 - 162.

Shehab, A.S. and Z.A. Abo-El-Khier 1983.
Comparative cytological studies on the effect of anti-histaminic drugs on mitosis of Vicia faba and Allium cepa
Annals Agr. Sci, Cairo - Under publication.

Table 1 : Total percentage of abnormalities and their percentage in each phase in *Vicia faba* after treatments with the two drugs.

Treatments	Total No of PMCs	NO. of abn. Cells	% of total abn	1 st Division			2 nd Division		
				% abn meta	%abn. ana	% Total abn.	% abn meta.	% abn ana.	% Total abn.
24 hr recovery									
Control	3789	43	1.2	1.5	1.1	1.3	1.2	0.55	0.8
Promethazine HCl									
20 ppm	3782	2228	58.8	66.5	47.5	61.8	94.0	21.5	51.9
40 ppm	3834	1408	36.7	46.5	42.3	46.7	26.0	11.4	20.2
Chlorpheniramine maleate									
20 ppm	2541	372	14.6	19.7	21.6	20.5	3. 4	13.5	10.2
40 ppm	2756	308	11.2	7.2	20.1	11.0	3.9	13.4	11.4
48 hr recovery									
Control	3106	41	1.3	4.2	0	2.3	5. 7	10.0	0.48
Promethazine HCl									
20 ppm	2878	570	20.2	14.8	1.1	11.0	55. 1	6.0	28.5
40 ppm	3342	476	14.2	11.8	17.3	14.4	41. 4	6.1	13.9
Chlorpheniramine maleate									
20 ppm	2618	998	38.1	12.6	0	10.4	81.7	23.9	44.2
40 ppm	2654	856	32.3	12.8	51.0	20.8	84.5	16.8	36.8

Table 2 : Total percentage of abnormalities and their percentage in each phase in *Allium cepa* after treatments with the two drugs.

Treatments	Total no of PMCs	NO of abn. PMCs	% of abn.	1 st Division			2 nd Division		
				% of abn.met.	% of abn.ana.	Total % of abn	% of abn.met	% of abn.ana.	Total % of abn.
24 hour recovery									
Control	2527	5	0.2	0.5	0.2	0.4	0	0	0
Promethazine HCl									
20 ppm	1235	318	25.7	53.8	2.6	29.4	78.9	6.7	20.4
40 ppm	2365	1265	53.5	93.1	29.3	64.1	100	8.4	34.5
Chlorpheniramine maleate									
20 ppm	1661	752	45.3	94.5	56.1	70.8	55.8	3.6	3
40 ppm	1330	288	21.7	66.9	1.9	30.5	16.7	9.4	10.8
48 hour recovery									
control	1161	20	1.7	4.5	0.9	2.1	3.8	0.3	1.3
Promethazine Hcl									
20 ppm	2124	908	42.8	92.8	5.7	38.8	79.3	0	44.4
40 ppm	1439	510	35.4	84.8	1.4	51.2	19.2	3.3	7.1
Chlorpheniramine maleate									
20 ppm	1530	560	35.2	90.5	0.67	55.6	52.1	0.9	16.1
40 ppm	1047	531	50.7	75.3	7.41	47.8	92.5	5.7	57.7

Table 3 : Percentage of different types of abnormalities in Vicia faba and Allium cepa PMCs after 24 and 48 hour recovery.

Treatments	24 h recovery							48 recovery				
	stick.	Sp. dist.	Bridges	Lagg-ing	Breaks	Desp.	Multi-Pol.	Stick.	Sp. dist.	Bridges	Lagg-ing	Breaks
Vicia faba												
Promerhazine HCl												
20 ppm	92.4	4.3	1.2	0.2	0	1.8	0	95.6	0	0.7	4.2	0.7
40 "	89.6	3.4	5.1	0.3	1.4	0.2	0	82.4	14.5	1.9	0.6	0.6
Chlorpheniramine maleate												
20 "	38.4	23.4	0	5.1	3.0	29.8	0.3	92.4	3.4	2.7	0.6	0.8
40 "	26.3	30.9	8.1	14.0	3.9	0	18.2	96.6	1.1	1.5	0.8	0
Allium cepa												
Promethazine HCl												
20 "	73.6	9.8	0	8.5	6.9	0	1.3	83.6	16.3	0.2	0	0.1
40 "	92.7	2.8	0.6	2.1	1.8	0	0	97.3	0.8	1.0	0.4	0.6
Chlorpheniramine maleate :												
20 "	95.5	3.2	0	0.4	0.9	0	0	94.6	2.3	0.9	0.4	1.8
40 "	75.7	13.5	0	10.4	0.3	0	0	71.6	23.9	0.9	0.9	2.6

Table 4 : Percentage of abortiveness in PGs of *Vicia faba* and *Allium cepa* plants treated with promethazine HCl and Chlorpheniramine maleate.

Treatments	Vicia		Allium	
	24 h	48 h	24 h	48 h
Control	1.9	3.4	0.8	1.6
Promethazine HCl				
20 ppm	4.7	9.6	1.8	1.5
40 ppm	2.9	4.1	1.9	4.1
Chlorpheniramine maleate				
20 ppm	2.7	8.9	2.?	3.4
40 ppm	3.2	6.7	1.6	2.9

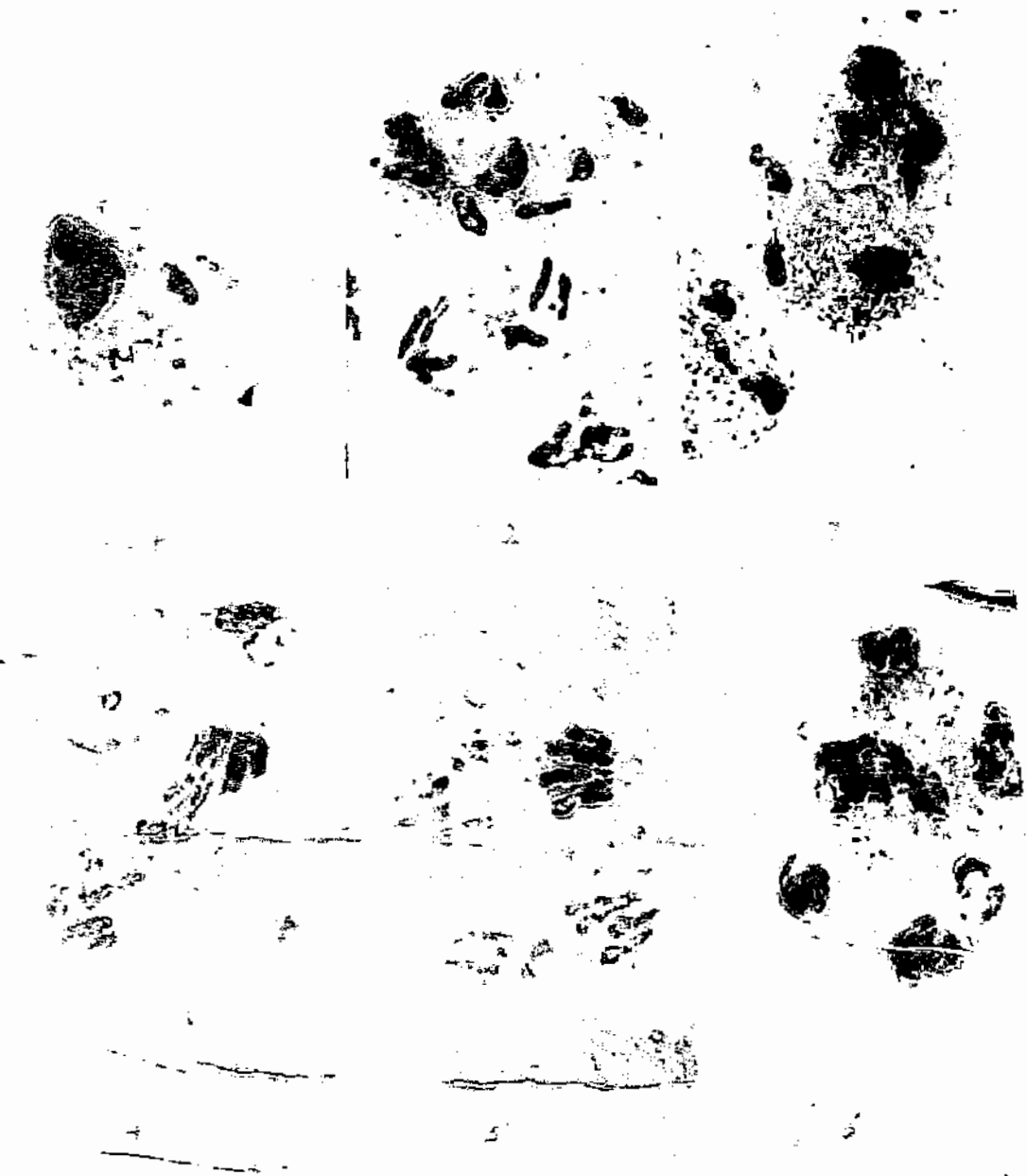

Fig 1 : Sticky metaphase I(20 ppm promethazine 48 h recovery).
Fig 2 : Disturbed A II with fragment(40 ppm chlorph.24 h rec.)
Fig 3 : Sticky multipolar A II with lagging chromosome.
(40 ppm chlorph. 24 h rec.).
Fig 4 : A I with chromosome bridge and fragments.
(40 ppm chlorph.24 h rec.).
Fig 5 : Despiralisation in A II (20 ppm chlorph. 24 h rec.)
Fig 6 : Multipolar T II (40 ppm chlorph. 24 h rec.).

تأثير بعض العقاقير المضاده للهستامين على الانقسام الاختزالى لنباتى الفول والبصـــــل

د ٠/ آمال شهاب د ٠ / زكيه ابو الخيـــر
قسم النبات ـ كليه البنات ـ جامعة عين شـــمس

يهدف هذا البحث دراستتاثير بعض العقاقير المضاده للهستامين مثل هيدروكلوريد البروميثازين ومالهات الكلورفنزامين على البراعم الزهريـــه لنباتى الفول والبصـــل ٠

وقد اعطى العقاران المستعملان نسبه عاليه من الشذوذ فـــى كلا النباتين ٠ وكانت هذه النسبه اعلى فى الانقسام الاول عن الانقســـام الثانى ٠ واعلى نسبه من الشذوذ كانت فى الطورين الاستوائيين ٠

وقد وجدت أنواع مختلفه من الشذوذ منها اللزوجه واضطـــراب الطورين الاستوائى والانفصالى وتعدد الاقطاب والكروموسوم المتاخـــــر والجسور والكسر الكروموسومى ٠ وقد ظهر الانفكاك الحلزونى للكروموسومات فى نبات الفول المعامل بكلا العاملين بعد ٢٤ ساعة من المعامله ٠

وقد اتضح كذلك أن العقاران المستعملان ليس لهما تاثير على خصوبه حبوب اللقـــاح ٠

THE INTERACTION BETWEEN PROTEIN DEFICIENCY AND NICOTINE: EFFECTS ON GROSS, HISTOLOGICAL, AND HISTOCHEMICAL FEATURES OF THE LUNG.

By:

Madiha A. Ashry , M. Yanni , and Sanaa M. Refaat.
" Zoology Dept. Ain Shams University College for Girls "

INTRODUCTION

Smoking hazards has been an international problem for several years. Experimentally, it has been proved that nicotine is the most effective extract of tobacco. It is absorbed into the blood circulation with each cigarette smoked, thus producing different toxicological effects. These effects might reach most; if not all of the body systems (Hug , 1970).

The vital role of dietary protein in the production, prevention, and repair of organ injury has been widely appreciated and extensively studied. Although the nutritional status in most of the developing communities is usually a protein deficient diet, yet smoking habit dominates, (Van Proosdij, 1960). Efforts are being done by the developed countries which are not governed by malnutrition to control smoking. It is worthwhile that developing countries governed by malnutrition should follow the same trend.

The present investigation deals with the interactive effect of protein deficiency and nicotine on the lung.

MATERIAL AND METHODS

A total number of 144 male weanling Albino rats, six weeks of age, and ranging from 50 : 60 grams of body weight were divided into four groups as shown in Table (1):

Table (I)
Experimental Design and Group Distribution

Group No.	Treatment	No. of Rats
Control (1)	Well balanced diet	32
Control (2)	Well balanced diet + Nicotine	36
Control (3)	Protein deficient diet	36
Experimental group	Protein deficient diet + Nicotine	40

The composition of the experimental diets used are shown in Table (2) :

Table (2)
Composition of the Experimental Diets

Dietary Component	Percentage Composition	
	Well balanced diet	Protein deficient diet
Casein	20%	5%
Corn starch	66%	81%
Cotton seed oil	7%	7%
Mineral mix.(Jones&Foster,1942)	5%	5%
Vitamin mix.(Woodruff, 1951)	2%	2%

Pure nicotine (BDH Chemicals Ltd., England) of the formula :

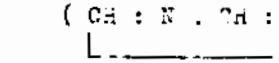

was mixed with diet at a dose rate of 30 mg. / kg. body wt. / day. Offered amounts were adjusted weekly according to fluctuations in body weights and amounts of food consumed.

Autopsies were performed at weekly intervals for five weeks. Gross structure of lungs was observed and lung weights were determined to the nearest 0.1 mg. using a Meopta torsion balance.

For histological and histochemical investigations, representative samples from each lung were subjected to the following fixation and staining techniques:

1- Bouin's fluid for routine Haematoxylin and Eosin.
2- 10% buffered formalin followed by staining in:
   Feulgen reaction for D.N.A.
   Pyronin / Methyl green stain for R.N.A.
3- Rossman's picro alcohol fixative and staining by P.A.S. reaction for polysaccharides.

The techniques used are those recommended by Pearse (1959).

RESULTS AND DISCUSSION

Lung Weights :

Relative lung weights, calculated as percentages per body weights are demonstrated by Table (3):

Table (3)
Average of Relative Lung Weights

Duration (weeks)	Control Groups: well balanced diet	well balanced diet+Nicotine	Low protein diet	Experimental group: L.P.D. + Nic.
1	0.610 ± 0.40	0.720 ± 0.014	0.710 ± 0.020	0.825 ± 0.007
2	0.615 ± 0.049	0.715 ± 0.007	0.695 ± 0.091	0.785 ± 0.120
3	0.723 ± 0.090	0.905 ± 0.106	0.820 ± 0.400	0.970 ± 0.110
4	0.750 ± 0.127	0.920 ± 0.110	0.950 ± 0.032	0.935 ± 0.007
5	0.[illegible] ± 0.049	0.890 ± 0.110	0.940 ± 0.100	0.910 ± 0.042

Data of the experimental group reveal a slight increase in the relative lung weights with respect to body weights. This increase is more clearly identified from the third week of the experiment and thereafter. Such finding was confirmed by Alexandrov and Raitchev (1963) in rats inhaling cigarette smoke and attributed this increase to the appearance of glandular tumours. Nevertheless, starving rats injected by nicotine showed a significant decrease in their relative lung weights, (Simkovich, 1973).

Gross and Microscopical Studies :

Normal lungs of the first control group were soft in consistency, bright pink in colour, and of uniform spongy appearance (Figure 1-i). Regular increase in size with growth of rats was evident throughout experimentation. All studied specimens had normal microscopical features (Figure 2).

In the second control group ; where rats were given nicotin with the well balanced diet, a fraction of examined lungs showed congested lobes ; predominently one of the left lobes. Congested lungs were slightly firm in consistency and dark red in colour. Lungs of rats autopsied at the end of experimentation showed areas of adhesions to the ribs. Such areas were markedly pale in colour and hard in the cut surface (Figure 1-ii). On microscopical examination, signs of internal haemorrhges were evident by the fourth week (Figure 3). Later, the alveolar walls became thickened and alveoli were filled with a firm network containing erythrocytes and polymorphs. Epithelial cells lining bronchioles were degenerative and distorted. The development of internal pulmonary haemorrhage during nicotine administration is also confirmed by Alexandrov and Raitchev (1963); while Mahrburg (1958) reported this lesion to be frequently transitory in subtoxic nicotine doses. Histochemically, lung tissue of this group showed gradual decline in the P. A. S. positive material.

While D.N.A. gave intense reaction throughout experimentation, (Figure 4), R.N.A. stained faintly prior the fourth week: after which it acquired normal staining affinity. Thus while Rosenkran and Sprague (1969) also reported similar elevations in lung D.N.A

n explanation for this unexpected finding is offered by oldblatt et al. (1975), to be due to the accumulation of .N.A. in small clumps located in the reticulum and membrane f the nucleus during the process of cellular necrosis. therefore iving intense reaction.

In the third control group where rats were maintained on the protein deficient diet, lungs were grossly unaltered during the whole experimental period (Figure 1-iii). On microscopical examination, the organs showed some degenerative bronchioles. Slight fragmentation of tissue or zonal necrosis characterized specimens examined by the fifth week (Figure 5). Histochemically, a slight increase in the P. A. S. positive material occured during the first two experimental weeks (Figure 6), followed by slight and gradual declino, while nucleic acids staining were not significantly faint.

In the experimental group, rats under the double stress of protein deficiency and nicotine showed severe grossly affected lungs. During the first two experimental weeks, the organ appeared wholly congested and dark red in colour. By the third week, multiple nodules of consolidation, predominently restricted to the left lobe charecterized most examined lungs. These white milky nodules were strongly adhered to the ribs where it was difficult to remove. Later, it invaded the whole lung (Figure 1-iv). Microscopical investigation showed degenerative bronchioles by the second week. During the fourth and fifth weeks, pulmonary tissue became wholly necrotic (Figure 7). No identifiable alveolar pattern could be distinguished besides the invesion of red blood cells and polymorphs (Figure 8). P. A. S. positive material appeared relatively dense during the first three weeks. Thereafter, it stained faintly (Figure 9). D.N.A. and R.N.A. were significantly faint and undifferentiated and therefore finelly depleted by the fifth week (Figure 10). Mortality of rats of this group after the fifth week ended the investigation.

ABSTRACT

Studies on the interactive effects of protein deficie diet and nicotine (30 mg./kg. body wt./day) on the lungs of male weanling Albino rats have indicated the following:

Relative lung weights showed slight increase. In the gross, lungs were wholly congested, dark red in colour, with multiple white nodules firstly restricted to left lobes and later extending to involve the whole organ. Microscopically, degenerative bronchiolitis, distorted alveolar pattern, zonal necrosis and internal haemorrahges were the main histological features. P. A. S. positive material gave an intense reaction during the early phase of investigation, followed by a gradua decline. D.N.A. and R.N.A. were finally depleted by the end o investigation.

REFERENCES

Alexandrov, K. and Raitchev, P. (1963)
C. R. Acad. Bulgare Sci., 16 , 329.

Goldblatt, P. ; Trump, B. and Stowell, R. (1975)
Amer. J. Pathol. , 47 , 183.

Hug, C. C. (1970)
Pharmacologist , 12 , 220.

Jones, J. and Foster, C. (1942)
J. Nutr. , 24 , 245.

Mahrburg, S. (1958)
Ann. Univ. Curie - Sklodowska , 13 , 35.

Pearse , A.E.G. (1959)
"Histochemistry , Theoretical and Applied" - London

Rosenkrantz, H. and Sprague, R. (1969)
Arch. Environ. Health (Chicago) , 18 , 917.

Simkovich, B. Z. (1973)
Latv. Psr. Zinat. Akad. Vestis. , 7 , 137.

Van Proosdij, C. (1960)
Smoking : Amsterdam Elsevier Publ. Comp. pp. 319.

Woodruff, A. W. (1951)
Brit. J. Exp. Pathol. , 31 , 405.

CAPTIONS OF FIGURES

Figure (1): Representative lungs from experimental and contro groups:
i- Well balanced diet.
ii- Well balanced diet + nicotine.
iii- Low protein diet.
iv- Low protein diet + nicotine.

Figure (2): Normal lung tissue from rat offered the well bala diet.
(H & E : X 150)

Figure (3): 4 weeks of well balanced diet + nicotine.
Internal pulmonary haemorrhage.
(H & E : X 400)

Figure (4): 3 weeks of well balanced diet + nicotine.
Intense staining for D.N.A.
(Feulgen reaction : X 300)

Figure (5): 5 weeks of protein deficiency.
Zonal necrosis of lung tissue.
(H & E : X 100)

Figure (6): 2 weeks of protein deficiency.
Increase in the P.A.S. +ve material.
(P.A.S. reaction : X 300)

Figure (7): 4 weeks of protein deficiency + nicotine.
Degenerative bronchioles invaded by fibroblasts.
(H & E : X 400)

Figure (8): 5 weeks of protein deficiency + nicotine.
Distortion of alveolar pattern, haemorrhage and infiltration.
(H & E : X 200)

Figure (9): 4 weeks of protein deficiency + nicotine.
Faint and undifferentiated P.A.S. +ve material.
(P.A.S. reaction : X300)

Figure (10): 5 weeks of protein deficiency + nicotine.
Depleted R.N.A.
(P.M.G. stain : X300)

(i)

(ii)

(iii)

(iv)

Fig. (1)

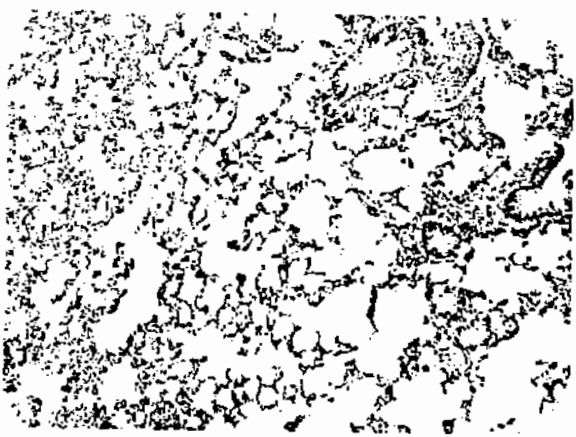

Fig. (2)

Fig (3)

Fig. (4)

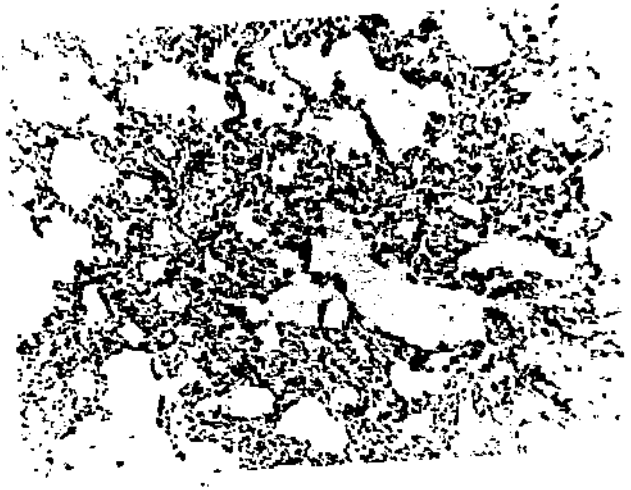

Fig. (5)

Fig. (6)

Fig. (7)

Fig. (8)

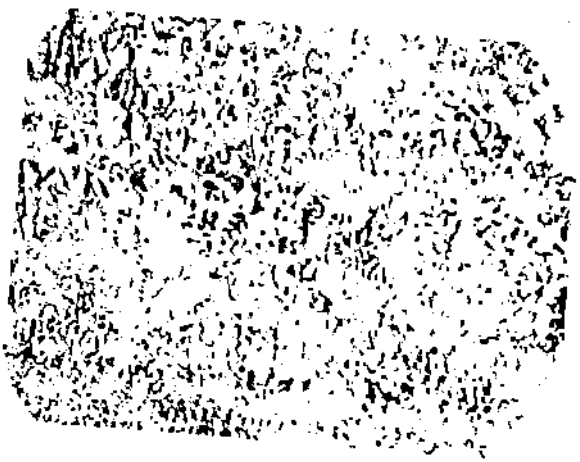

Fig. (9)

Fig. (10)

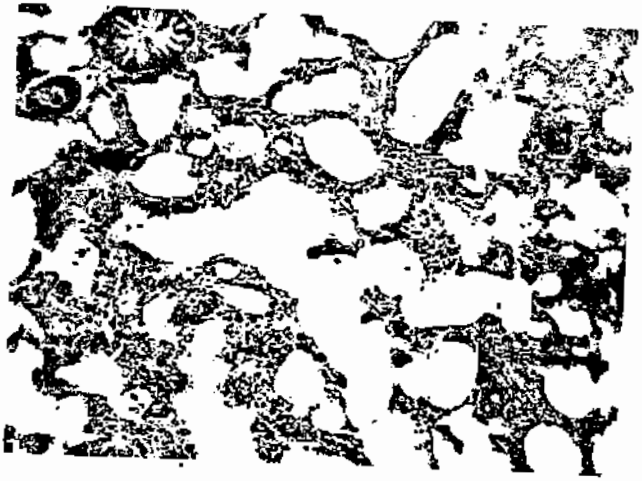

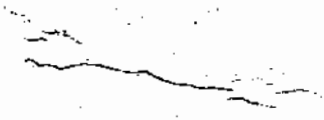

Serum Ceruloplasmin And Copper In Filariasis

By

M.A.Rifaat ; T.S.Kholief ; M.Kh.Makled

from

Parasitology Department, Faculty of Medicine and Nutrition &
Food Chemistry Department, University College for Women,
Ain Shams University.

Abstract

Serum ceruloplasmin and copper levels were assayed in 42 filariatic patients. They were divided into elephantiatic and microfilariatic cases according to the severity of infection. Both serum copper and ceruloplasmin were in the normal range in elephantiatic stage except 36 % of tested cases showed elevated serum copper than normals. In microfilariatic cases, both serum copper and ceruloplasmin were markedly increased, while 29 % of cases showed normal serum copper. Both were highly significantly different as compared to controls. The significance of these data is fully discussed.

Introduction

Filariasis occurs in man as a result of infection with certain filarial worms including Wuchereria bancrofti, Wuchereria malayi, Loa Loa & Onchocerca Volvulus. Infection with Wuchereria bancrofti is commonly called bancroftian filariasis. The full manifestation of the disease develops in youth and is seldom recorded

in very young children under the age of two years. The adult worms inhibit lymphatic vessels and nodes. The microfilariae are first expelled into these areas and later into blood stream.

The present study is to investigate the effect of filariasis on serum ceruloplasmin and copper levels. Ceruloplasmin is a copper-containing alpha$_2$-globulins. It is believed to play a role in copper transport and absorption.

Materials and Methods

The material of study consisted of 59 cases from endemic areas. They aged from 25 to 40 years. 17 cases were taken as controls, they gave negative intradermal test on using Dipetalonema evansi antigen, 17 cases with microfilariae in the blood as diagonised by thick blood film at mid-night. This group was selected to represent the inflammatory stage of the disease. 25 cases were chosen to represent the elephantiatic stage of the diceass and diagonised by the clinical picture and by the indirect haemagglutination test using Dipetalonema evansi antigen. Blood samples were taken in the mid-night, sera separated. Ceruloplasmin (copper - oxidase) has been estimated according to the method described by Ravin (1961) in which it can catalyze the oxidation of P-phenylenediamine and the extent of the latter process is used as a measure of ceruloplasmin amount present in serum. Serum copper was estimated by the method of Gubler et al (1952 A) depending on the measurement of the depth of the colour of its reaction with sodium diethyldithiocarbamate.

Results

The data obtained for serum ceruloplasmin and copper in the material of study are shown in Tables I, II, III and g figure. In normals, ceruloplasmin level ranged from 49.0 - 117.8 (90.7 ± 5.6) mg /100 ml serum. The normal serum copper level was 88 - 170 (138 ± 6.9) Ug / 100 ml. Whereas the serum levels of ceruloplasmin and copper in the 25 cases showing symptoms of elephantiasis were 46.0 - 135.3 (75.4 ± 4.7) mg / 100 ml a nd 103 - 225 (154.4 ± 6.4) Ug / 100 ml, respectively. However, 9 cases (case no. 14, I5, I6, I7, I8, I9, 20, 2I, 25) out of the 25 showed higher serum copper values (i.e. 36 %) of elephantiatic cases. Their ceruloplasmin was in the normal level. Both serum ceruloplasmin and copper were significantly different from control values ($P < 0.05$).

In our group of microfilaraemia, serum ceruloplasmin and copper valuea were 117.9 - 248.7 (151.2 ± 8.9) mg / 100 ml and 145 - 260 (195.9 ± 9.4) Ug / 100 ml serum, respectively. Levels of ceruloplasmin were elevated than normals for all cases. The same increase for serum copper except 5 cases (case no. 1, 2, 3, 4, 5)out of 17 (i.e.29 %) have normal serum copper. Both ceruloplasmin and copper levels were highly significantly different as compared to control values ($P < 0.05$).

Table: I Serum Ceruloplasmin (mg /100 ml) and Copper (Ug /100 m
for Normals

case no.	serum ceruloplasmin	serum copper
1	117.80	141
2	101.20	158
3	91.50	168
4	57.60	144
5	78.50	170
6	96.00	88
7	117.80	105
8	87.30	146
9	102.10	158
10	49.00	141
11	117.80	167
12	70.00	158
13	96.00	88
14	49.00	103
15	96.00	140
16	117.80	117
17	96.00	115
Range	49.00 - 117.80	88 - 170
Mean	90.70	138
± S.E.	5.56	6.87

Table II: Serum Ceruloplasmin (mg /100 ml) and Serum Copper (Ug /100 ml) in Elephantiasis (25 cases)

Case no.	serum ceruloplasmin	serum copper
1	61.1	145
2	65.4	145
3	87.3	135
4	71.6	155
5	101.2	153
6	46.0	145
7	68.1	105
8	49.0	155
9	56.7	I45
10	56.7	I05
11	69.0	I55
12	82.9	I53
13	49.0	LI7
14	65.4	I90°
15	69.8	I75 °
16	78.5	I78 °
17	52.4	225 °
18	6I.I	200 °
19	6I.I	I97 °
20	I35.3	I75 °
21	65.5	I78 °
22	I09.I	I03
23	II3.4	I45
24	I04.7	I05
25	I04.7	I75 °
° denotes higher values than controls.		
Range	46.0 - 135.3	103 - 225
Mean	75.4	154.4
± S.E.	4.7	6.4
P	< 0.05 (significant)	< 0.05 (significant)

Table III: Serum ceruloplasmin and Serum copper in Microfilarae

(17 cases)

Case no.	serum ceruloplasmin	serum copper
1	I26.5	I55 N
2	II8.2	I45 N
3	I30.9	I45 N
4	I20.4	I60 N
5	I70.2	I55 N
6	I26.5	260
7	II7.9	I85
8	I26.5	250
9	I35.3	I75
IO	I20.7	I95
II	I92.0	205
I2	I83.0	250
I3	I5I.8	I95
I4	248.7	2IO
I5	I70.2	235
I6	I96.3	235
I7	I35.3	I75
N denotes normal level.		
Range	117.9 - 248.7	145 - 260
Mean	15I.2	I95.9
± S.E.	8.95	9.42
P	< 0.0I (significant)	< 0.0I (significant)

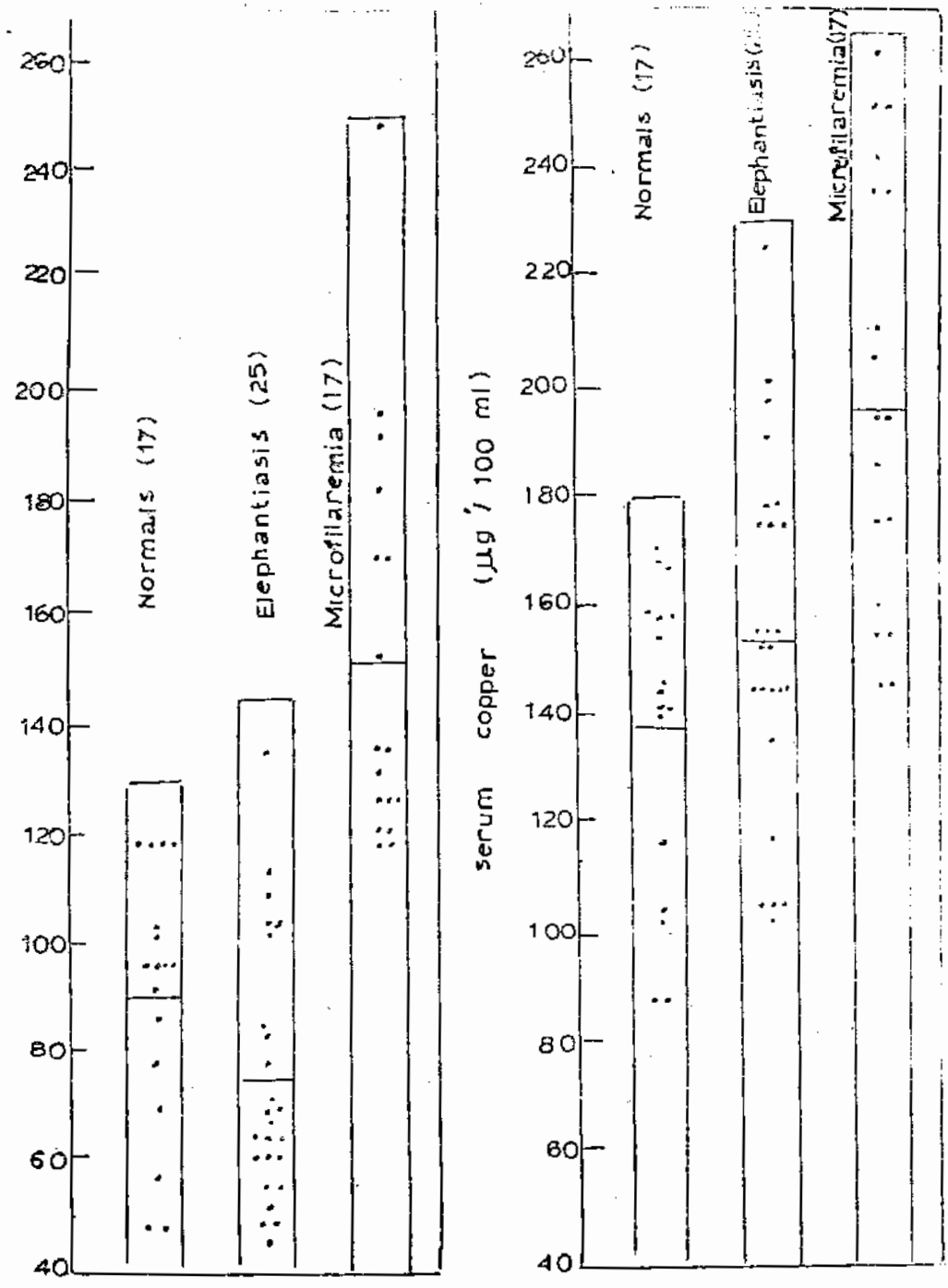

Serum ceruloplasmin and copper levels for normals, elephantiasis and microfilaremia

Discussion

Blood samples were taken at mid-night because the filariall worms migrate to prepheral blood vessels at night.

The present data indicates the normal level for both s copper and ceruloplasmin are in accordance with data previous reported for normals (El-Nabawi et al, 1970 and El-Hawary et 1973). The normal serum ceruloplasmin and copper in cases showing elephantaisis is a result of normal liver function. T is moderate increase in serum copper level for 36 % of the tested cases. This moderate serum copper increase is in acco ance with the findings of Wysock (1958) in cases of uncompl fibrosis. It is suggested that this finding may denote liver involvement leading to the release of some of its copper cont into circulation (El-Hawary et al, 1973 and Khalifa et al,19

On the other hand, the microfilaraemic tested cases sh significant increase in both ceruloplasmin and copper than n This overall tendency of hyper-cupraemia in severe infection i in agreement with reports of other workers (Gubler et al, 19 Heldig, 1954 and Khalifa et al, 1972).

Several studies showed that viral and microbial infec portal, biliary cirrhosis and mycardial infarctions showed a in ceruloplasmin content which has been found concomitant wit the increase in copper concentration (Markowitz et al, 1955 These diseases are characterized by a change in serum protein distribution. This change can be possibly due to inability o the damaged liver tissue to synthesise the polypeptide, as it is well known that the liver is the main site for its formati It is also suggested that the increase in serum copper and ceruloplasmin was found to be related to the activity of the disease. The enzymatic activity determination might be utili

s a non-specific laboratory test for establishing the severity f infection. In our opinion ceruloplasmin level is a more ensitive laboratory investigation and should put the physician n guard for more close and longer follow up of cases.

The findings in the present work of uniform increase in serum ceruloplasmin in microfilariasis lead one to suggest the possibility of considering increased serum ceruloplasmin level as a criterion of the extent and magnitude of tissue destruction in an immunologic disease, of proved streptococcal infective antecedence. It is of interest to add the finding reported by Bazhkov (1967) concerning changes in oxidase activity of ceruloplasmin in rats after successive infection with B.hemolytic streptococcus strain H-46-A every two weeks to produce experimental myocarditis. Ceruloplasmin synthesis was increased during the active phase of the process and dropped with its decline.

References

Bazhkov, B.(1967): Patal Fiziol. Exp. Ter., 11, 20.

El-Hawary,M.F.S., Kamel,H.B., Abdin,M.A. & El-Henedy,F. (1973): Gaz.Egypt.Paad., 21, 51.

El-Nabawi,M., Abdel-Aal,A.M.A., El-Hawary,M.F.S., Kamel,H. & Abdel-Khalik,M.K.(1970): J.Egypt.Med.Assoc., 53, 150.

Heldig,G. (1954): Z.Kinderheilk, 74, 622.

Gubler,C.J., Lahey,M.E., Aschmbrucker,H.,Cartwright,G.E. & Wintrobe,M.M.(1952A): J.Biol.Chem., 196, 205.

Gubler,C.G.,Brown,H.,Markowitz,H.,Cartwright,G.E. & Wintrobe, M.M.(1952B): J.Biol.Chem., 196, 209.

Khalifa,K., Doss,H., Hafez,T.A., Awadallah,R. (1972):
J.Egypt.Med.Assoc., 55, 859.

Khalifa,K.,Doss,H., Hafez,T.A., (1973): J.Egypt.Med.Assoc.,5

Markowitz,H.,Gubler,C.J., Mahoney,J.P., Cartwright,G.E. &
Wintrobe,M.M. (1955): J.Clin.Invest.,34, 1498.

Revin, H.A.,(1961): J.Lab.Clin.Med., 58, 161.

Wysocki,K1.,(1958): Bull.Soc.Ami.Sci.et Lettres.Pozman C 8 3

THE CORROSION BEHAVIOUR OF ALUMINIUM IN SODIUM HYDROXIDE SOLUTIONS CONTAINING TUNGESTATE IONS.

by

Kh.M.Kamel, A.Kassab and E.Abdel Hamid.

Chemistry department, University college for girls, Heliopolis, Cairo(Egypt).

INTRODUCTION

Brasher[1] suggested that some anions are corrosive when present in large dilutions and become inhibitive at high concentrations. In testing this theory the corrosion behaviour of aluminium in sodium hydroxide solutions containing sodium phosphate and sodium chromate were previously studied.[2,3]

In this work we studied the corrosion behaviour of Aluminium in alkaline tungestate solutions.

EXPERIMENTAL

The polarisation measurements on the aluminium electrode were carried out in a cell described in an earlier publication.[4] This cell is constructed from the arsenic-free hard borosilicate glass, Hysil, and thus it permits the vigorous purification of the solutions under investigation through pre-electrolysis.

For this purpose we used a platinum electrode(2 cm^2 platinum sheet welded to a platinum wire sealed to glass).

The electrode were prepared from extra-pure aluminium rods 3 mm in diameter(Shering Kahlbaum company).

The electrode area was I cm^2.Each run was carried out with a new electrode. All Solutions were prepared from A.R.materials.Before each run,the cell was cleaned with a mixture of nitric and sulphuric acids(A.R.)and thoroughly washed with a conductance water.

Determination of the corrosion rate was carried out using the weight-loss technique.Experiments were performed on pieces of aluminium measuring 5 X I0 cmm and 0.8 mm thick,cut from analar aluminium sheet.

The test pieces were first degreased with acetone,washed with conductivity water,dried in alcohol and ether,and then weighed.

Corrosion tests were carried out in awide 200 ml Jar, in which the specimen was suspended for 2 hours in the test solution.The specimen was then removed,rinsed with conductivity water and finally dried and weighed.

All corrosion tests were carried out in aerated,unstirred solutions.Results were duplicated and the mean was computed.

For measuring the corrosion potential,the potential of the aluminium electrode was followed as a function of time over a period of 3 hours.In all solutions studied the potential became constant constant within Ca 2 hours.

All measurements were carried out at 30°c in an air thermostat controlled to $\pm$ 0.5°c.

RESULTS AND DISCUSSION

-Corrosion potential and corrosion rate:

The potential of aluminium electrode was measured in 0.001-1 M Na_2WO_4. The steady state potentials obtained after 4 hours immersion were plotted against the logarithm of the molar tungestate concentration for the different NaOH solutions.

As evident from Fig(1):the first part designated by (a) represents a region of almost constant potential.The range of tungestate concentration within which the potential remains constant increases with the alkali concentration.The second part designated by(b)shows considerable increase of potential with tungestate concentration.

The corrosion rate, V_{corr} mg/hour,has also been determined in the different solutions.An example of the results is shown in Fig(2).In this figure the corrosion rates in the corresponding free sodium hydroxide solutions are represented by dotted lines,these are taken as reference values to those obtained in presence of the different tungestate concentration.The plots can be roughly divided into two parts a,b which correspond respectively to the parts a and b of the potential log C relationships.

Part a covers the concentration range 0.001-0.05 M Na_2WO_4. At such concentrations tungestate ions hardly affect the corrosion rates.However,in very dilute alkali solutions(0.01-0.02 M NaOH)addition of small amounts of tungestate leads to the decrease of the corrosion rate down to a minimum value at 0.005 M WO_4^{2-}.

Part b covers the concentration range 0.02 - I M Tungestate. In this range, increase of tungestate concentration bring about marked increase in the corrosion rate in all NaOH solutions studied. It is to be observed that hydrogen evolved, while there was no indication for the reduction of tungestate ion.

The above results are interesting so far as Bracher's[6] equation is concerned. This equation requires that, for a corrosion activating anion the potential of the corroding metal decreases linearly with the logarithm of the anion concentration. In the present investigation, increase of the corrosion rate is accompanied with increase of the corrosion potential. This shows that the addition of Na_2WO accelerates the cathodic reaction. Similar behaviour was observed in case of Na_3PO_4.[2]

Galvanostatic corrosion current:

In this technique we measured the current passing in a cell composed of two aluminium electrodes, one immersed in the pure alkali solution and referred to "Reference electrode", and the other immersed in the same alkali solution containing sodium tungestate "Test electrode". The difference in corrosion potential brought about by the tungestate leads to the passage of the so called galvanostatic corrosion current. The galvanostatic corrosion currents as well as the potentials during the passage of those currents were followed as a function of time, and the steady state values are plotted versus log C of WO_4^{2-}

for the different NaOH solutions.As example,Figs 3a and 3b show the results obtained in case of 0.2 M NaOH.

It is obvious that the potential of the reference electrode remains practically constant.For the test electrode,on the other hand,the potential increases linearly with Log C of Na_2WO_4,in agreement with the behaviour observed from the measurments of corrosion potential under open-circuit conditions.

As a result of increase of the potential with tungestate, galvanostatic corrosion current flows from the reference electrode(negative pole),which undergoes anodic reaction, to the test electrode at which a cathodic reaction proceeds.We have,therefore,assigned negative signs to the value of galvanostatic corrosion currents.

As evident from Fig 3a minute corrosion currents are observed at low tungestate concentrations.Then at a certain tungestate concentration dependent on the alkali concentration,the galvanostatic current begins to increase significantly with further increase of WO_4^{2-} concentration. The results of these experiments show again that the presence of sodium tungestate accelerates the cathodic reaction.

-Anodic polarisation:

In order to throw light on the anomalous corrosion behaviour in the tungestate solutions,anodic polarisation measurements were carried out in 0.2,0.1 and 0.05 NaOH

solutions, containing different Na_2WO_4 concentrations. An example of the results is given in (Fig 4). Polarisation was conducted within the current density range 10^{-6} . 10^{-2} A/cm^2 .

Generally, the polarisation curves exhibits a region of stationary potential which extends up to a certain current density dependent on the tungestate concentration .The electrode is subjected to low overpotential and then at higher current densities the potential rises rapidly.The rapid increase is likely due to the lack of supply of OH^- ions at the anode leading to incomplete dissolution of metal oxide as Aluminium ALO_2^- . The metal oxide accumulation the metal surface, with the result that the metal is passivated.

The important phenomenon exhibited by polarisation measurements is that passivation occurs at a decreasing current density as the concentration of tungestate is increased. Such a behaviour may reveal that WO_4^{2-} ions participate only in the electrolytic transport of the current, but they are not evolved in the anodic reaction. Passivation current decreases with tungestate concentration owing to the decrease of the supply of OH^- ions to the anode. This is because the fraction of the current carried by OH^- ions (viz. their transport number) decreases as more tungestate ions are added. According to this argument, the passivation current, at a given tungestate concentration, should increase as the alkali concentration increased.

This is actually true as evident from (Fig 5) which show

the passivation currents in 0.0I, 0.02,0.05,0.I,0.2 and 0.5 M NaOH solutions in presence of I M tungestate. Morever,some experiments were carried out in stirred solutions,whereby the passivation currents increased markedly.

-Cathodic Polarisation:

Cathodic polarisation measurements were carried out in 0.05 - 0.2 M NaOH solutions at different concentrations of Na_2WO_4. Hydrogen was always observed to evolve at the cathode. (Fig 6)shows the results in case of 0.2 M NaOH. It is clear that the polarisation curve is markedly shifted to less negative potentials as the salt concentration is increased.This confirms the activations of the cathodic reaction.

The activation of the cathodic reaction, and consequently the promotion of corrosion rate on adding the salt might be attributed to the adsorption of Na^+ ion on the electrode surface(5) This is because the adsorption of Na^+ ion leads to the increase of the negative charge density on the area around the ion, and consequently,an active cathodic area is formed.

-Behaviour in low alkali concentration:

At low alkali concentrations(0.I M),addition of very small amounts of Na_2WO_4 leads to the decrease of the corrosion rate to a certain minimum(Fig 2).This is of course important from the economic point of view.More interesting

however,is the theoretical meaning of the phenomenon. From the observation that the corrosion potential is also decreased on adding the tungestate salt(Fig I), it is concluded that the cathodic reaction is retarded. This most probably indicated that the activity of reacting entities,viz.,the water molecules in the double layer,decrease as the activity of the Na^+ ions in solution is increased.It seems that Na^+ ions are preferentially attracted to the double layer,while the originally oriented water molecules are displaced.
On further increase of sodium tungestate concentration Na^+ ions became adsorbed,and the usual increase of V_{corr} with Na_2WO_4 concentration is observed.

SUMMARY

The corrosion rate and potential of aluminium were measured in 0.01-0.2 M NaOH solutions containing 10^{-3} - I M Na_2WO_4 at 30°c. It was found that above 0.05 M Na_2WO_4,the corrosion rate and potential increase with tungestate concentration.The galvanostatic corrosion current increased also with the salt concentration.The results of these measurements indicated the activation of the cathodic reactions.
Anodic polarisation curves were measured in alkali solutions containing(0.001 - 1 M)Na_2WO_4. The results revealed that WO_4^{2-} ions participate only in the electrolytic transport of current but they are not involved in the anodic reaction. The results confirmed the acceleration of the cathodic reaction.This is attributed to the adsorption of Na^+ ions on the metal surface.

REFERENCES

(I) D.M.Brasher , Nature.Lond., I93(1962) 868.

(2) Kh.M.Kamel,S.A.Awad and A.Kassab, J.Electronal Chem,00(I98I) Jec 6000.

(3) Kh.M.Kamel,S.A.Awad and A.Kassab, J.Electronal Chem(under publication).

(4) S.A.Awad. Electrochim.Acta. 7(I962)677

(5) S.A.Awad,Kh.M.Kamel and A.Kassab,J.Electronal Chem,I05(I979)29.

EFFECT OF CONCENTRATION OF Na_2WO_4 DISSOLVED IN DIFFERENT CONCENTRATIONS OF NaOH, ON TH POTENTIAL OF ALUMINIUM.

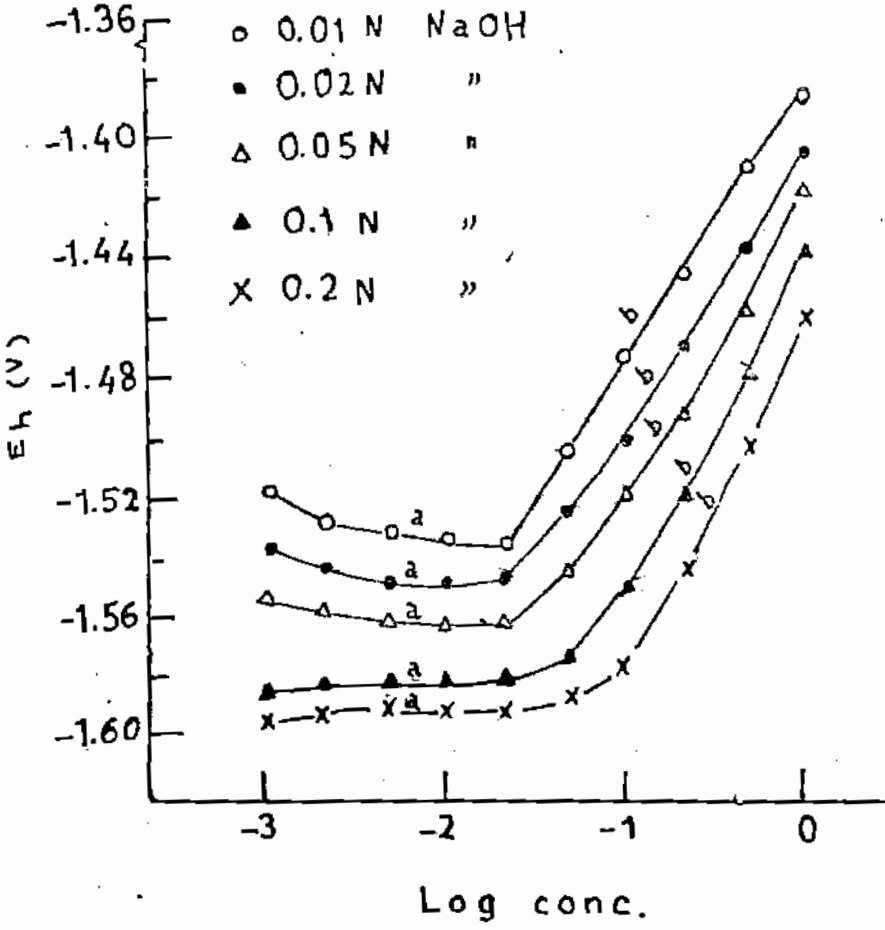

Fig (1)

EFFECT OF TUNGSTATE CONCENTRATION ON THE CORROSION RATE OF ALUMINIUM IN 0.2 M, 0.1M AND 0.05 N NaOH.

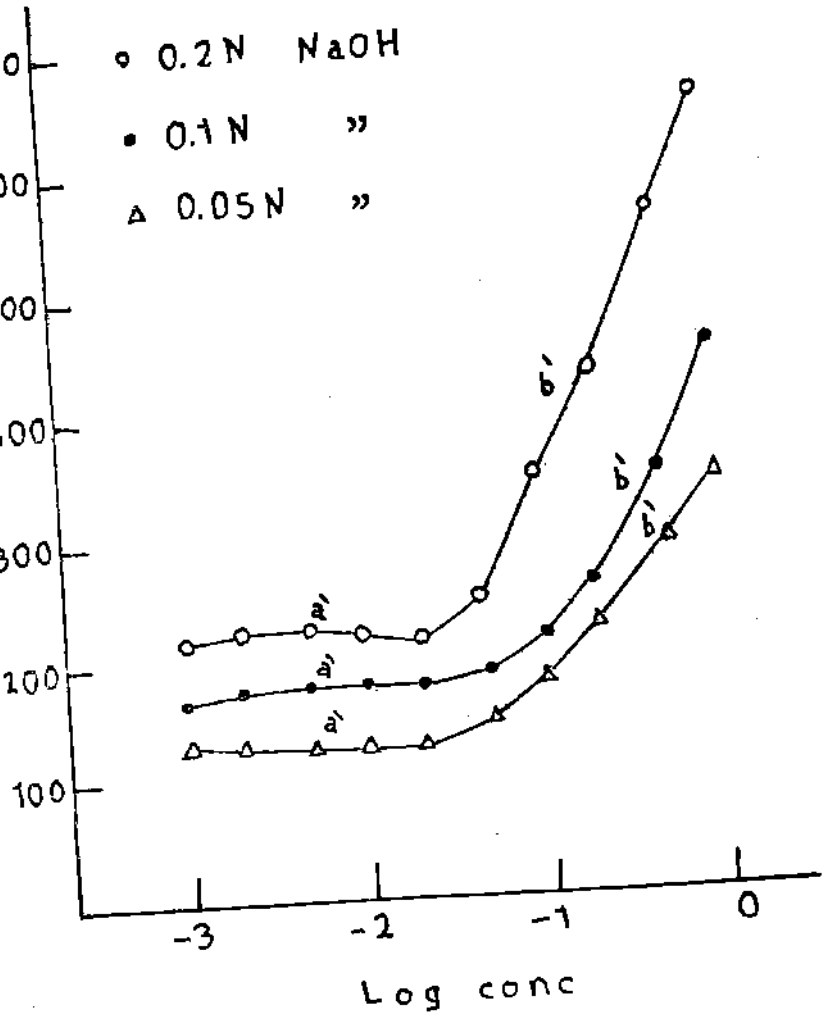

CORROSION CURRENT OF ALUMINIU
IN 0.2N NaOH AT DIFFERENT
CONCENTRATION OF TUNGSTATE

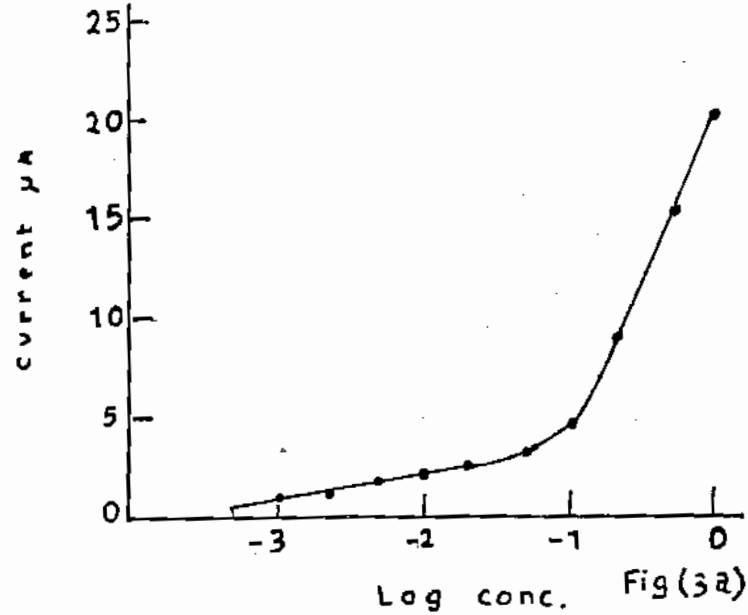

Fig (3a)

EFFECT OF CONCENTRATION OF
TUNGSTATE DISSOLVED IN 0.2N NaO
ON THE POTENTIAL OF ALUMINIUM

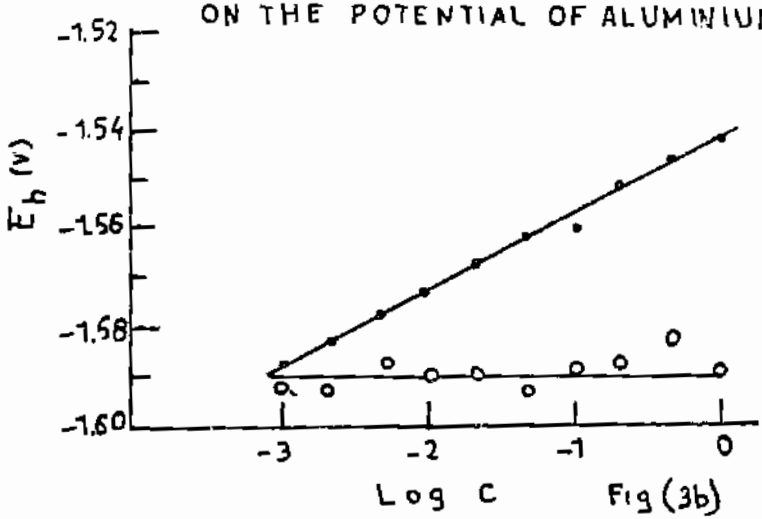

Fig (3b)

ANODIC POLARISATION CURVES FOR ALUMINIUM IN DIFFERENT CONCENTRATIONS OF Na_2WO_4, DISSOLVED IN 0.1N NaOH.

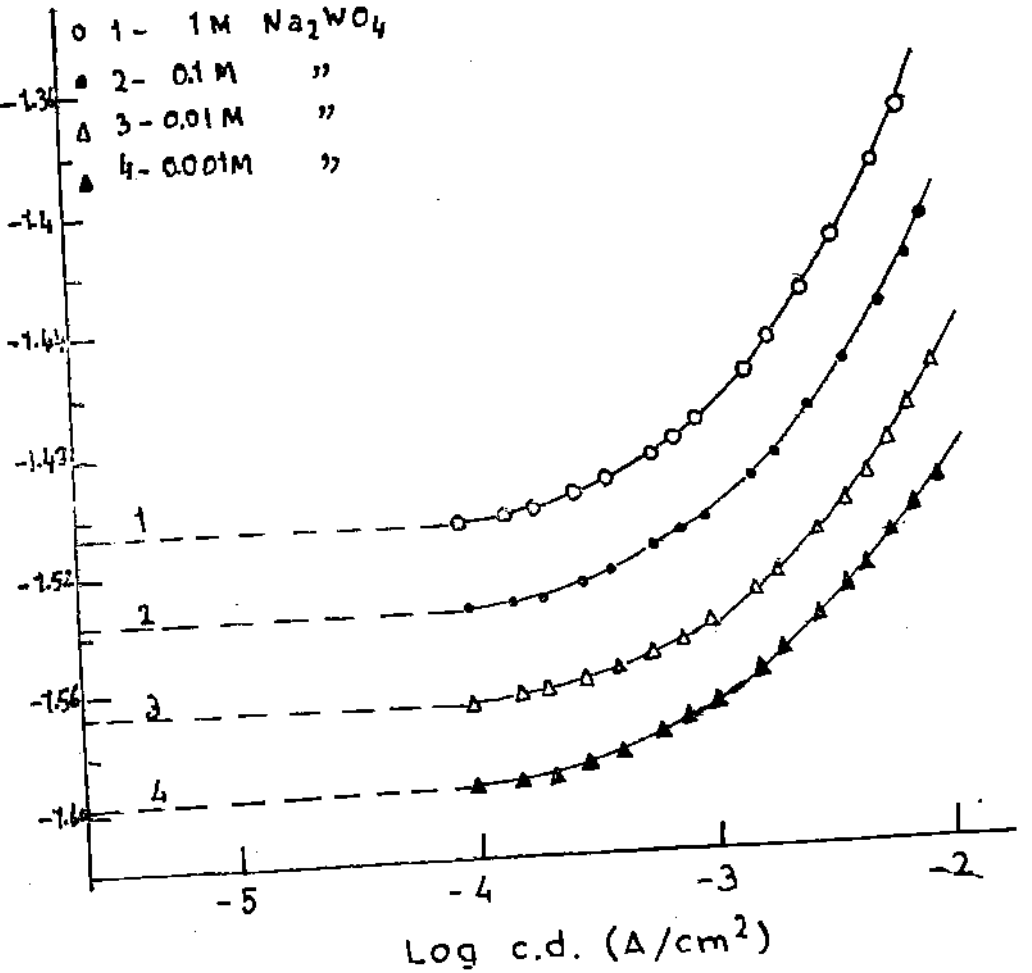

Fig (4)

ANODIC POLARISATION CURVES FOR ALUMINIUM IN DIFFERENT CONCENTRATIO OF NaOH , DISSOLVED IN 1M TUNGSTATE.

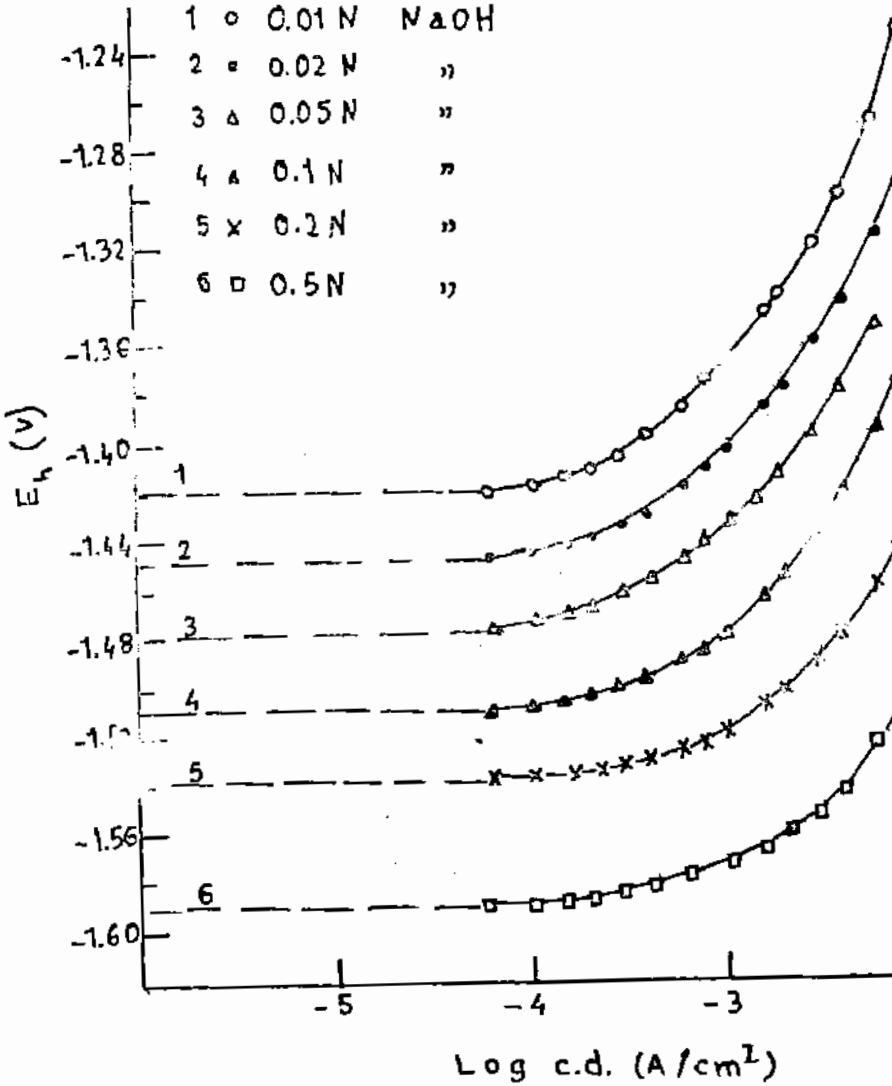

Fig (5)

CATHODIC P[illegible]RISATION CURVES FOR ALUMINIUM IN DIFFERENT CONCENTRATIONS OF Na_2WO_4, DISSOLVED IN 0.2 N NaOH.

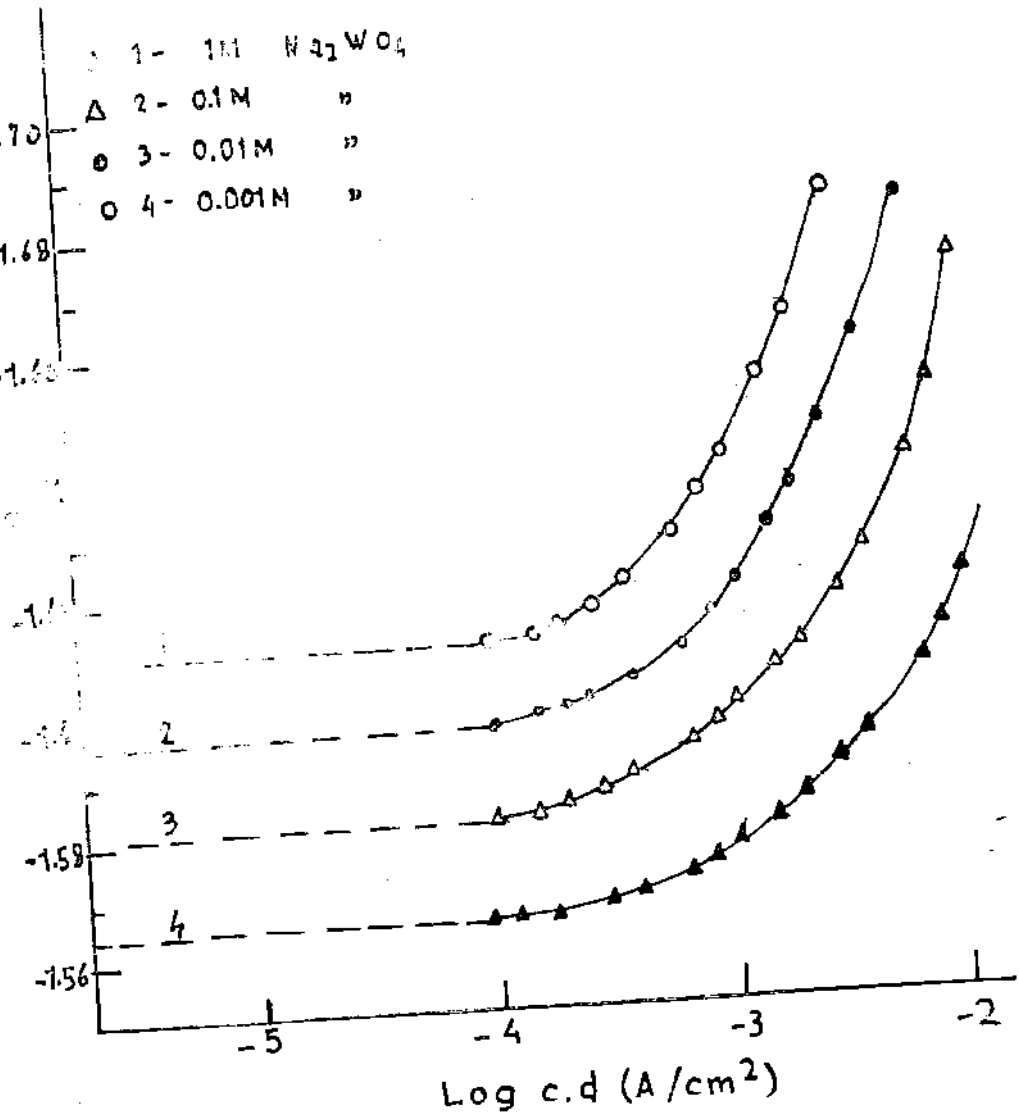

Fig (6)

NATURAL PLANT COVER IN THE DESERT FRINGE WEST OF NILE DELTA

BY

M. A. HAMMOUDA

Professor, Botany Department, Women's College,
Ain Shams University, Cairo.

Introduction

The area west of Rosetta Branch of the Nile gives an ample of a desert fringe where xeric and mesic habitats me.in contact at a margin line. In such an area reciprocal fluences and interactions of factors occur. This paper is vocated to a study of natural plant cover in the area. ttern and features of plant communities in this area were nvestigated.

The scope of survey covers a traingular area, the head f the traingle is SW of Cairo and its base represents a line assing from Khatatba on Rosetta branch to k. 106 on Cairo-lexandria desert road. The study was made along four trans-cts traversing longitudinal and horizontal planes of the urveyed area.

The effect of wind ercsion and deposition in auch an area is quite pronounced. Sand is drifted from the desert uplands and deposited on the lower contours to the east and threatens the fertile land. Wind-transported sand exerts clear effects on soil and vegetation.

Geology

The general geological characteristics of the norther part of the western desert of Egypt has been reported on b some authors e.g. Shatta (1955). Recent series include th Nile silt and alluvium occuring in the limited area border the Nile Delta. Its thickness averages from 20m. to the s of Cairo to 40m. to the north, Attia, (1954). Pleistocene deposits as sands and gravels of assorted sizes border the cultivated areas west of the Nile Delta forming a series terraces of various heights. Pliocene rocks exist in the [illegible]t. Outcrops of porcelaneous limestone and black s alternating with argillaceous sandstone are distinguished. Miocene deposits composed essentially of limestone changin partly into a fluviatile series and exposed Eocene sedimen occur at Abu Rawash area and the Pyramids plateau.

The general axial trend of the surface anticlines is NE-SW.

Topography

The area under investigation (see Fig. 1) shows in ge a characteristic uneven relief, of an undulated landscape SW-NE sloping trends and an eastward depressed area which provides the fertile land bordering Rosetta branch of the N (contour about 12-15m.). A prominently broad sand bar -4

t Katta- is developed west of and parallel to Rosetta channel xtending northward to a long distance from Katta to Wardan. Behira channel has its way along sandy area (contour about 0m.) in the south. To the west, the land rises steeply to ontour 50m. or more forming the terrace side seen westward of bu Rawash-Birkash and further to the north along Imbaba - hatatba desert road. From this side some runnels slope down ith a prevailing SW-NE direction. There exist also few wide nd sloping dry streams of which may be mentioned Wadi Farah ith a west-eastward course joining the eastward depressed ea opposite to k.30 on Imbaba-Khatatba desert road. Westwards the undulated gravel desert prevails; Cairo-Alexandria desert road traverses it SE-NW and Khatatba-Tahrir province desert road E-W.

Especially to the south exist calcareous prominent uplifts .g. G. Abu Rawash (174 m.), G. Mansuria (182m) and Garet l Hadadin (233 m.).

Climate

The following table, (Table 1) shows monthly variations f the climatic factors in Giza (G), at the south of the studied area, and Badr Centre in Tahrir province (T), at the orth. The data given represents mean values of 1966 and 1967.

Transects

Vegetation study was made along four transects as follo

Transect 1: (SE-NW) Imbaba-Khatatba eastern road (eas of Behira channel).

Transect 2: (SE-NW) Desert border from Abu Rawash to Birkash-Nikla-Khatatba desert road.

Transect 3: (SE-NW) Cairo-Alexandria desert road till k. 106.

Transect 4: (E-W) Khatatba-k. 82 Cairo-Alexandria des road.

Vegetation

The main types of plant communities and habitats along the studied transects are given in the following:

Transect 1:

The prominent effects pertaining on vegetation are cau by Nile water (Behira channel) and by drifted sand. Alhagi maurorum or Phragmites australis occasionally appear forming pure or mixed stands indicating near water table. A communit type (stand 2, Table 2, Fig. 2) is remarkable on elevated areas.

Table 2: Floristic composition of Alhagi maurorum community type.

	Stand 1	Stand 2
Alhagi maurorum	(pure stand)	d.
Phragmites australis	.	cod.
Imperata cylindrica	.	c.
Cynodon dactylon	.	c.
Panicum turgidum	.	c.
Launaea nudicaulis	.	r.

		J	F	M	A	M	J	J	A	S	O	N	D
Air temperature:													
mean for day (C)	G:	11.8	11.6	15.6	21.0	23.5	27.1	27.2	27.9	26.0	23.1	19.4	14.2
	T:	11.6	13.5	15.2	20.1	23.0	26.0	26.5	27.9	25.0	22.7	19.0	14.3
highest mx. °(C)	G:	26.6	22.1	33.5	40.1	42.8	44.0	38.2	38.8	39.4	34.9	34.9	28.5
	T:	29.2	22.9	34.8	41.0	40.3	46.0	38.8	38.8	38.5	35.3	33.1	28.1
lowest min. °(C)	G:	1.1	3.3	2.2	6.7	11.9	16.6	18.3	19.5	16.1	13.1	4.2	3.0
	T:	1.1	3.6	2.6	7.5	11.0	15.8	17.4	19.5	14.7	13.1	5.6	4.2
Relative humidity:													
mean for day (%)	G:	70	67	46	51	54	51	61	63	63	67	70	65
	T:	66	62	50	57	61	60	70	63	65	71	78	72
Wind speed:													
mean for day (m/sec.)	G:	1.7	2.2	2.5	2.6	2.8	2.7	2.7	2.2	2.2	2.2	2.8	2.8
	T:	2.6	2.6	3.1	2.7	2.6	2.9	2.9	2.3	2.3	2.1	2.1	2.3
highest gust (knots)	G:	30	29	37	30	32	29	25	28	24	26	26	27
	T:	39	38	50	42	34	30	27	28	27	26	34	42
Rain fall (mm.)	G:	4.4	1.4	2.8	0.7	3.7	0	0	0	0	0	8.9	0.8
	T:	3.0	4.1	12.8	tr.	23.3	0	0	0	0	0	7.4	8.2

On moist areas of low contours C.6., south of Abu Galeb evelops an aquatic community type composed of Panicum epens on water, the cattail Typha domingensis and bordered y the reed-grass Phragmites australis and the sedge Cyperus lternifolius. The series of flat sand dunes west of Rosetta ranch hold a dune plant community (Table 3) dominated Aristida coparia in the top stands: (Fig 3) and by Polycarpea repens n the foot stands.

Table 3: Floristic Composition of Aristida scoparia Plant community type.

	Stand 1 Katta: foot of dune	Stand 2 Katta: top of dune	Stand 3 T3 k.55	Stand 4 T3 k.56
Aristida scoparia	Cod.	d.	d.	d.
Polycarpea repens	d.	.	r.	.
Pennisetum divisum	a.	.	.	.
Panicum turgidum	.	.	cod.	c.
Heliotropium luteum	O.	.	.	.
Moltkea Calosa	O.	O	r.	.
Hammada elegans	.	.	r.	r.
Monsonia nevea	O.	.	O.	.
Bassia muricata	r.	.	.	.

The windward side- height may reach 4 mts.-is dev id of plant cover which is only restricted to its base.

Transect 2:

The terrace side to the west is almost devoid of vegetation except scarcely on the eastward inclining slopes.

The sand flats by the terrace base on the border of fertils land sustain Moltkea callosa community; type, Table 4 and Figs. 4,5). Of the characteristic species may be mentioned Heliotropium luteum and Panicum turgidum.

Table 4: Floristic composition of Moltkea calosa Plant community type.

	Stand 1 T2	Stand 2 T2	Stand 3 T2	Stand 4 T3 K41
Maltkea callosa	d.	d.	d.	d.
Heliotropium luteum	cod.	c.	c.	.
Panicum turgidum	a.	O.	a.	.
Pennisetum divisum	O.	r.	.	.
Aristida plumosa	C.	cod.	.	.
Pulicaria crispa	O.	C.	.	.
Eremobium lineare	O.	.	.	.
Launaea nudicaulis	O.	.	.	.

Passing northward, the transect traverses the gravely desert and on drifted sand, distinct stands of Aristida scopar appear. Blown sand fall along the slopes, and despite windbreaks the effect of blown sand is clear e.g. at fences (Fig.6 Panicum turgidum scatterly appears and dominates on sand sheet along Wadi Farah runnel (opposite k. 30 Imbaba-Khatatba desert road) and especially at its mouth.

Opposite to Khatatba appears Artemisia monosperma and comes codominant with Panicum turgidum.

A soil profile in a cultivated area just at the desert rder SW or Birkash-near the southern end of the transect-is presented (Fig. 7), Table 5). The upper soil is formed of layer of light sand, one meter thick, below which exists a ver of heavier silty sand '20 cm).

This sublayer has been formed by earlier silting from le flood irrigation water where as the upper layer is built by wind drifted sand.

able 5: Granulometric analysis of the soil Profile at the desert limit (SW. Birkash)

Particle size	50 cm	125 cm
00 - 0.20 mm.	75.7%	27.5%
20 - 0.15 mm.	8.5	11.0
15 - 0.07 mm.	15.2	21.4
0.07 mm.	0.6	10.1

Transect 3:

At the foot of Abu Rawash uplift a community of Alhagi rorum is located (Fig. 8). A community dominated by gophyllum coccineum (e.g. at K. 24) inhabits the shallow l at the foot of the limestone elevations. Plant cover

is scanty on the gravel desert (e.g. k. 34–53), however, a community type dominated by Hammada elegans occasionally appears (e.g. K. 32) on depressed areas. From k. 53–64 the landscape changes to a desert grassland. By k.55–57 Aristi scoparia community type is remarkable on loose drifted sand on the eastwardly directed runnels (Table 3. Fig. 9). Stan of Moltkea callosa are located on drifted sand at the borde (e.g. k. 41, Fig. 10, and k. 67). A second grassland commu type dominated by Panicum turgidam inhabits wide and conti

Table 6: The floristic Composition of Panicum turgidum Plant community type.

T3:	Stand 1 k.55	Stand 2 k.58	Stand 3 k.70	Stand k.72
Panicum turgidum	d.	d.	d.	d.
Pituranthos tortuosus	O.	h.	c.	c.
Aristida scoparia	O.	.	O.	O.
Hammada elegans	O.	.	O.	O.
Moltkea callosa	c.	c.	O.	O.
Fagonia cretica	O.	O.	r.	r.
Polycarpea repens	c.	c.	c.	c.
Ifloga spicata	O.	O.	O.	O.
Dawthonia forskalei	O.	.	.	.
Neurada procumbens	r.	.	r.	.
Convolvulus lanatus	r.	.	r.	.
Cotula cinerea	o.	.	.	.

Table 7: Floristic composition of Pituranthos tortuosus plant community type.

T3:	Stand 1 k.72	Stand 2 k.83	Stand 3 k.87	Stand 4 k.89	Stand 5 k.95	Stand 6 k.105
Pituranthos tortuosus	d.	d.	d.	d.	d.	d.
Panicum turgidum	c.	c.	c.	r.	.	.
Zilla spinosa	.	r.	r.	r.	o.	o.
Farsetia aegyptisca	.	.	.	r.	.	r.
Schismus barabatus	o.	c.	o.	o.	c.	o.
Moltkea callosa	o.	c.	.	o.	.	.
Zygophyllum album	.	o.	o.	o.	c.	r.
Fagonia glutinosa	.	r.	o.	o.	r.	c.
Artemisia monosperma	c.	cod.	o.	c.	r.	a.
Crotalaria aegyptiaca	.	.	o.	o.	.	.
Stipa lagasca	.	.	o.	o.	o.	.
Hoplophyllum tuberculatum	.	.	r.	.	c.	.
Atractylis flava	.	r.	.	.	o.	.
Hyoscyamus muticus	.	.	.	r.	c.	.
Neurada procumbens	.	r.	o.	.	.	.
Helianthemum lippii	.	.	.	.	o.	.
Convolvulus lanatus	.	.	o.	o.	.	.
Lamarkia sp.	.	r.	r.	.	.	.
Launaea nudicaulis	.	.	.	.	r.	.

Table 8: Floristic composition of Zilla spinosa Plant Community type.

T:3	Stand 1 k.96	Stand 2 k.97	Stan k.9
Zilla spinosa	d.	d.	d.
Pituranthos tortuosus	c.	a.	c.
Farsetia aegyptiaca	o.	o.	o.
Panicum turgidum	.	.	c.
Hammada elegans	.	c.	.
Zygophyllum coccineum	.	o.	.
Z. album	o.	o.	o.
Z. simplex	r.	.	.
Fagonia arabcea	.	o.	.
Artemisia monosperma	o.	cod.	.
Atractylis flava	o.	.	.
Hyoscyamus muticus	r.	o.	.
Senecio coronopifolius	r.	o.	.
Cotula cinerea	o.	o.	.
Launaea nudicaulis	o.	o.	.
Pteranthus dichotomus	o.	o.	.
Helianthemum lippii	c.	r.	.

Table 9: Floristic composition of Artemisia monosperma plant community type

	Stand 1 T4 k.16	Stand 2 T4 k.24	Stand 3 T4 k.28	Stand 4 T3 k.100	Stand 5 T5 k. 104
Artemisia monosperma	d.	d.	d.	d.	d.
Pituranthos tortuosus	a.	c.	o.	c.	c.
Panicum turgidum	c.	o.	o.	c.	c.
Zilla spinosa	c.	c.	o.	c.	c.
Farsetia aegyptiaca	r.	.	.	.	.
Hyoscyamus muticus	o.	o.	.	c.	.
Hammada elegans	o.	.	r.	r.	r.
Fagonia glutinosa	o.	.	o.	o.	c.
Salsola kali	r.	.	o.	.	.
Trigonella stellata	c.	.	o.	.	.
Polycarpea repens	o.	.	.	o.	.
Pancratium sickenbergi	r.	.	.	.	r.
Helianthemum lippii	r.	.	r.	.	.
Medicago hispida	c.	.	.	.	.
Filago spathiolata	o.	.	r.	r.	.
Ifloga spicata	o.	r.	r.	r.	.

sheets of sand, (Fig. 1). Table 6 shows the [illegible] position of four stands of this community type. Fur[illegible] the north, Pituranthos tortuosus dominates a characteristic community type of sandy furrows: (Fig. 12). The floristic composition is shown in Table 7. In some runnels, pure stands of Pituranthos tortuosus, the suffrutescent perennial are seen. Roots of Pityranthus tortuosus are known to be deep penetrating, the plant shows good growth in its sandy habitat. By k.96-98, Zilla spinosa community type prevails, (Table 8). Artemisia monosperma begins to appear near k. 77, but further north it appears frequently and dominates a plant community type (e.g. stands k. 100 and 104). Artemisia monosperma is commonly codominated by Pituranthos tortuosus, and occasionally by Zygophyllum album in some stands, (e.g. k. 100). However pure stand of Zygophyllum album may exist, (e.g. k. [illegible]).

Transect 4:

The desert west of Khiva is gravelly [illegible] poor vegetation on the drifted sand, but further west Artemisia monosperma plant community type richly colonizes the area, (Fig. 13, Table 9) till the reaches of the end of the transect. The S-N runnels are densely grass oriented by September due to the new growth of Artemisia monosperma; the green runnels alternate with barren slightly elevated gravelly areas. In some localities Pituranthos tortuosus, or Zilla spinosa, codominates with Artemisia monosperma, whereas in several other

localities Artemisia monosperma forms almost pure stands. Artemisia monosperma actually characterizes the open desert scrub landscape of nearly the whole length of Transect 4. For few kilometers at both ends of the transect - higher elevations-, the vegetation is very scarce.

Discussion

It is evident that the features of the plant cover in the studied area are greatly regulated by the complex of the climatic, especially rainfall and wind, (Table 1), and physiographic factors especially topography (Fig. 1), and soil characteristics.

The natural plant cover in the area under investigation is oriented in six distinct plant community types, as follows:

1- Aristida scoparia community type.
2- Moltkea callosa " "
3- Panicum turgidum " "
4- Pituranthos tortuosus " "
5- Zilla spinosa " "
6- Artemisia monosperma " "

and three subcommunity types, namely:

7- Zygophyllum coccineum subcommunity type
8- Hammada elegans " "
9- Zygophyllum album " "

A quatic and moist soil communities are also represented.

- 4.4 -

Each of the above mentioned community types is characterized by the dominant species which give it a homogeneity of plant growth. The phytoceonsis varies from an open desert grassland in Aristida scoparia and Panicum turgidum community types to an open desert sub Serub as Artemisia monosperma community type.

The pattern of the different plant community types is regulated by the interacting complex of factors of the environment . Tolerance limits of the different species to various factors determine the floristic composition of the different localities of the above mentioned vegetation units; some are transitional types. While few Zygophyllum coccineum subcom. appears on shallow soil on limestone at the southern sector of the area, Zygophyllum coccineum forms a rich community type representing stages in the development of wadi, Kassas (1952) and Kassaa and Imam (1954). Hammada elegans appears commonly on gravel desert.

Panicum turgidum grassland represents a stage in the general building up of sand soil. The last two examples may thus represent stages in allogenic retrogressive and progressive successional changes, respectively.

Pityranthos tortuosus community type is sand preferable and merges to Panicum turgidum type to one side and to Artemisia monosperma community type to the other side. Orientation of Zilla spinosa and Artemisia monosperma community

types appears to be greatly governed by factors such as soil depth, runoff, and moisture regime.

Moltkea callosa community type is a transitional one. Moltkea callosa is a pioneer plant on newly drifted sand and develops on sand flats and dune bases. Aristida scoparia too, a pioneer sand binder is higly wind tolerant and inhabits tops of dunes. Both species are endowed with the ability of colonizing moving sand.

The six plant community types above mentioned are dominated mostly by sand loving plants. They represent stages of plant succession on sand exhibiting a form of communities of a psamosere. However, some of these community types could reach a relatively stable subclimax state.

It may be stated here that the community types here represented exhibit some relationship with community types distinguished by Kassas and Abid (1962) for the Eastern desert.

The role of wind, through erosion and deposition is quite evident in the area. Sand creeps gradually from the north-west to the low cultivated land in the east. Movement of soil is controlled by grain size and wind velocity. Thus according to Stockes law, a grain of sand 0.125 mm. in diamter could be moved by a threshold wind velocity of 4, 5-6.7 m./sec. (about 16.0-24.0 km./h). Soil may be moved by saltation,

-40b-

supension or surface creep, Stallings, (1959). While saltation is responsible of moving grains ranging in diameter from 0.1- 0.2 mm., particles less than 0.1 mm. are carried in suspension. Grains of about 0.5 - 1.0 mm. in diameter derive their kinetic energy by the impact of grains moving in saltation to form surface creep. Deposition occurs as wind carrying soil material either in suspension or saltation subsides so it deposits its soil load, (see Fig. 6). Exceptional wind storms and gusts of increasing frequency and severity occur in the desert, (Table 1). They are responsible of building up of surface sand soil, (Fig. 7), the observed movement of sand and sometimes its oncroschment on fertile land. Worthwhile to emphathize here the advantageous role of wind breaks and tree and shrub plantation.

Summary

A vegetation study of the desert fringe area west of the Nile Delta was made. The following vegetation units were distinguished: Aristida scoparia, Moltkea callosa, Panicum turgidum Pituranthos tortuosus, Zilla spinosa, Artemisia monosperma, Zygophyllum coccineum, Hammada elegane, and Zygophyllum album.

An aquatic and moist soil comm. type sppears at water habitats.

The features and characteristics of these vegetation units were shown. The community types distinguished are dominated by sand loving plants and they represent stages of plant succession on sand.

The role of wind erosion and deposition is disscussed.

References

Attia, M.I. 1954. Deposits in the Nile valley and the Delta, Egypt. Geological Survey, Cairo.

Kassas, N. 1952. Habitats and plant communities in the Egyptian deserts. I Introduction. J. Ecol. 40, 342.

_____, and Imam, M. 1954. Habitat and plant communities in the Egyptian deserts. III The wadi bed ecosystem J. Ecol. 42, 424.

_____, and Abyad, M. 1962. On the phytosociology of the desert vegetation of Egypt. Annals of Arid Zone 1,1.

Shatta, A. 1955. An introductory note on the geology of the northern portion of Western desert of Egypt. Bull. Desert Inst. 5 II, 96.

Stallings, 1959. Soil Conservation. Prentice-Hall Incorp.

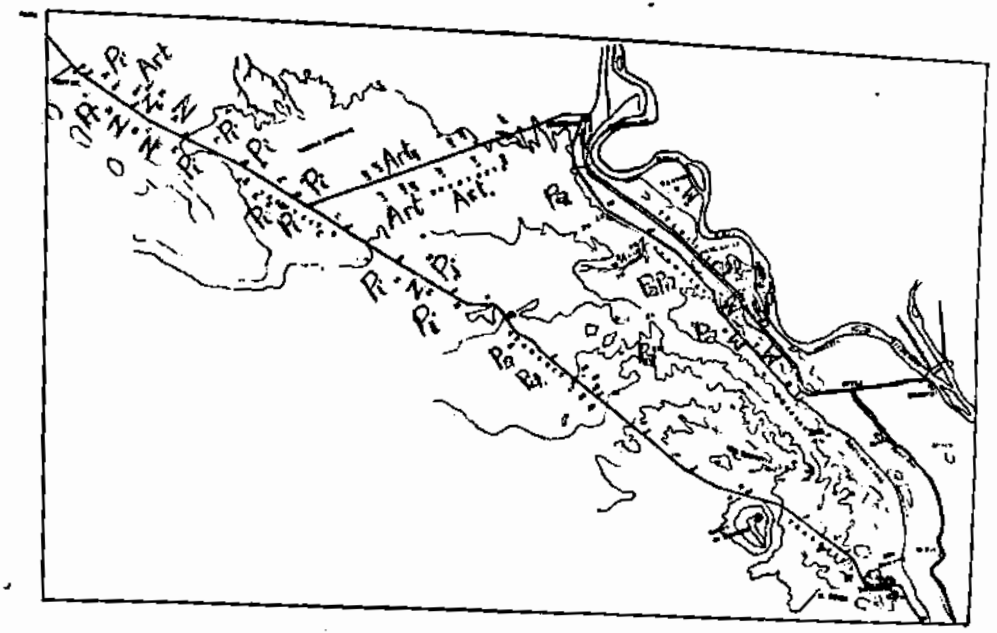

Fig. 1: Map of the studied area west of the Nile Delta showing orientation pattern of vegetation.

Fig. 2: (Tr 1) A stand of Alhagi maurorum; Phragmites australis is invading the area.

Fig. 3: (Tr 1, near Katta) Aristida scoparia on sand dunes.

Fig. 4: (Tr 2) Moltkea callosa plant community type, in neighbourhood of cultivation.

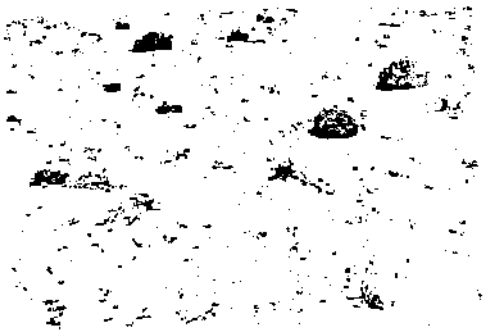

Fig. 5: (Tr 2) Moltkea callosa plant community type.

Fig. 6: (Tr 2) A semi natural stand with plantations of Opuntia. Note deposited sand beyond the fence.

Fig. 7: (Tr 2) A soil profile near Birkash. Note the silty layer below the layers of deposited sand.

Fig. 8: (Tr 3) Alhagi maurorum stand at the foot of G. Abu Rawash.

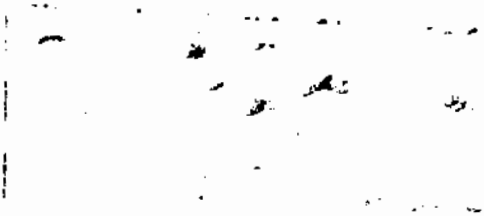

Fig. 9: (Tr 3, k.57) Aristida scoparia plant community type.

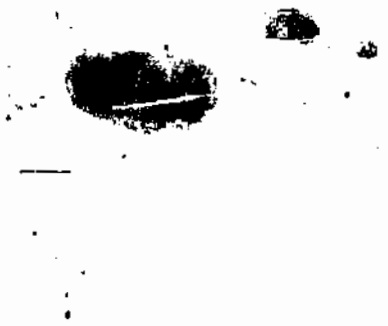

Fig. 10: (Tr 3, k. 41) Meltkea callosa plant community type.

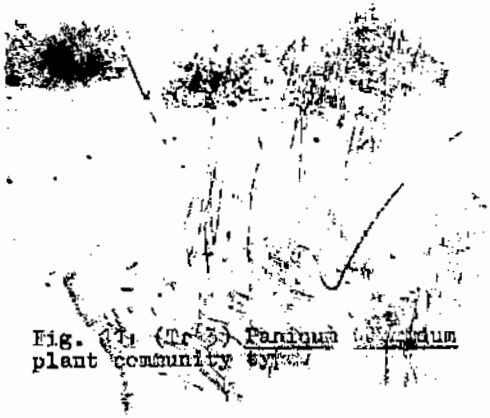

Fig. 11 (Tr 3) Panicum [illegible]dum plant community type.

Fig. 12: (Tr 3, k. 97) Pituranthos tortuosus plant community type.

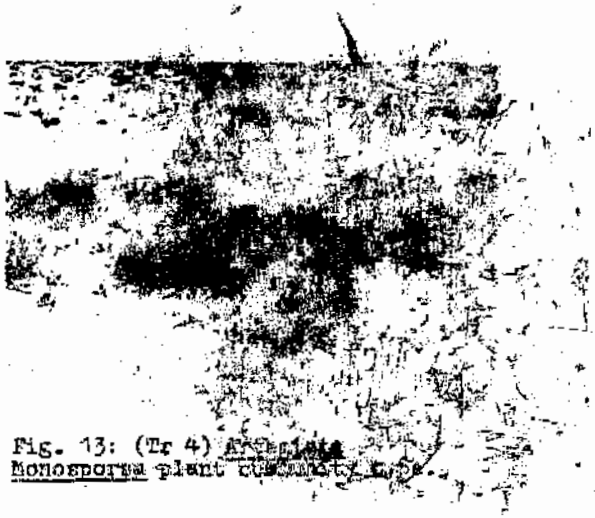

Fig. 13: (Tr 4) [illegible] Monosperma plant community type.